

Water-Gas-Shift Membrane Reactor for High-Pressure Hydrogen Production: A Comprehensive Project Report (FY 2010 – FY 2012)

January 2013



The INL is a U.S. Department of Energy National Laboratory
operated by Battelle Energy Alliance

DISCLAIMER

This information was prepared as an account of work sponsored by an agency of the U.S. Government. Neither the U.S. Government nor any agency thereof, nor any of their employees, makes any warranty, expressed or implied, or assumes any legal liability or responsibility for the accuracy, completeness, or usefulness, of any information, apparatus, product, or process disclosed, or represents that its use would not infringe privately owned rights. References herein to any specific commercial product, process, or service by trade name, trade mark, manufacturer, or otherwise, does not necessarily constitute or imply its endorsement, recommendation, or favoring by the U.S. Government or any agency thereof. The views and opinions of authors expressed herein do not necessarily state or reflect those of the U.S. Government or any agency thereof.

Water-Gas-Shift Membrane Reactor for High-Pressure Hydrogen Production: A Comprehensive Project Report (FY 2010 – FY 2012)

John Klaehn¹, Eric Peterson¹, Christopher Orme¹

**Dhaval Bhandari², Scott Miller², Anthony Ku², Kimberly Polishchuk²,
Kristi Narang², Surinder Singh²
Wei Wei², Roger Shisler², Paul Wickersham², Kevin McEvoy², William Alberts²,
Paul Howson²**

Thomas Barton³, Vijay Sethi³

January 2013

¹Idaho National Laboratory, Idaho Falls, ID 83415

²General Electric Global Research, Niskayuna, NY 12309

³Western Research Institute, Laramie, WY 82072

www.inl.gov

www.ge.com

www.westernresearch.org

**Prepared for the
U.S. Department of Energy
Office of Energy Efficiency and Renewable Energy
Under DOE Idaho Operations Office
Contract DE-AC07-05ID14517**

ABSTRACT

Idaho National Laboratory (INL), GE Global Research (GEGR), and Western Research Institute (WRI) have successfully produced hydrogen-selective membranes for water-gas-shift (WGS) modules that enable high-pressure hydrogen product streams. Several high performance (HP) polymer membranes were investigated for their gas separation performance under simulated (mixed gas) and actual syngas conditions. To enable optimal module performance, membranes with high hydrogen (H_2) selectivity, permeance, and stability under WGS conditions are required. The team determined that the VTEC PI 80-051 and VTEC PI 1388 (polyimide from Richard Blaine International, Inc.) are prime candidates for the H_2 gas separations at operating temperatures ($\sim 200^\circ\text{C}$). VTEC PI 80-051 was thoroughly analyzed for its H_2 separations under syngas processing conditions using more-complex membrane configurations, such as tube modules and hollow fibers. These membrane formats have demonstrated that the selected VTEC membrane is capable of providing highly selective H_2/CO_2 separation ($\alpha = 7\text{--}9$) and H_2/CO separation ($\alpha = 40\text{--}80$) in humidified syngas streams. In addition, the VTEC polymer membranes are resilient within the syngas environment (WRI coal gasification) at 200°C for over 1000 hours. The information within this report conveys current developments of VTEC PI 80-051 as an effective H_2 gas separations membrane for high-temperature syngas streams.

ACKNOWLEDGEMENTS

The authors wish to extend their heartfelt thanks to the following DOE-HQ individuals for their support of this project.

Dr. Bhima Sastri

Dr. Robert Gemmer

Dr. Dibyajyoti Aichbhaumik (Debo)

Dr. Mahesh Jha

Dr. Stephen Sikirica

Dr. Harvey Wong

Dr. Isaac Chan

CONTENTS

| | |
|--|----|
| INTRODUCTION | 9 |
| Background..... | 10 |
| A New Approach: “Tightening Up” Polymer Structures | 17 |
| SECTION 1 MODEL PERFORMANCE OF THE MEMBRANE REACTOR AND SYSTEM | 19 |
| Systems Modeling for Coal to Ammonia | 19 |
| Water Gas Shift Kinetics | 22 |
| Counter Current Membrane Model | 23 |
| Integrated Model and Results | 24 |
| Sizing and Cost Analysis | 26 |
| Summary | 28 |
| SECTION 2 DEVELOPMENT OF HYDROGEN-SELECTIVE POLYMER MATERIALS | 30 |
| High Performance Polymers..... | 30 |
| Development of Gas Permeation Experiments for Polymer Evaluation | 35 |
| Conclusion..... | 42 |
| SECTION 3 HIGH PERFORMANCE POLYMERS ON POROUS SUPPORTS | 43 |
| Evaluation of VTEC Pi Polyimide on Ceramic and Porous Metal Discs in Gasified Coal Syngas Streams | 43 |
| Development and Testing of VTEC Coated Porous Tube Modules..... | 47 |
| Membrane Layer Development for Porous Supports | 51 |
| Summary..... | 68 |
| SECTION 4 DEVELOP MANUFACTURING PROCESSES FOR SUPPORTS WITH DEFECT- FREE INTERMEDIATE LAYERS AND MEMBRANE MODULES (POROUS SUPPORTS)..... | 70 |
| Background Analysis to Module Design and Development..... | 70 |
| Hollow Fiber Module Development and Separation Performance Testing..... | 87 |
| BENEFITS ASSESSMENT | 95 |
| COMMERCIALIZATION | 95 |
| Adjacent Market Opportunities | 96 |
| Corporate Commitment | 97 |
| ACCOMPLISHMENTS | 97 |
| Journal Articles..... | 97 |
| Presentations..... | 97 |
| Publications | 97 |
| Patent Activitie | 97 |
| TECHNICAL ACCOMPLISHMENTS..... | 98 |

| | |
|---|-----|
| Conclusions | 100 |
| OVERALL SUMMARY AND CONCLUSION | 101 |
| Recommendations and Future Work | 101 |
| BIBLIOGRAPHY | 103 |
| APPENDICES | |
| Appendix A. Dry Permeability Gas Analysis | |
| Appendix B. Mixed Gas Separation Apparatus Description | |
| Appendix C. Gas Humidification Procedure. | |
| Appendix D. Gas Permeability Calculations. | |
| Appendix E. Thermal Analysis | |
| Appendix F. High Performance Polymers on Porous Inorganic Supports | |
| Appendix G. High Performance Polymers on Porous Supports – Polyimide Hollow Fiber Membranes for Gas Separation and Modules | |
| Appendix H. H ₂ /CO ₂ Gas Permeability Testing of Hollow Fibers | |
| Appendix I. Summary of Tests, Major Milestones, and Deliverables | |

FIGURES

| | |
|---|----|
| Figure 1. Overview of the program..... | 9 |
| Figure 2. Syngas markets and technical opportunity. The WGS reaction and CO ₂ removal are critical steps in the processing of syngas in the chemical petroleum and power generation industries. | 11 |
| Figure 3. WGS-MR concept. A H ₂ -selective membrane is located in the midst of the packed bed of the shift reactor catalyst, operating at temperatures between 250° and 350°C. H ₂ permeates the membrane into the tubes, where a high pressure N ₂ sweeps the gas to produce a high pressure H ₂ /N ₂ gas stream. The H ₂ -selective membrane allows continuous removal of the H ₂ produced in the WGS reaction, allowing the equilibrium conversion of CO to CO ₂ to proceed to near completion, while also separating the H ₂ from the CO ₂ | 12 |
| Figure 4. Technical approach to developing membrane materials and manufacturing processes. INL and GEGR applied innovative methods in polymer processes, support engineering, and manufacturing to develop high performance membranes. | 15 |
| Figure 5. Syngas market segments..... | 15 |
| Figure 6. Materials targets for ammonia production..... | 19 |
| Figure 7. Conventional systems diagram for ammonia production from coal..... | 20 |
| Figure 8. Systems diagram using WGS–MR for ammonia production from coal..... | 20 |

| | |
|--|----|
| Figure 9. An example of ASPEN™ Plus model utilizing a WGS–MR in a coal-to-ammonia plant. | 21 |
| Figure 10. A typical profile of gas composition through HTS (left) and LTS (right). | 23 |
| Figure 11. A WGS–MR conceptual design. | 25 |
| Figure 12. Composition of gases through a WGS–MR. | 25 |
| Figure 13. Example of modeling the WGS–MR in ASPEN™ Custom Modeler. | 26 |
| Figure 14. CAPEX breakdown of the conventional system vs. a system utilizing WGS–MR for coal-to-ammonia process. | 29 |
| Figure 15. Robeson plot of H ₂ permeance and H ₂ /CO ₂ selectivity, showing Robeson’s 1991 and 2008 upper bound lines. | 31 |
| Figure 16. Dry-gas testing on mixed-gas feed streams—E _p data collected on Matrimid 5218 films from 30–275°C. | 41 |
| Figure 17. Humidified (2-4% water vapor) gas testing on mixed-gas feed streams—E _p data collected on Matrimid 5218 films from 30–200°C. | 41 |
| Figure 18. Mixed-gas permeability test on VTEC PI 1388 for 72 hours using a humidified feed stream (2-4% water) at 200°C. | 42 |
| Figure 19. Asymmetric composite membrane structure. | 44 |
| Figure 20. WRI facilities (left) and sample coupons prior to exposure test (right). | 45 |
| Figure 21. Coupons after exposure testing: labels indicate the support materials (steel, Inconel, or alumina), the intermediate layer (γ-alumina or zeolite), and the type of polymer membrane (VTEC 080-051 or VTEC 1388). | 45 |
| Figure 22. Syngas simulant feed stream test for 168 hours at 250°C on the polymer coated discs. The test was designed to expose these polymer-coated discs to syngas conditions at 250°C. | 46 |
| Figure 23. SEM Pictures of the polyimides after 168 hours of syngas exposure at 250°C. | 47 |
| Figure 24. Leak site at interface between epoxy potting and stainless steel end fitting. | 53 |
| Figure 25. (a) Standard tube in fitting geometry, (b) butt joint, and (c) modified butt joint that mimics seal to flat disk. | 54 |
| Figure 26. Close-up of a tube with a machined end (top) and a tube that has been machined and then swaged on both ends (bottom). | 55 |
| Figure 27. Performance of ferrule materials during thermal cycle to 250°C. | 56 |
| Figure 28. Sample laser weld results. | 57 |
| Figure 29. Schematic of tubular membrane testing protocol. | 57 |
| Figure 30. Image of the tube housing and the fixtured sample tube. | 58 |
| Figure 31. Performance of Tube 50. | 60 |
| Figure 32. Performance of Tube 50. | 61 |
| Figure 33. Tube 50 process exhaust line after elevated temperature testing. | 61 |
| Figure 34. Performance of Tube 50. | 62 |
| Figure 35. Performance of Tube 50. | 63 |

| | |
|--|----|
| Figure 36. Performance of Tube 50. | 64 |
| Figure 37. Performance of Tube 50. | 65 |
| Figure 38. Performance of Tube 50. | 65 |
| Figure 39. Performance of Tube 50. | 66 |
| Figure 40. Performance of Tube 50. | 66 |
| Figure 41. Stability of Tube 50 over time. | 67 |
| Figure 42. Cost breakdown for the membrane module. | 67 |
| Figure 43. Single-tube module. | 71 |
| Figure 44. Multi-tube configuration. | 71 |
| Figure 45. Bench-top-module design for laboratory testing. | 72 |
| Figure 46. Schematic representation of a binodal curve used to determine core layer spin dope composition. | 75 |
| Figure 47. Schematic representation of cloud point study to determine spin dope composition. | 75 |
| Figure 48. Cross-section SEM image of Gen-2 polyamic acid hollow fiber membrane. The fibers were found to have a nice open cell uniform morphology with a thin-selective skin layer. Macrovoids were eliminated by carefully tuning the fiber morphology (GE ID: Spin 4). | 77 |
| Figure 50. Images of Spin 2: State 2 hollow fibers at different stages of cure. | 78 |
| Figure 51. SEM images of the cross-section of the middle of hollow fibers (Spin 4: State 8) exposed to maximum temperatures of (a) 30°C, (b) 150°C, and (c) 250°C. | 79 |
| Figure 52. SEM images of the cross-section of the inner diameter of hollow fibers (Spin 4: State 8) exposed to maximum temperatures of (a) 30°C, (b) 150°C, and (c) 250°C. | 79 |
| Figure 53. SEM micrographs of the membrane surfaces of hollow fibers (Spin 4: State 4) cured at the temperature and nitrogen flows specified. Micrographs a, b, and c were higher magnification images of micrographs d, e, and f, respectively. | 80 |
| Figure 54. Spin 4 – SEM images of Spin 4: State 4 hollow fibers: as-spun (left), and after steam exposure (right). | 81 |
| Figure 55. Spin 4: State 1 Optical microscope images of the various stages of hollow fiber processing. | 82 |
| Figure 56. Spin 4: State 1 SEM images of the various stages of hollow fiber processing, external view of the fibers. | 82 |
| Figure 57. Spin 4: State 7 SEM images of the various stages of hollow fiber processing, internal bore (internal diameter) of the fiber. | 83 |
| Figure 58. SEM images of a Spin 2: State 3 hollow fiber cured under nitrogen. | 83 |
| Figure 59. SEM images of a Spin 2: State 3 hollow fiber cured under vacuum. | 84 |
| Figure 60. ATR-IR spectra of cured, uncured and semi-cured Spin 2 hollow fibers. The spectra were all normalized to the aromatic ring stretch at 1499 cm ⁻¹ | 85 |

| | |
|--|----|
| Figure 61. ATR-IR spectra of the exterior and interior surfaces of the 1-hour cured Spin 2: State 2 hollow fiber. The spectra were all normalized to the aromatic ring stretch at 1499 cm^{-1} . The inset contains an optical image of the split fiber. | 86 |
| Figure 62. Typical Hollow Fiber Module Constructed from 1/4" Swagelok® Fittings..... | 87 |
| Figure 63. Gas-separation testing of polyimide tubing potted with four different potting materials. All permeances greater than ~2 GPU were assumed to be caused by potting materials leaks. | 89 |
| Figure 64. Cracks in Durapot™ 863 potting material after thermal cycle at 200 °C, as indicated by white circle. | 89 |
| Figure 65. Permeance increase with temperature for hollow fiber module potted with Cotronics 4525-IP epoxy: (a) hydrogen, (b) carbon dioxide..... | 90 |
| Figure 66. Cross section of potted VTEC fibers potted in module with Duralco™ 4525-IP. | 91 |
| Figure 67. H ₂ /CO ₂ selectivity performance of Module 23..... | 93 |
| Figure 68. Gas-separation performance of Module 23 over time. | 93 |
| Figure 69. Ends of Module 23 before and after testing at WRI, showing potting material changes: (a) end 1 before testing (b) end 2 before testing (c) end 1 after testing (d) end 2 after testing..... | 94 |

SCHEMES

| | |
|--|----|
| Scheme 1. Polyamic acid (pre-polymer) goes through a condensation reaction to yield polyimide polymers. | 33 |
| Scheme 2. Two 6-FDA polyimides that were utilized. | 35 |

TABLES

| | |
|---|----|
| Table 1. Membrane performance parameters..... | 13 |
| Table 2. Pure gas data at 30°C — Polyimide blends and Kapton®. | 18 |
| Table 3. Summary of results from ASPEN™ Plus systems model for mass and energy balances for coal-to-ammonia process using WGS–MR..... | 22 |
| Table 4. Model assumptions and results. | 24 |
| Table 5. Gas-stream composition..... | 24 |
| Table 6. Specific costs used to estimate capital costs (Kreutz, 2005)..... | 27 |
| Table 7. Component cost estimates..... | 28 |
| Table 8. Decrease in production cost of ammonia by utilizing WGS–MR..... | 30 |
| Table 9. General properties of commercially-available polyimides. | 32 |
| Table 10. Gas-separation properties of commercial polyimides..... | 32 |
| Table 11. Mixed-gas data collected beyond 200°C [dry gas]. | 34 |

| | |
|---|----|
| Table 12. Kinetic gas diameter and critical temperatures of selected gases. | 37 |
| Table 13. Pure-gas permeabilities of selected polyimides at 30°C (dry-gas data)..... | 38 |
| Table 14. Humidified mixed-gas data collected at 30°C. | 38 |
| Table 15. Dry and humidified mixed-gas permeation at 150°C for Matrimid 5218..... | 40 |
| Table 16. Energy of activation (E_p) for Matrimid 5218 under dry and humidified conditions in mixed-gas streams. | 40 |
| Table 17. Material screening samples for the syngas exposure test..... | 45 |
| Table 18. Trade-off table for Screening Intermediate Layer Processes. | 48 |
| Table 19. Performance of Tube 50 in preliminary gas testing at GE Global Research. | 59 |
| Table 20. Performance of Tube 50 in syngas and steam at WRI. | 59 |
| Table 21. Gas compositions. | 60 |
| Table 22. Summary of the membrane module testing parameters. | 69 |
| Table 23. Mechanical risks enumeration and ranking for shell and tube design module. | 73 |
| Table 24. Spin dope compositions identified for hollow fiber membrane creation (units in wt. %) | 76 |
| Table 25. Summary of bore fluid compositions (units in wt. %). | 76 |
| Table 26. TGA analysis: difference in percent weight loss at 250°C after 3 hours and 24 hours with and without humidity in a nitrogen gas stream. | 81 |
| Table 27. Curing Oven Parameters for Spin 4 – State 4 Hollow Fibers. | 84 |
| Table 28. IR samples of Polyimide Hollow Fiber and Flat Sheets. | 84 |
| Table 29. Potting Materials Ranked by Performance. | 88 |
| Table 30. Summary of Permeability Testing: Hollow Fiber Module 23. | 92 |
| Table 31. Summary of Permeability Testing: Hollow Fiber Module 25. | 92 |
| Table 32. Summary of Permeability Testing: Hollow Fiber Module 23. | 92 |
| Table 33. A list of the project’s patent activities. | 98 |
| Table 34. Membrane Performance Accomplishments. | 98 |

ACRONYMS

| | |
|---------|--|
| AMO | Advanced Manufacturing Office |
| ASU | air separation unit |
| CAPEX | capital expenditure |
| CCS | carbon capture and storage |
| CTE | coefficient of thermal expansion |
| DMAc | N,N-dimethylacetamide |
| DSC | differential scanning calorimetry |
| EPD | electrophoretic deposition |
| FTE | full time equivalent |
| FT-IR | Fourier transform-infrared |
| FWP | field work proposal |
| GEGR | General Electric Global Research |
| GPU | gas permeation unit |
| GWth | Gigawatt thermal |
| HCl | hydrochloric acid |
| HDPE | high-density polyethylene |
| HP | high-performance |
| HTS | high-temperature shift |
| IGCC | integrated gasification combined cycle |
| IR | infrared |
| INL | Idaho National Laboratory |
| LHV | Lower Heating Value |
| LTS | low-temperature shift |
| MAF | Moisture Ash Free |
| MDEA | methyldiethanolamine |
| MR | membrane reactor |
| NDA | Non-disclosure agreement |
| NETL | National Energy Technology Laboratory |
| NMP | N-methylpyrrolidone |
| NMR | Nuclear magnetic resonance |
| PBI | polybenzimidazole |
| PBI-TMS | poly(bis(trimethylsilylmethyl)polybenzimidazole) |
| PDMS | polydimethylsiloxane |
| PEG | poly(ethylene glycol) |
| PSA | pressure swing adsorption |
| PVA | poly(vinyl alcohol) |
| PVP | polyvinylpyrrolidone |
| RBI | Richard Blaine International |
| SEM | scanning electron microscopy |

| | |
|------|------------------------------------|
| TGA | thermogravimetric analyses |
| THF | tetrahydrofuran |
| TMA | thermomechanical analysis |
| TRL | Technology Readiness Level |
| VTEC | (polyimide, products of RBI, Inc.) |
| WRI | Western Research Institute |
| WGS | water-gas shift |

INTRODUCTION

Idaho National Laboratory (INL), in conjunction with GE Global Research (GEGR) and Western Research Institute (WRI), has developed hydrogen-selective membranes for water-gas-shift (WGS) membrane reactors that produce *high-pressure* hydrogen product streams. This alternate thermo-chemical approach to syngas processing improves the separation of H₂ from CO and CO₂, with significant energy savings through process intensification of the WGS reactor and downsizing of the CO₂ clean-up operation. To enable optimal system performance, membranes with high selectivity, permeance, and stability under WGS conditions were developed. To encourage widespread adoption, scalable manufacturing processes were considered during development to ensure favorable economics.

Our program—which is illustrated in Figure 1—addressed this technical challenge by combining the critical institutional knowledge and capabilities in the areas of polymer materials and processing (as provided by INL), inorganic materials processing and scalable coating technologies (as provided by GEGR), with expertise in the modeling and deployment of gasification systems (as provided by both GEGR and WRI). INL initially collaborated with GEGR to develop high-flux hydrogen-selective membranes incorporating novel polymer layers on a surface-engineered inorganic support. These membranes were tested under WGS conditions at a WRI gasification facility, with the intent to advance Technology Readiness Level (TRL) from TRL 2 to TRL 3. This goal was accomplished building upon INL and GEGR's earlier TRL 1 development level.

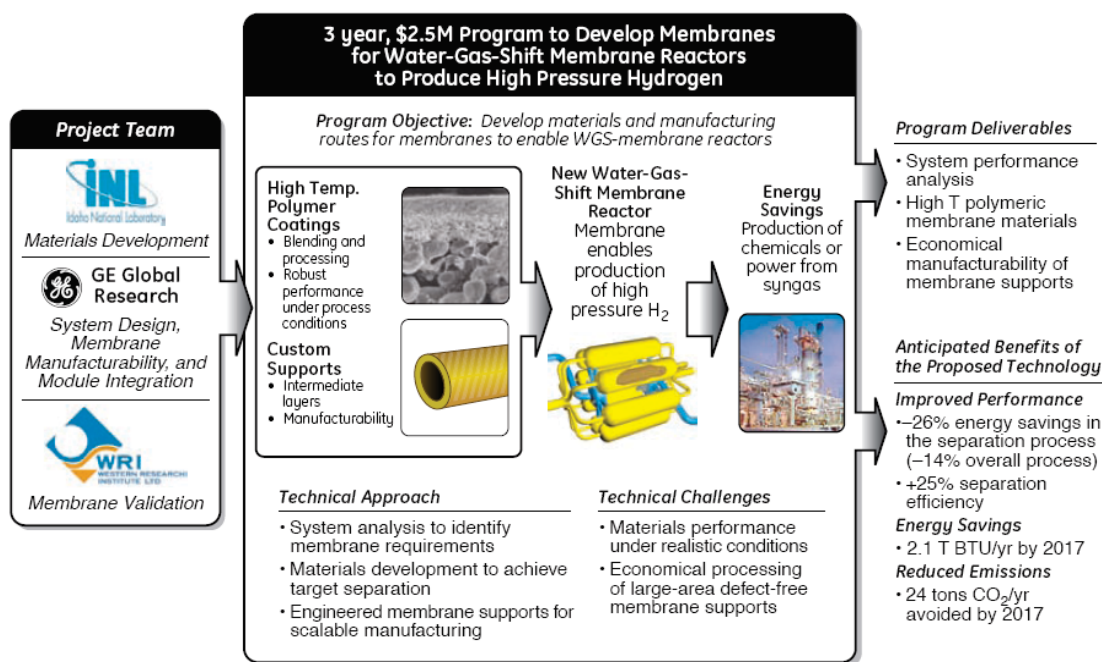


Figure 1. Overview of the program.

Operationally INL—located in Idaho Falls, Idaho—was the lead research organization for this project, and managed the activities of GEGR and WRI under contract. INL developed the new membrane materials, while GEGR created processes for the surface preparation of steel and/or ceramic membrane supports. INL collaborated with GEGR on the development of novel materials and processes for producing the supported polymeric membranes with the required selectivity and permeance. GEGR—with input from INL and WRI—designed, built, and tested the new membrane modules. WRI led the final performance and validation testing of the membrane modules on a stream of synthesis gas at WRI's demonstration facilities and ensured that all requirements for hydrogen separation were met throughout the development project phases.

This program developed hydrogen-selective membranes for an innovative gas-separation process based on WGS membrane reactor for syngas to hydrogen-gas stream production at high temperatures. For context, syngas is a gas mixture containing H_2 and CO produced from water steam reforming of methane, and other hydrocarbons or coal gasification. WGS technologies are used in a variety of industrial processes to drive additional H_2 production from the syngas CO component with additional steam. Integration of our membrane into the shift unit operation leads to process intensification with concomitant reductions in energy use and environmental emissions, as well as improvements in process economics and increased fuel flexibility. As contrast to other WGS membrane reactor (MR) concepts, our approach produces a hydrogen stream at high temperatures that can be directly used for the production of chemicals such as ammonia and methanol, combustion in CO_2 -free power generation, or production of high purity hydrogen gas.

Details concerning the research and development of polymer membranes, membrane modules, and membrane testing for hydrogen separations are divided into three sections:

1. Modeling performance of the membrane reactor and system
2. Development of hydrogen-selective polymer materials, which include polymer selection, membrane processing and gas permeability testing with humidity
3. Development of manufacturing processes for membrane modules, which include development and selection of porous supports and subsequent testing, development and testing of a prototype porous tube module in an actual WGS stream, and development and testing of a polymeric hollow fiber based upon the selected polymer.

The polymer membrane development was not straightforward for a WGS stream. New techniques were needed for gas-permeability testing of mixed gases at high temperatures. These testing protocols are new to the polymer membrane field because water vapor at high temperature was historically neglected during these measurements. Also, membrane-module development and testing was difficult due to the well known failures associated with high temperature seals. Thus novel high temperature designs were developed, tested, and incorporated into prototype modules.

This report includes successful membrane-module designs that fulfill the following requirements:

- (1) a selective layer with hydrogen permeance, high selectivity, and stability under WGS conditions; and
- (2) pathways towards developing economical manufacturing processes for large-scale production of the membranes via demonstration of successfully operating WGS prototype modules.

Background

This program is aligned with the Advanced Manufacturing Office's (AMO) goals of developing robust high-temperature membranes to enable efficient membrane separation systems that operate with real process streams and can seamlessly integrate with other industrial processes.

The WGS reaction is widely used in the chemical and petroleum industries to produce hydrogen from syngas streams. As seen in Figure 2, the shifted stream is then cleaned of by-product CO_2 . Conventional options for CO_2 removal use solvent-based absorption, leading to energy intensive methods that require cooling of the syngas stream to prevent solvent losses. In the final conditioning step, the temperature, pressure, and purity of the hydrogen product are adjusted to the specific requirements needed for end-use applications. Some applications, such as fuel cells and certain refinery applications, require ultra-high purity H_2 . Other applications, such as synthetic ammonia production or power generation, have less rigorous purity requirements, but need high pressure.

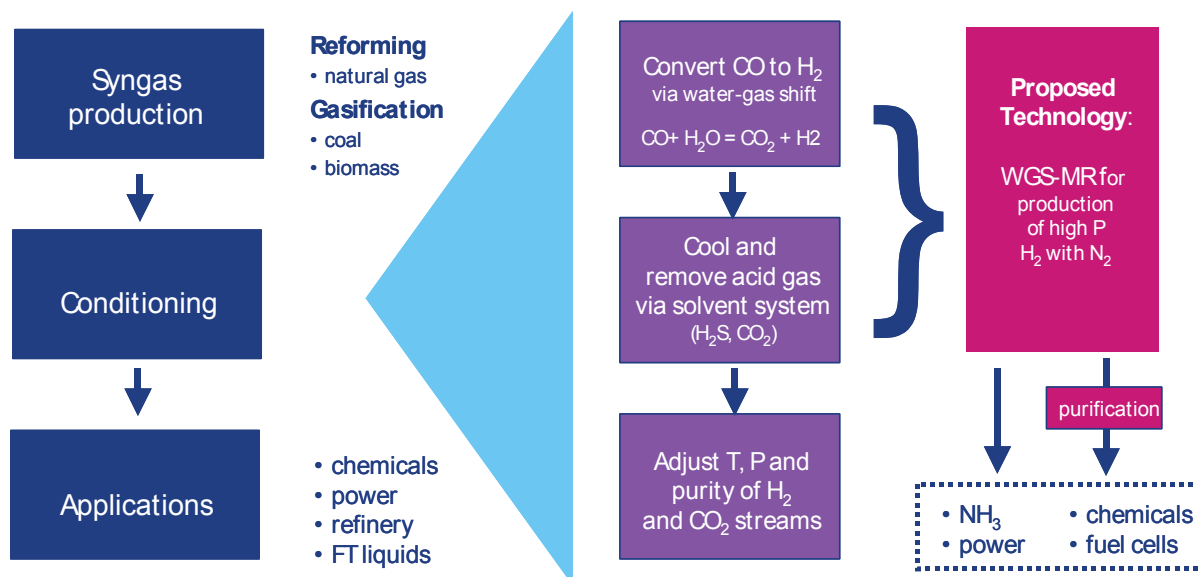


Figure 2. Syngas markets and technical opportunity. The WGS reaction and CO₂ removal are critical steps in the processing of syngas in the chemical petroleum and power generation industries.

High CO conversion in the shift reaction is achieved by adjusting reaction conditions to enhance output of products by using LeChatelier's principle. The introduction of excess steam enhances conversion, but exacts an energy penalty on the overall system performance. Steam-to-CO ratios of three to one and greater are used industrially (Criscuoli, 2001, An economic feasibility study for water gas shift membrane reactor). The slightly exothermic reaction is performed in a two-stage configuration involving a high and low temperature (T) stage. In the high T stage, the rapid kinetics lead to relatively small reactor sizes, but thermodynamics limits the equilibrium CO conversion to about 70%. Higher conversions are achieved by cooling the stream and using a second, low T shift. CO conversions above 90% are possible with this approach, but due to slower kinetics low T reactors tend to be physically larger than their higher T counterparts.

In our concept, shown in Figure 3, the WGS reactor and solvent-based CO₂ removal system are replaced by an integrated WGS-MR. To produce a high-pressure product stream, compressed nitrogen is used to sweep the core of the membrane tube. The purity and pressure of the H₂ stream can be adjusted by the nitrogen sweep rate. This configuration enhances CO oxidation through the continuous removal of H₂, improves energy efficiency by reducing the need for excess steam driving CO conversion, reduces the size and cost of the shift reactor, and leads to a downsizing of the downstream CO₂ removal operation. The high-pressure streams can be directly used for the production of ammonia, methanol, and fuel for CO₂-free power generation, or further purified to produce high purity hydrogen for fuel cells. The CO₂-rich retentate could be further purified for use in chemical manufacturing or compressed for sequestration.

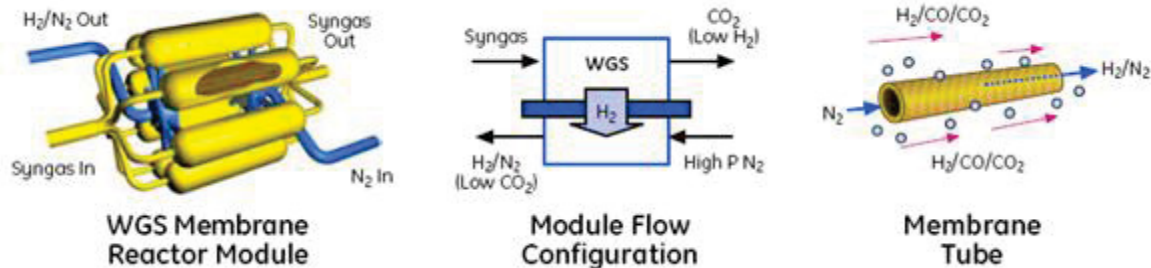


Figure 3. WGS-MR concept. A H_2 -selective membrane is located in the midst of the packed bed of the shift reactor catalyst, operating at temperatures between 250° and 350°C . H_2 permeates the membrane into the tubes, where a high pressure N_2 sweeps the gas to produce a high pressure H_2/N_2 gas stream. The H_2 -selective membrane allows continuous removal of the H_2 produced in the WGS reaction, allowing the equilibrium conversion of CO to CO_2 to proceed to near completion, while also separating the H_2 from the CO_2 .

The project's preliminary analysis indicated that this approach has the potential to reduce energy intensity by 26% relative to a WGS reactor with methyldiethanolamine (MDEA) CO_2 separation unit, as well as to improve the efficiency of the separation process by 25%. Applied to a chemical process such as ammonia synthesis, our analysis indicated that a 26% savings in the WGS/ CO_2 clean-up unit translates into a 14% overall energy savings. The custom Aspen™ model confirms reduced energy intensity in two ways. First, active removal of H_2 from the shift reactor drives the WGS equilibrium towards production of more H_2 and CO_2 for higher conversion efficiency. This reduced the need for excess steam leading to energy savings and reduced water use. Second, a substantial amount of the H_2/CO_2 separation is performed in the shift reactor thus decreasing the size of the CO_2 removal operation. A detailed explanation, using a more robust Aspen™ model, of the potential energy savings is provided in the *Potential Energy, Carbon, Economic, and Environmental Benefits* section.

Previous efforts to develop WGS MRs have been supported by DOE-EERE's hydrogen production and gasification programs, with the goal of producing *very high purity* H_2 (2010, Hydrogen from Coal Program: Research, Development and Demonstration Plan for the period 2007 to 2016.) The unique feature in our approach compared to other WGS-MR approaches is a pressure vs. purity balance. Conventional technologies exist for both compression and purification and the exact economics will depend upon the hydrogen requirements. Compression is expensive due to issues with materials, seals, and reliability. Purification using pressure swing adsorption (PSA) is an option, but the costs must be evaluated on a case-by-case basis. The option of either high pressure or purity hydrogen lends flexibility to the industrial base as well as allowing adjustments for optimizing energy use, thus minimizing costs.

By focusing on both materials and manufacturability, we address the key technical challenges associated with membrane development. The performance of the WGS-MR and the composition of the streams it produces are strongly sensitive to the membrane performance; in particular, the selectivity and permeance. The *selectivity* controls the extent that CO and CO_2 leak through the membrane into the H_2 product stream. The minimum selectivity is set by the amount of CO and CO_2 that can be tolerated by the downstream processes. The *permeance* describes the rate of H_2 transport through the membrane. The permeance controls the enhancement of CO conversion in the WGS reactor and the size of the reactor.

To address the demands of favorable transport characteristics and the mechanical requirements of the membrane, we use a supported membrane structure in which a thin, H_2 selective layer is supported on a thicker, more mechanically robust support. A critical enabler for this structure is an intermediate layer on the support that enables the formation of a thin selective layer. Presently, intermediate layers for inorganic

supports are produced by the consolidation of nanoparticles produced through dip-coating. This process requires strict environmental controls, leading to higher costs. Alternate methods of forming intermediate layers with controlled microstructures under favorable manufacturing economics would facilitate the adoption of inorganic membrane technologies. The following analysis provided a guide for development of the membranes.

Performance and Microstructural Targets

An analysis of the gas transport, mechanical, and economic constraints for the membrane was performed to determine microstructural and performance targets for an intermediate layer. The key membrane performance parameters, relevant physical constraints, and resulting (measurable) intermediate layer performance targets are listed in Table 1.

Table 1. Membrane performance parameters.

| Parameter | Physical Constraint | Target (measurable) |
|-------------|---|---|
| Selectivity | Overall membrane permeance and selectivity were controlled by polymer layer | Intermediate layer permeance >5,000 gas permeation unit (GPU) |
| | Bypass flow through pinhole defects contributes less than 1% of total flow | Ultrafiltration rate: <5% tracer pass-through; Intermediate layer selectivity ~ Knudsen |
| Permeance | Low surface roughness to allow coating of continuous 100 nm polymer layer | Intermediate layer RMS roughness <30 nm |
| | Intermediate layer pore size was smaller than solvated polymer coil size to avoid infiltration during coating | Intermediate layer pore size <30 nm |
| Stability | Chemical compatibility with syngas components at realistic operating temperatures and pressures | No reaction upon 100 h slipstream exposure |
| | No delamination or thermal stress-driven cracking of polymer layer due to coefficient of thermal expansion (CTE) mismatch | |
| Economics | Cost per unit H ₂ from the membrane system was less than baseline SMR technology | Cost of H ₂ (membrane) < Cost of H ₂ (baseline) |

Selectivity

A preliminary analysis of the WGS-MR system indicated that the membrane H₂/CO₂ selectivity (alpha) should be close to 10 to achieve meaningful benefits in energy efficiency. As explained later, laboratory mixed gas selectivities of the VTEC PI 80-051 polyimide material approach this target. However, in order to realize the full potential of the material, the composite membrane structure must be constructed so that the polymer layer controls the transport through the composite structure. Consequently, the permeance of the intermediate layer and support must exceed that of the polymer layer.

The numerical target for the intermediate layer permeance was derived from the assumption that the polymer layer has a permeability of approximately 50 barrer and a target thickness of 0.1 μm , resulting in an upper bound on the permeance of about 500 gas permeation units (GPUs). For the selectivity of a composite membrane to exceed 90% that of the polymer layer alone, the permeance of the intermediate layer and support should be greater than 5,000 GPU.

The intermediate layer must also be free of pinhole defects, which can allow flow to bypass the selective layer. For this project, defects were defined to be pores larger than about 50 nm, which was about half the target thickness of the polymer selective layer. In the limit where 1% of the total flow through the membrane passes through defects as non-selective viscous flow, the selectivity of the composite membrane selectivity will still approach about 90% of the polymer layer alone.

Permeance

Gas transport through a multilayer structure is controlled by the least permeable layer. In an ideal structure, the permeance of the polymer layer should be as high as possible, but still about an order of magnitude less than the permeance of the intermediate layer and support to ensure high selectivity. One simple way to increase the permeance of the polymer layer is to make the membrane as thin as possible. To accommodate an ultrathin polymer layer, the intermediate layer must have low surface roughness. In a liquid-based coating process, the surface roughness should be at most half the target thickness of the polymer coating. For a 100 nm thick polymer coating, this means the RMS roughness should be less than about 50 nm to limit the coating's imperfection. The pore size of the intermediate layer should be small enough to prevent infiltration of the polymer during coating. The numerical target will vary because the hydrodynamic size of the solvated polymer depends on the polymer chain length, the quality of the solvent, degree of aggregation, and presence of ternary components such as binders. As a starting point, a nominal pore size of about 30 nm, as determined by ultrafiltration experiments were used during intermediate layer development.

Stability

The chemistry and microstructure of the intermediate layer must exhibit chemical and mechanical stability of the membrane under realistic operating conditions. Syngas produced from the gasification of coal contains a number of components that may react with the polymer or intermediate layers, such as steam, H_2S , COS , HCl , HCN , various metals.

Economics

The overall economic constraint for the membrane is that the cost of hydrogen must be competitive with hydrogen produced from conventional technology. The overall economics will be strongly influenced by the permeance of the membrane, as that parameter sets the required area. High permeance membranes have allowable costs, due to the lower area requirement. Historically, inorganic supports have been favored over polymeric ones for higher temperature conditions, because of their ability to handle the extreme conditions. Conversely, the higher cost of inorganic membranes arises from the materials processing costs and lower surface area-to-volume form factors.

Figure 4 graphically summarizes the key aspects of our approach in developing high performance membranes that met or exceeded the above requirements in Table 1. INL and GEGR worked in parallel to improve the performance of the polymer coating and the manufacturability of the intermediate layer and support. INL identified some approaches in addition to the traditional materials chemistry methods for improving membrane permeance and selectivity. GEGR developed custom methods for the fabrication of intermediate layers on inorganic membrane supports to enable the coating of thin, uniform, defect-free films to enable improved membrane permeance without sacrificing selectivity via defects. In the second part of the program, GEGR and INL worked together to integrate the polymer onto the support to optimize the membrane performance and manufacturability at scale. The performance of the membranes was then tested at WRI's gasification facility.

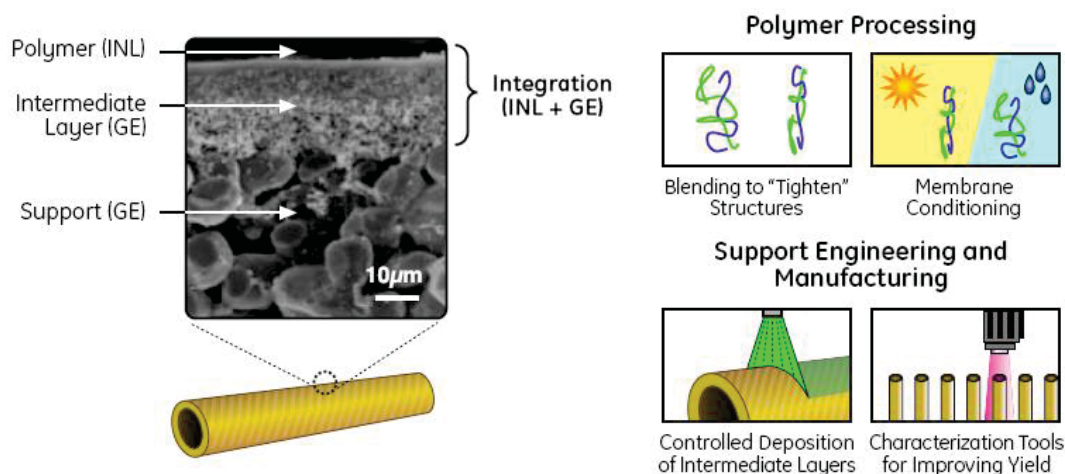


Figure 4. Technical approach to developing membrane materials and manufacturing processes. INL and GEGR applied innovative methods in polymer processes, support engineering, and manufacturing to develop high performance membranes.

Syngas is a starting point for a wide range of processes in the chemical, petroleum, and power generation industries. The WGS reaction is a critical step in the conditioning of syngas for its varied end uses. According to the National Energy Technology Laboratory's (NETL) Gasification World Database 2007, U.S. syngas production was 7.7 Gigawatts thermal (GW_{th}), which accounted for 14% of global capacity (2007, Gasification World Database: Current Industry Status: Robust Growth Forecast). Global capacity is expected to increase from 56 GW_{th} in 2007 to 73 GW_{th} by 2010, which corresponds to an annual growth rate of 9%. Figure 5 shows a breakdown of the world syngas market by segment (van der Drift, 2004, Bio-syngas: key intermediate for large scale production of green fuels and chemicals.). About three-fourths of the syngas is used for ammonia production and refineries, both of which require a WGS reaction to produce H_2 . An additional 4% is used in electricity generation. A WGS-MR capable of producing high-pressure hydrogen would be immediately useful in the ammonia and electricity generation segments, and could also penetrate other markets depending on the quality of H_2 required.

The specific markets that will be impacted are:

Ammonia production. Globally, ammonia (and fertilizer) production ranks as one of the major consumers of syngas, particularly from methane reforming. In 1998, U.S. ammonia production was 17.5M tons, ranking it 7th among chemicals by production (Syntex, Intro to Ammonia Manufacturing). However, high natural gas prices have led to a stagnating domestic market (note, this analysis was performed before the relatively recent drop in natural gas prices due to fracking technology). But, there is a strengthening trend towards gasification-fed ammonia production due to the possibility of using less expensive coal feedstocks, and the potential for CO_2 capture and sequestration. DOE-NETL, in its 2007 gasification roadmap, highlighted the successful retrofit of the Coffeyville facility, which now operates as an economically competitive coal-to-ammonia process (Syntex, Intro to Ammonia

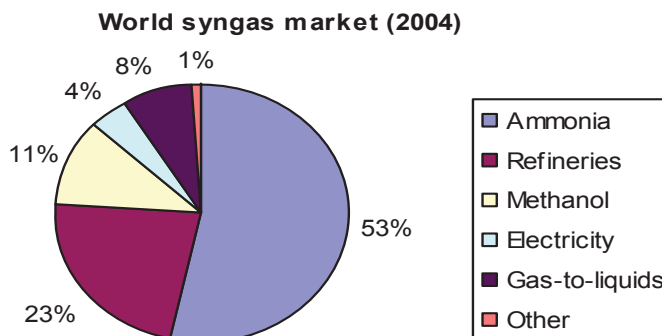


Figure 5. Syngas market segments.

Manufacturing). This suggests the possibility of stronger growth in the domestic coal-to-chemicals market that would increase the projected impact of our proposed WGS-MR technology, which could be applied as retrofits to existing plants using methane reforming, or in new builds using coal gasification and would offer energy savings in both situations.

Electricity. There is growing interest in integrated gasification combined cycle (IGCC) for the production of electricity, due to its potential for reduced emissions, including carbon capture with lower energy penalties. In capture-ready IGCC systems, high-pressure hydrogen is combusted and expanded in a turbine to produce electricity. A key step in the pre-combustion capture of CO₂ in IGCC is the use of the WGS reaction to transfer the chemical energy of CO into H₂. Although DOE did not project any new gasification plants in North America before 2020, the changing dynamics of the power generation market in 2007 were thought to possibly lead to a sizeable market for WGS-MR by 2017. However, by 2010, unanticipated market shifts in the energy markets due to abundant supplies of natural gas created a real shift away from use of syngas for virtually any application until the natural gas supply tightens up again.

Fundamentals of membrane transport

Permeability (P) of any particular gas through a membrane can be simply thought of as the product of its solubility (S) and diffusivity (D) terms, as shown in Equation (1).

$$P = D \times S \quad (1)$$

Robeson expressed the empirical relationship between D and S in a graphical format (permeability vs. selectivity) that created an “upper bound” in transport (Robeson, 1991, Correlation of Separation Factor Versus Permeability for Polymeric Membranes.). This “upper bound” is an empirical limitation in the degree to which both D and S can be enhanced. At some point, efforts to enhance one particular parameter cause a reduction in the other. This relationship is termed the trade-off in membrane performance. However, it should be noted that the trade-off, while commonly observed, is not absolute. And in fact, trade-offs can be non-linear in which a better membrane can be formed by a slight loss of one parameter that results in a large enhancement to the other.

Dense rubbery polymers, such as PDMS, are characterized by strong contributions to P from S in which a permeant gas must possess a high affinity for the membrane substrate to exhibit high fluxes (Freeman, 1999, Basis of Permeability/Selectivity Tradeoff Relations in Polymeric Gas Separation membranes.). This is not to say that D plays no role, only that S may be dominant. High free volume polymers represent an opposite relationship where D is the dominant term. In this circumstance, as a gas molecule is transported effectively when it is physically small enough to pass through intramolecular voids easily and with little interaction with the membrane material.

Diffusion, in an ideal case, can be thought of as laminar flow of a gas through membrane voids. In actuality, Knudsen diffusion more adequately describes diffusion in a high free volume ceramic or polymeric material. In Knudsen diffusion, penetrant permeability is dictated by the gas mean free path, or the distance it travels without collision with other gas atoms/molecules and the membrane substrate. The tortuosity of the membrane structure, the size of the penetrant gas, and the pressure differential across the membrane (driving force) also are important factors. Gases that exhibit high mean free paths within a membrane should exhibit relatively high permeabilities. Likewise, gases with lower mean free paths should have lower permeability. In a gas separation, it is helpful to have a size difference between the gases such that the smaller gas may pass preferentially, thus resulting in a large separation. In gases that are close in size, high free volume membranes, such as the poly(trimethylsilyl)propyne, with low tortuosity generally yield lower selectivity. Modifications of the membrane structure to reduce pore size or increase tortuosity would be expected to increase separation factors; however, some reduction in permeability is expected. Feed side pressure with respect to permeate side pressure is another factor that must be considered. Increases in pressure differentials (ΔP) across the membrane can force Knudsen flow into more laminar flows, which results in lower selectivity between similar-sized gases and negates the

effect that membrane modification may have on permeant transport. A more complete treatment of transport mechanisms can be found in the literature (Hwang, 1984, Membranes in Separations).

Flux through the membrane is also a function of the membrane thickness. The relationship between flux and membrane thickness is described by Equation (2).

$$J = [D S (\Delta P)]/l \quad (2)$$

In Equation (2), J is the flux of gas through the membrane, ΔP is the pressure differential across the membrane, and l is the membrane thickness. Flux and thickness have an inverse relationship in which thinner membranes yield high fluxes. However, in the case of membranes that operate by diffusion dominant mechanisms, loss of separation factor can occur, thus it is important to characterize the permeability, flux, and selectivity in terms of the membrane thickness.

Pure gas permeability determinations. Pure gas permeability determinations were made using a barometric technique. In this method, the membrane is mounted into a system with calibrated volumes upstream (feed side) and downstream (permeate side) of the membrane. In the experiment, both volumes are evacuated, and then the feed side is charged with the analyte gas at a known pressure, while the pressure is monitored on the permeate side. Initially, there is a lag in permeate side pressure increase as the gas permeates through the polymer. This time lag can be thought of as a function of the diffusivity of the polymer. Longer time lags correlate with a polymer that has a lower diffusivity. Likewise, short time lags suggest that the polymer is highly diffusive. Once a steady-state gas transport condition has been established, pressure increases in a nearly linear fashion, and from this linearity, the permeability can be calculated. An estimation of how a membrane can perform a separation is provided by a simple ratio of the pure gas permeabilities for any gas pair. This parameter is termed the “ideal separation factor.”

Mixed-gas permeability determinations. Determinations of permeability of gas mixtures are performed differently from those of the pure gas experiments. In a mixed-gas experiment, an analysis of the feed and permeate gases is required. This is accomplished by a sampling of the feed and permeant gases followed by separation and analysis by gas chromatography. A membrane cell is connected to a series of gas delivery and sampling tubing that allows for periodic analyses of the composition of both sides of the membrane. The system is then interfaced with an automated data collection system so that multiple data points may be taken and steady state transport measured. The entire system is housed in a temperature-controlled enclosure, which may be adjusted to perform measurements at higher-than-ambient temperatures. INL has two testing systems, one of which is limited to $\sim 90^\circ\text{C}$, and the other capable of temperatures as high as 400°C .

A New Approach: “Tightening Up” Polymer Structures

There are six ways to modify transport in polymers: (1) vary the types of polymers, (2) modify the chemical structure of the individual polymers, (3) thermally process the polymers, (4) expose the polymers to controlled environments, (5) control the polymer morphology, and (6) form interpenetrating networks and blends. Items 1, 2, and 3 are “traditional” approaches to controlling transport. The Team came into this project with an extensive experience in these approaches. However, this project focused upon using the less traditional approaches (4, 5, and 6) because recent work has shown these approaches to be more effective when attempting subtle separations.

Based upon these studies, several high performance polymers (polyimides, polyamides, and polybenzazoles) have been blended with the functionalized PBI. This technical approach has been used for many different blended polymer systems with success. Several polymer blends were created using a polyimide as the base polymer and blending it with poly[bis((trimethylsilyl)methyl)-benzimidazole] (PBI-TMS); poly(vinyl alcohol) (PVA); and poly(ethylene glycol) (PEG). In some cases, The Team was able to blend a large amount of secondary polymer, like 35 wt% of PEG into the parent VTEC (a polyimide precursor) without deleterious effects. This is significant as it shows the stability of the parent polyimide polymers even blended with known unstable polymers at high temperature ($> 250^\circ\text{C}$). Table 2 shows

some of the resulting polyimide blends along with Kapton[®]. Remarkably, 50 wt% PBI-TMS can be included in VTEC, and they exhibited the best gas transport properties when compared to the parent polymers. However, the VTEC-PEG blend showed a reduction in permeability for all of the gases tested—leading us to conclude that the overall structure of the polymer had “tightened up.”

The selected approach to the hydrogen separation membranes can use the same logic as given above. The basic polyimide structure may be tightened by forming interpenetrating networks and simple polymer blends (Klaehn, 2008, CO₂ Separation Using Thermally Optimized Membranes: A Comprehensive Project Report.).

Table 2. Pure gas data at 30°C — Polyimide blends and Kapton[®].

| Polymer | Permeability (barrers) ^a | | | | | | Selectivity α | | |
|----------------------------------|-------------------------------------|-------------------|----------------|----------------|-----------------|-----------------|----------------------------------|---------------------------------|--------------------------------|
| | H ₂ | Ar | N ₂ | O ₂ | CH ₄ | CO ₂ | CO ₂ /CH ₄ | H ₂ /CO ₂ | O ₂ /N ₂ |
| VTEC w/ ~50wt% PBI-TMS | 12.05 | 1.077 | 0.907 | 1.392 | 0.849 | 3.987 | 4.7 | 3.0 | 1.5 |
| VTEC w/ ~50wt% PBI-TMS | 6.655 | 0.156 | 0.064 | 0.442 | 0.026 | 1.896 | 72.9 | 3.5 | 6.9 |
| VTEC w/ ~35wt% PEG | 1.392 | 0.017 | 0.009 | 0.07 | 0.006 | 0.25 | 41.7 | 5.6 | 7.8 |
| VTEC w/ ~5 wt% PVA | 3.223 | 0.035 | 0.017 | 0.132 | 0.008 | 0.511 | 63.9 | 6.3 | 7.8 |
| Kapton [®] -HN (DuPont) | 1.56 | <i>Not tested</i> | 0.007 | 0.075 | 0.008 | 0.297 | 71.1 | 4.8 | 10.7 |

^a Barrers - (10⁻¹⁰)(cm³ (STP) x cm)/(cm² x sec x cmHg).

Preliminary targets for membrane performance were H₂/CO₂ selectivity of 10 to 100 and a permeance of 200 GPU. A simple mass balance calculation was used to estimate the minimum selectivity and permeance needed for a WGS membrane reactor (see Figure 6). Under typical operating conditions, the H₂/CO₂ selectivities of between 10 and 100 are required to recover about 80 to 90% of the H₂, while allowing 10% CO₂ slip into the permeate. This level of slip allows substantial downsizing of the CO₂ capture unit. With H₂/CO₂ selectivities of 100 to 1,000, the CO₂ slip is sufficiently low to eliminate the CO₂ recovery unit. The permeance targets are driven by the rate of removal of hydrogen and the membrane area needed to recover the H₂. The initial target for this project was set at the 2015 DOE H₂ production target of 300 scfh/ft² at ΔP_{H_2} = 20 psi or about 200 GPU (i.e., 1000 barrer at 5 μ m thickness, or 200 barrer at 1 μ m thickness) (DOE-EERE, 2007, Hydrogen, Fuel Cells, and Infrastructure Technologies Multi-Year RD&D Plan).

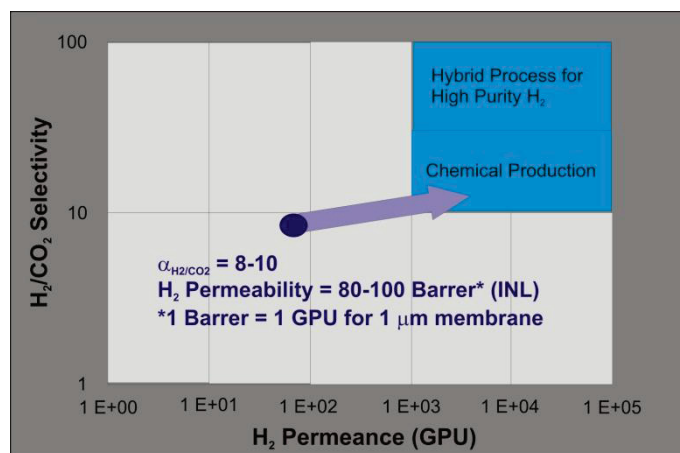


Figure 6. Materials targets for ammonia production.

Efforts to improve support manufacturability focused on engineering the microstructure of the intermediate layer and identifying scalable coating processes. GEGR leveraged its wide range of experience in the development of coatings for harsh environmental applications to define the specific microstructural properties (surface roughness, mechanical properties, and gas transport characteristics) needed to maximize the overall performance and stability of the membrane. Criteria for the selection process included a material's potential to produce microstructures that satisfy the targets and its potential to be economically scaled for manufacturing. Success in this part of the program has led to engineered substrates could reduce costs and improve yields in the manufacturing of supported metal or ceramic membranes. Details of these efforts are provided in the following three sections of the report.

SECTION 1 MODEL PERFORMANCE OF THE MEMBRANE REACTOR AND SYSTEM

Systems Modeling for Coal to Ammonia

System modeling was carried out on a water-gas-shift-membrane reactor (WGS–MR) designed for a coal-to-ammonia process. Modeling was carried out in multiple steps. First, an ASPEN™ Plus model was constructed for completing a mass and energy balance of the process and also to size the main equipment. A WGS–MR model was also built in ASPEN™ Custom Modeler for developing performance targets for the membrane reactor. The results from the two models were then used to develop an economic model that calculated the production cost of ammonia from coal and compared the conventional process (see Figure 7) to the improved process (see Figure 8).

In a conventional coal-to-ammonia system, a gasifier produces syngas by using oxygen from an air separation unit (ASU). After cleanup, the syngas (primarily H_2 and CO) goes through a two stage WGS (high-temperature shift [HTS] and low-temperature shift [LTS]) process to produce a gas that contains mainly H_2 and CO_2 . The product from the shift reactors goes to a CO_2 removal system. After CO_2 removal, the leftover gas (mainly H_2) goes to a methanator in which leftover carbon-containing gases are converted to methane. This carbon reduction is done because the ammonia synthesis catalyst is poisoned by CO and/or CO_2 . The hydrogen is then mixed with the N_2 from the ASU and, following compression, is sent for ammonia synthesis.

A process using a WGS–MR in the overall coal-to-ammonia process is illustrated in Figure 7 as a block-flow diagram. The syngas (primarily H_2 , CO, and steam) from the gasifier, following cleanup, is sent to the WGS–MR. The WGS–MR is essentially a porous tube with a highly robust membrane coated on the tube wall and with the catalyst packed inside. The feed gas is clean syngas and the sweep gas is N_2

from the ASU. A chemical reaction takes place inside the WGS–MR where $\text{CO} + \text{H}_2\text{O} \rightarrow \text{H}_2 + \text{CO}_2$. Hence, hydrogen is produced and CO is consumed. Also, the hydrogen-selective membrane is transferring H_2 from the feed gas to the sweep gas. The WGS reaction is an equilibrium-limited reaction, when product gas (H_2) removed the reaction is driven in the forward direction producing more hydrogen. Hence, by utilizing a WGS–MR, higher conversion for CO can be achieved, and also lower $\text{H}_2\text{O}/\text{CO}$ ratio may be required; hence, less steam is used. The H_2 mixed with N_2 in the sweep gas, then goes to a CO_2 removal system by which the CO_2 is removed (some CO_2 goes to the permeate side from the membrane, which is removed by the MDEA system). The clean N_2 and H_2 is then compressed and sent for ammonia synthesis.

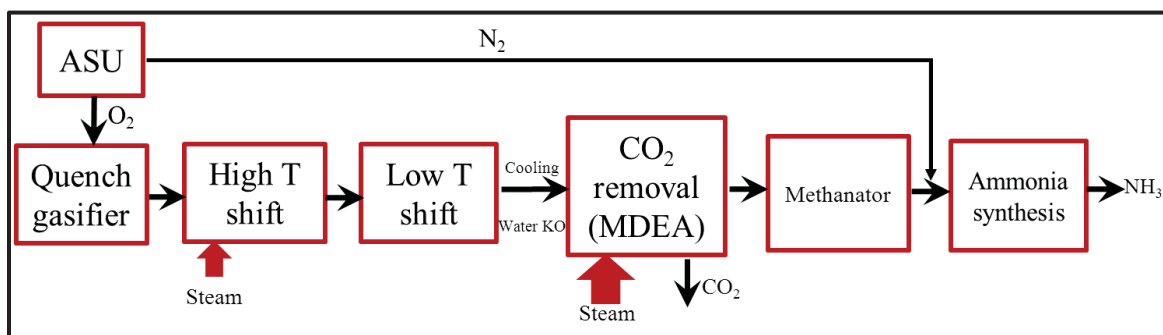


Figure 7. Conventional systems diagram for ammonia production from coal.

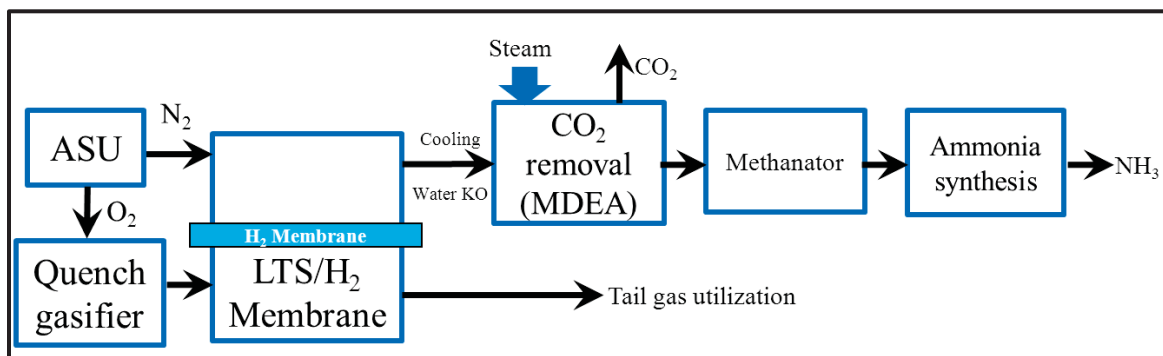


Figure 8. Systems diagram using WGS–MR for ammonia production from coal.

Conventionally, WGS is carried out in two stages: an HTS and an LTS. The high temperature is used to produce a higher reaction rate, but it suffers from poor conversion (equilibrium is favored at lower temperatures). The LTS is then used in the second stage to produce a better conversion (a lower reaction rate). The improved method, Figure 9, eliminates the need for the HTS component within the process.

Systems Model in ASPEN™ Plus for Overall Sizing

A model was constructed in ASPEN™ Plus for a base case for benchmarking the membrane case models. The base case model was developed using descriptions from (Heaven, 2004, Synthesis Gas Purification in Gasification to Ammonia/Urea Complex). Another model was constructed with the modifications, as shown in the block-flow diagram in Figure 8, to adjust the system to utilize a WGS–MR. Mass and energy balances were carried out for a plant producing 2000 TPD of ammonia. An example of the ASPEN™ Plus model is shown in Figure 9. A summary of the results is provided in Table 3.

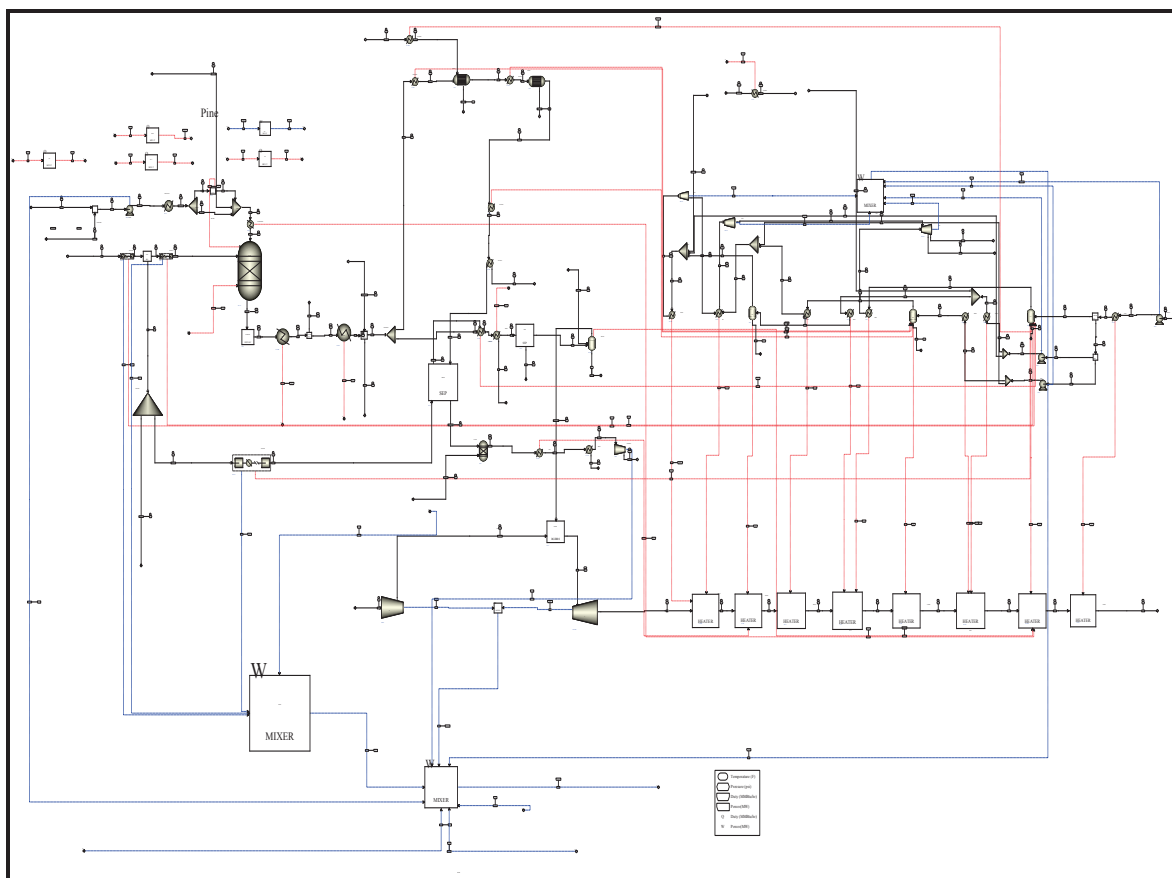


Figure 9. An example of ASPEN™ Plus model utilizing a WGS–MR in a coal-to-ammonia plant.

Table 3. Summary of results from ASPEN™ Plus systems model for mass and energy balances for coal-to-ammonia process using WGS–MR.

| | | | Case 1a | Case 6a | Case 7a |
|---|-------------------------------------|----------|---------|------------|------------|
| | | | Base | Membrane 1 | Membrane 2 |
| Coal | TPD | | 2722 | 2722 | 2722 |
| Gasifier | | | | | |
| | H ₂ | lbmol/hr | 8355 | 8355 | 8355 |
| | CO | lbmol/hr | 10450 | 10450 | 10450 |
| Conversion | | | | | |
| | H ₂ /Coal | ton/ton | 0.067 | 0.067 | 0.067 |
| | CO/Coal | ton/ton | 1.170 | 1.170 | 1.170 |
| WGS | WGS Ratio | | 2.700 | | 1.700 |
| | H _{out} /H _{in} | | 2.192 | 2.192 | 2.192 |
| | | | | | |
| | CO Conversion | | 95.299 | 95.309 | 95.309 |
| Hydrogen through membrane | | | - | 0.970 | 0.900 |
| CO ₂ through membrane | | | - | 0.360 | 0.200 |
| Hydrogen/ton of coal in ammonia synthesis | | | 0.128 | 0.128 | 0.128 |
| | | | | | |
| Ammonia Synthesis | N ₂ /(H ₂ /3) | | 1.047 | 1.011 | 1.066 |
| | | | | | |
| | Ammonia Conversion | | 0.996 | 0.996 | 0.996 |
| Ammonia yield per ton of coal | | ton/ton | 0.726 | 0.775 | 0.722 |

Custom Modeler

The integrated WGS–MR model consists of three key modules: the WGS kinetic module, which describes the WGS reaction kinetics and heat generation; the Counter Current Membrane module, which describes the mass transfer of gas species across membrane in the presence of feed gas and sweep gas; and the Integrator module, which connects the kinetic model and the membrane model and conducts an integrated mass and energy calculation at each point along the membrane reactor.

Methodology

The WGS membrane reactor was developed using ASPEN™ Custom Modeler software. This software provides a unique platform for countercurrent-membrane reactor modeling as well as easy implementation of the WGS kinetics and heat and mass transfer.

Water Gas Shift Kinetics

The WGS is an important reaction that converts CO and H₂O into H₂ and CO₂.



WGS is exothermic and is often carried out in two modes: an HTS and an LTS. WGS kinetics are fairly fast in the HTS zone, where the exothermic heat of the reaction quickly raises the reactor temperature to above 450°C. At this temperature, however, the WGS reaction quickly reaches equilibrium, and the reaction is swiftly stopped. At this point, typically only 75% of the CO has been converted. The gas phase will then have to be cooled down to about 200°C in a heat exchanger before the WGS reaction resumes in the LTS zone, where the kinetics are slower, with a mild temperature rise.

At the end of the two-stage WGS reactor, the majority of the remaining 25% of the CO is converted into H₂ and CO₂ with overall CO conversion of above 95%.

WGS kinetics are fairly well known, and an iron-based catalyst is assumed for the kinetic model in this study. Figure 10 illustrates the typical composition profiles in the HTS and LTS reactors.

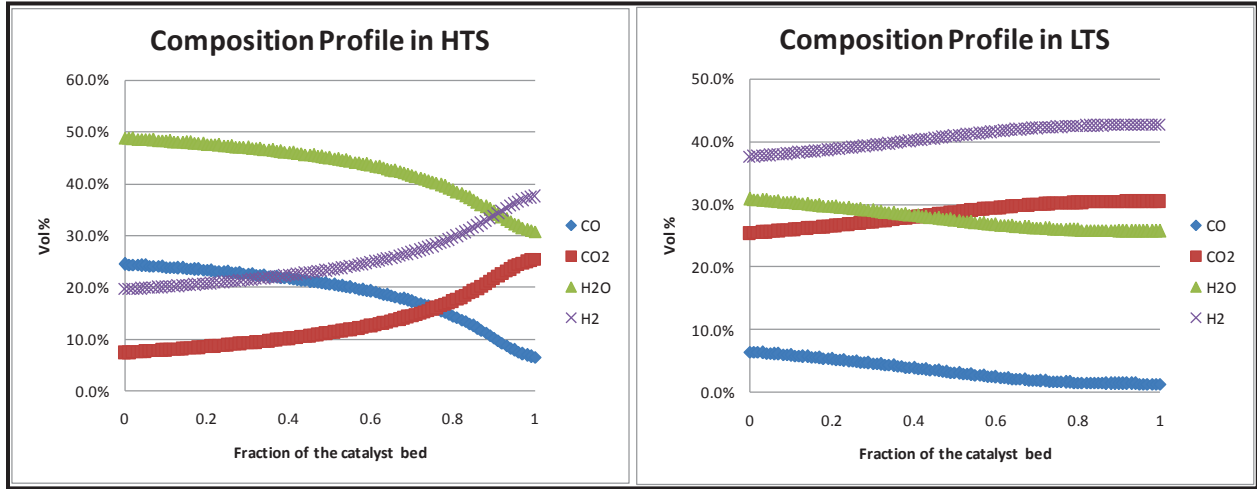


Figure 10. A typical profile of gas composition through HTS (left) and LTS (right).

Counter Current Membrane Model

The mass balance of a counter-current membrane can be modeled as following:

Feed side:

$$dn_i/dz = 1/4\pi d^2 r_i - \pi d J_i$$

Sweep side:

$$dn_i/dz = -\pi d J_i$$

where n_i is the molar flow rate of species i , z is the axial direction, d is the ceramic-tube internal diameter, r_i is the volumetric reaction rate of species i , and J_i is the permeation flux of species i across the membrane surface area. The permeation flux can be expressed as:

$$J_i = B_i \cdot \Delta(P_i) / \Theta$$

where B_i is the permeability of component i , P_i is the partial pressure difference of the component across the ceramic membrane, and Θ is the thickness of the membrane functional layer.

Model Capabilities

Specifically, the model takes into account the key material and process drivers—such as membrane selectivity and permeability, functional-layer thickness, cross membrane pressure differential, WGS reaction kinetics, feed- and sweep-gas concentrations and flow rates, etc.—and predicts the hydrogen separation efficiency, including hydrogen recovery rate, CO_2 , CO and H_2S slips, and final-product gas compositions.

Model Results

Table 4 shows the modeling calculation assumptions and results. This preliminary analysis suggests that—in order to achieve >90% H_2 recovery in the membrane reactor, >90% CO conversion in WGS reaction, and <10% CO_2 slip—the membrane must achieve (H_2/CO_2) selectivity of about 80, and a permeance of 1,000 GPU. Other key driving forces for gas-separation efficiency include pressure differential across membrane, membrane functional-layer thickness, etc. Table 5 gives the gas-stream compositions.

Table 4. Model assumptions and results.

| | Value | Units |
|-----------------------------------|-------|--------|
| Reactor Design | | |
| Number of membrane bundles | 8 | |
| Membrane tube length | 2 | m |
| Membrane tube ID | 1 | cm |
| Number of tubes per bundle | 5283 | |
| Membrane Property | | |
| Permeability | 1000 | GPU |
| Selectivity | 80 | |
| Functional layer thickness | 1 | micron |
| Pressure differential | 25 | Bar |
| Results | | |
| H ₂ recovery | 93.3% | |
| CO ₂ slip | 6.9% | |
| CO conversion | 95.5% | |
| Feed side H ₂ vol% dry | 8.6% | |
| Feed side H ₂ vol% wet | 7.2% | |
| Feed side linear velocity | 0.32 | m/s |
| Feed side residence time | 6.19 | s |

Table 5. Gas-stream composition.

| | Feed In | Feed Out | Sweep In | Sweep Out |
|--------------------------|---------|----------|----------|-----------|
| Flow Rate (kmol/hr) | 4000 | 1942.61 | 650 | 2707.39 |
| P (Bar) | 32 | 32 | 7 | 7 |
| T (°C) | 280 | 394.575 | 200 | 422.603 |
| Composition (Vol%) | | | | |
| Vol%("CO") | 30.0% | 2.8% | 0.0% | 0.6% |
| Vol%("CO ₂ ") | 9.0% | 72.0% | 0.0% | 3.4% |
| Vol%("H ₂ ") | 24.0% | 7.2% | 0.0% | 72.0% |
| Vol%("H ₂ O") | 36.0% | 16.0% | 0.0% | 0.0% |
| Vol%("N ₂ ") | 1.0% | 2.1% | 100.0% | 24.0% |

Integrated Model and Results

The integrated WGS-membrane model accounts for mass balance on both the permeate and retentate side of the membrane, heat transfer across the membrane walls, detailed WGS kinetic reaction rate, reaction conversion, adiabatic heat release during the reaction, membrane geometry, membrane area needed, etc. The membrane reactor model was validated against similar reactor models [Huang, 2005]. A conceptual drawing of the WGS-MR and its composition of gases are shown in Figures 11 and 12, respectively.

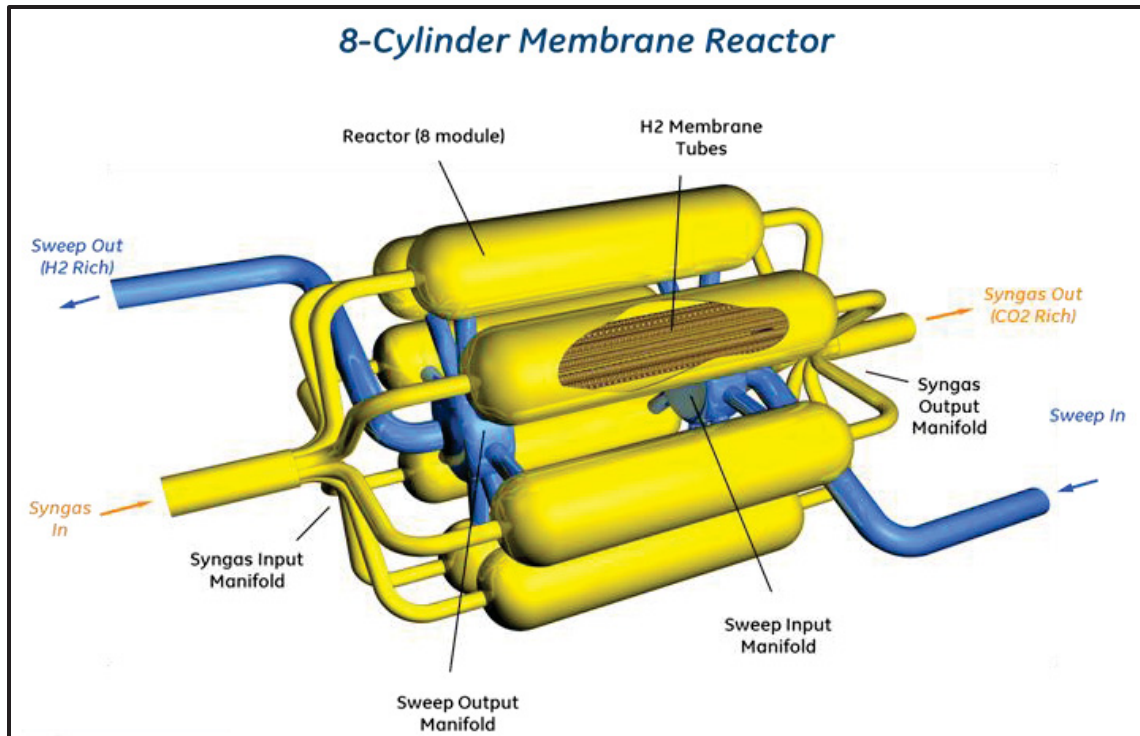


Figure 11. A WGS–MR conceptual design.

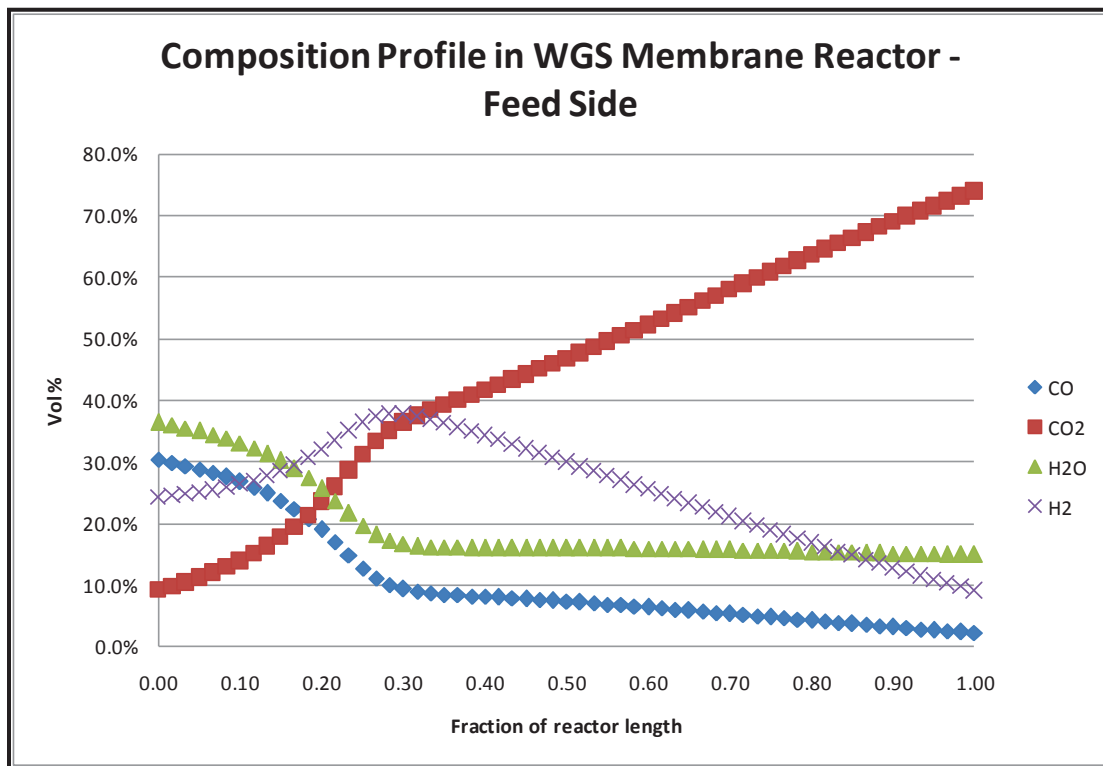


Figure 12. Composition of gases through a WGS–MR.

An integrated WGS–MR model was completed and used to conduct first-order estimation of process mass and energy balance, hydrogen-separation efficiency, and membrane material-property evaluation. Figure 13 provides a picture of the model in ASPEN™ Custom Modeler.

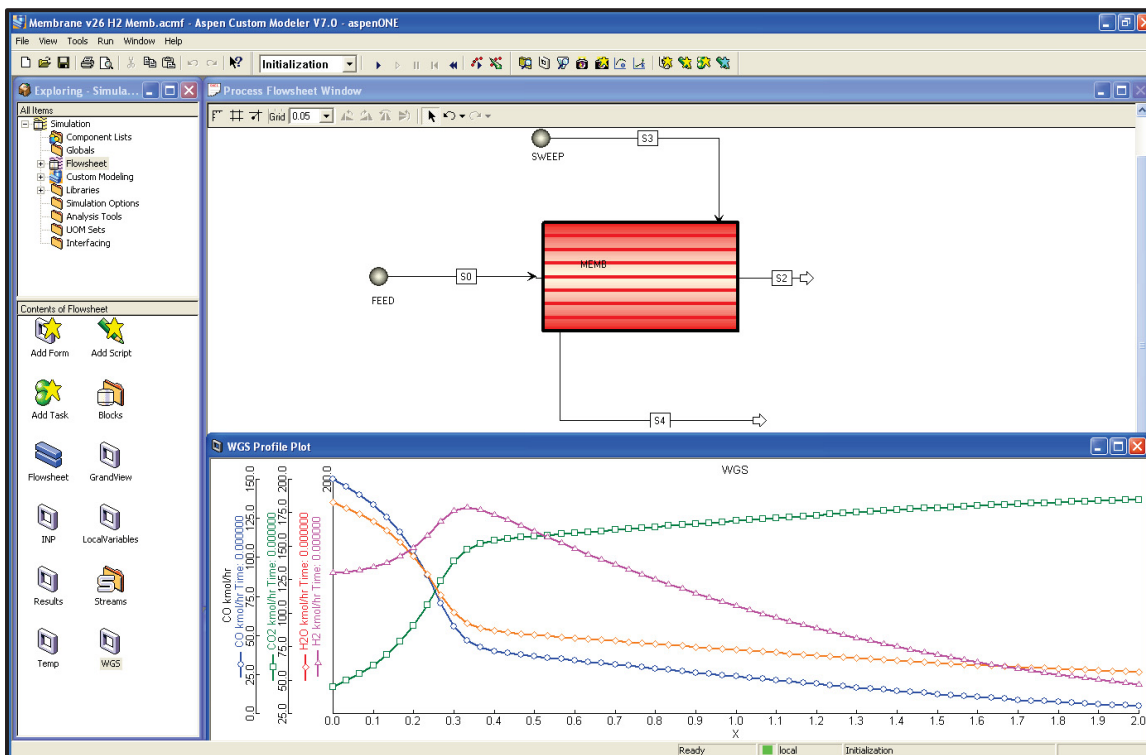


Figure 13. Example of modeling the WGS–MR in ASPEN™ Custom Modeler.

The first objective of the reactor model was to provide a mechanism that links the macro-level process performance, such as separation efficiency, with the micro-level material property, such as selectivity and permeability. This enables the back-calculation of membrane performance targets that would satisfy the overall system efficiency and economics requirements.

Sizing and Cost Analysis

Capital and operating costs were estimated in order to calculate a cost for ammonia.

Plant equipment for all cases was sized to produce 2,000 MTD of ammonia according to the layout of (Heaven, 2004, Synthesis Gas Purification in Gasification to Ammonia/Urea Complex) to generate enough electricity to exactly match the electrical requirements for the ammonia-production process.

Equipment-cost estimates were scaled according to their size per (Kreutz, 2005, Co-production of hydrogen, electricity, and CO₂ from coal with commercially ready technology. Part B: Economic analysis) as shown in Table 6. The specific costs are indexed to 1st quarter 2010 with the Chemical Engineering's Plant Cost Index.

Table 6. Specific costs used to estimate capital costs (Kreutz, 2005).

| Plant Component | Scaling Parameter | CO (M\$) | So | Specific Cost | f |
|---|---|----------|------------------------|---------------------------|------|
| Air separation unit (O ₂ at 1.05 bar) | Pure O ₂ produced | 56.79 | 1839 tonne/day | 30.88 \$/kg/day | 0.5 |
| O ₂ compression (from 1.05 bar) | Compression power | 8.82 | 10 MWe | 881.52 \$/kWe | 0.67 |
| N ₂ compressor (NH ₃ process) | Compression power | 6.61 | 10 MWe | 661.14 \$/kWe | 0.67 |
| N ₂ compressor (Sweep + GT) | Compression power | 6.61 | 10 MWe | 661.14 \$/kWe | 0.67 |
| H ₂ compression (from 1.05 bar) | Compression power | 7.43 | 10 MWe | 881.52 \$/kWe | 0.67 |
| Coal storage, prep, handling | Raw coal feed | 39.87 | 2367 tonne/day | 16.84 \$/kg/day | 0.67 |
| Gasifier + quench cooling/scrub | Moisture Ash Free (MAF) coal input Lower Heating Value (LHV) | 86.86 | 680 MWth | 127.74 \$/kWth | 0.67 |
| Gasifier + syngas cooler & scrub | MAF coal input (LHV) | 202.52 | 697 MWth | 290.56 \$kWth | 0.67 |
| WGS reactors, heat exchangers | MAF coal input (LHV) | 56.05 | 1377 MWth | 40.71 \$/kWth | 0.67 |
| Selexol H ₂ S removal & stripping | Sulfur input | 47.41 | 81 tonne/day | 585.34 \$/kg/day | 0.67 |
| Sulfur recover (Claus, SCOT) | Sulfur input | 32.18 | 81 tonne/day | 397.24 \$/kg/day | 0.67 |
| Selexol CO ₂ absorption, stripping | Pure CO ₂ captured | 45.90 | 327 tonne/hr | 140.37 \$/kg/hr | 0.67 |
| CO ₂ drying and compression | Compression power | 20.46 | 13 MWe | 1573.54 \$/kWe | 0.67 |
| Pressure swing absorption | Pure gas flow | 9.90 | .294 k mole/s | 33.69 M\$/kmole/s | 0.74 |
| PSA purge gas compressor | Compression power | 8.82 | 10 MWe | 881.52 \$/kWe | 0.67 |
| Methanation | Methane generated | 34.14 | 2.69 kg/sec | 3525.17 \$/kg/hr | 0.67 |
| Ammonia synthesis | Ammonia product | 13.14 | 2.1 kg/sec | 1738.37 \$/kg/hr | 0.67 |
| H ₂ Ultra Membrane | Surface Area | 150.00 | 50,000 m ² | 3000.00 \$/m ² | 1 |
| Syngas expander | Expander power | 4.41 | 10 MWe | 440.76 \$/kWe | 0.67 |
| Siemens V64.3A gas turbine | Gas turbine power | 42.89 | 67 MWe | 640.08 \$/kWe | 1 |
| Siemens V94.3A gas turbine | Gas turbine power | 102.31 | 266 MWe | 384.61 \$/kWe | 1 |
| Gas Turbine | Gasturbine power | 116.61 | 276 MWe | 422.51 \$/kWe | 0.67 |
| Heat recovery steam generator | HX surface area | 96.014 | 225,000 m ² | 426.72 \$/m ² | 0.67 |
| Steam cycle (ST+condenser) | ST gross power | 83.04 | 136 MWe | 610.61 \$/kW | 0.67 |

The specific costs were then used to calculate the total equipment-component costs for the two cases considered here, as shown in Table 7. It can be seen that the cost (size) of the coal-handling equipment was reduced for the membrane case due to the improved efficiency. The cost of the methanation equipment was reduced by ~73%. Costs for a membrane reactor was estimated at 3000/m².

Table 7. Component cost estimates.

| Case No. | 1 | 6 |
|---|-------------------------|----------|
| Case Descriptions | Baseline No Membrane | Membrane |
| CO ₂ Venting vs. Capture | C | C |
| Cost of plant components (M\$) | | |
| Coal storage, prep, handling | 53.7 | 50.3 |
| Air separation unit (O ₂ at 1.05 bar) | 71.8 | 68.4 |
| O ₂ compression (from 1.05 bar) | 12.0 | 11.3 |
| N ₂ compressor (NH ₃ process) | 8.2 | 0.0 |
| N ₂ compressor (Sweep + GT) | 0.0 | 6.4 |
| H ₂ compression (from 1.05 bar) | 12.2 | 14.2 |
| Gasifier, syngas cooling, scrubbing | 111.8 | 104.7 |
| WGS reactors, heat exchangers | 45.0 | 42.1 |
| Selexol H ₂ S removal & stripping | 5736 | 53.9 |
| Sulfur recovery (Claus, SCOT) | 39.1 | 36.6 |
| Selexol CO ₂ absorption, stripping | 39.2 | 18.9 |
| CO ₂ drying and compression | 563.4 | 44.5 |
| Pressure swing absorption | 0.8 | 0.0 |
| PSA pure gas compressor | 0.0 | 0.0 |
| Methanation | 20.6 | 5.6 |
| Ammonia synthesis | 82.5 | 82.5 |
| H ₂ Membrane | | 4.1 |
| Gas turbine | 51.8 | 44.1 |
| Heat recovery steam generator | 38.8 | 33.1 |
| Steam cycle (turbine + condenser) | 48.9 | 47.7 |
| Total overnight cost (M\$) | 747.4 | 668.4 |

Summary

The H₂ membrane-based WGS–MR model in this project provided a detailed account of the mass and energy balance for the hydrogen-separation process in this reactor. As more experimental data on membrane performance became available, the integrated model was updated to improve reactor sizing and separation-performance projections. At the same time, the integrated model can be used to explore trade-offs between various membrane-performance parameters, such as selectivity, permeability, pressure drop, etc. Such a trade-off provides important information about future research directions while setting material development targets.

The benefits of coal-based synthesis-gas WGS–MRs are related to driving the equilibrium reaction in the forward direction to get higher CO conversion at medium temperatures (280–420°C) and lower H₂O/CO (1–4.5) ratios resulting from active, continuous H₂ membrane removal. For this process, N₂ sweep was used. Specifically, when the WGS–MR is used for coal-to-ammonia process, a number of benefits are seen: (1) a smaller methanator, (2) a smaller CO₂ separator, and (3) an integrated system/improved efficiency. These benefits translate to a lower capital expenditure (CAPEX), as shown

in Figure 14, and lower ammonia-production cost as shown in Table 8. Figure 14 shows CAPEX being reduced from \$747M to \$668M for a 2000 TPD ammonia plant. The price of coal used for the study was assumed to be 24\$/ton. The production-cost decreases from ~320\$/ton to ~290\$/ton. We recognize that these results were obtained when the price of natural gas was relatively high, in 2010 the price of natural gas dropped dramatically due to discovery and extensive use of fracking methodologies. As a result we recommend future work utilizing the developed ASPEN™ process model to examine cost savings and added value manufacturing options under newer energy costs reality.

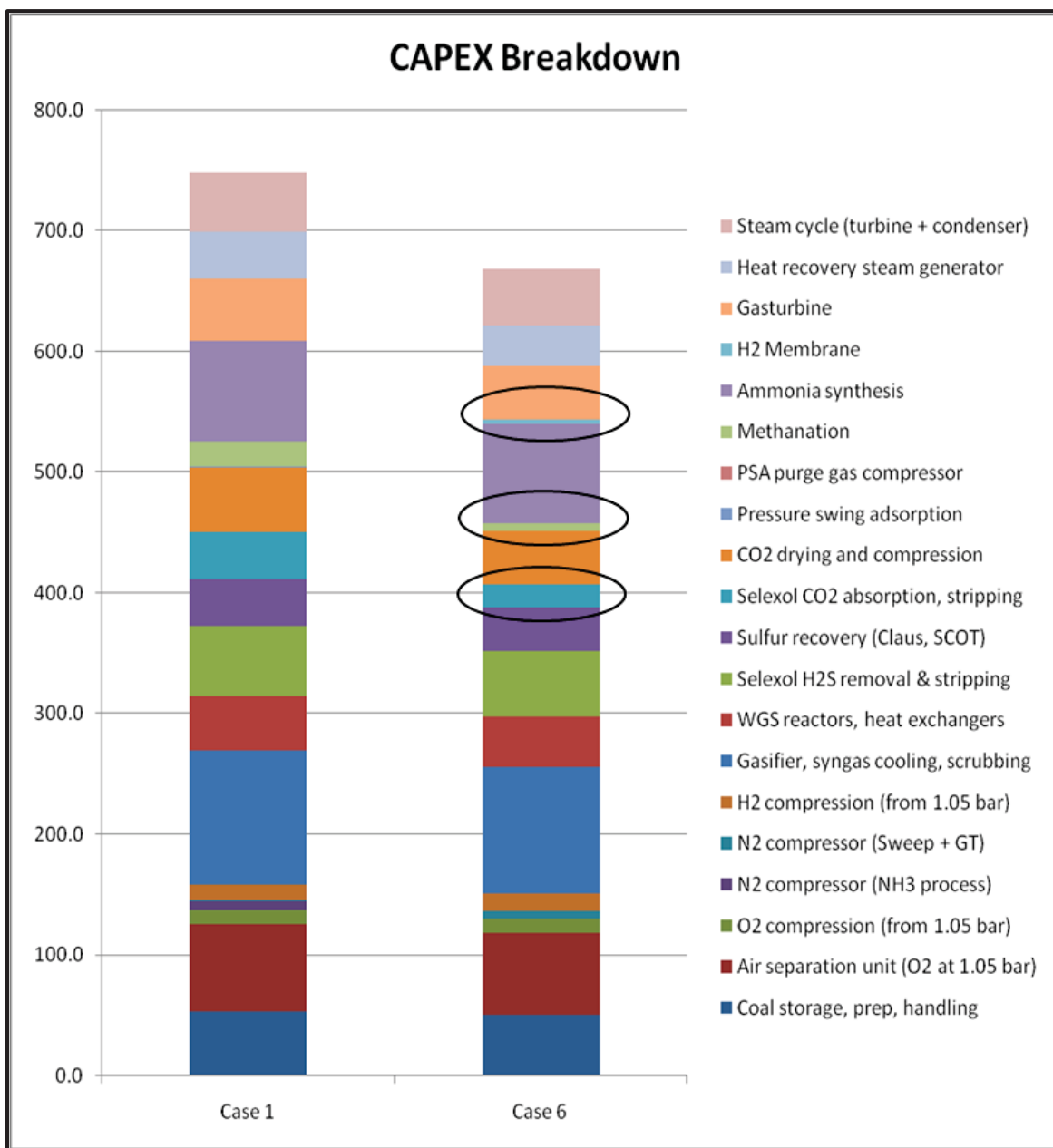


Figure 14. CAPEX breakdown of the conventional system vs. a system utilizing WGS–MR for coal-to-ammonia process.

Table 8. Decrease in production cost of ammonia by utilizing WGS–MR.

| Case# | Case 1 | Case 6 |
|---|--|-------------------------------------|
| Case Descriptions | Baseline no membrane generate electricity | membrane generate electricity |
| CO ₂ Venting vs. Capture | C | C |
| Total overnight cost (M\$) | 747.4 | 668.4 |
| Construction interest (12.30% of OC) | 91.9 | 82.2 |
| Total plant investment (M\$) | 839.3 | 750.7 |
| Specific overnight cost (k\$/tonne/day) | 374 | 334 |
| NH ₃ cost components (\$/tonne) | | |
| Capital (15% of TCR) | 215.59 | 192.80 |
| O&M (4% of OC per year) | 51.19 | 45.78 |
| Electricity @ \$.077/kWh | | |
| Fuel (at 1.26 \$/GJ, LHV) | 52.88 | 47.96 |
| Total CoNH ₃ (\$/tonne) | 319.66 | 286.55 |
| Cost of NH ₃ +- % (compared to Case 1) | | -10.4% |
| Capex increase %(compared to Case 1) | | -11% |

SECTION 2

DEVELOPMENT OF HYDROGEN-SELECTIVE POLYMER MATERIALS

High Performance Polymers

Polymer membranes are known to be economical and effective gas separators; however, for the described high-temperature applications, more durable polymers are necessary. Under high temperature environments, a special class of glassy polymers, called high performance (HP) polymers is used. For example, several known HP polymer families have good thermal resistance, like polybenzazoles (polybenzimidazole [PBI]), polyamides (Nylon[®], Nomex[®]), and polyimides (Kapton[®], VTEC PI series). Most of these polymers are known to have high thermal stabilities, while some have operating temperatures up to 400°C. These high-temperature stabilities allow their use in applications with which other organic polymers are incompatible. Additionally, many HP polymers are chemically resistant to organic solvents. Many of them are known to be mechanically robust, with high compressive strength. Therefore, the temperature stability and robust nature of these HP polymers make them ideal candidates for the described high-temperature hydrogen separations.

High gas-pair selectivity is an interesting characteristic of HP polymers. The high selectivity is due to the combination of size-based and solubility-based molecular separation and a “dual-mode” mechanism not shared by size-driven inorganic membrane separators. This dual-mode mechanism is derived from the basic relationship of gas-transport properties: permeability (P), solubility (S), and diffusivity (D) ($P = D \cdot S$) (Bernando, et. Al., 2009; Brunetti, et. Al., 2010; Powell, 2006; Ayala, et. Al., 2003; Hirayama, et. Al., 1996; Koros, 1993). Permeability (P) is the resulting product for overall gas transport. HP polymers have inherently high glass transitions (T_g) that limit the interactions of the gases with the polymer matrix; however, solubility can still have an effect. Gas-separation research using HP-polymer membranes has focused mainly on optimizing materials at near-ambient conditions. Thus, the development of high-temperature polymeric membranes for gas separations has significance for economic and environmental contributions.

Although glassy polymers are known to give effective gas separations, their gas permeabilities show low gas fluxes at ambient temperatures. These permeability issues can be overcome by increased temperatures. However, as a rule, when gas permeabilities increase, the gas-pair separation factors (selectivities) decrease. Robeson (1991, 1999, 2008) compiled an extensive list of gas-separation properties for polymeric membranes presented in the literature. The Robeson Upper Bound is an empirical limit that all glassy and rubbery polymers show with the permeability/selectivity tradeoff. Here, polyimide membranes tend to have separation properties close to the designated upper bound lines, which are shown in Figure 15. This permeability/selectivity tradeoff in Robeson's selectivity/permeability correlation plot was acquired near ambient temperatures for most of these data sets. Temperature is not typically shown in this tradeoff; nevertheless, it should be noted when comparing gas permeability/selectivity data using the Robeson's plot. Reports of high-temperature gas separations using HP polymers are found in the literature using binary gas mixtures at 100°C (Fink, 2008, Polyimides: in *Plastics Design Library. High Performance Polymers.*). These data show that glassy polymers can provide good gas separations, even at temperatures beyond ambient. During the past decade, interest in high-temperature gas separations (such as H₂) has provided new opportunities for application of HP polymers. However, most high-temperature gas-separation studies beyond 150°C were not investigated using HP polymers.

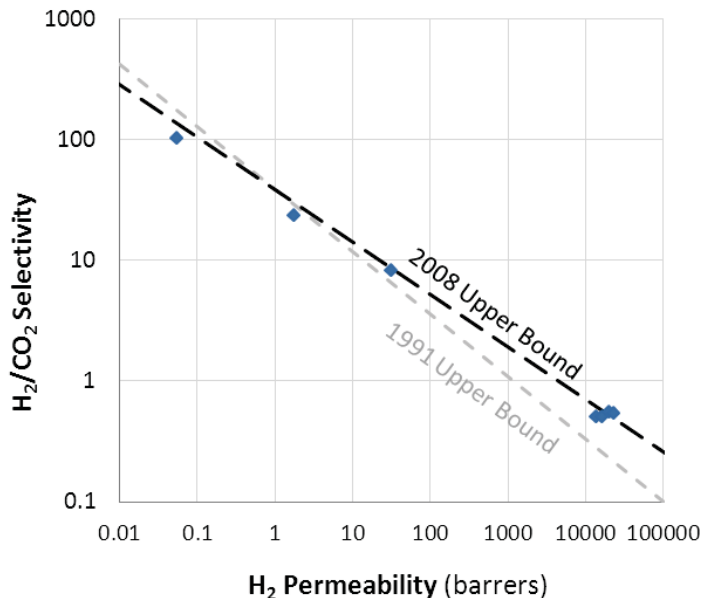


Figure 15. Robeson plot of H₂ permeance and H₂/CO₂ selectivity, showing Robeson's 1991 and 2008 upper bound lines.

Several synthetic routes have been developed for the functionalization of polybenzimidazole (PBI), where the resulting PBI is soluble in common organic solvents (THF and chloroform) (Klaehn, 2011, *High Temperature Gas Separations Using High Performance Polymers, In Inorganic, Polymeric and Composite Membranes: Structure, Function and other Correlations, Eds.*). Based upon these studies, several high-performance polymers (polyimides, polyamides, and polybenzazoles) have been dissolved into solution with relative ease and blended with the functionalized PBI. The Team has used this technical approach for many different polymer systems and successfully blended them. For example, several polymer blends were created using a polyimide as the base polymer and blending it with the following polymers: PBI-TMS; poly(vinyl alcohol), PVA; and poly(ethylene glycol) (PEG). In some cases, a large amount of secondary polymer, such as 35 wt% of PEG, was blended with the parent VTEC polyimide. This is significant because it demonstrates the stability of the parent polyimide polymers, even blended with known unstable polymers at high temperature (> 250°C). The Team's approach to the hydrogen-

separation membrane proposed here is to use the same logic as given above. The basic polyimide structure may be changed by forming interpenetrating networks and simple polymer blends. Based upon the above results, the Team has shown that a number of options for blending commercial polyamides with PEG, other polyamides, and some oligomers of other high-temperature polymers exist.

For this project, the research was focused on polyimides. Polyimides are chemically resistant, thermally robust, high-strength polymers. They also have good dielectric properties, are flame retardant, have a high resistance to radiation, and exhibit low deformation at elevated temperatures (Lee, 2007, Polyimides). High T_g 's and T_M 's give polyimides an advantage over other polymers for high-temperature gas-separation applications, such as being used in conjunction with WGS systems. Chemical resistance is a requirement for the harsh conditions seen in power plant applications, including water vapor and sulfur content. In addition, the polyimides exhibit flexibility and toughness and provide advantages over ceramic membranes. Select properties for three commercially available polyimide materials are given in Table 9. While this research focuses on H_2/CO_2 transport, polyimides have also been used to separate other gases, such as carbon dioxide from methane and oxygen from nitrogen (White, 1995, Properties of a Polyimide Gas Separation; Xiao, 2009, The Strategies of Molecular Architecture and Modification of Polyimide-Based Membranes for CO_2 Removal from Natural Gas: A Review). Hydrogen-gas-separation properties for a few commercially available polyimides are given in Table 10. Permeabilities and selectivities are based on pure-gas tests at room temperature.

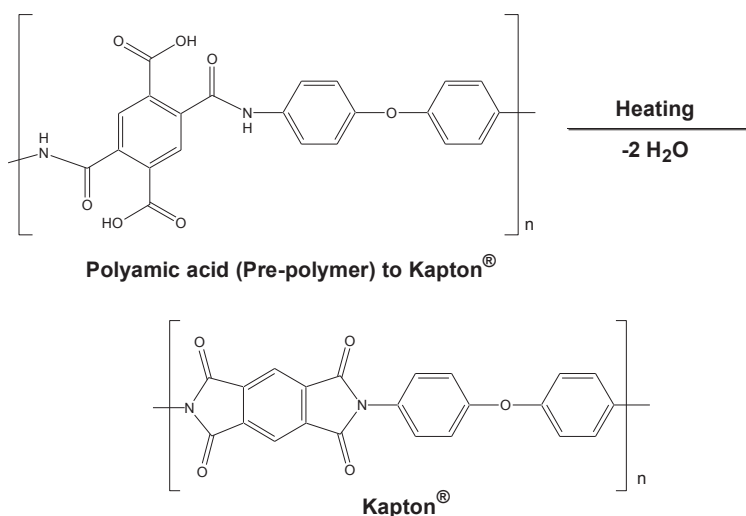
Table 9. General properties of commercially-available polyimides.

| Property | Units | Ultem 1000 ^a | Kapton [®] -HN ^b | VTEC PI ^c |
|---|-----------------|-------------------------|--------------------------------------|----------------------|
| Density | g/cm^3 | 1.27 | 1.42 | 1.41 |
| Water Absorption | % | 1.3 | 1.8 | <0.1 |
| Tensile Modulus | GPa | 3.59 | 2.50 | -- |
| Tensile Yield Strength | MPa | 110 | 69 | 89 |
| Hardness | -- | 109 (Rockwell) | -- | 86 (Durometer D) |
| Thermal Conductivity | $Wm^{-1}K^{-1}$ | 0.22 | 0.12 | 0.308 |
| Thermal Expansion | $ppm/^\circ C$ | -- | 20 | 45 |
| Glass Transition Temp | $^\circ C$ | 219 | 360–410 | >320 |
| Decomposition Temp | $^\circ C$ | -- | -- | >500 |
| a. (Fink, 2008, Polyimides: in Plastics Design Library. High Performance Polymers.) b. (2010, Kapton Product Sheet) c. (2010, VTEC PI Polyimide Data Sheet) | | | | |

Table 10. Gas-separation properties of commercial polyimides.

| Trade Name | Supplier | Selectivity (α) | | | Permeability |
|---|----------------|-------------------------------------|------------------|------------------|-----------------------------------|
| | | H_2/CO_2 | H_2/N_2 | H_2/CH_4 | H_2 (barrer) |
| Upilex | Ube Industries | -- | 145 ^a | -- | 0.8 ^a |
| Kapton [®] Type HN | Du Pont | 5.6 ^b – 5.7 ^c | 42 ^b | 40 ^c | 1.6 ^c |
| VTEC PI 080-051 | RBI | 7.4 ^c | 59 ^c | 120 ^c | 3.6 ^c |
| Matrimid [™] 5218 | Huntsman | 3.9 ^d | 97 ^d | 118 ^c | 27 ^d – 32 ^c |
| where 1 barrer = 3.347×10^{-16} (mol)/(Pa-m-s). | | | | | |
| a. (Nakagawa, 1994, Industrial Applications of Membranes for Gas Separation in Japan) (2010, Kapton Product Sheet) b. (Klaehn, 2008, CO2 Separation Using Thermally Optimized Membranes: A Comprehensive Project Report.) c. (Hosseini, 2008, Hydrogen Separation and Purification in Membranes of Miscible Polymer Blends with Interpenetration Networks) d. (Gorgojo, 2008, Mixed Matrix Membranes from Nanostructured Materials for Gas Separation) | | | | | |

From these data, a set of polyimide-based materials (VTEC PI polyimides; Richard Blaine International, Inc. [RBI, Inc.]) has been identified as having the desired gas separations in themselves (without blending or special additives). VTEC PI polymers are new materials which are made in multi-gallon quantities and have not been previously available for the described membrane applications. VTEC PI materials start as polyamic acids in a solution of N-methylpyrrolidone (NMP). As the polyamic acid, the polymer is soluble in other polar organic solvents, like dimethylacetamide (DMAc) and dimethylformamide (DMF), and can be blended with many different types of polymers or additives, as described previously. These VTEC solutions can be cast into films on a glass plate. After the solvent is removed (typically by low heating), a polymer film is left on the glass surface. The film is a polyamic acid precursor, which requires heat processing to form the resulting polyimide structure. The films are heat-treated, as illustrated in Scheme 1 (polymeric condensation reaction), eliminating water as a by-product and forming a highly heat-resistant, virtually insoluble film of a polyimide, similar to Kapton®. Specific structures for the VTEC polymers are considered proprietary and not provided in this report.



Scheme 1. Polyamic acid (pre-polymer) goes through a condensation reaction to yield polyimide polymers.

The VTEC materials when converted to their respective polyimides (similar to Kapton®) possess stable thermal properties and are robust and flexible even after numerous thermal cycles (up to 350°C). INL's preliminary studies have shown that these promising HP polymers produce exciting results for high-temperature gas separations. VTEC polyimides can be formed into films and tested for their gas-transport properties at elevated temperatures (250–300°C), and they are attractive polymers for the described challenging applications. The VTEC polyimides showed good permeabilities and selectivities when they were blended with other HP polymers, like N-substituted PBIs. Based upon these previous results, experiments were designed mainly for polyimides and their blends with an emphasis on the VTEC polyimides for their gas transport properties and other potential processing techniques that can enhance permeability and selectivities.

Hydrogen-Selective High Performance Polymers

The Team have been investigating and developing many different types of HP polymers for several years. Prior knowledge and capabilities using polymeric membranes with the carbon capture and storage (CCS) processes was utilized (Klaehn, 2008, CO₂ Separation Using Thermally Optimized Membranes: A Comprehensive Project Report.). The Team's previous documented work provided the basis for the synthesis and casting of several HP polymers and obtained consistent gas permeability data from these polymers for high-temperature mixed-gas analysis. The Team performed a down selection of HP polymers for further development and gas-permeability testing for this project. The first selected HP

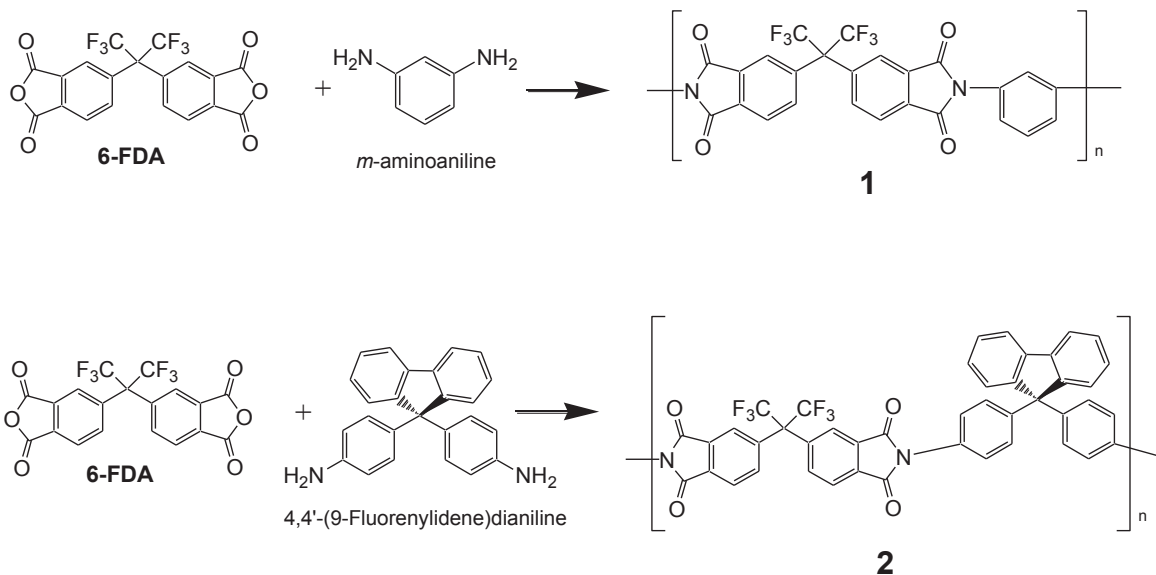
polymers were two polyimides, named VTEC PI 80-051 and VTEC PI 1388. These polyimides were chosen due to their easy film casting and thermal processing properties. The selected VTEC polymers are able to handle high temperatures (for polymers), 300°C or greater, and perform high H₂/CO₂ gas pair separations (H₂/CO₂ separation factor = 7–9; Table 11) at 250°C. The gas permeability tests were conducted using a mixed-gas stream from ambient temperatures to 250°C. These polymers meet the project's desired gas separation properties, which are beyond those of many other HP polymers currently in use. Therefore, the selected two VTEC polymers (VTEC PI 80-051 and PI 1388) needed to be tested under simulated syngas stream conditions to determine their performance.

Table 11. Mixed-gas data collected beyond 200°C [dry gas].

| Polymer | Permeability (Barrers) ^a | | | Selectivity α | |
|---|-------------------------------------|-----------------|-----------------|---------------------------------|----------------------------------|
| | H ₂ | CH ₄ | CO ₂ | H ₂ /CO ₂ | CO ₂ /CH ₄ |
| VTEC PI 80-051 (250°C) | 83.0 | 2.3 | 9.3 | 8.9 | 4.0 |
| VTEC PI 851 (250°C) | 55.4 | 1.8 | 5.6 | 9.9 | 3.1 |
| VTEC PI 1388 (250°C) | 66.8 | 0.85 | 9.2 | 7.3 | 10.8 |
| DuPont – Kapton-HN (250°C) | 37.5 | 4.1 | 11.8 | 3.2 | 2.9 |
| PBI Performance Products – PBI (250°C) | 33.1 | 1.69 | 4.7 | 7.1 | 1.9 |
| a. Permeabilities measured in Barrers: [(10 ⁻¹⁰)/((cm ³ (STP) x cm)/(cm ² x sec x cmHg))] | | | | | |

Improving VTEC Polyimides' Gas Permeabilities

The key issue for the parent VTEC polyimides is their gas fluxes; therefore, to increase their flux, we attempted to blend VTEC polymers with other polymers to improve the overall gas transport over the parent VTEC polyimides without changing H₂/CO₂ selectivity. One polymer for blending, 6-FDA polyimides [polyimide condensation reactions based on 2,2-bis(3,4-carboxyphenyl)-hexafluoropropane dianhydride] was chosen (see Scheme 1), since these polymers have shown both high-temperature stability and excellent gas transport while being blended with the VTEC solutions. The 6-FDA polymers were synthesized for the project because a manufacturer could not be found (M., 1999, New Polyimides for Gas Separation). The 6-FDA polyimide reactions were carried out near room temperature, which causes the reactions to take to complete. Two different 6-FDA polymers, **1** and **2** (see Scheme 2), were successfully isolated, and they were found to be good film formers using either tetrahydrofuran (THF) or dimethylacetamide (DMAc) as solvents. There were many other synthetic attempts with other aromatic diamines to make 6-FDA polymers; however, these products did not produce good films. The failed synthetic attempts occurred with ortho substituted and/or sterically encumbered aromatic diamines. The two isolated 6-FDA polymers (**1** and **2**) could be blended up to a 1:1 ratio with either VTEC polyimide. Several polymer films were cast from both the parent 6-FDA polymers and the blended 6-FDA/VTEC polymer solutions with excellent films resulting.



Scheme 2. Two 6-FDA polyimides that were utilized.

Preliminary gas-permeability (pure gas) data showed that the 6-FDA polymer is much more permeable than the VTEC polymers, but the selectivities are not as good as either of the VTEC polymers. The parent films of the 6-FDA polymers from DMAc are completely clear and colorless; however, the films would not pass leak checks after thermal processing at 250°C. The blended 6-FDA and VTEC polyimides resulted in good films with the features of the parent VTEC polymeric films. Two different concentrations of the two 6-FDA polymers were made with both VTEC PI 80-051 and 1388. One film contained a 1:1 and the second was 2:1 (VTEC:6-FDA polyimide). These blended films were heat processed at 250°C without issues, and gas-permeability testing was conducted on them. The gas permeability results for these blended polymers did not show any advantage over the parent VTEC PI polymers. The permeabilities of these polymers were found to be only slightly higher, but the selectivity was diminished compared to the parent VTEC. Upon completion of these studies, The Team concluded that these mixtures could not be used for this project, and the blended 6-FDA polymers were no longer pursued.

Development of Gas Permeation Experiments for Polymer Evaluation

Dry pure and mixed gas polymer permeation measurements have been commonplace for several decades. There exists a rather large hole in the literature with respect to humidified gas streams. One of the tasks in the project was to extend the teams' ability to make accurate measurements of gas permeation with humid gas streams at high temperature. Noting the high temperatures with acid-gases present, several gas-permeability tests were conducted in higher concentrations of CO₂ because the syngas stream itself has at least a 15–20% CO₂ composition. CO₂, an acid gas itself, can have deleterious effects on many polymers that have polar functional groups. Most of the gas-permeability measurements made for this project using the VTEC polymers were between 2–4% CO₂ (mixed-gas composition). The Team validated that the increased percentage of CO₂ (10–15% composition) did not affect the gas separations, even at higher temperatures (250°C). In fact, the VTEC polymers did not show any appreciable problems (such as membrane failures) when subjected to these conditions. This was a success for the project with these polymers, in regards to their stability towards higher-percentage composition CO₂ streams.

A typical syngas stream can have high concentrations of water (>10% by volume in total gas composition) at high temperatures. This makes for a difficult endeavor for gas permeability testing

because water can greatly affect the analytical instrumentation (gas chromatography). In addition, high-temperature steam ($> 150^{\circ}\text{C}$) can inflict damage upon gaskets and seals in a practical system.

Analytical information on gas-permeability analysis with water vapor is not well represented in the literature, which required The Team to develop a robust method that gives consistent analyses. The Team was successful with introduction of a high-temperature humidified gas stream into the mixed-gas permeation system. The humidified gas stream was obtained using a heated water reservoir to match the gas pressure on the front side of the membrane (see Appendix C). The feed stream's humidity level was calculated to be 2–4% water composition. These analyses were performed using VTEC PI 1388 ranging in temperatures from 100 – 200°C . During the analysis, the system sometimes needed time to stabilize (as much as 24 hours) before data could be collected, due to the water interaction (possible condensation) with the membrane. The testing apparatus took longer to stabilize, when the system temperatures were 100°C or lower. These experiments suggest that water is having a strong influence on the system. However, when the humidified gas stream was heated to higher temperatures, the gas permeability measurements were easier to quantify. In fact, the data at 200°C shows that the membrane behaves in a similar manner as a dry-gas-stream. This is somewhat astonishing when water is part of the gas stream, but we speculate that all gases in the humidified gas stream behave as permanent gases at higher temperatures ($> 100^{\circ}\text{C}$). However, there are extreme technical difficulties involving water vapor in these systems, and we proceeded to use known HP polymers that have been previously investigated to accurately measure the gas permeation rates in humidified gas streams.

Measuring Gas Permeability with Water Vapor


Mixed-gas permeation measurements provide data that are industrially relevant; however, the majority of studies published in the literature have been performed in the absence of water and at ambient temperatures ($<30^{\circ}\text{C}$) (Bernardo, 2009, Membrane Gas Separation: A Review/State of the Art.; Brunetti, 2010, Membrane technologies for CO_2 separation.; Powell, 2006, Polymeric CO_2/N_2 gas separation membranes for the capture of carbon dioxide from power plant flue gases.; Ayala, 2003, Relation of gas permeability with structure of aromatic polyimides; Hirayama, 1996, Relation of gas permeability with structure of aromatic polyimides I.; Koros, 1993, Membrane-based gas separation.; Robeson, 1991, Correlation of Separation Factor Versus Permeability for Polymeric Membranes.; Sridhar, 2007, Separation of Carbon Dioxide from Natural Gas Mixtures through Polymeric Membranes - A Review; Adhikari, 2006, Hydrogen Membrane Separation Techniques). Characterization of the influence of water on gas-separation performance must be considered. However, there are few gas permeability data in the literature that include water vapor as a component above ambient temperatures, and these studies are limited to 80°C (Sijbesma, 2008, Flue gas dehydration using polymer membranes; Potreck, 2009, Mixed water vapor/gas transport through the rubbery polymer PEBAX-1074). Thus, new system designs are needed using humidified gas-permeation studies at temperatures greater than 100°C , especially for applications where operational temperatures are nearly 200°C (syngas).

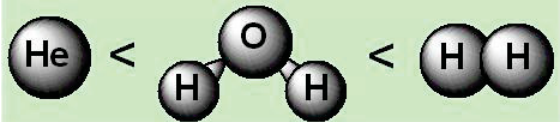
When determining humidified gas streams at high temperatures, one needs to recognize how water vapor can influence the polymer structure and the gas permeability measurements. Two factors associated with water vapor characterization are: (1) high permeability, which can be attributed to water's small Lennard-Jones kinetic gas diameter; (Breck, 1974, Zeolite Molecular Sieves: Structure, Chemistry and Use) and (2) condensed liquid water that can swell the polymer membrane (Lide, 2004, CRC handbook of chemistry and physics: a ready-reference book of chemical and physical data). Water vapor has a high permeation rate when compared to the permanent gases, with the exception of helium (see Table 12). The Lennard-Jones kinetic gas diameter for water vapor is 2.65 \AA , which is smaller than hydrogen (2.89 \AA) and carbon dioxide (3.30 \AA). Thus, water vapor is more penetrating than the other gases for most polymeric systems (Tock, 1983, Permeabilities and water vapor transmission rates for commercial polymer films). Changes in the polymer structure/matrix can be pronounced for polymers that have polar sites or additives where water vapor can bind or associate. For example, many HP polymers have functional groups (ketones, imines) that may enhance or restrict permeation in the presence of water

vapor. Deliquescent salts (e.g. LiCl) that are used to enhance polymer processability are also quite problematic (Fink, 2008, Polyimides: in *Plastics Design Library. High Performance Polymers*). Previous reports have shown that LiCl can dramatically change gas-separation performance by sorption of atmospheric moisture (Klaehn, 2011, *High Temperature Gas Separations Using High Performance Polymers, In Inorganic, Polymeric and Composite Membranes: Structure, Function and other Correlations, Eds.*). Another noted problem with water vapor is its high critical temperature (647.2 K), which can lead to difficulties in controlling the phases of water present in the experiment. Whether water is found as a gas or a liquid, it is influenced by temperature and pressure. Therefore, exact measurements below water's boiling point can be problematic. Typically, the percentage of water vapor in a gas stream will be limited to the dew point (saturation at 2–4 vol.%) at nominal temperatures (20–30°C). We recognize that above 150°C, a gas stream can contain much higher water vapor content. For these studies, the water vapor in the feed-gas stream was limited to 2–4 vol.%, a relevant set of values for these studies.

Table 12. Kinetic gas diameter and critical temperatures of selected gases.

| Gas | Kinetic Gas Diameter (Å) | Critical Temp (K) |
|------------------|--------------------------|-------------------|
| He | 2.60 | 5.2 |
| H ₂ O | 2.65 | 647.2 |
| H ₂ | 2.89 | 32.98 |
| CO ₂ | 3.30 | 304.2 |
| O ₂ | 3.46 | 154.58 |
| Ar | 3.54 | 130.86 |
| N ₂ | 3.64 | 126.2 |
| CH ₄ | 3.80 | 190.46 |





Water vapor permeates easily through most polymeric membranes, resulting in water sorption and/or swelling of the polymeric membrane, which can have a significant influence on permeability and selectivity. At ambient temperature, water sorption has been observed when additives are entrained in the polymer matrix (Klaehn, 2011, *High Temperature Gas Separations Using High Performance Polymers, In Inorganic, Polymeric and Composite Membranes: Structure, Function and other Correlations, Eds.*). Water vapor also can bind to polar functional groups on a polymer and change the polymer matrix (Roman, 2011, *Gas permeation measurement under defined humidity via constant volume/variable pressure method.*). During these studies, many measurements were performed at temperatures that were well above the boiling point of water. Water vapor may be destructive to polymer membranes where the polymer can undergo hydrolysis induced by heated steam. In these aggressive conditions, HP polymers offer distinct advantages in terms of membrane durability and performance. Polyimides exhibit good stability at high temperatures. However, there is nothing in the literature discussing the performance of polyimides against humidified gas streams at temperatures higher than 150°C.

For these gas-permeation studies, known HP polymers were compared to the VTEC polyimides. Generally, HP polymers exhibit poor gas permeabilities at ambient temperatures due to their high glass transition temperatures (Bernardo, 2009, *Membrane Gas Separation: A Review/State of the Art.*; Brunetti,

2010, Membrane technologies for CO₂ separation.; Powell, 2006, Polymeric CO₂/N₂ gas separation membranes for the capture of carbon dioxide from power plant flue gases.; Ayala, 2003, Relation of gas permeability with structure of aromatic polyimides; Hirayama, 1996, Relation of gas permeability with structure of aromatic polyimides I.; Koros, 1993, Membrane-based gas separation.; Robeson, 1991, Correlation of Separation Factor Versus Permeability for Polymeric Membranes.; Sridhar, 2007, Separation of Carbon Dioxide from Natural Gas Mixtures through Polymeric Membranes - A Review; Adhikari, 2006, Hydrogen Membrane Separation Techniques). Surprisingly, several HP polymers have relatively high water-vapor permeability at 30°C (Tables 13 and 14). The gas permeability data collected for selected polyimide and polyetherimide (Ultem 1000) membranes water vapor permeabilities that are 10–100 times greater than hydrogen were observed. Ultem 1000 showed the highest water vapor permeability of over 1,000 Barrers, which was over 350 times greater than hydrogen. Kapton resulted with water vapor permeabilities that were nearly 300 times greater than hydrogen. The VTEC polyimides did not yield consistent data at 30 °C, but these data show that water is much more permeable than any of the tested gases.

Table 13. Pure-gas permeabilities of selected polyimides at 30°C (dry-gas data).

| Polymer | Permeability (Barrers) ^a | | | Selectivity α | |
|---|-------------------------------------|-----------------|-----------------|---------------------------------|----------------------------------|
| | H ₂ | CH ₄ | CO ₂ | H ₂ /CO ₂ | CO ₂ /CH ₄ |
| VTEC PI 80-051 | 3.56 | 0.03 | 0.48 | 7.4 | 16.0 |
| VTEC PI 1388 | 3.97 | 0.05 | 0.53 | 7.5 | 10.6 |
| Ultem 1000 | 12.85 | 0.026 | 1.8 | 7.1 | 69.2 |
| Matrimid 5218 | 15.42 | 0.181 | 6.16 | 2.5 | 34.0 |
| Kapton-HN (DuPont) | 1.56 | 0.008 | 0.297 | 5.3 | 37.1 |
| a. Permeabilities measured in Barrers: $[(10^{-10})((\text{cm}^3 (\text{STP}) \times \text{cm})/(\text{cm}^2 \times \text{sec} \times \text{cmHg}))]$. | | | | | |
| b. Experimental difficulties with permeability measurements below 100°C. | | | | | |

Table 14. Humidified mixed-gas data collected at 30°C.

| Polymer | Permeability (Barrers) ^a | | | | Selectivity α | |
|---|-------------------------------------|----------------|-----------------|-----------------|---------------------------------|----------------------------------|
| | H ₂ O ^b | H ₂ | CH ₄ | CO ₂ | H ₂ /CO ₂ | CO ₂ /CH ₄ |
| VTEC PI 80-051 ^c | 50 ^c | 5.1 | 0.2 | 3.7 | 1.4 | 18.5 |
| VTEC PI 1388 ^c | 100 ^c | 7.6 | 0.35 | 2.60 | 2.9 | 7.4 |
| Ultem 1000 | 1311.4 | 3.8 | 0.6 | 4.3 | 0.9 | 7.2 |
| Matrimid 5218 | 872.7 | 24.5 | 0.5 | 13.5 | 1.8 | 27.0 |
| Kapton-HN (DuPont) | 410.9 | 1.5 | 0.1 | 0.8 | 1.9 | 8.0 |
| a. Permeabilities measured in Barrers: $[(10^{-10})((\text{cm}^3 (\text{STP}) \times \text{cm})/(\text{cm}^2 \times \text{sec} \times \text{cmHg}))]$. | | | | | | |
| b. 2–4 vol% Water Vapor Composition. | | | | | | |
| c. Below 100°C, vapor-liquid equilibria as a function of pressure can lead to poor reproducibility. | | | | | | |

Due to the difficulty of making measurements on the humidified gas streams, Matrimid 5218 was selected as a “model polyimide” because it gave sufficient flux for the other gases to be measured along with water. Matrimid 5218 thin dense films have also been studied extensively for various small gas separations. (Bernardo, 2009, Membrane Gas Separation: A Review/State of the Art.; Brunetti, 2010, Membrane technologies for CO₂ separation.; Powell, 2006, Polymeric CO₂/N₂ gas separation membranes for the capture of carbon dioxide from power plant flue gases.; Roman, 2011, Gas permeation measurement under defined humidity via constant volume/variable pressure method.; Shishatskiy, 2006, Polyimide Asymmetric Membranes for Hydrogen Separation: Influence of Formation Conditions on Gas Transport Properties; Zhao, 2008, Effects of cross-linkers with different molecular weights in cross-linked Matrimid 5218 and test temperature on gas transport properties; Reijerkerk, 2011, On the effects of plasticization in CO₂/light gas separation using polymeric solubility selective membranes.; Tin, 2003, Effects of cross-linking modification on gas separation performance of Matrimid membranes.; Liu, 2001, Chemical cross-linking modification of polyimide membranes for gas separation). In recent work, water-vapor permeation with Matrimid 5218 has been explored. These experiments focused on water-vapor permeability at 35°C, along with analysis of the effects of water in a mixed-gas stream at different pressures (Chen, 2011, Water vapor permeation in polyimide membranes). This study suggested that water vapor at ambient temperatures may be causing polymer plasticization through water clustering, which in turn, altered the permeability of other gases.

Measurement of permeability of water vapor in a mixed-gas permeation scenario, required modification of the gas testing apparatus. Water vapor contained in high-temperature gas streams is difficult to quantify, especially *in-situ* (see Appendix B). Typically, water vapor is measured by using cooled gas line traps on gas permeation systems; however, these water-filled traps allow analysis after the gas analysis is completed. INL’s system was designed to analyze water vapor and the other gases simultaneously. This means that the entire gas analysis system has to be maintained at higher temperatures for proper water-vapor analysis (to minimize water condensation in the system). Initial studies found that gas chromatography is not sufficiently accurate for water-vapor analysis, especially at high concentrations of water vapor. The Team found that infrared (IR) spectroscopy (LI-COR, model LI-840) is required in parallel with GC for proper gas analysis with water vapor. When GC and IR are combined, they result in a powerful and accurate analysis of the water vapor-containing stream that is generated for these experiments. Matrimid 5218 was characterized against the three gases (CH₄, CO₂, and H₂) at 150°C under both humidified and dry conditions, as seen in Table 15. The permeability of water vapor was measured to be over 1,700 Barrers, which is over 10 times the H₂ permeability, consistent with the data derived at 30°C. Under dry conditions, CH₄, CO₂, and H₂ also were found to be significantly more permeable at 150°C. Addition of 2–4 vol.% water vapor resulted in significant permeation increases for all three gases. H₂ was a little over 250 %, CH₄ was nearly 300%, and CO₂ has the largest percent increase at over 320 %. All of the gas permeabilities were influenced by water vapor entrained in the feed stream. It is also believed that water vapor also influences the polymer membrane’s morphology. Table 15 provides details of the selectivity of H₂/CO₂ at 150°C, which is close to the Knudsen diffusion value for both the humid and dry experiments and is higher than the ambient temperature selectivities (see Tables 13 and 14). However, the CO₂/CH₄ selectivity alphas are much higher than expected from Knudsen diffusion; therefore, it can be assumed that the polymer membrane is not compromised due to cracks/fissures under either dry or humidified conditions described.

Table 15. Dry and humidified mixed-gas permeation at 150°C for Matrimid 5218.

| Gas Conditions | Permeability (Barrers) ^a | | | | Selectivity α | |
|-------------------------|-------------------------------------|----------------|-----------------|-----------------|---------------------------------|----------------------------------|
| | H ₂ O | H ₂ | CH ₄ | CO ₂ | H ₂ /CO ₂ | CO ₂ /CH ₄ |
| Humidified ^b | 1769.5 | 143.8 | 8.1 | 37.7 | 3.9 | 4.6 |
| Dry | --- | 56.5 | 2.5 | 12.7 | 4.4 | 5.2 |

a. Permeabilities measured in Barrers: $[(10^{-10})((\text{cm}^3 \text{ (STP)} \times \text{cm})/(\text{cm}^2 \times \text{sec} \times \text{cmHg}))]$.

b. 2–4 vol% Water Vapor Composition.

Table 16. Energy of activation (E_p) for Matrimid 5218 under dry and humidified conditions in mixed-gas streams.

| Gas | Energy of Activation [kJ/(mol K)] | |
|------------------|-----------------------------------|-------------------------|
| | Dry | Humidified ^a |
| H ₂ O | - | 3.8 |
| H ₂ | 8.0 | 15.5 |
| CO ₂ | 5.0 | 8.4 |
| CH ₄ | 21.0 | 23.5 |

a. 2–4 vol% Water Vapor Composition.

The energy of activation of permeation (E_p) was calculated for the Matrimid 5218 membrane from the Arrhenius plots of humidified (see Figures 16 and 17) transport data for CO₂, CH₄, and H₂. These calculated E_p values from dry gas streams correlate well to earlier reports on Matrimid 5218, which were taken over a narrower temperature range (Shishatskiy, 2006, Polyimide Asymmetric Membranes for Hydrogen Separation: Influence of Formation Conditions on Gas Transport Properties; Zhao, 2008, Effects of cross-linkers with different molecular weights in cross-linked Matrimid 5218 and test temperature on gas transport properties). When dry, the E_p values of these three gases fall in the following order: CO₂ < H₂ < CH₄. CO₂, which is the most condensable gas in this data set, gives the lowest E_p (see Table 16). Transport of CO₂ can be thought of as largely influenced by solubility; although it can be argued that there are significant contributions from diffusion, since the permeation barrier for CO₂ is quite small. H₂ is the smallest gas, except for water, in this data set, and its transport is known to be highly penetrating through polymeric membranes; thus, its low E_p seems reasonable. CH₄, which is substantially larger than H₂ and less condensable than CO₂, yields the largest E_p value. This can be interpreted to be a result of larger amount of energy required for CH₄ to transport due to lower contributions from both solubility and diffusivity of the gas within the polymer matrix.

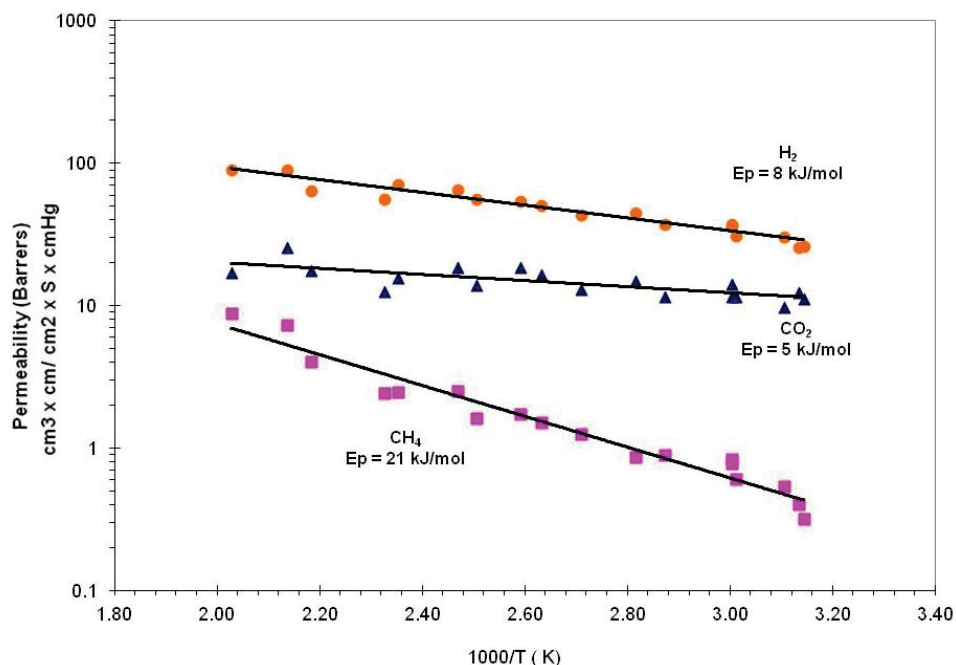


Figure 16. Dry-gas testing on mixed-gas feed streams— E_p data collected on Matrimid 5218 films from 30–275°C.

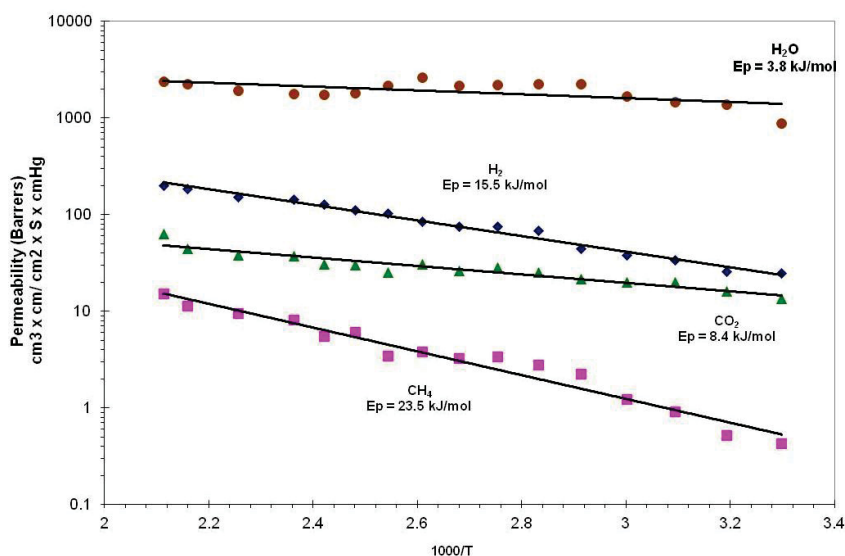


Figure 17. Humidified (2-4% water vapor) gas testing on mixed-gas feed streams— E_p data collected on Matrimid 5218 films from 30–200°C.

Addition of water to the feed resulted in two notable observations. First, the E_p for water was quite low at 3.8 KJ/mol, which can be rationalized by both its highly condensable nature and its relatively small kinetic gas diameter. Second, water appears to have a significant influence on the permeation of the other gases in the study. For all three gases, an increase in E_p was observed, Table 16. The greatest magnitude increase was with H_2 , which suggests that although there may be water-induced plasticization of the polymer substrate, a significant increase in diffusional barrier is present as a function of temperature.

Our data (ambient) are very close to the reported literature values for water permeation through Matrimid. What is interesting in the energy of activation (E_p) data is that the E_p of water vapor is relatively flat (3.8 kJ/mol); however, water has the highest permeation rate. This means that there is little resistance (the solubility mechanism is a minor component of transport) for water-vapor permeation through Matrimid from ambient to higher temperatures. In addition, the other tested gases (H_2 , CO_2 , and CH_4) do not show dramatic changes relative to dry-gas streams. The Matrimid data show that water does not affect the other gases; therefore, the H_2/CO_2 gas separation was not changed, see Figure 17.

Long-term Gas-permeability Measurements with VTEC

A gas-permeability study was conducted on VTEC polyimides as free-standing films, before the long-term exposure tests at WRI using gasified coal syngas. This study was to establish stability and gas separations at the operational temperature in a coal gasifier. Both VTEC polyimides were tested in a humidified mixed-gas stream, which was a composite of H_2 , CO_2 and CH_4 . In Figure 18, gas permeability data were obtained using VTEC PI 1388 for continuous operation in a humidified mixed-gas stream (2–4% water composition in the feed stream) for 84 hours at 200°C. The H_2/CO_2 separation factor (α) remained **steady** at nearly 8 throughout the mixed-gas permeability test. This high separation factor is an exciting result because it is well above the Knudsen diffusion H_2/CO_2 separations ($\alpha = 4.7$). Based upon these experiments, the VTEC PI membrane systems are able to give H_2/CO_2 separations in the presence of water, so long as water is a vapor at high temperatures. Additional studies on VTEC PI 80-051 were subjected to the same gas feed stream conditions as VTEC PI 1388. The gas permeability data showed that VTEC PI 80-051 had similar performance to VTEC PI 1388, where the H_2/CO_2 separation factor (α) resided at 7–8. These initial humidified-gas permeation studies showed that VTEC PI 80-051 and 1388 were fully capable of surviving these extreme environments and afford high H_2/CO_2 separations. Therefore, these two VTEC polyimides were evaluated further for their adhesion properties on various porous supports with and without metal-oxide coatings under the described conditions.

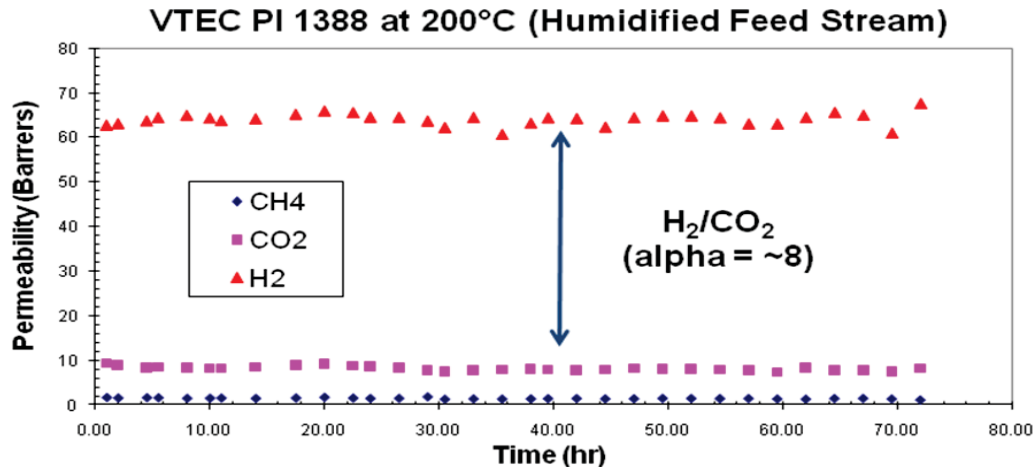


Figure 18. Mixed-gas permeability test on VTEC PI 1388 for 72 hours using a humidified feed stream (2–4% water) at 200°C.

Conclusion

The Team has developed a method to obtain consistent gas permeability data from HP polymers for high-temperature mixed-gas analysis. The selected HP polymers are two polyimides, named VTEC PI 80-051 and VTEC PI 1388 (RBI, Inc.). These polyimides were chosen due to their ease of casting films and thermal processing of these films.

The Team has studied various HP polymers for several years and evaluated their gas permeabilities and separations using a mixed-gas stream from ambient temperatures to 250°C. The VTEC polymers handle high temperatures, 300°C or greater, and delivered high H₂/CO₂ gas pair separations (H₂/CO₂ separation factor = 7–9) at 250°C. These polymers perform to the project's desired gas separation levels, and perform well beyond many other HP polymers currently in use. Also, preliminary tests with elevated concentrations of CO₂ (>10 vol.%) with the VTEC membrane remained stable at temperatures ranging from ambient to 200°C. Therefore, these two VTEC polymers were tested under simulated conditions for a syngas stream (humidified) to determine their performance.

A noted issue is water vapor that is a common component in many industrial gas mixtures. The literature is limited regarding humidified gas streams, and none show water vapor analysis at temperatures beyond 100°C. Due to water vapor's high condensability and small kinetic gas diameter, water vapor can be aggressive and has the potential to destroy polymer membranes. Therefore, new system designs were needed to analyze for water–vapor-containing gas streams. The modified gas-permeability apparatus is capable of analyzing water vapor along with other gaseous components in a mixed-gas stream simultaneously at high temperatures.

A series of gas permeation tests (dry pure gas, dry mixed gas, and humidified mixed gas) were performed using a proxy polyimide, Matrimid 5218, which has been studied extensively in the literature. The literature data were used to compare and evaluate our experimental results. The initial studies show that Matrimid 5218 membranes were found to be both chemically and dimensionally stable at temperature in the presence of water. The permanent gases CO₂ and water vapor encompassed a range of kinetic gas diameters and critical temperatures (condensability). Across the temperature range, permeability of all components was observed to increase with increasing temperature. Addition of water into the feed stream resulted in an increase in permeability for all gases with a slight loss in selectivity. This observation was made at both 30°C and 150°C. Increases in permeability with membrane hydration were greatest for CO₂, suggesting that water-induced plasticization of the polymer plays a role in transport. The data suggest that humidified-gas separation processes are possible if the humidified gas stream is kept at high temperatures at which water will remain a vapor and the polymer membrane will remain stable.

Several different HP polymers were analyzed for their gas permeation characteristics using three common industrially significant gases (H₂, CO₂, and CH₄) at temperatures ranging from 30°C to 200°C, both with and without added humidity. The initial gas-permeability data showed that VTEC PI 80-051 and VTEC PI 1388 membranes do not perform consistently at ambient temperatures (up to 100–150°C), but they do show stable performance at high temperatures (>150°C). As stated previously, water is possibly plasticizing these polymer membranes, thus changing their permeabilities and selectivities. However, free-standing films of VTEC polyimides demonstrate that they have exceptional physical stability towards water-vapor-containing gas streams for long durations. A long term study was undertaken with the VTEC polyimides. The membranes were tested in a mixed-gas stream at 200°C in the presence of humidity (2–4 vol%). Remarkably, both VTEC polyimides consistently performed (H₂/CO₂ separation = 7–8) for over 80hrs. These studies confirmed that the VTEC PI polymers are excellent candidates for the actual syngas experiments that were pursued in this project.

SECTION 3

HIGH PERFORMANCE POLYMERS ON POROUS SUPPORTS

Evaluation of VTEC Pi Polyimide on Ceramic and Porous Metal Discs in Gasified Coal Syngas Streams

Another objective of this project was to develop intermediate layers that can enable the formation of ultrathin polymer layers. The target polymer layer thickness was nominally 1 µm, with a stretch goal of 0.1 µm. Figure 19 shows an asymmetric membrane structure comprising the selective polymer layer, a sizing intermediate layer (zeolites or alumina), and a porous support. The porous support provides

mechanical support and robustness, while the polymer layer provides gas selectivity. The role of the intermediate layer was to enable the deposition of a continuous, uniform polymer layer on the relatively large pored support.

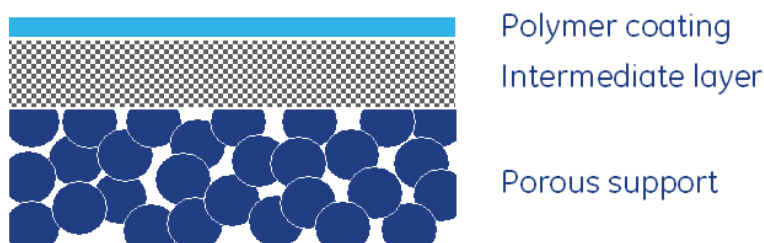


Figure 19. Asymmetric composite membrane structure.

The gasified coal, syngas stream environment can be very aggressive towards many materials, including metals and polymers. To be successful, the polymer, intermediate layer and porous support (metal or ceramic) need to survive this harsh environment without the polymer delaminating, cracking/fissuring and/or degrading. Initial tests used the VTEC polymers (INL) to coat metal and ceramic porous supports (coupons or discs from GE) then subjected them to a gasified coal, syngas stream from a power plant at WRI. These tests provided evidence that the proposed systems for gas separations will be able to handle these harsh conditions for extended periods. Several polymer coated metal and ceramic porous supports (VTEC PI 80-051 and 1388) are used, and the postmortem analysis of the polymer coated discs were evaluated for different degradation mechanisms.

Materials Selection and Testing

Early concerns were raised about how an acidic atmosphere could produce a loss of polymer adhesion to the porous supports. To address these concerns, aqueous acid exposure tests were done, prior to the syngas exposure experiments using WRI's gasified coal syngas stream. Several exposure tests with VTEC PI polyimide coated discs (both stainless steel and alumina) were done by submerging them into 4M sulfuric acid for one week. To simulate the most severe conditions that one might anticipate for the membranes, the membranes were heated to nearly boiling while in the acid solution for about 10-15 minutes, no observable physical changes (delamination, cracks/fissures or degradation) were found with an optical microscope, and the polymers remained affixed to the discs. These results demonstrated that the polymers maintained their adhesive properties to the supports and may be expected to operate under acidic conditions without reservation.

A syngas exposure test was performed on test coupons to aid in material selection. The test entailed exposure of coupons to syngas at WRI's facility. Table 17 lists the samples prepared for the syngas exposure test. Support coupons consisted of porous stainless steel buttons (Mott Corp., 1 in. diameter, SS316), porous Inconel buttons (Mott Corp. 1 in. diameter, Inconel), and porous alumina buttons (Tape-cast Taimei α -Al₂O₃, 1in. diameter). Intermediate layer consisted of either a γ -alumina coating or a zeolite coating spin-coated onto the support. Polymer membrane layers were applied by coated with either VTEC PI 080-051 or VTEC PI 1388 solutions onto the support followed by thermal imidization (see appendices).

The coupons listed in Table 17 were exposed to coal-derived syngas. The exposure test was performed at WRI (Figure 20), and WRI's syngas test (33% H₂; 18% CO; 44% CO₂; 2% H₂O) was at 300 psi for 168 hours at 250°C.

Table 17. Material screening samples for the syngas exposure test.

| Quantity | Support | Intermediate Layer | Membrane Layer | Position |
|----------|-------------------|---------------------------|----------------|-----------|
| 2 | Stainless (316) | -- | -- | Level 1 |
| 2 | Stainless (316) | γ -alumina coating | -- | Level 1 |
| 6 | Stainless (316) | γ -alumina coating | Polymer | Level 3 |
| 4 | Stainless (316) | Zeolite | Polymer | Level 1-2 |
| 6 | Stainless (316) | -- | Polymer | Level 3 |
| 2 | Inconel | -- | -- | Level 1 |
| 2 | Inconel | γ -alumina | -- | Level 1 |
| 8 | Inconel | γ -alumina | Polymer | Level 2 |
| 6 | Inconel | -- | Polymer | Level 4 |
| 2 | α -alumina | -- | -- | Level 1 |
| 2 | α -alumina | γ -alumina | -- | Level 1 |
| 6 | α -alumina | γ -alumina | Polymer | Level 2 |
| 4 | α -alumina | Zeolite | Polymer | Level 1-2 |



Figure 20. WRI facilities (left) and sample coupons prior to exposure test (right).



Figure 21. Coupons after exposure testing: labels indicate the support materials (steel, Inconel, or alumina), the intermediate layer (γ -alumina or zeolite), and the type of polymer membrane (VTEC 080-051 or VTEC 1388).

After the first test, it was discovered that the temperature in the chamber was not uniform. This caused the samples on the lower level (Level 1) of the chamber to be exposed to temperatures greater than 250°C. The temperature gradient made direct comparison of samples difficult. Polymer coated samples on the bottom layers all appeared dark in color compared to those on upper levels due to the higher temperatures. For example, image #12 in Figure 21 shows two identical samples, the left sample having been on level 1 and the right sample having been on level 4 during the test. However, some qualitative observations could be made:

- *Alumina Reduction:* The alumina buttons developed a slight gray color during the test, as shown in image #3 of Figure 21, indicating a reduction of Al_2O_3 to $\text{Al}_2\text{O}_{3-x}$. This reduced phase of alumina did not appear in an XRD spectrum of the samples, indicating less than 1% change in stoichiometry. Since this slight reduction does not appear to lead to delamination, alumina was determined to be a suitable support/intermediate layer material.
- *Zeolite Delamination:* The zeolite intermediate layer delaminated from the alumina buttons, as shown in image #18 of Figure 21. This occurred because the CTE of the polymer was greater than that of the zeolite and the adhesion between the zeolite and the alumina was weak. Zeolite will *not* be considered for future work.
- *Metal Support:* Both the stainless steel and the Inconel supports survived the exposure testing with no noticeable degradation or delamination of coatings. Work will continue with the metal support; however, long term testing was needed to evaluate corrosion of the steel.

A second exposure test was done using the same described conditions as previous stated, and the temperature was monitored for congruency throughout the testing vessel. After this exposure test, the polymer coated discs showed almost no changes in appearance (carbonization) by visual inspection. All polymer coatings survived without peeling or flaking from the porous substrates. This was a milestone for this project, which shows that these polymers will be able to withstand these harsh conditions for long-term. Several of these discs were retained for evaluation (SEM and optical microscope). The rest of these samples are repackaged into their original containers and sent to the other Team members for their microscopy evaluations. From Figure 22, the polymer coatings are still present on the discs that were coated with alumina or zeolites, and the polymer coatings don't have any visual imperfections or discolorations.



Figure 22. Syngas simulant feed stream test for 168 hours at 250°C on the polymer coated discs. The test was designed to expose these polymer-coated discs to syngas conditions at 250°C.

A postmortem scanning electron microscopic (SEM) study was done on the polymer coated discs from WRI. Several SEM pictures were taken of the polymer coated discs (Figure 23). These discs did not show any apparent deformation or fissures on the surface of the polymer (Figure 23; right picture). Also, SEM pictures show that the VTEC polymers shows effective adhesion to the surface of the disc (including the alumina and zeolite coated discs) without peeling or fracturing from the surface of the disc. The interesting point with the VTEC polyimides is that there is no penetration into the porous substrates. The polymer coating does not penetrate into the porous structure, even with the inorganic coatings on the substrates (Figure 23; middle picture). Based on the initial exposure testing studies, it is clear that the VTEC polyimides will survive these harsh conditions. Some initial experiments were conducted using porous alumina or stainless steel ½” button supports prior to scaling up to 20 cm tubular supports.

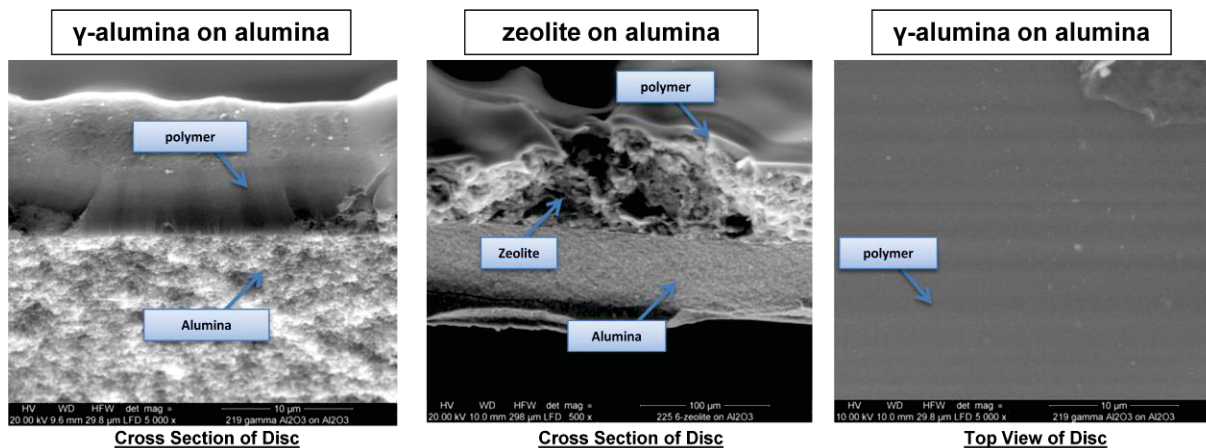


Figure 23. SEM Pictures of the polyimides after 168 hours of syngas exposure at 250°C.

Porous Metal Support Layer Selection

At initiation of the project, GEGR, INL, and WRI agreed to use tubular and flat-sheet porous metallic supports. The porous tubes used for the membrane support were seamless stainless steel sintered tubes manufactured by the Mott Corporation. The specifications for these tubes and flat-sheet supports were:

- OD=0.5" Nominal
- ID=0.375"+/-0.020"
- Length=8.0"+/0.040"
- 0.2 micron media grade
- Material: 316L SS.

Development and Testing of VTEC Coated Porous Tube Modules

Intermediate Layer Development for Porous Tube Modules

Intermediate Coating Process Down-select

There were five candidate processes that were screened according to ten selection criteria, as summarized in Table 18. The scoring procedure was designed to emphasize the trade-offs between different options. Criteria directly related to a specific metric were assigned a high weighting. For each criterion, each process was scored (high, moderate, low) according to literature analysis and initial experiments designed to provide insight into the entitlement. Scores were tabulated for each process, and are summarized in Appendix F.

Table 18. Trade-off table for Screening Intermediate Layer Processes.

| Criteria | Options | | | | | | | Total |
|---------------------------------------|------------|----------------|-------------|----------------------------------|-----------------------------|-----------------|--|-------|
| | Importance | Slurry casting | Dip coating | Electrophoretic deposition (EPD) | Hollow fiber co-fabrication | Sol-gel coating | | |
| Compatible with polymer | 9 | M | M | M | M | M | | 135 |
| Compatible with support (defects) | 9 | H | M | M | H | L | | 225 |
| Compatible with syngas-tolerant matls | 9 | H | H | H | M | H | | 351 |
| Economic entitlement | 9 | M | L | L | H | L | | 135 |
| Structure meets performance targets | 9 | M | M | M | M | M | | 135 |
| Compatible with sealing options | 3 | M | M | M | M | M | | 45 |
| Continuous process | 3 | M | M | M | M | M | | 45 |
| Low processing complexity | 3 | H | H | M | M | H | | 99 |
| Potential for IP | 3 | M | L | M | M | L | | 33 |
| Existing mfg supply chain | 3 | H | H | M | H | M | | 99 |
| Total | | 324 | 246 | 216 | 306 | 210 | | |

Process Compatibility with Polymer

This criterion was concerned with the compatibility of the process used to fabricate an intermediate layer with the subsequent application of the selective polymer layer. Potential failure modes include poor structural adhesion to the underlying substrate leading to delamination during the polymer application process. The coefficient of thermal expansion (CTE) for the polymer is greater than that of the ceramic intermediate layer (Xiao, 2009, The Strategies of Molecular Architecture and Modification of Polyimide-Based Membranes for CO₂ Removal from Natural Gas: A Review). Contraction of the polymer during cooling introduces a tensile stress on the intermediate layer. Mechanical delamination can occur in cases where there is poor structural adhesion (Chan, 1997, Layered Ceramics: Processing and Mechanical Behavior). Delamination can occur at either the support-intermediate layer interface, or the intermediate layer-polymer interface. Adhesion of the intermediate layer can be a function of the coating process, but detailed experiments are needed to ascertain the specific degree of risk associated with each process. Based on a literature review, there was insufficient information to rule out any of the five processes during the screening stage. Consequently, all of the processes were rated “moderate” for compatibility, pending direct experimental evidence.

Process Compatibility with Supports

This criterion assesses the ability of each process to deposit a conformal intermediate layer on the porous support. Specific concerns include: propagation of defects and pinholes from the support structure, through the intermediate layer, and into the selective polymer layer, and poor structural adhesion to the underlying substrate leading to delamination during the intermediate layer coating or polymer application process. In the target membrane structure shown in Figure 19, the role of the intermediate layer is to

enable the deposition of a continuous, uniform polymer layer on the relatively large-pored support. Physically, the intermediate layer must fill the surface roughness and pinholes in the support layer. Failure to do so will result in the propagation of these defects into the selective polymer layer, compromising gas selectivity.

Both slurry casting and dip coating are capable of forming layers that fill underlying gaps of up to several tens of microns, with slurry casting benefiting from the added effects of pressure induced deposition. Through careful manipulation of the current density at the surface, electrophoretic deposition (EPD) methods have the potential to preferentially deposit the intermediate layer material into defective regions (Xiao, 2009, *The Strategies of Molecular Architecture and Modification of Polyimide-Based Membranes for CO₂ Removal from Natural Gas: A Review*). Sol-gel approaches have the lowest entitlement, given the high degree of shrinkage associated with the conversion of the gel to a ceramic structure (Kaya, 1999, *Processing and Characterization of 2-D Woven Metal Fibre-Reinforced Multilayer Silica Matrix Composites Using Electrophoretic Deposition and Pressure Filtration*). The hollow fiber approach has the potential to solve this problem by eliminating the need for an intermediate layer.

Based on a literature review, surface characterization of the stainless steel supports, and initial coating experiments, slurry casting was rated “high, dip-coating, EPD and polymeric hollow fiber coating were rated “moderate” and sol-gel processing was rated “low.”

Process Compatibility with Syngas-tolerant Materials

The chemical environment presented by syngas necessitates the use of materials that are tolerant to sulfur corrosion, steam exposure, and reducing environments. This criterion addresses the ability of each coating process to handle syngas-tolerant materials.

Preliminary syngas exposure testing suggests that oxide materials were suitable for use as intermediate layers, but that the specific effects of minor components must be studied further (Tremblay, 2007, *The Effect of IGFC Warm Gas Cleanup System Conditions on the Gas-Solid Partitioning and From the Trace Species in Coal Syngas and Their Interaction with SOFC Anodes*). All of the ceramic candidate processes were compatible with oxide coatings. The ability to fabricate polymeric hollow fibers comprising syngas-tolerant materials is addressed in a separate report.

Based on initial screening work, all of the processes were rated “high,” except the hollow fiber approach, which was rated “moderate” pending direct experimental evidence of feasibility.

Potential to Produce a Structure that Meets Performance Targets

This criterion considers the ability of each process to produce a membrane that has the desired gas separation properties, life, and economic entitlement needed for meet the overall system performance targets.

Slurry and dip-coating processes are used in the manufacturing of ceramic membranes for catalyst deposition and water separation applications (Bonekamp, 1996, Chapter 6 *Preparation of Asymmetric Ceramic Membrane Supports by Dip-Coating*). While not yet proven for the manufacturing of membranes for gas separation applications, currently available structures approach the requirements needed for the intermediate layer (Verweij, 2006, *Microporous Silica and Zeolite Membranes for Hydrogen Purification*). Membranes comprising sol-gel coated intermediate layers on metal supports have been fabricated at the laboratory scale, but several layers are required to build sufficient thickness to overcome the underlying roughness of the supports (Kaya, 1999, *Processing and Characterization for 2-D Woven Metal Fibre-Reinforced Multilayer Silica Matrix Composites Using Electrophoretic Deposition and Pressure Filtration*). Polymeric hollow fibers for gas separation have been demonstrated for lower temperature gas separation applications.

Slurry and dip-coating approaches were rated “high” due to their use in adjacent applications. Other approaches were rated “moderate” pending experimental evidence.

Economic Entitlement of the Process

The final high weight criterion is economic entitlement. Favorable manufacturing economics are critical to meeting the cost of hydrogen targets. Factors which can reduce manufacturing costs include high yields (or low scrap rates), simple and scalable processing equipment, low waste material, low processing cycle times, fewer coating layers, and lower temperatures in thermal processing steps.

The hollow fiber-based approach was estimated to have the most favorable economic potential, owing to the low costs associated with the polymer supports. Of the remaining processes, slurry casting and dip coating have the potential to be operated in a semi-batch or continuous manner, and are already used commercially in the coating of ceramic elements for the catalyst and membranes industries (Verweij, 2006, Microporous Silica and Zeolite Membranes for Hydrogen Purification). EPD can also be operated continuously, but the process complexity associated with controlling deposition using the electric field introduces additional costs into the manufacturing process. Finally, sol-gel approaches have the lowest economic entitlement given the need to apply multiple coats due to significant shrinkage during drying and thermal processing. The polymeric hollow fiber approach was rated “high,” slurry casting and dip coating were rated “moderate,” and the remaining approaches rated “low.”

Compatibility with Sealing Options

This criterion arises from the need to establish hermetic and thermo-mechanically stable junctions between the membrane and module housing, in order to eliminate paths for bypass of gas and achieve the necessary gas separation performance.

Relevant sealing options under the conditions of interest (syngas, 250°C) include ceramic glasses, metal welds, metal brazes, and, potentially, high temperature epoxies (Qi, 2001, Ceramic-Glass Composite High Temperature Seals for Dense Ionic-Conducting Ceramic Membranes; Weil, 2006, Brazing as a Means of Sealing Ceramic Membranes for Use in Advanced Coal Gasification Processes.). In the case of inorganic seals, a thermal treatment step is needed. If the required temperatures of the seal exceed the temperatures used in the intermediate layer coating process, the seal must be applied before the coating. This may introduce additional constraints during process optimization.

Based on a literature review, there was insufficient information to rule out any of the five processes during the screening stage. Consequently, all of the processes were rated “moderate” for compatibility with seals, pending further work.

Continuous Process

This criterion is linked to the economic considerations (Tenison, 2000, Current Hurdles in the Commercial Development of Inorganic Membrane Reactors.). Continuous coating processes offer the potential for reduced manufacturing costs, through the improved utilization of capital equipment and lower labor costs due to higher production throughputs.

Based on a literature review, there was insufficient information to rule out any of the five processes during the screening stage. All of the processes were rated “moderate” for compatibility, pending further process definition.

Low Processing Complexity

This criterion was linked to the economic considerations (Tenison, 2000, Current Hurdles in the Commercial Development of Inorganic Membrane Reactors.). Simple coating processes offer the potential for reduced manufacturing costs and lower labor costs due to higher production yields.

Liquid-based coating processes for ceramic processing are used commercially for a range of applications, and polymeric hollow fibers are prepared at large scale for membranes. However, the fabrication of high temperature polymeric hollow fibers is still under development and EPD processes

require electrode fixturing, which introduces complexity. Consequently, EPD and hollow fiber processes were rated “medium,” while the other liquid-based coating processes were rated “high” for simplicity.

Potential for Intellectual Property

This criterion is relevant to the long term commercial prospects of the coating approach. The ability to develop intellectual property around the coating process or resulting membrane structure increases the chances of successful commercialization of the technology.

A preliminary survey of the existing intellectual property landscape suggests the potential for high temperature polymeric hollow fibers was “high,” slurry processes and EPD were “medium,” and dip-coating and sol-gel coatings were “low.”

Compatibility with and Availability of Existing Manufacturing Supply Chain

This criterion also relates to the long term commercial prospects of the coating approach. The ability to leverage an existing supply chain reduces the risks associated with scale up, and can accelerate the commercialization of the technology.

Since slurry casting, dip-coating, and polymeric hollow fiber technologies are used commercially in adjacent applications, these options scored a “high” rating. EPD and sol-gel processes require additional development before they can be readily applied to the form factors encountered in the large scale manufacturing of membranes. These options scored a “moderate” rating.

Summary

Based on the literature survey, laboratory test results and preliminary economic analysis, two approaches were selected for further development. The primary approach was a slurry-casting process based on a multicomponent inorganic precursor suspension. This approach has the potential to produce defect free structures compatible with polymer coating on sub-scale structures, operate as a continuous process, and may be compatible with the existing manufacturing base for ceramic membranes.

A secondary approach involving polymeric hollow fiber supports was also identified for further investigation. Although this falls outside the original scope of work for the project, this approach was selected because of its potential for significant reductions in the manufacturing costs associated with an all-polymeric structure. The hollow fiber development effort was added to the work scope in the project, and it is covered later in this report.

Membrane Layer Development for Porous Supports

The H₂ selective polymer material was selected based on gas permeance experiments with various polymer films (Klaehn, 2008, CO₂ Separation Using Thermally Optimized Membranes: A Comprehensive Project Report.;Klaehn, 2011, High Temperature Gas Separations Using High Performance Polymers, In Inorganic, Polymeric and Composite Membranes: Structure, Function and other Correlations, Eds.). Initial experimental work at GE Global Research was performed on 0.5 in. button samples composed of α -Al₂O₃ supports with γ -Al₂O₃ intermediate layers and polyimide membranes (Polishchuk, 2012, Supported Polyimide Membrane for Gas-Separation). The permeabilities of these composite membranes were in good agreement with those measured on film samples of the same polymer. Hence, the polymer solution coating and curing process was developed to create defect-free membrane layer on porous stainless tube structures (see Appendix F).

Porous Support Module Prototypes

Sealing Methods

Hermetic and thermomechanical stable junctions between the membrane and module housing must be formed in order to eliminate paths for gas to bypass the selective layer, enabling the module to achieve the necessary gas separation performance. These important items are not generally researched for most

module systems; however, the temperatures and conditions are beyond the specifications of most common epoxies found for membrane modules. Therefore, relevant sealing options have to be developed under the conditions of interest (syngas conditions, 250 to 300°C) include glasses, metal welds, metal brazes, and high temperature epoxies (Qi, 2001, Ceramic-Glass Composite High Temperature Seals for Dense Ionic-Conducting Ceramic Membranes; Weil, 2006, Brazing as a Means of Sealing Ceramic Membranes for Use in Advanced Coal Gasification Processes.). In the case of inorganic seals, a thermal treatment step was found to be necessary. If the required temperatures of the thermal treatment exceeded the temperatures used in the intermediate layer coating process, the seal must be applied before the coating. This may introduce additional constraints during process optimization.

The two sealing options used for testing were high temperature epoxies and metal welds (see Appendix F). For short term evaluation of membrane performance, high temperature epoxy seals provided a hermetic seal with a short cure time with no additional process steps for integration into a test module. These seals can be used for room temperature testing and pressure gradients up to 70 psig. Once defect-free membrane coatings were established, the performance of high temperature epoxy for long term testing was further evaluated and found to be unsuitable for thermal cycling.

The welding of steel tubing to the ends of the porous steel substrate was chosen as the preferred sealing method. Standard sealing methods or welds can then be used to integrate the solid tubing ends of the membrane unit into the module housing. The substrates must be joined to the solid tubing prior to coating due to the heat of welding and to the potential of damage that could be incurred by machining done at the weld area to smooth the interface between substrate and tubing. After coating, the polymer layer must fully cover this interface, with no leak paths for gas. The following two sections describe the two sealing techniques in greater detail.

High Temperature Epoxy Sealing Technique

The epoxy seals were evaluated by sealing a dense steel tube to a fitting and testing it in the same way that a membrane would be tested. Since there will be no gas flow through the walls of the dense tube, any gas flow detected through the part represents a seal leak. The tube was pressurized up to 50 psig at room temperature and found to be leak tight. The seal was heated from room temperature to 250°C while being pressurized on the inside with a mixture of H₂/CO₂. No leak could be detected through the seal by mass spectrometer. However, upon cooling, a leak developed between the epoxy and the inner diameter of the Swagelok® fitting.

H74 epoxy was chosen because it had been successfully used for membrane sealing in other systems that cycled to temperatures as high as 250°C and exhibited no leaks during heating or cooling. It was shown to maintain its adherence between a ceramic part and a steel surface during thermal cycling, but in a different geometry than was used to seal a tube into a fitting.

For the tube seal, the leak that occurred upon cooling was a failure in the adhesion of the epoxy to the stainless steel fitting that contained it, as shown in Figure 24.



Figure 24. Leak site at interface between epoxy potting and stainless steel end fitting.

Several factors were considered to see if the epoxy failure upon cooling could be prevented, including seal geometry, surface preparation, epoxy cure temperature and system cooling temperature. Additional epoxies were also tested. Test parts were made using steel tubing in place of the porous steel membrane substrate. Test parts were sealed with epoxy and subjected to thermal cycling to 200°C. After heating and cooling, the parts were checked for leaks.

The standard tube-in-fitting geometry was compared against a flat butt joint and a modified butt joint that mimicked sealing the flat end of the steel tube to a flat disk. The modified butt joint geometry was included based on previous experience with H74 epoxy at high temperature. Pictures and schematics of the joints are shown in Figure 25 (see the next page).

In order to improve the adhesion of the epoxy to the steel, the surface preparation of the metal parts was modified. The standard tube-in-fitting geometry was used, since no benefit was seen from geometry modifications. The surface of the steel that was to contact epoxy was roughened by sand blasting. After sandblasting, the parts were ultrasonically cleaned in solvent to remove any residue from the surface. After this surface preparation, several samples were assembled, epoxied, and tested. Out of several samples tested, most showed leaks but one or two samples did not show leaks after one thermal cycle. Additionally, the amount of force required to break the epoxy seal was found to be greater than for a sample without pre-roughened surfaces.

Two other high temperature epoxies were considered: Cotronics Duralco™ 4525-IP and Aremco-Bond™ 526N-ALOX-BL. Test parts were assembled with these epoxies, utilizing the improved surface preparation and the modified curing schedule. These epoxies showed a leak at the same interface between the epoxy and the steel fitting. A more exhaustive survey of epoxies would be necessary to identify a better candidate for thermal cycling. It was decided to keep using the H74 epoxy with the understanding that samples could be heated only one time. This was used as an intermediate sealing method that allowed samples to be tested while developing membrane samples with welded steel ends.

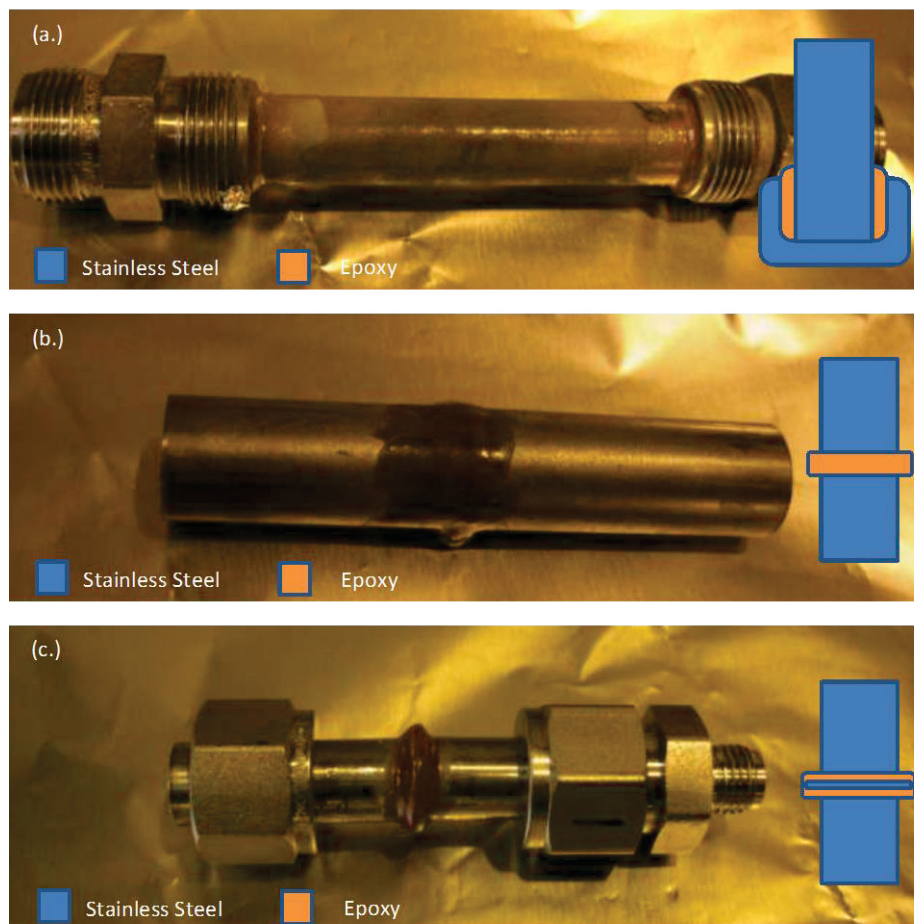


Figure 25. (a) Standard tube in fitting geometry, (b) butt joint, and (c) modified butt joint that mimics seal to flat disk.

Machined End Tubes

One of the methods attempted for sealing the ends of the porous stainless steel Mott tubes was to machine the ends on a lathe. During the machining process the lathe cutting tool shears and presses the metal particles together, filling in the gaps between them. Figure 26 shows a close-up of a tube with a machined end (top) followed by one that has been machined and then swaged on both ends (bottom). To test the method an entire tube was turned on the lathe, swaged on both ends, capped on one end, pressurized with hydrogen, and then valved off on the other end. Pressure was measured over a period of ten minutes. Approximately ten different samples were tested in this manner. In two cases the tubes were found to be leak free (e.g., no detectable drop in pressure) at 40 psig of hydrogen for ten minutes. In all other cases leaks were found. No systematic study was performed to determine the optimal machining parameters that result in a good seal since other sealing options were available as described later.

One of the important lessons learned was that swaging torque is a critical parameter. These sintered porous tubes were much more deformable than their solid stainless steel counterparts. Swaging has the effect of deforming the tube and reopening some of the pores near the ferrule. Additionally, too much deformation will result in a compromised ferrule to tube seal. This was shown to be the case by performing “snoop” leak testing on one of the tubes while tightening. Initially there were no leaks near the ferrule, but after a critical amount of tightening was performed bubbles began to form. As the ferrule was tightened further, bubbling became more vigorous indicating that the leak rate was getting worse. It

was discovered that using nylon ferrules resulted in far fewer leaks near the ferrules than stainless ferrules since less torque need be applied. However, in most cases where nylon ferrules were used, leaks were found elsewhere on the machined surface.



Figure 26. Close-up of a tube with a machined end (top) and a tube that has been machined and then swaged on both ends (bottom).

Welded Steel End Seals

The most reliable and scalable sealing solution was to have solid steel tubing welded to porous substrates prior to coating. Tubes of this sort were acquired from two sources: (1) supplied directly from the substrate manufacturer, and (2) fabricated on site using existing porous substrates and standard seamless tubing. In both cases, the tubing was welded to the substrate and machined as necessary to provide a smooth interface between the porous and solid tube. There was no performance difference noted between the two types of tubes.

For laboratory testing, a standard compression seal to each end of the tube was used so that the module shell and test fixture could be reused for successive samples. In commercial practice, the tube would likely be welded into place. For leak tight compression seals, the tubing used must be close to the nominal diameter 0.500", not out-of-round and have a significantly smooth outer surface. According to Swagelok[®] Company (2011, An Installer's Pocket Guide to Swagelok(r) Tube Fittings), "tubing with any kind of depression, scratch, raised portion, or other surface defect will be difficult to seal, particularly in gas service." Surface roughness along the tube provided a leak path for gas molecules between the ferrule and the tube wall. Several of the substrate tubes received had unacceptably rough surface finishes on the solid ends that had to be machined smooth to permit compression sealing. The surface machining required material removal, reducing the outer diameter of some tubes by as much as two thousandths of an inch.

The results of the ferrule material tests are shown in Figure 27 and compared to the permeance measured through a typical coated tube. The leak through the seals needs to be at least an order of magnitude lower than the tube permeance so that the gas selectivity performance of the coating was not compromised by poor seals. The Teflon[®] ferrule leaked initially, but the leak decreased as the sample was heated. Upon cooling to room temperature, the leak was evident again, making the Teflon[®] unsuitable for thermal cycling.

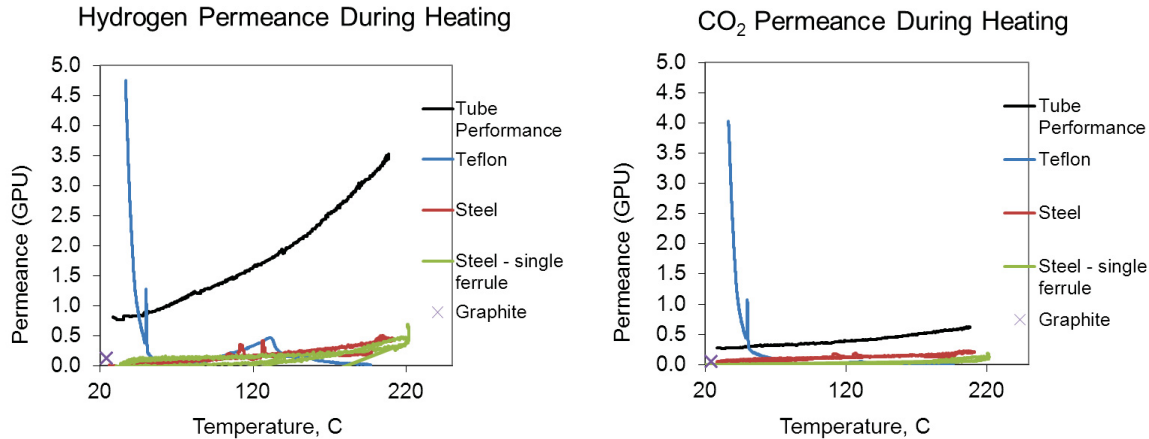


Figure 27. Performance of ferrule materials during thermal cycle to 250°C.

Both the single and double stainless steel ferrules showed a permeance that was much less than the permeance of a coated tube ($\sim 10\%$ at temperature), and both types of ferrules showed no detrimental effects from thermal cycling. The graphite ferrule had a higher leak rate than the steel ferrules at room temperature and was not heated. Of the two steel ferrule types, the single ferrule showed a lower CO₂ permeance than the two piece ferrule. The ParkerCPITM fitting with the single ferrule design was chosen to seal membrane tubes with solid ends to the test fixture.

Laser Welding of Tubes

There was concern that the heat generated by the welding process would compromise the coating, so to mitigate this risk we decided to use laser welding to attach the fittings to the dense ends. Because the laser energy can be precisely controlled and the weld can be precisely located, it was possible to create welds without generating large amounts of excess heat. However due to the precise nature of the weld, some additional prep work was needed. Before welding, the tube ends were turned on a lathe so that their OD matched that of the weld-on fitting (see Figure 28). It was also necessary to machine the ends flat (also on the lathe) to assure a good mate between the pieces.

Laser welding was attempted a total of 6 times and 2 out of the 6 joints were found to be leak free. Samples were leak tested by pressurizing with Helium to 50 PSIG and applying Snoop to the weld. Examples of a successful and unsuccessful weld are shown in Figure 28. Even though the yield rate was only 33%, this was sufficient to prove that the laser welding method can be successfully implemented. There were a number of parameters that can be adjusted for this process such as pulse energy, laser focus, part rotation, fixture alignment, etc. Parameter optimization would be required in order to improve the yield rate above 33%. With optimization, we would expect close to a 100% yield rate.

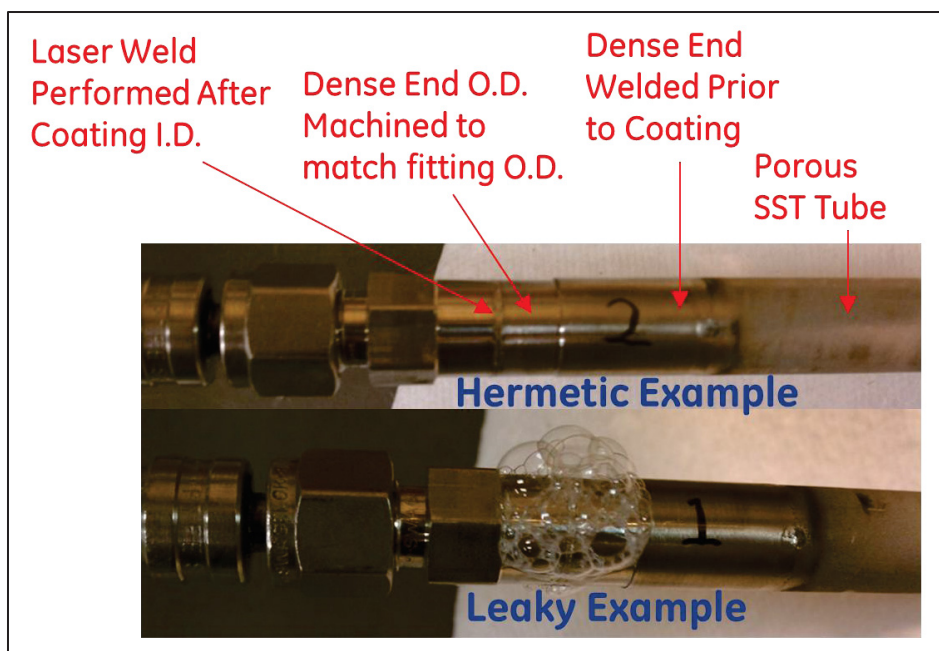


Figure 28. Sample laser weld results.

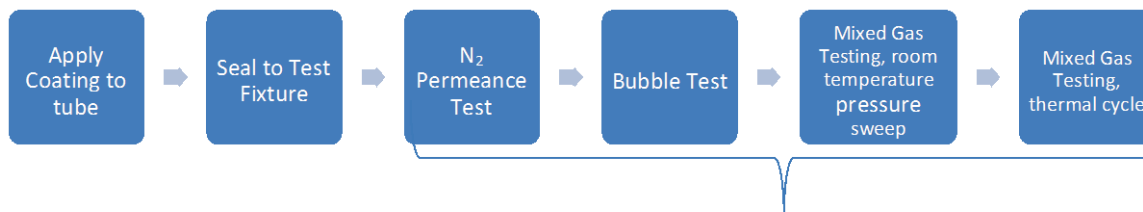
Porous Support Module Housing

The membrane tubes must be integrated into a module housing which directs flow on each side of the membrane for gas permeance testing, yielding separation performance. Membrane tubes were integrated into a metal piping network that supplied feed gas and enclosed by a gas tight shell with inlets and outlets for the sweep gas and permeate. The module was a freestanding unit which can be installed into the required test set-up either at GEGR or WRI (see Appendices F and G).

Gas Permeability Testing

Gas permeability testing capabilities for each of the partner institutions are summarized in Appendices.

After the intermediate and membrane coating was applied to the porous tube support, it was sealed to the test fixture and tested for the presence of any large viscous leaks. Following the leak check, the tubular membrane was tested for H_2/CO_2 separation performance testing. The general testing protocol for tubes is shown in Figure 29 and described in detail in Appendices B and F.



Testing

Figure 29. Schematic of tubular membrane testing protocol.

GE Tube #50 after clearing the N_2 permeance bench test and bubble test and was mounted into a test module using Parker CPI™ fittings to make the seal to the sample. The module consists of two

components: coated porous tube with 0.5 in. stainless steel tube end connections and tube housing, as shown in Figure . The tube housing was about 58 in. long with an internal diameter of 1.6 in. The housing was sealed by KF flanges and silicone o-rings, limiting the maximum operating temperature to around 220°C and maximum shell pressure to 75 psig. The process line entered the housing through the end flanges and was constructed of stainless steel tubing assembled with Swagelok® fittings. The tube was connected to the Parker CPI™ fittings on the sample and a 6 in. length of convoluted steel tubing was connected to one end of the sample to enable the tube to be constrained and aligned on both ends of the module shell. Due to the convoluted tubing, the maximum operating pressure of the process line was limited to 90 psig.

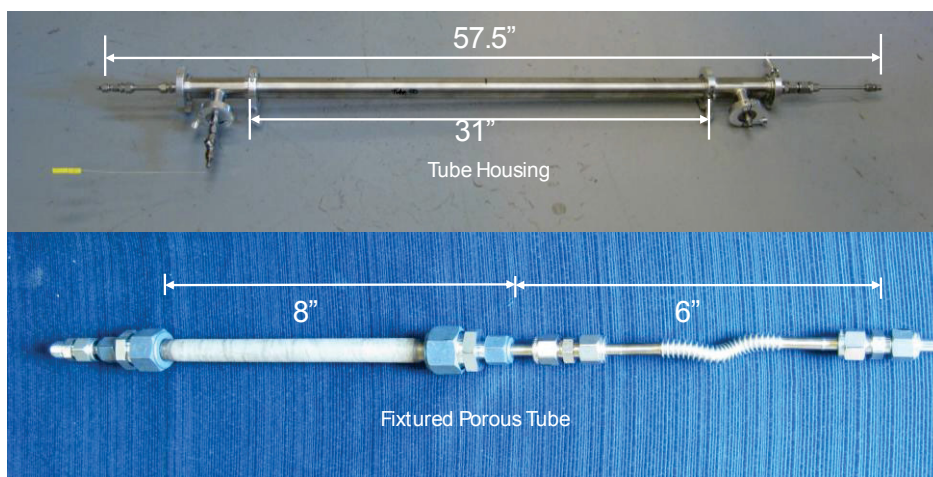


Figure 30. Image of the tube housing and the fixtured sample tube.

The gas separation performance of Tube 50 was measured at GEGR using simulated syngas (H_2/CO_2 - 50/50 mole %) fed through the inside of the tube at 1 slpm. A nitrogen sweep gas was delivered on the shell side at 1 slpm in a countercurrent flow configuration. For initial testing, the module was at ambient temperature. The differential pressure (Δp) across the tube and the shell side was increased from 0 to 5 psid. The module was then held at $\Delta p = 5$ psid and the temperature was increased to 200°C. The module was held at temperature for 15 hours then cooled back to room temperature. The H_2 and CO_2 concentration in the permeate was measured continuously during this period. The H_2 permeance did not increase with increasing pressure, indicating minimal viscous flow through the membrane. The H_2/CO_2 selectivity was above 5 and did not drop below Knudsen at increased pressure gradient.

Upon heating to 200°C, H_2 and CO_2 permeances typically increased between 2 to 10 times, with the H_2 permeance increasing more than the CO_2 permeance. This caused the selectivity of the sample to increase to around 8 from a value close to Knudsen selectivity. The samples were stable at temperature, and the values did not change significantly after an overnight soak. There was an initial period of 2 to 4 hours at temperature when the sample reaches equilibrium.

The H_2 permeance of Tube 50 was in the range of 1-6 GPU, and H_2/CO_2 selectivity was between 4 and 8. Both H_2 permeance and, as a consequence, H_2/CO_2 selectivity increased with elevated sample temperature. H_2/CO_2 selectivity higher than the Knudsen selectivity ($S_{H_2/CO_2} = 4.7$) indicates significantly defect-free polymer coating layer and tube end seals. The data set is summarized in Table 19. The complete module containing Tube 50 was shipped to WRI for long term testing in coal-derived syngas and steam.

Table 19. Performance of Tube 50 in preliminary gas testing at GE Global Research.

| Summary of GEGR Testing | | | Average values | | |
|-------------------------|---------------|---------------------------------|----------------|-----------------|---------------------------------|
| | Feed Pressure | | H ₂ | CO ₂ | |
| | | | permeance | permeance | |
| Temp, °C | psig | Gas | GPU | GPU | H ₂ /CO ₂ |
| 25 | 0.5 | H ₂ /CO ₂ | 0.34 | 0.07 | 4.7 |
| 25 | 2.5 | H ₂ /CO ₂ | 0.33 | 0.07 | 4.6 |
| 25 | 5 | H ₂ /CO ₂ | 0.32 | 0.07 | 4.3 |
| 200 | 5 | H ₂ /CO ₂ | 6.17 | 0.80 | 7.7 |

Exposure/Slip-Stream Testing at WRI

At WRI, the membrane Tube 50 was exposed to temperatures from 200 to 280°C, feed pressures of 5 to 450 psig, and multiple syngas compositions, some of which included steam and H₂S at ppm concentration levels. H₂ permeate concentration was measured at periodic intervals by gas chromatograph with N₂ carrier gas. CO₂ and CO permeate concentration was measured using a Draeger-Tube[®] after collecting the gas and storing it in a plastic bag and measured at frequent time intervals. The main test conditions and results are summarized in Table 20.

Table 20. Performance of Tube 50 in syngas and steam at WRI.

| Summary of WRI Testing | | | | | Average values | | | | |
|---------------------------|-----|--------|----------------|---|---------------------------|----------------------------|---------------------------------|---------------|--------------------|
| | | | Feed pressure, | | H ₂ permeance, | CO ₂ permeance, | selectivity | CO permeance, | selectivity |
| Test | hrs | Temp C | psig | Gas | GPU | GPU | H ₂ /CO ₂ | GPU | H ₂ /CO |
| Sample baseline | 200 | 200 | 5 | NETL | 3.5 | 0.6 | 5.8 | | |
| Steam exposure | 30 | 200 | 5 | NETL + steam | 4.4 | 0.7 | 6.3 | | |
| Syngas | 200 | 200 | 10 | syngas + steam | 4.7 | 0.7 | 6.7 | 0.1 | 47 |
| H ₂ S exposure | 50 | 200 | 10 | syngas + steam + 150 ppm H ₂ S | 3.7 | | | | |
| dP increased 50 psig | 6 | 200 | 50 | syngas | 3.5 | 0.5 | 7.0 | 0.1 | 35 |
| Thermal cycling | 30 | 200 | 10 | syngas | 3.5 | 0.5 | 7.0 | 0.1 | 35 |
| Steam exposure | 280 | 200 | 50 | syngas + steam | 4.4 | 0.6 | 7.3 | 0.2 | 22 |
| dP increased to 90 psig | 20 | 200 | 90 | NETL + steam | 3.5 | 0.8 | 4.4 | 0.1 | 35 |
| Temp increased to 280C | 20 | 280 | 50 | NETL | 13.7 | 2.6 | 5.2 | 1.4 | 10 |
| dP increased to 450 psig | 50 | 280 | 450 | NETL | 11.2 | 2.9 | 3.9 | 1.0 | 11 |

The sample remained stable over 1,700 hours of elevated temperature testing. At 200°C and feed pressures less than 50 psig, the H₂ permeance remained between 3.5 – 4.7 GPU and H₂/CO₂ selectivity was between 6 and 7. This was in reasonable agreement with the GEGR data under equi-molar H₂ and CO₂ feed streams. The sample was exposed to NETL protocol gas, syngas, steam, and up to 150 ppm H₂S. The gas compositions for the NETL protocol gas and the syngas as shown in Table 21.

Table 21. Gas compositions.

| Gas composition | % H ₂ | % CO ₂ | % CO |
|-------------------|------------------|-------------------|-------|
| NETL protocol gas | 60.68 | 38.34 | 0.975 |
| Syngas | 43.70 | 26.33 | 28.01 |

As temperature increased > 200°C or feed pressure increased > 50 psig, H₂/CO₂ selectivity decreased. This decrease in performance was reversible, with the performance returning to its baseline level after temperature and/or pressure was reduced. An overview of the results is shown in Figure with a timeline of the testing shown in Figure 32.

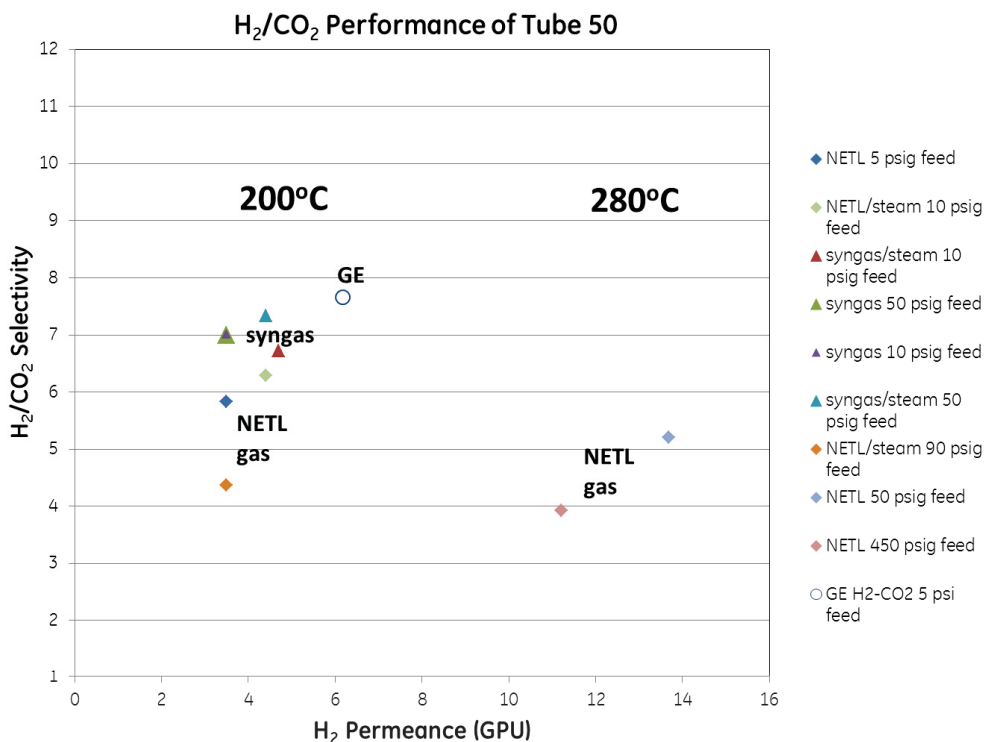


Figure 31. Performance of Tube 50.

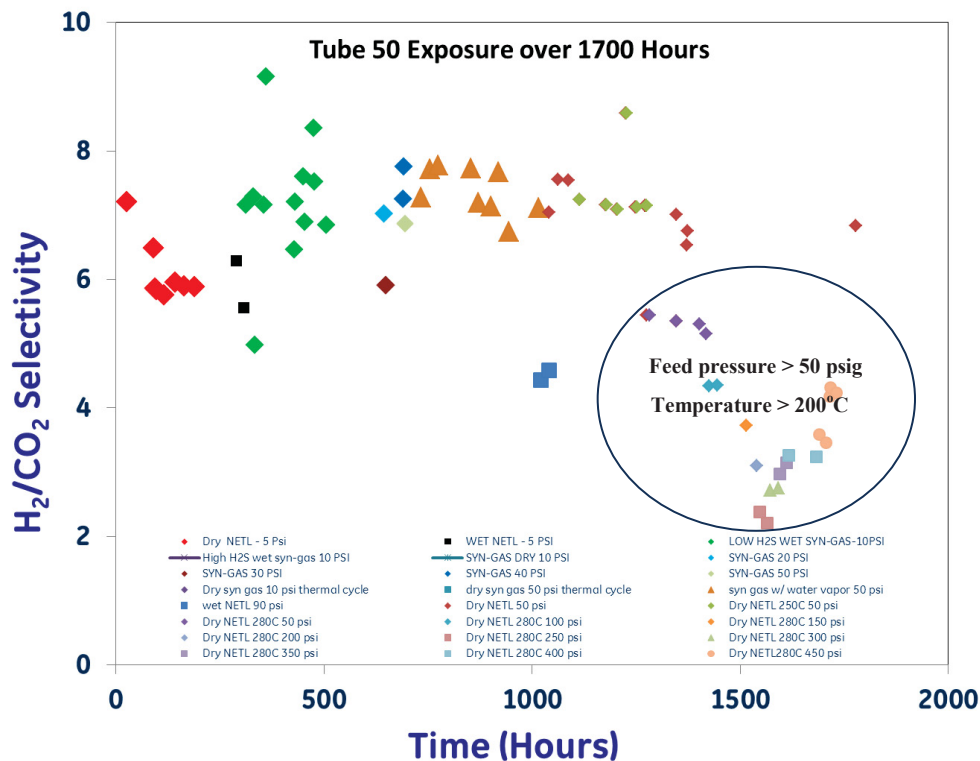


Figure 32. Performance of Tube 50.

The test was performed in two phases. In the first phase of testing, maximum temperature was limited to 200°C, and maximum feed pressure was limited to 90 psig. These limits were determined by module materials of construction as described earlier. After 1,000 hours of testing, the module was returned to GEGR for modification to allow higher temperature and pressure operation.

After the end of Phase I testing, it was found that there was some discoloration of the process gas exhaust line and softening of the silicone o-ring used to seal the module, as shown in Figure 33. The silicone o-rings were replaced with Kalrez[®] 4059 o-rings, which have a maximum operating temperature of 327°C.

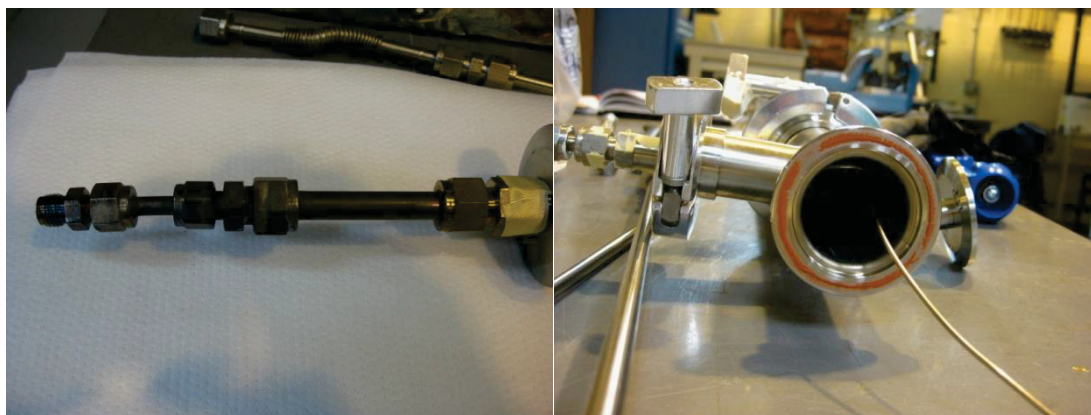


Figure 33. Tube 50 process exhaust line after elevated temperature testing.

The H₂/CO₂ selectivity was seen to decrease as the process gas pressure was increased above 50 psig. The pressure capability of the process tube circuit was increased to 1736 psig by replacing the flexible

steel hose on the process line inside the shell with a hose rated to higher pressure (Swagelok® SS-FM4SL4SL4-12). The pressure rating of the shell remains the same, 75 psig, as limited by the NW40 KF o-ring seals with overpressure rings.

As the operating temperature of the module was increased, the permeance of both H₂ and CO₂ increased. From 200°C to 250°C, there was no decline in selectivity. When temperature was increased to 280°C, H₂/CO₂ selectivity decreased (Figure 34). The change in membrane performance likely stemmed from the operating temperature approaching the T_g of the polymeric membrane material (270-280°C).

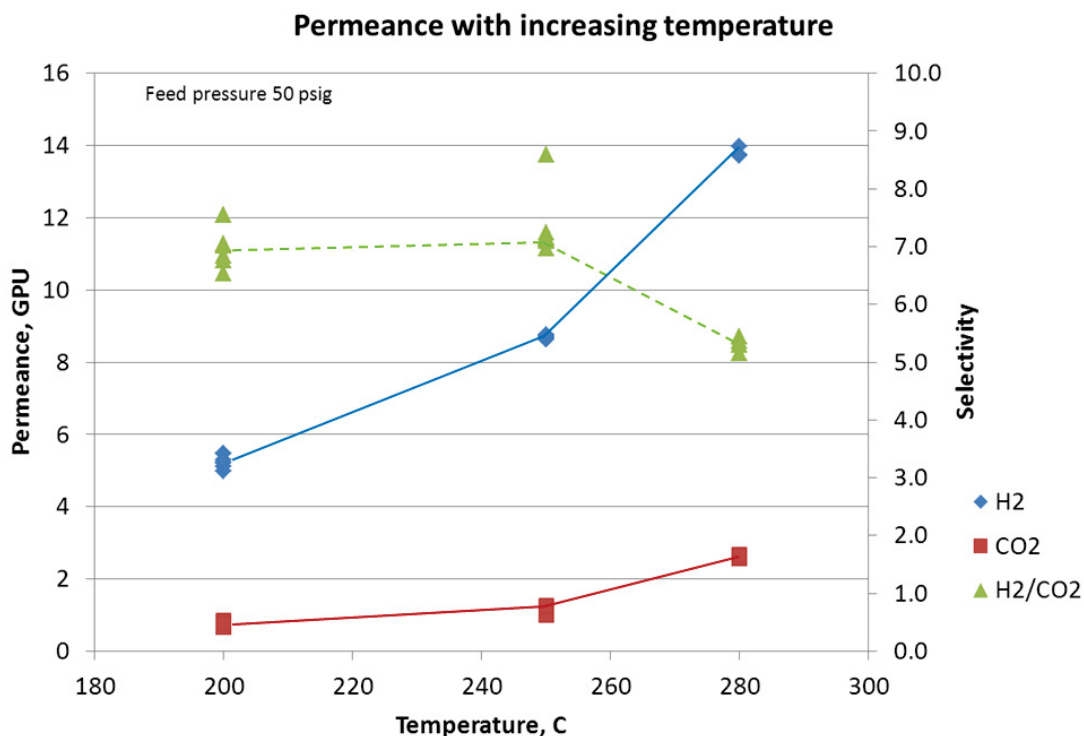


Figure 34. Performance of Tube 50.

The H₂/CO selectivity was found to decrease with temperature. This decrease was seen when the operating temperature was increased from 200°C to 250°C. The H₂/CO selectivity decreased further when operating temperature was increased to 280°C (Figure 35).

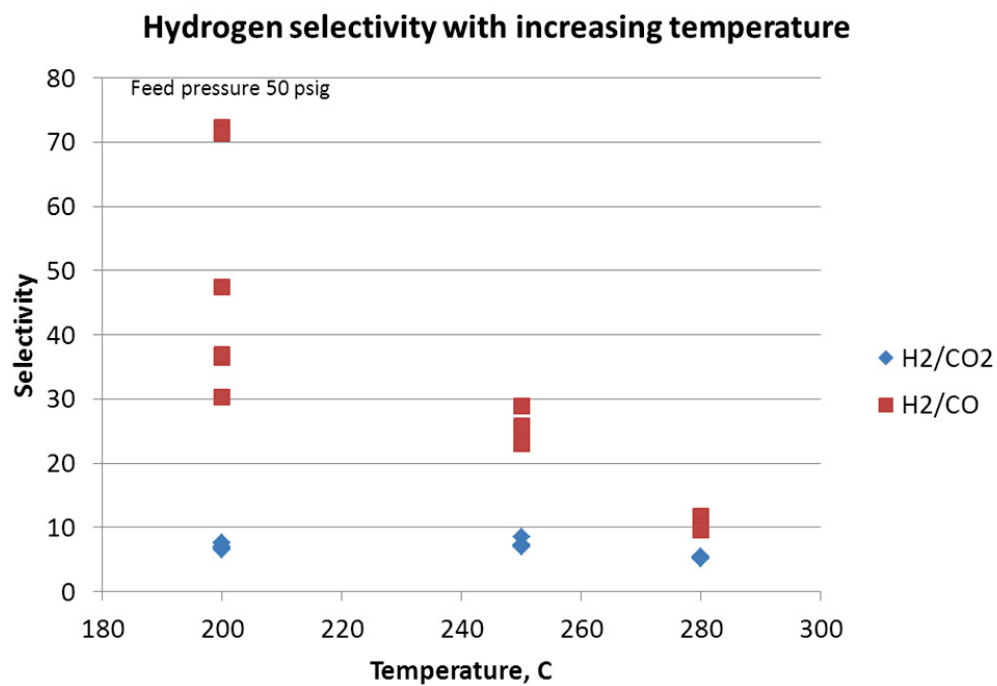


Figure 35. Performance of Tube 50.

The initial round of pressure testing was done with a pressure gradient between the feed and sweep side of the membrane from 0 to 50 psig. The gas was syngas with a composition of 44% H₂, 26% CO₂ and 28% CO. H₂/CO₂ and H₂/CO selectivity decreased as feed pressure was increased from 0 to 50 psig (Figure 36).

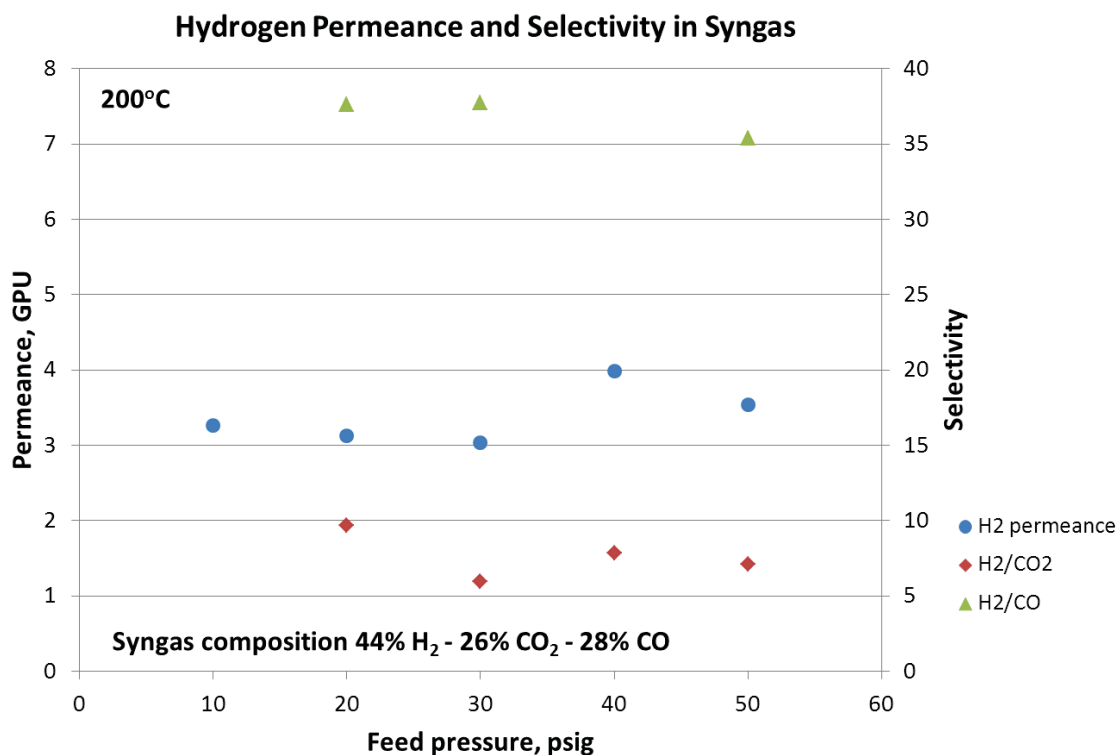


Figure 36. Performance of Tube 50.

To ensure that the decrease in selectivity was not due to a leak within the module, the module was modified and a second round of elevated pressure experiments were performed with feed pressures from 50 to 450 psig. This test was performed with a dry NETL gas with the composition 61% H₂, 38% CO₂ and 1% CO. In this test, the H₂/CO₂ selectivity decreased from 5 to 4 as feed pressure was increased from 50 to 450 psig. As feed pressure was increased, the permeate flow rate increased. The permeate flow rate increased enough that the H₂ fraction in the retentate was significantly lower than the H₂ fraction in the feed and the majority of the feed flow was going through the membrane. At a feed pressure of 300 psig, the feed flow rate was increased to compensate for this effect. At the maximum feed flow rate and feed pressure of 450 psi, the H₂ fraction in the retentate was close to the H₂ fraction in the feed at a feed pressure of 50 psig. This point could be directly compared to the 450 psig point (see Figure 37).

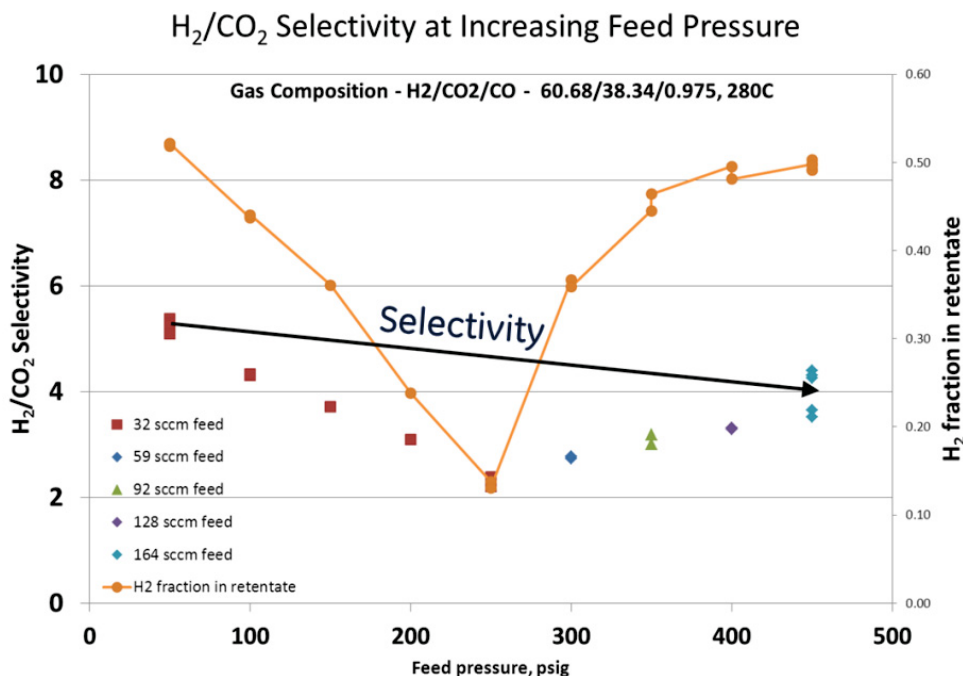


Figure 37. Performance of Tube 50.

Stage cut is the ratio of permeate flow to feed flow for a given component, and pressure ratio was the ratio of the feed pressure to the permeate pressure. As the feed pressure, and as a consequence the pressure ratio, increases the stage cut also increases. At 200°C, stage cut increased from 2 to 9 as the feed pressure was increased from 10 to 50 psig (Figure 38).

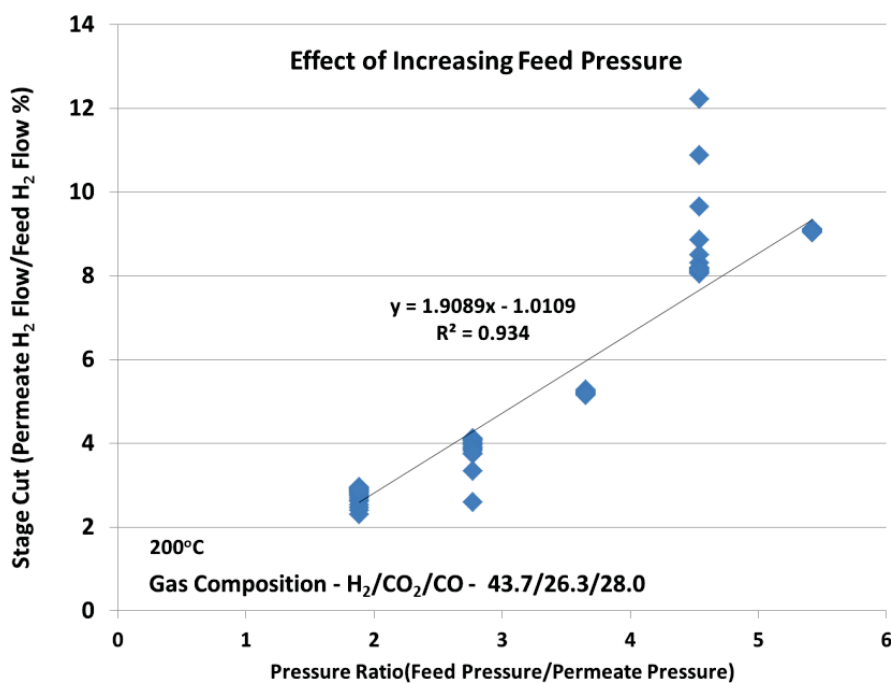


Figure 38. Performance of Tube 50.

At a feed pressure of 50 psig, the sample temperature was increased from 200 to 280°C. Stage cut increased from 10 to above 30 with an increase in temperature to 280°C (Figure 39).

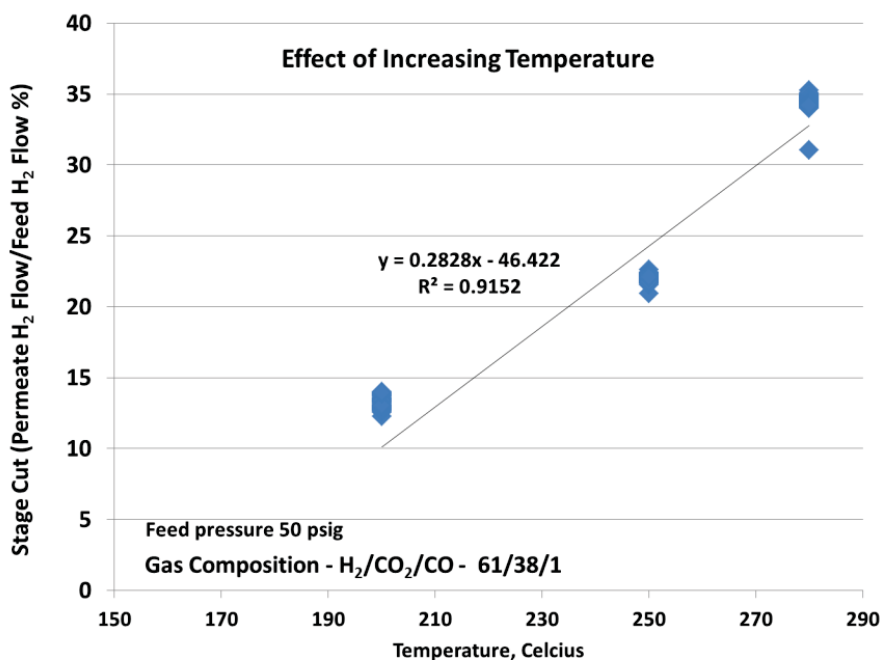


Figure 39. Performance of Tube 50.

At 280°C, an increase in feed pressure from 50 to 450 psig caused stage cut to increase from 35 to 43 (Figure 40).

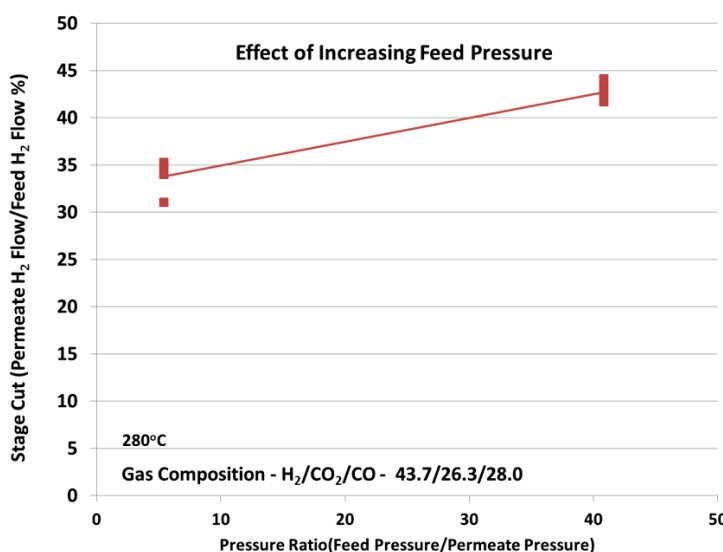


Figure 40. Performance of Tube 50.

Temperature increases up to the materials maximum operating temperature had a more significant effect on stage cut than pressure ratio increase. After 1,700 hrs of elevated temperature testing in varying syngas compositions, the membrane performance returned to and remained stable when the membrane module was returned to the original starting conditions (Figure 41).

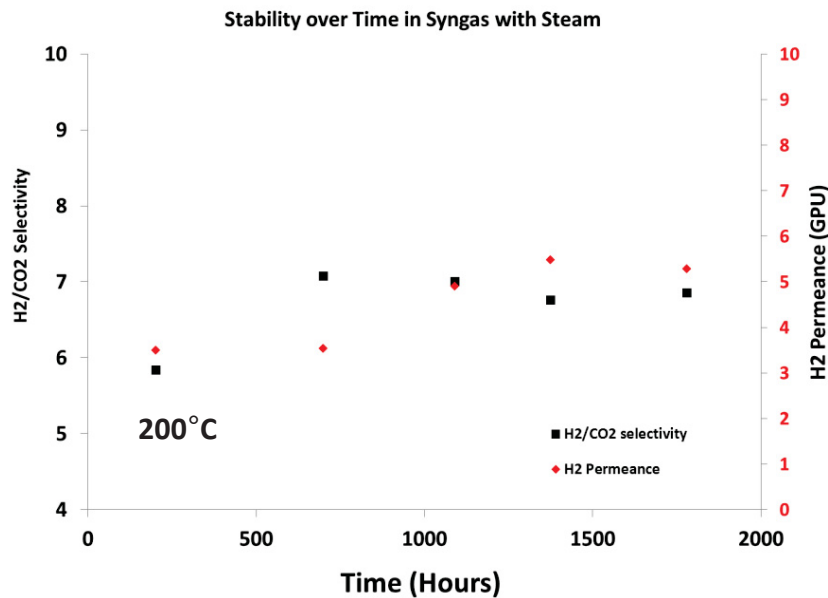


Figure 41. Stability of Tube 50 over time.

Economic Entitlement

A preliminary economic assessment was performed for the tube coating and development process. Figure 42 shows a cost breakdown according to the various cost contributors for the membrane module.

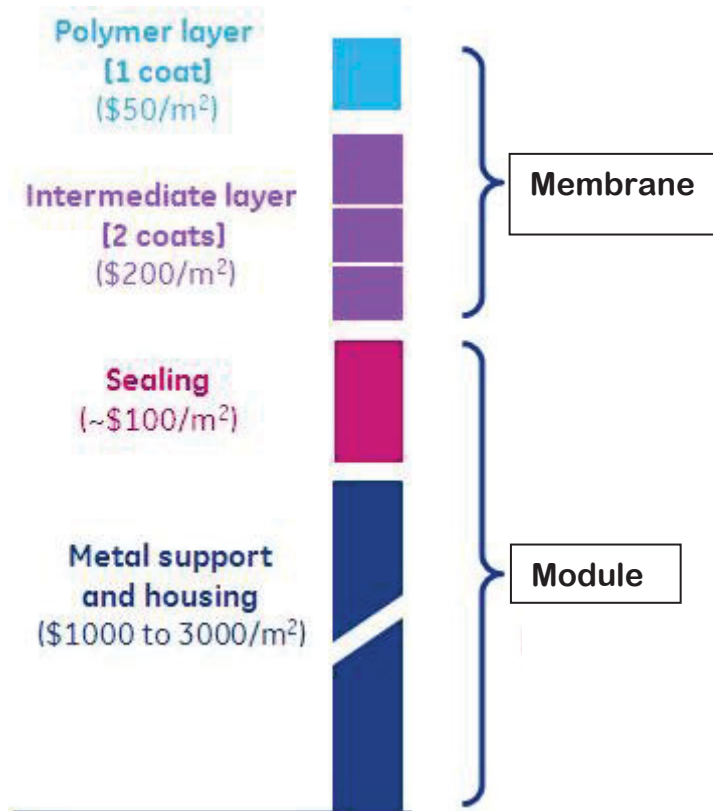


Figure 42. Cost breakdown for the membrane module.

The most significant cost factor was the porous metal support. Cost estimates vary depending on producer, but previous work by Pall suggests that the cost entitlement for a porous support is about \$1000/m². The housing and valving costs will vary, depending on the exact design module design. Engineering approximations typically assume the module costs are 100% of the elements.

Sealing costs were estimated at about \$100/m². This estimate was strictly a placeholder value, and will be sensitive to the type of seals, the form factor (length) of the membrane elements, and the materials of construction of the module housing.

The initial estimate for the slurry-casted intermediate layer was \$200/m². This estimate assumed that two coats were required to meet the membrane performance targets. The costs were further broken into estimates for energy and processing costs (\$40/m²/coating), raw material costs (\$30/m²/coating) and

labor (\$30/m²/coating). Finally, costs for the polymer coating layer were estimated by considering energy and processing costs, raw materials, and labor. The combined cost for a single polymer layer was \$50/m².

Together, the costs of the intermediate layer and polymer layer were estimated to be around \$250/m². This was a fraction of the cost of the support, module packaging, and seals. The significant contribution from the porous metal supports suggests that alternate supports such as polymeric hollow fibers, may offer significant cost advantages, assuming the technical manufacturing challenges can be solved. The development of polymeric polyimide hollow fiber membranes was added to the project work scope at no cost addition and is described in a separate section.

Summary

The H₂ selective polymer material was selected based on gas permeance experiments with various polymer films (Klaehn, 2008, CO₂ Separation Using Thermally Optimized Membranes: A Comprehensive Project Report.;Klaehn, 2011, High Temperature Gas Separations Using High Performance Polymers, In Inorganic, Polymeric and Composite Membranes: Structure, Function and other Correlations, Eds.). Initial experimental work at GE Global Research was performed on 0.5 in. button samples composed of α -Al₂O₃ supports with γ -Al₂O₃ intermediate layers and polyimide membranes (Polishchuk, 2012, Supported Polyimide Membrane for Gas-Separation). The permeabilities of these composite membranes were in good agreement with those measured on film samples of the same polymer. Hence, the polymer solution coating and curing process was developed to create defect-free membrane layer on porous stainless tube structures. Future work should focus on evaluating other bond coat layer materials to allow further reductions in membrane thicknesses.

The Team's primary goal was to successfully create a H₂/CO₂ selective, defect-free 20 cm VTEC polyimide coated membrane and sealing methods to enable high temperature, high Δp module testing under coal syn gas conditions. However, the membrane coating layer was thick (1-5 μ m) with a H₂ permeance \approx 10 GPU. The target membrane H₂ permeance for the coal-to-ammonia process was estimated to be between 500-1000 GPU. The Team has successfully demonstrated on 1/2" button samples that defect-free performance with high permeance can be achieved. Future work must focus on transitioning the bond-coat or secondary intermediate layer formation on tubular structures to achieve thinner membrane coatings leading to higher permeances.

The Team successfully demonstrated performance of 20 cm H₂ selective tubular membrane inside a module. Future work should focus on the scale up of the process to full scale modules (1 meter or greater) and employing multiple coated tubes in a module. Two 20 cm polymer coated composite membrane tubes (Tubes 50 and 51) encased individually in larger modules with a shell-and-tube design for testing at WRI under coal derived syngas. Tube 50 successfully completed 1000 hours of continuous testing under coal derived syngas streams of various compositions. The module was tested up to its maximum temperature and pressure rating of T = 200 °C and p = 90 psi. The modules were returned to GEGR for retrofit to increase the maximum temperature and pressure rating of the module to T = 300°C and p = 400 psi. The retrofitted modules wereshipped to WRI for further testing under syngas conditions for an additional 700 hours (total testing time of continuous on stream testing was 1,700 hours). Table 22 provides a summary of all of the tests conducted at WRI.

Table 22. Summary of the membrane module testing parameters.

| | | |
|---------------------|---|---|
| Membrane properties | Parameter | value |
| | Material(s) of fabrication for selective layer | Polymer |
| | Material(s) of fabrication for support layer (if applicable) | metal/ceramic |
| | Selectivity of key gas components for pre-combustion technology (Permeance of fast gas [GPU]/Permeance of slow gas [GPU]) | H ₂ /CO ₂ = 7-9 |
| | | H ₂ /CO = 40-60 |
| | | H ₂ O/H ₂ = 7-8 |
| | Type of selectivity measurement (ideal or mixed gas) | mixed |
| | Pressure normalized flux for more selective gas component (GPU) | P _{H2} = 3-5 GPU @ 6 bar |
| | Syngas composition (vol. %) | H ₂ =30.6, CO ₂ =18.4, CO=19.6, H ₂ O=30.0, CH ₄ =1.4 |
| | Maximum H ₂ S exposure (ppm) | 150 |
| | Maximum temperature (°C) | 280°C |
| | Lab-scale testing under simulated syngas without significant performance degradation (hours) | 24 |
| | Bench-scale testing under coal syngas without significant performance degradation (hours) | 1700 |
| | Membrane area (cm ²) | 45 |
| | Maximum pressure differential achieved without significant performance degradation or failure (bar) | 30 |
| Module Properties | Module configuration (hollow-fiber, spiral-wound sheet, shell-and-tube, plate-and-frame, other) | Shell-and-tube |
| | Packing density (m ² /m ³) | - |
| | Pressure drop (bar) | - |
| | Estimated cost of manufacturing and installation (\$/m ²) | 1500-2000 |
| Product Quality | CO ₂ purity (Retentate - vol. %) | 20-40 |
| | H ₂ purity (Permeate - vol. %) | 90-95 |
| | CO ₂ recovery (vol. %) | > 90 |

SECTION 4

DEVELOP MANUFACTURING PROCESSES FOR SUPPORTS WITH DEFECT-FREE INTERMEDIATE LAYERS AND MEMBRANE MODULES (POROUS SUPPORTS)

Background Analysis to Module Design and Development

Lab Scale Module Design and Development

Under this task, a 1-m²-long small-scale module was designed to provide a path towards scale-up of production. Initially, a laboratory-scale module was designed. This model can be set-up and tested on a table, but withstands operational syngas conditions (pressures, temperatures, etc.). Following a literature survey, various design embodiments were evaluated to help select a form factor that can be adapted for the membrane module. Previous module designs used for a range of technologies—such as heat exchangers, solid-oxide fuel cells, and water purification—were examined. A trade-off analysis was performed between three broad possible design concepts: tube and shell, planar, and monolithic (similar to that used in catalytic converters). These designs were evaluated for their structural robustness/durability, the processability of their coating, the complexity of sealing/packaging required, and their scalability, cost, ease of repair, etc. A tube-in-shell design was deemed to be optimal for the membrane module, due to lower bending stresses, reduced sealing areas, and ease of processing. A preliminary module design was conceived, and analyses (analytical, computational, and experimental) were performed to optimize the design and mitigate risks of mechanical failure.

Description of Module Design Concepts

Tube-and-shell Design

Tubular designs typically consist of tubes enclosed in shells/pressure vessels, such that the separating membrane is coated on the inside or outside of porous tubes, with the syngas and sweep gas flowing on either side of the tube. Figure 43 shows a proposed single-tube module. An internally coated porous stainless steel tube (single channel or multi-channel) is attached to two metallic flanges on either end via appropriate seals. The flanges are then welded to a tubular vessel, creating a chamber through which sweep gas flows. Two hemispherical caps are welded onto either side of the tubular vessel, creating a chamber to help flow the syngas through the membrane-coated porous tube. Inlet and outlet ports (not shown in the figure) help feed the syngas and sweep gas through the fittings. The syngas/sweep gas may be flowed on either side of the tube (as co- or counter-flow). The module geometry can be optimized to the operational conditions (temperatures, pressures, flow rates, etc.) via a range of modifications. Figure 44 shows a method for scaling up production via multiple tubes in a vessel.

The key advantages of this family of designs are:

- Efficient flow characteristics
- Structurally robust/durable due to tubular geometry
- Minimal sealing areas
- Economical manufacturing
- Ease in scaling up.

However, compared to planar designs, these designs are prone to greater coating defects.

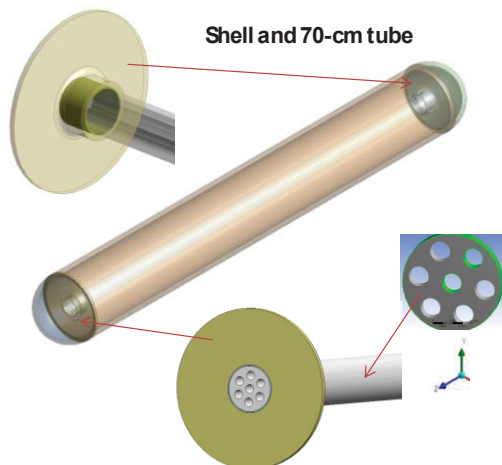


Figure 43. Single-tube module.

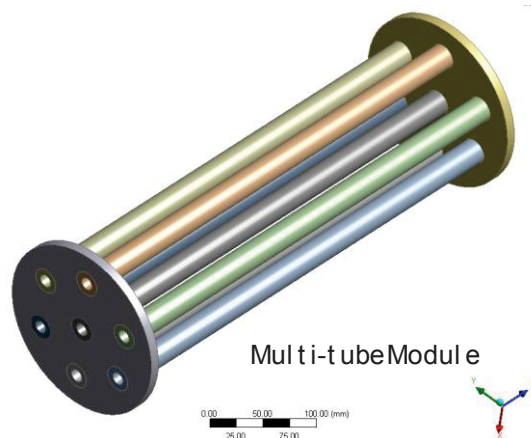


Figure 44. Multi-tube configuration.

Planar Design

Planar designs consist of coated planar substrates, housed in metallic assemblies, that provide flow paths for the syngas and sweep gas on either side of the coated substrate (such designs are commonly used for solid-oxide fuel cells [SOFCs]). Chambers with flow fields are built on either side of the substrate. Appropriate spacers help separate and deliver the gases, and the assembly is brazed/sealed together. Repeating cells can be stacked up to increase production.

The key advantages of this design are:

- Minimization of coating defects, with defects easier to repair on the planar substrates
- Compact stackable design
- Choice of co-, cross, or counter flow.

However, the disadvantages are:

- Structurally weak due to planar substrates' being less resilient to bending stresses
- Flow characteristics that are complex and inefficient
- Extensive sealing areas, making the design more prone to failure and less economical.

Monoliths, similar to those used in catalytic converters and filtration, can also be chosen as substrates. Such designs are highly compact; however, the complexities of coating and packaging such geometries preclude their being a viable option for the current application.

Bench-top-module Design

Figure 45 shows a schematic of a tubular module that can be built using off-the-shelf components. A porous SS tube coated with the functional layers (Figure 42) is attached to dense stainless steel tubes on either end by an appropriate seal (e.g., epoxy). These dense stainless steel tubes are passed through Conax flanges as shown and help provide the flow path for feed gas and syngas. Each of the Conax flanges is threaded into its ring joint (RJ) flange. The Conax flanges utilize grafoil or Viton seals at the interface between the dense stainless steel tube and the metal housing. The interface is secured by applying compressive pressure onto the grafoil seal. The RJ flanges are bolted onto weld-neck flanges on either end with a stainless steel oval ring seal between them. A stainless steel vessel/tube is welded between the two-weld neck flanges as shown. Ports into the stainless steel vessel will provide for the flow of the sweep gas. The entire module will rest on a support that will allow for thermal expansion/contraction of

the module. The stainless steel tube, weld neck, and RJ flange specifications were chosen to follow ASME pressure vessel and AMSE B16.9 flange protocols with a large factor of safety. The materials for the vessel and flanges can be chosen to help reduce the thermo-mechanical stresses and withstand the corrosive environment of syngas (Alloy 625 is recommended). The vessel was designed to withstand pressures exceeding ~450 psi (30 bar) and temperatures exceeding ~300°C.

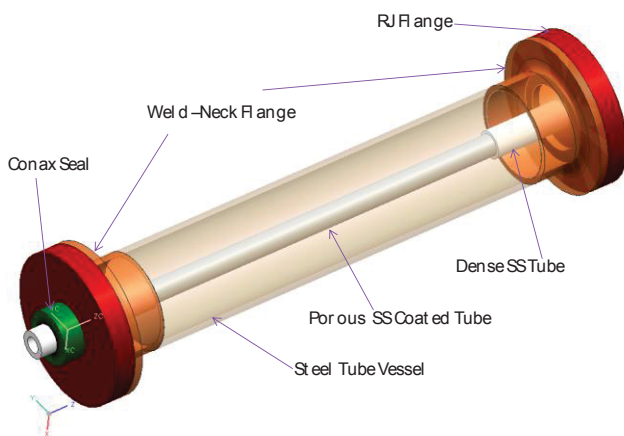


Figure 45. Bench-top-module design for laboratory testing.

Mechanical Risks Assessment and Mitigation

Risks Enumeration

Efforts were made to methodically enumerate, rank, assess and mitigate risks related to mechanical failure. A risk review workshop was conducted with external reviewers (project leaders from various GE businesses), and a comprehensive list of risks was identified and ranked at a component level (coating, substrate etc.), module level (tube and shell design), and system level. The list accounted for failures arising from various thermal, mechanical, and environmental factors, such as gas pressures, temperatures, residual stresses, chemical attacks, vibrations, etc. The ranking methodologies are described in Table 23. Based on the rankings, mechanical risks of the greatest and most immediate concern were identified as the risks related to the membrane and seals failures at operational conditions. Hence, analyses and experiments were being devised and performed to assess and retire these risks.

Table 23. Mechanical risks enumeration and ranking for shell and tube design module.

| Risk | Probability | Impact |
|---|-------------|--------|
| Component level | | |
| Selective Membrane and Intermediate layer | | |
| Coating/Intermediate layer failure/tearing/rupture due to gas pressure | L | H |
| Delamination between coating and int. layer due to gas pressure | L | H |
| Coating/Int. layer debond/delam from substrate due to gas pressure | L | H |
| Drop in failure pressure as the length is scaled up | U | H |
| Coating/Intermediate layer failure/tearing/rupture due to CTE mismatch | L | H |
| Delamination between coating and int. layer due to CTE mismatch | L | H |
| Coating/Int. layer debond/delam from substrate due to CTE mismatch | L | H |
| Pinholes exacerbating other failure modes | L | H |
| Coating/Intermediate layer degradation due to high temp. creep | U | H |
| Chemical degradation of coating/Intermediate layer | L* | H |
| Coating/Intermediate layer failure/fatigue due to thermal cycling (cumulative damage from CTE mismatch) | L | H |
| Coating/Intermediate layer failure/fatigue due to pressure spikes (pressures drops from both sides) | L | H |
| Coating/Intermediate layer failure due to thermal shock | U | |
| Coating/Intermediate layer wear due to gas flow | U | |
| Polymer plasticization | U | |
| Seals (swagelok) | | |
| Seals failure due to gas pressure | L(SL) | |
| Seals failure due to CTE mismatch | L | |
| Seals failure due to high temperature creep | | |
| Seals failure/fatigue due to thermal cycling (cumulative damage from CTE mismatch) | L | |
| Seals failure/fatigue due to pressure spikes(shutdowns) | L | |
| Seals failure due to thermal shock | U | |
| Wear of seals due to gas flow | U | |
| Seals failure due to vibration-induced mechanical fracture | U | |
| Failure due to misalignment | L | |
| Corrosion/Degradation of seals | | |
| H2 embrittlement | | |
| Polymer damage due to excessive temperature | | |
| Substrate | | |
| Substrate failure/buckling due to gas pressure | L | H |
| Substrate failure due to CTE mismatch | L | H |
| Substrate clogging/failure due to chemical degradation | | |
| Substrate failure due to thermal shock | L | H |

| Risk | Probability | Impact |
|--|-------------|--------|
| Substrate wear due to gas flow | L | L |
| Pressure vessel/Housing/Flange | | |
| Vessel/housing failure due to gas pressure | L | H |
| Vessel/housing failure due to CTE mismatch | L | H |
| Vessel/housing failure/fatigue due to pressure spikes (shutdowns) | L | H |
| Weld joints in the pressure vessel/housing | | |
| Weld joint failure due to gas pressure | L | H |
| Weld joint failure due to CTE mismatch | L | H |
| Weld joint failure/fatigue due to pressure spikes (shutdowns) | L | H |
| Module level (interacting components) | | |
| Failure/buckling due to gas pressures | L | |
| Failure/buckling due to CTE mismatch (tubes/seals/housing) | L | |
| Failure/buckling due to temperature gradients | U | |
| Failure/buckling due to pressure gradients | | |
| Low cycle fatigue due to pressure profiles | U | |
| High cycle fatigue due to pressure profiles | U | |
| failure due to flow induced vibrations | U | |
| Environment induced vibrations | U | |
| Corrosion (stress, chemical..) | | |
| Any particulates in gas causing impact damage? | | |
| System level | | |
| Maintenance | | |
| Turndowns/valves | | |
| replaceability/repairability | | |
| Table Key: PROBABILITY High (H) - Known risk with mitigation plan needed or not known yet if it is a risk Medium (M) - Known risk with mitigation plan identified Low (L) - Not a risk or risk already mitigated IMPACT High (H) - Severely affects operation and requires shutdown Medium (M) - Affects operation, but can be tolerated or can be repaired without shutdown Low (L) - Does not affect operation *Newly updated | | |

Hollow Fiber Moldules for Coal SynGas Streams

When using the VTEC polyimide for an industrial gas stream, an obvious issue is its ability to handle large gas throughput and giving an effective hydrogen gas separation. This requires a high capacity module that has a high surface area. During FY 2011 and FY 2012, hollow fiber development became a major part of the project because they are considered to be the best support design of choice in high volume applications. Hollow fibers provide the optimum geometry for high production rates and ease of

module formation while providing high surface area and membrane packing density compared to flat sheets. The selected polymer for highly selective H_2/CO_2 separations should be commercially available, easily processed with high mechanical and chemical stability and must be formulated into an asymmetric structure with a highly porous support and a thin selective skin layer. In the project, the Team focused their efforts on developing defect-free polyimide-based asymmetric hollow fiber membranes for hydrogen purification from syngas streams.

Determination of spin dope composition

In hollow fiber membrane creation it is desired to choose a one-phase dope composition in close proximity to the binodal curve to ensure rapid phase separation and high porosity of the membrane. Figure 46 shows the schematic representation of a binodal curve used to determine the spin dope composition.

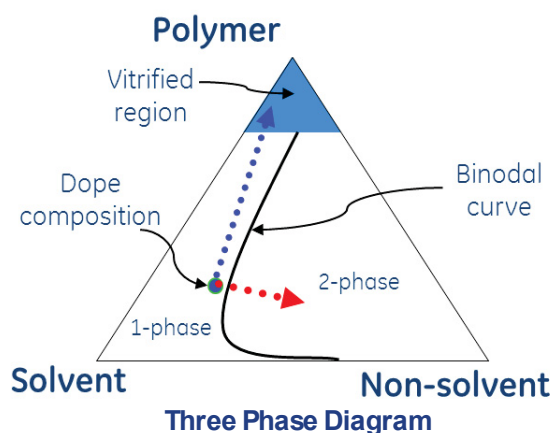


Figure 46. Schematic representation of a binodal curve used to determine core layer spin dope composition.

In the cloud point technique to determine the binodal curve, one-phase dopes in small quantities (15 ml) were made with varying amounts of polymer solution (VTEC PI-80-051)/solvent (THF)/non-solvent (ethanol)/additive (polyvinylpyrrolidone; PVP). These dope samples were then visually observed as shown schematically in Figure 47 to determine a 1-phase solution (transparent and homogenous), a cloudy solution (translucent) indicating the onset of phase separation and a 2-phase solution (non-homogenous and phase separated). The ‘cloudy’ dope solution composition was defined as the practical binodal point.



Figure 47. Schematic representation of cloud point study to determine spin dope composition.

The Generation 1 (Gen-1 fibers) dope composition in close proximity to the cloud point having appropriate viscosity (determined by viscosity measurements) was selected for scale-up (500 mL dope mixtures). From the cloud point experiments and observations during the fiber spinning process, two sets of dope compositions were developed as shown in Table 24.

Table 24. Spin dope compositions identified for hollow fiber membrane creation (units in wt. %)

| ID | Polyamic acid solution | THF | PVP | Ethanol |
|-------|------------------------|------|-----|---------|
| Gen-1 | 80.1 | 10.9 | 6 | 3 |
| Gen-2 | 89 | 0 | 8 | 3 |

A mixture of solvent and non-solvent, referred to as the bore fluid (or internal coagulant) was also prepared by adding measured quantities of solvent and non-solvent. The bore fluid composition was carefully tuned as per spin dope formulation. Gen-1 and Gen-2 bore fluid compositions used in this work are summarized in Table 25. Bore fluid compositions of 95/5 wt. % (Gen-1) and 70/30 wt. % (Gen-2) NMP/Water mixture were used (see Appendix G).

Table 25. Summary of bore fluid compositions (units in wt. %).

| Bore Fluid | NMP | Water |
|------------|-----|-------|
| Gen-1 | 75 | 25 |
| Gen-2 | 70 | 30 |

For the Gen-2 fibers, the spinning temperatures (spinneret, pumps and transfer lines temperature) were adjusted to 40°C and were found to give appropriate viscosity to spin hollow fibers. The adjusted viscosity led to elimination of the macro voids from the fiber morphology as shown in Figure 49 (GE ID: spin 4). The polyamic acid hollow fibers have a desired porous uniform sub-structure with a thin outer skin layer. Fibers were found to be strong and could be easily collected on to the take-up drum with collection rates up to 70 m/min possible, with typical collection rates of 30 m/min. Typically, take-up rates of 60 m/min are desired for industrial scale operations. Fibers spun at a low dope flow rate (180 to 300 mL/hr) and correspondingly low bore fluid flow rate (60 to 100 mL/hr) were found to be more concentric possibly due to a lower die swell at the nozzle annulus. An air-gap of 10 cm was found to be optimum.

Even though the dope composition and spinning conditions were optimized, the nozzle alignment did get disturbed due to the high viscosity dope fluid. Once misaligned it was difficult to align the nozzle once the spinning run was underway. The nozzle misalignment could be resolved by the fabrication of next generation nozzles which can sustain the high dope pressure build-up without leading to bore needle misalignment. Nozzle design, however, was outside the project's work scope. Fibers with a misaligned bore structure are shown in Figure 49. The nozzle misalignment primarily affected the concentricity of the fiber, leading to variation in the fiber wall thickness as shown in Figure 49. The solvent exchanged polyamic acid hollow fibers were then stepped to imidization or curing. Three spin runs (GE ID: Spin 3, 4, and 5) were completed using Gen-2 spin dope and bore fluids compositions. GE ID: Spin 4 hollow fibers were found to be circular in shape, concentric with the desired porous substructure and thin skin layer. GE ID: Spin 5 hollow fibers were found to be slightly non-concentric due to misalignment of the nozzle bore needle.

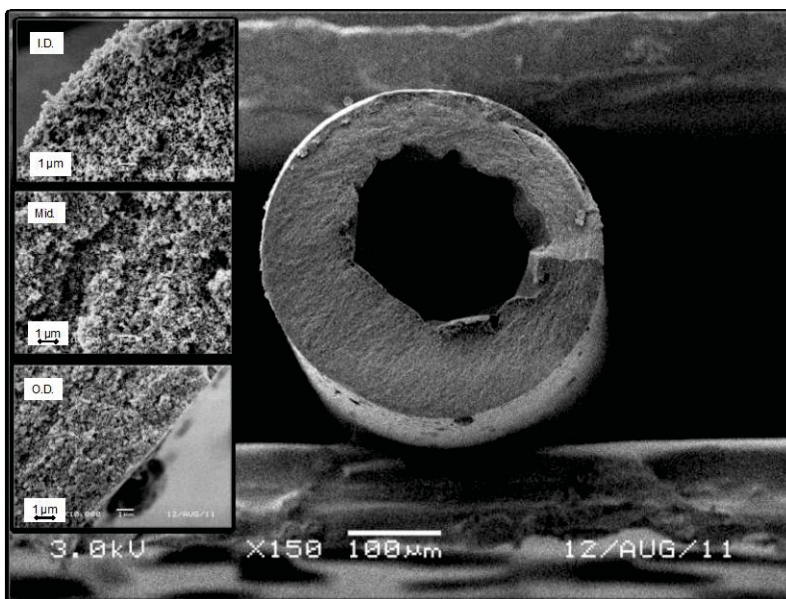


Figure 48. Cross-section SEM image of Gen-2 polyamic acid hollow fiber membrane. The fibers were found to have a nice open cell uniform morphology with a thin-selective skin layer. Macrovoids were eliminated by carefully tuning the fiber morphology (GE ID: Spin 4).

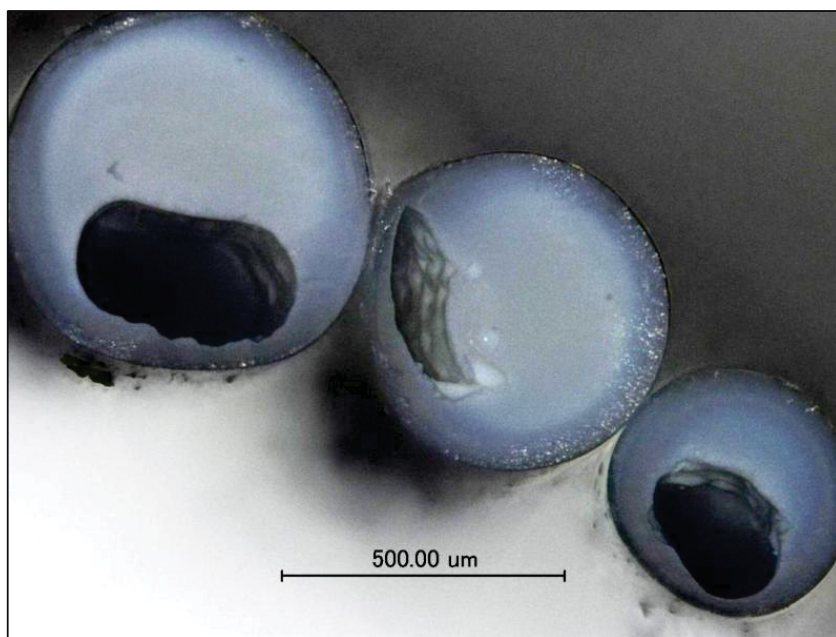


Figure 49. Cross-section optical image of the hollow fibers from the same spin state formed with a non-concentric bore possibly due to nozzle bore needle misalignment (i.e., spun under identical conditions).

Curing Polyimide Hollow Fibers Testing and Development

Curing Process Development

The solvent exchanged VTEC polyamic acid hollow fibers were imidized to form a thermally and chemically robust polyimide hollow fiber membrane. Upon discussion with INL, a thermal imidization

method was chosen due to simplicity of use and scale-up compared to chemical imidization. The baseline imidization protocol was obtained by flat sheet film studies conducted collaboratively by the Team (Appendix G).

Imidization of the fibers is affected by a number of factors including: the type of atmosphere, amount of water present, solvents/byproducts removal rate, heating rates, and temperatures and soak times. Due to time constraints, a thorough examination of these factors was not possible. However, some optimization of the curing process was made possible by thermogravimetric (TGA) analysis, nuclear magnetic resonance (NMR) spectroscopy, infrared (IR) spectroscopy, and scanning electron microscopy (SEM) studies. A bench-scale fiber curing oven was designed and fabricated to scale-up the curing protocol allowing imidization of multiple polyamic acid hollow fiber strands of up to 1 m in length (see Appendix G).

Effect of Temperature on Hollow Fiber Curing

Fibers were cured on either a graphite shelf or a quartz tray positioned near the middle of the oven (see Appendix G). The effect of temperature on the pore structure of the hollow fibers was studied using Spin 4: State 8 fibers that were cured at 150°C for 24 hours and imidized at 250°C for three days. The pore structure of the fibers did not change significantly during the drying phase. The most significant changes occurred during the imidization phase, with the bulk of the fiber becoming denser, as shown in Figure 51, and more ductile. The densification led to a decrease in gas permeance. However, the pores on the inner diameter actually increased in size and retained their open structure, as shown in Figure 52. It was not immediately clear why the pores on the inner diameter retained an open pore structure, but if such a microstructure could be promoted throughout the bulk of the hollow fiber, higher permeances could be achieved.

Modification in hollow fiber features during curing

As the VTEC polyamic acid hollow fibers cured they become darker in color and smaller in diameter with Spin 2: State 2 fibers. The as-spun fibers were white or slightly off-white in color. Drying resulted in some shrinking of the hollow fiber, but most of the changes occur during imidization. Fibers that were imidized for only 30 minutes shrunk to ~75% of their original size, but did not change color significantly. As the fibers were held at the imidization temperature (250°C) for longer and longer times, they continued to shrink and become darker in color, changing from yellow to bronze to black. SEM images provided additional insight into microstructural changes that occurred with the hollow fibers during curing.

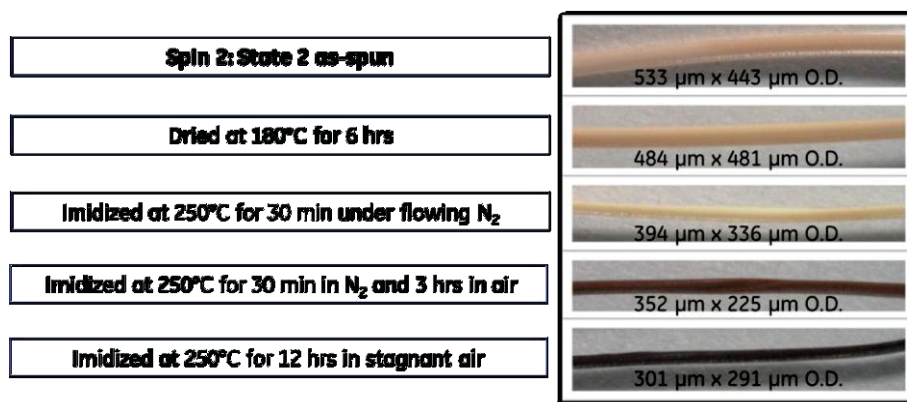


Figure 50. Images of Spin 2: State 2 hollow fibers at different stages of cure.

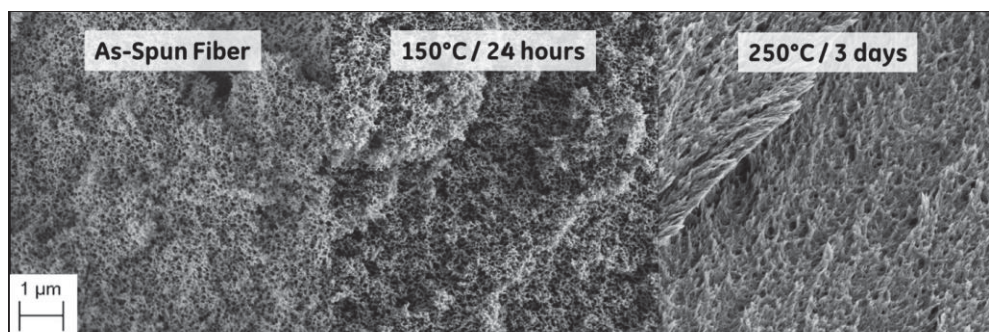


Figure 51. SEM images of the cross-section of the middle of hollow fibers (Spin 4: State 8) exposed to maximum temperatures of (a) 30°C, (b) 150°C, and (c) 250°C.

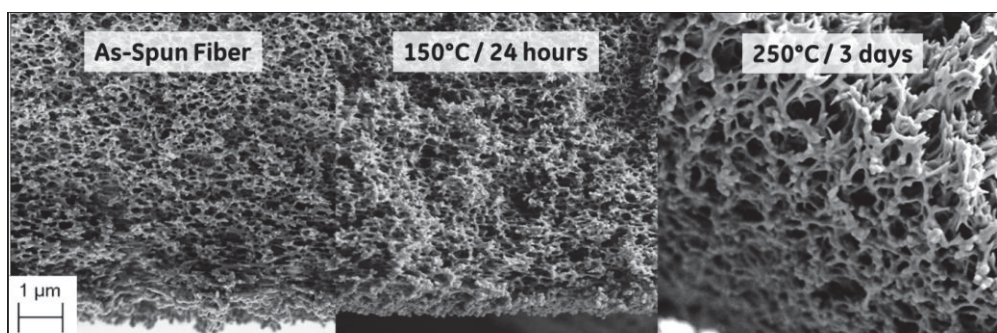


Figure 52. SEM images of the cross-section of the inner diameter of hollow fibers (Spin 4: State 8) exposed to maximum temperatures of (a) 30°C, (b) 150°C, and (c) 250°C.

Effect of purge gas flow rate on hollow fiber curing

Previous experience with polyimide coatings on stainless steel tubes (Bonekamp, 1996, Chapter 6 Preparation of Asymmetric Ceramic Membrane Supports by Dip-Coating) showed that curing the VTEC 080-051 material in stagnant air led to a brittle, cracked polyimide film. It was hypothesized that excessive NMP or water produced during the imidization process was the cause. The cracking problem in the dense films was resolved by flowing gas through the tubes during the curing process. Hollow fibers go through an additional solvent exchange process to remove the NMP solvent prior to curing. However, water is still produced during the imidization process, the removal of which could be aided by a flowing atmosphere.

Although not confirmed with multiple samples, there was anecdotal evidence that higher flow rates resulted in smoother membrane surfaces on the hollow fibers. The three sets of Spin 4: State 4 fibers that were cured at 230°C, 240°C, and 250°C were imaged with SEM. The fibers cured at 240°C had a lower flow of nitrogen (0.5 lpm, 0.15/min exchange rate) compared to the other two sets (3.6 lpm, 1.05/min exchange rate). This “low flow” set of fibers had a rougher surface texture than fibers cured at higher flow rates, as shown in Figure 54. The surfaces of the fibers cured with the higher flow rate were smooth with occasional defects or rough spots (Figure 53, Figure 52a, and Figure 53c). By comparison, the fiber cured with the low flow rate was highly textured over its entire surface (Figure 53b).

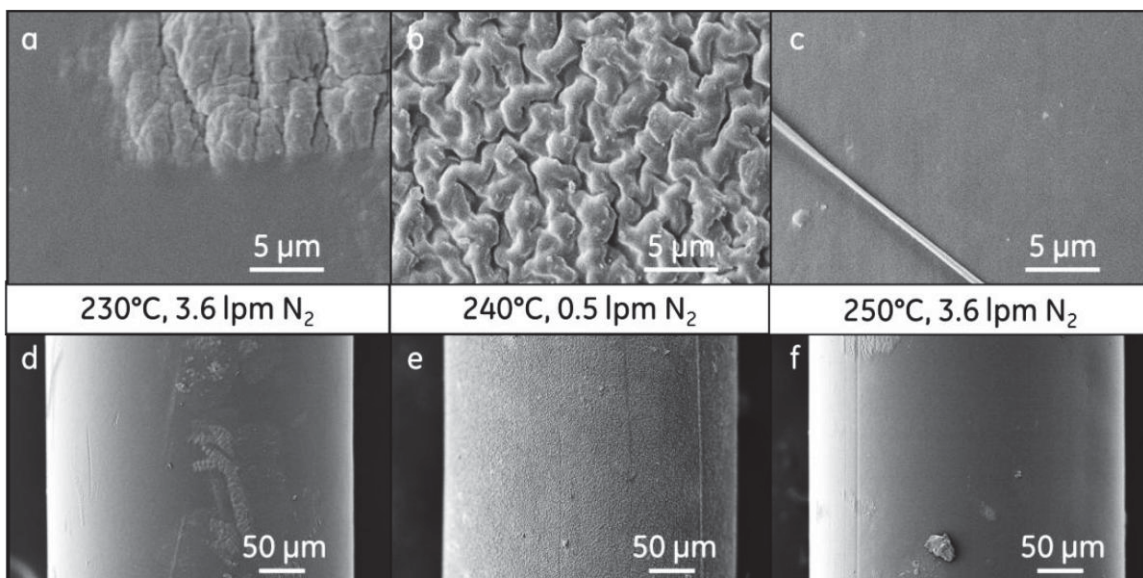


Figure 53. SEM micrographs of the membrane surfaces of hollow fibers (Spin 4: State 4) cured at the temperature and nitrogen flows specified. Micrographs a, b, and c were higher magnification images of micrographs d, e, and f, respectively.

Effect of environment on hollow fiber curing

The hollow fiber curing atmosphere also was observed to affect the pore structure and surface texture of the fibers. Poly(amic acid) fibers from spin4 : state 4 were exposed to steam (205°C, 240 psig, saturated atmosphere) for 89 hours. This pressure was representative of the partial pressure of H₂O that the membranes would ultimately be exposed to if used for pre-combustion separation in a gasification operation.

The experimental test protocol is described as follows. The autoclave was partially filled with water and heated to the desired temperature resulting in saturated or “wet” steam. The air inside the autoclave was then bled off so that a pure water environment was obtained. Using wet steam greatly simplified the control process since it was only necessary to make sure liquid water was present inside the autoclave to guarantee saturated conditions. The test stand was originally designed to hold button style membrane samples, but was also used to hold the hollow fibers. The fibers were placed inside the holding tabs to keep them from rolling off the stand and down into the liquid water. All of the parts inside the autoclave were made of 316 SST, except for the tabs which were made of nichrome ribbon tack welded to the ring stand. Temperature and pressure control capability were better than 0.1 PSI and 1°C.

When the fiber cross-section was imaged by SEM, the size of the pores was found to have increased, but dense areas also appeared, as shown in Figure 54. Since exposed to a temperature of 205 °C, it most likely had a low degree of imidization, while the majority of the structure still consisted of poly(amic acid) and some traces of PVP.

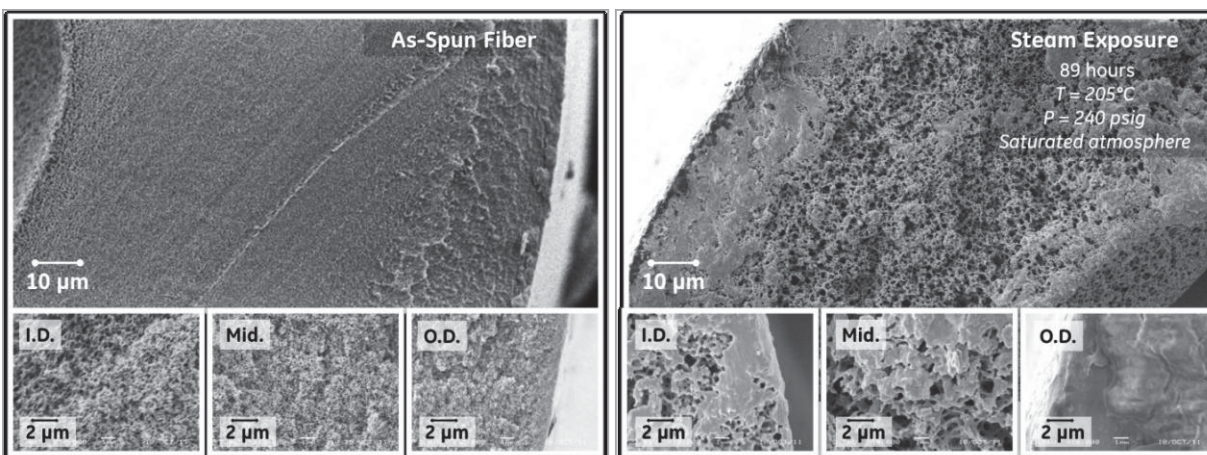


Figure 54. Spin 4 – SEM images of Spin 4: State 4 hollow fibers: as-spun (left), and after steam exposure (right).

Additional studies were performed in an effort to validate the effects of humidity on curing hollow fibers. Some of the hollow fibers (Spin 4) were thermally cured, and the fibers were investigated thermal processing pathways, so that the fibers' porosity was preserved. TGA analysis was performed on all fibers up to 250°C under a nitrogen atmosphere with and without humidity for all tests. Water vapor content was calculated between 2-4 vol% in gas stream (100% RH). The thermal tests were maintained at 250°C for 3 hours (dry and humidified) for all of the samples, except for Spin 4 State 1, which was tested for 24hrs in the humidified conditions. The data in Table 26 were obtained after 1 hour at a steady state of 250°C. Initial findings showed that wet gas streams do not significantly impact weight loss in the TGA after 3 hours. Even after 24 hours the hollow fiber's "State 1" percent weight loss difference is relatively close to the dry gas stream.

Table 26. TGA analysis: difference in percent weight loss at 250°C after 3 hours and 24 hours with and without humidity in a nitrogen gas stream.

| Time period (water composition) | State 1 | State 4 | State 5 | State 7 | State 8 |
|---------------------------------|---------|---------|---------|---------|---------|
| From 1 to 3 hrs. (dry) | 1.72% | 3.62% | 2.15% | 1.97% | 1.37% |
| From 1 to 3 hrs. (humidified) | 0.61% | 2.41% | 0.59% | 1.77% | 0.25% |
| After 24 hrs. (humidified) | 2.63% | N/A | N/A | N/A | N/A |

Optical microscopy and SEM were used to identify differences with the uncured and cured fibers under the various conditions described in Table 26. Figure 55 shows the optical micrograph with an interesting feature resulting from processing with a humidified gas stream for 3 hours (wet N₂), and these fibers are not as discolored when compared with those processed in a dry gas stream (dry N₂) for the same period of exposure. This suggests that the humidified gas stream does not affect the hollow fiber in the same manner as a dry gas stream. The SEM pictures of the various fibers show interesting trends with these processing parameters. Due to imidization of the polyamic acid, the most notable item is the densification/ shrinking of the hollow fibers after they are processed (Figure 56). However, a more important item is the loss of the internal porous structure in these fibers. After 3 hours of processing at 250°C (Figure 57), these fibers show that there is a difference between the dry and humidified gas streams. These images show the surface of the inner bore in the hollow fiber. Surprisingly, the humidified gas streams do show different porous structural features than the dry gas stream. However, the porosity appears to be somewhat compromised due to the processing temperatures when compared against the uncured fibers. The porous structure is still visible in the fibers processed with either dry or

humidified gas streams. These are very encouraging results for hollow fiber curing methods. It was concluded that curing with a humidified stream certainly has some advantages as discussed above.

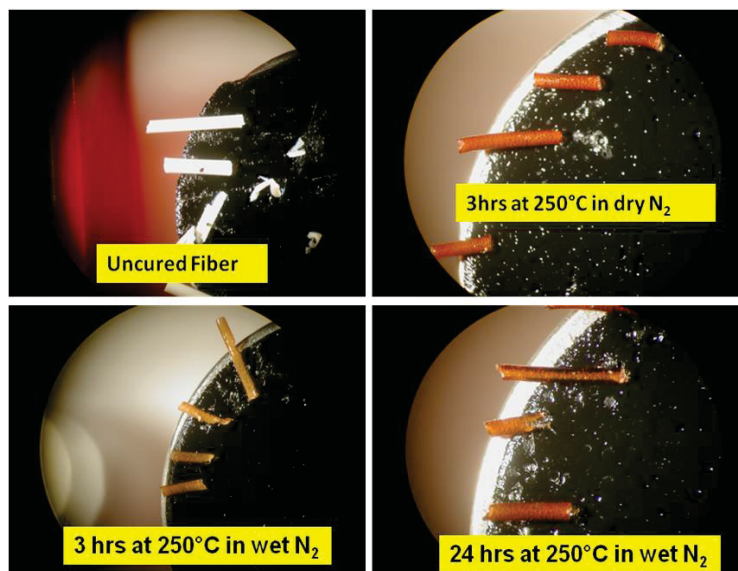


Figure 55. Spin 4: State 1 Optical microscope images of the various stages of hollow fiber processing.

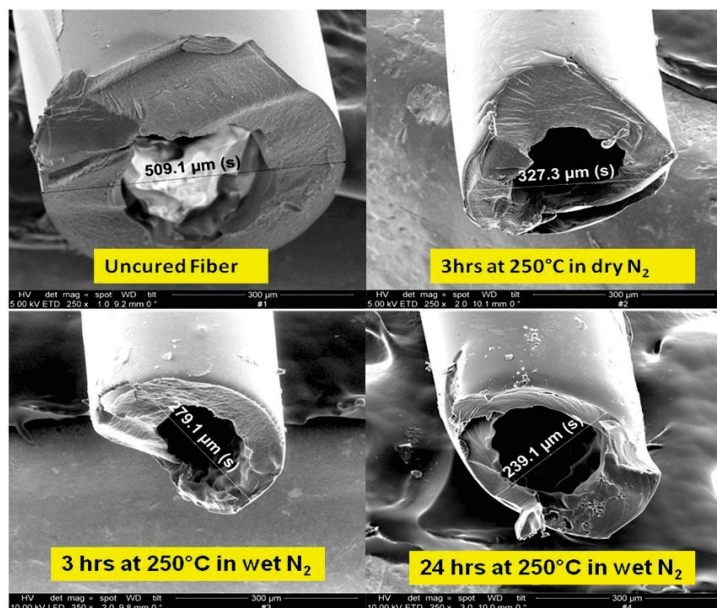


Figure 56. Spin 4: State 1 SEM images of the various stages of hollow fiber processing, external view of the fibers.

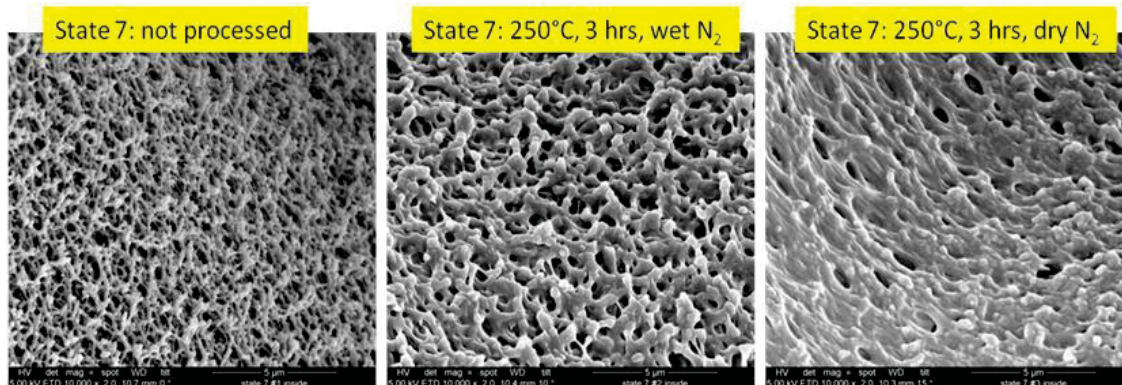


Figure 57. Spin 4: State 7 SEM images of the various stages of hollow fiber processing, internal bore (internal diameter) of the fiber.

Use of inert curing atmospheres was also considered. Early studies were performed on Spin 2: State 3 hollow fibers, which were not suitable for gas-separation membranes due to their large oblong pores and off-center bores. These fibers were cured at 250°C for 24 hours in either a nitrogen atmosphere or under vacuum. The fibers cured under the nitrogen atmosphere had a white layer of fine, sponge-like structure on their inner diameters, as shown in Figure 58. The spongy structure was very similar to the spongy structures observed in later fiber batches, which did not possess the undesired oblong pores. By comparison, the fibers that were cured under vacuum did not exhibit the fine spongy structures anywhere, as shown in Figure 59. Furthermore, the fibers did not retain their straight shape when cured under vacuum, instead they self-curved into a small ball, which was obviously is unsuitable for making hollow fiber modules for gas-separation. Fibers cured in nitrogen also took on curved shapes during curing, but remained relatively straight.

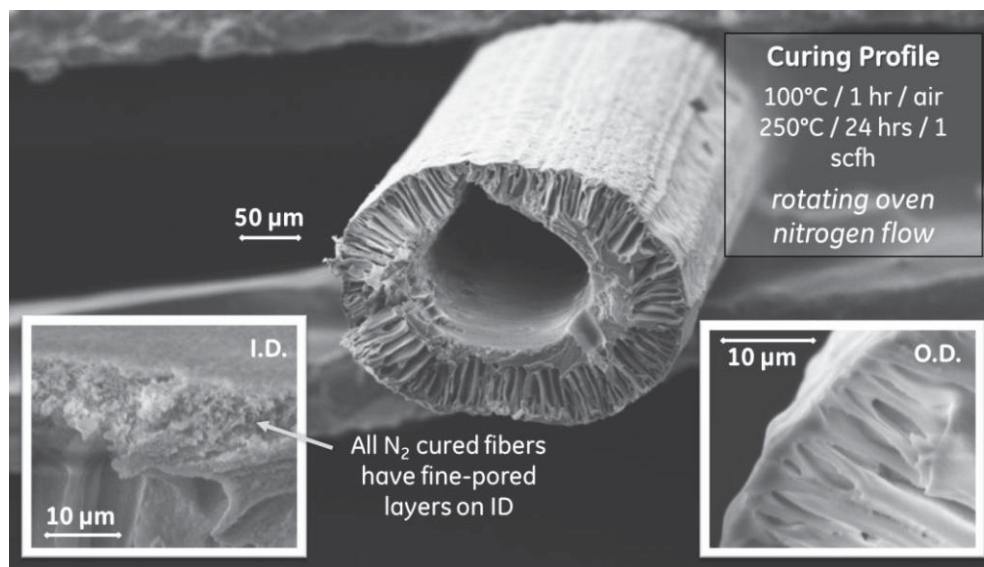


Figure 58. SEM images of a Spin 2: State 3 hollow fiber cured under nitrogen.

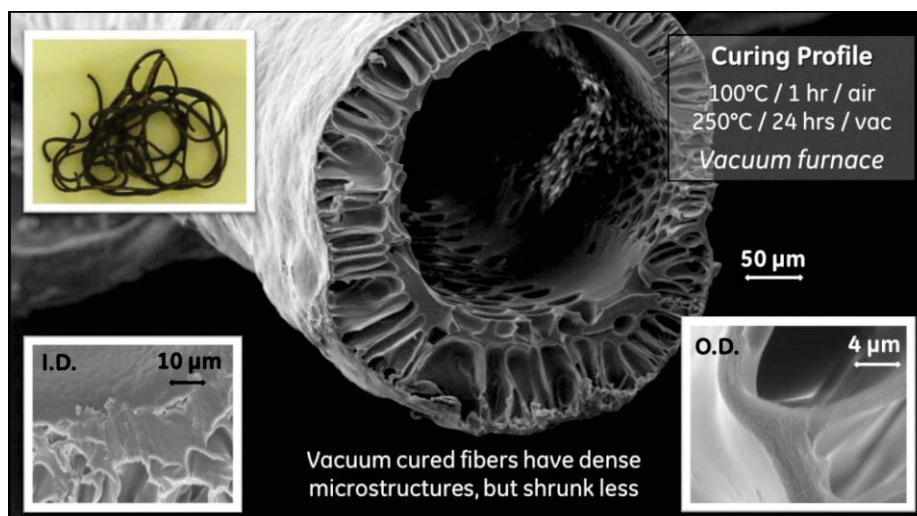


Figure 59. SEM images of a Spin 2: State 3 hollow fiber cured under vacuum.

The curing process of poly(amic acid) hollow fibers has been analyzed with a variety of techniques and modified as appropriate. However, further analysis and optimization is required to improve on hollow fiber permeances. Further analyses were needed to determine the mechanisms that result in the densification of the porous bulk of the hollow fibers.

Based on the experimental studies described above, various curing protocols were developed to conduct hollow fiber imidization as shown in Table 27. IR and NMR analyses were conducted to examine the imidization and crosslinking of polyamic acid hollow fibers from Spin 4: State 4 hollow fibers.

Table 27. Curing Oven Parameters for Spin 4 – State 4 Hollow Fibers.

| Run # | Run 1 | Run 2 | Run 3 |
|-------------------------|-----------------|----------------|----------------|
| N ₂ Flowrate | 0.5 lpm | 3.6 lpm | 3.6 lpm |
| Ramp 1 | 2 °C/min | -- | -- |
| Hold 1 | 100 °C / 1 hr | -- | -- |
| Ramp 2 | 2 °C/min | 2 °C/min | 2 °C/min |
| Hold 2 | 150 °C / 20 hrs | 150 °C / 6 hrs | 150 °C / 6 hrs |
| Ramp 3 | 2 °C/min | 2 °C/min | 2 °C/min |
| Hold 3 | 240 °C / 24 hr | 250 °C / 6 hr | 230 °C / 6 hr |

Spectroscopic Analysis of Hollow Fibers

Infrared (IR) Analysis

Three hollow fiber samples and two cured film samples, Table 28, were analyzed by infrared spectroscopy to gain insight into the imidization process.

Table 28. IR samples of Polyimide Hollow Fiber and Flat Sheets.

| Batch | Condition | Curing Profile | Atmosphere |
|-----------------|-----------|----------------|--------------|
| Spin 2: State 2 | uncured | N/A | N/A |
| Spin 2: State 2 | cured | 250 °C / 1 hr | stagnant air |
| Spin 2: State 1 | cured | 250 °C / 12 hr | stagnant air |

The ATR-IR spectra of cured and uncured fibers are shown in Figure 60. The conversion of poly(amic acid) in the uncured fiber to polyimide in the 24-hour cured fiber was readily apparent from the loss of the broad amide C=O stretch centered at 1651 cm^{-1} and secondary amide II band at 1545 cm^{-1} in the spectrum of the uncured fiber. The loss of these amide bands was concomitant with the appearance of phthalimide C=O stretching modes at 1776 and 1713 cm^{-1} and imide C-N stretching mode at 1371 cm^{-1} following closing of the imide ring in the cured fiber (Snyder, 1989 #19). Both the phthalimide C=O stretches and imide C-N noted in the cured fiber spectrum in Figure 60 served as useful markers for the curing of the fibers, particularly when normalized to the aromatic ring stretch at 1499 cm^{-1} whose peak shape and intensity remains largely unchanged with curing.

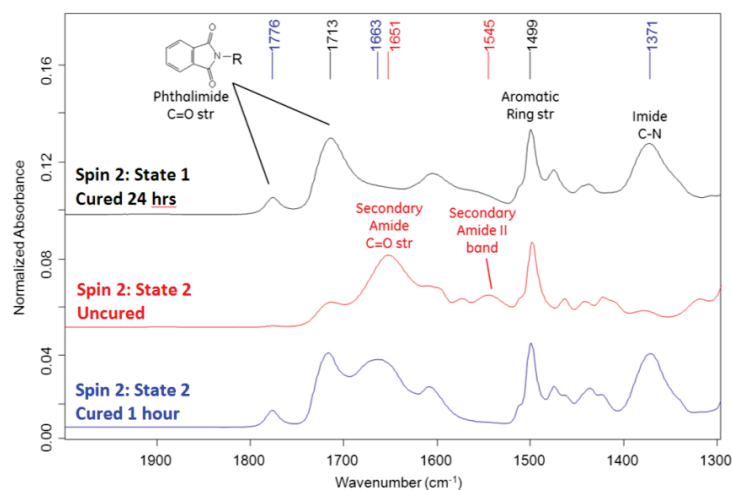


Figure 60. ATR-IR spectra of cured, uncured and semi-cured Spin 2 hollow fibers. The spectra were all normalized to the aromatic ring stretch at 1499 cm^{-1} .

The ATR-IR spectrum of the 1-hour cured fiber is also shown in Figure 60. The 1-hour cured fiber contained the spectral characteristics of both the 24-hour cured and uncured fibers, including the imide C=O stretches and C-N stretch associated with the cured fiber and the broad C=O stretch at $\sim 1660\text{ cm}^{-1}$ observed for the uncured fiber. While the presence of modes associated with both the uncured and 24-hour cured states might suggest that the 1-hour cured fiber was only partially cured, closer examination of peak shape and intensity of the imide C=O stretches at 1776 and 1713 cm^{-1} —as well as the imide C-N stretch at 1371 cm^{-1} relative to intensity of the backbone aromatic ring stretch at 1499 cm^{-1} —strongly suggests that poly(amic acid) was largely converted to poly(imide) in the 1-hour cured fiber. The broad C=O stretch centered at $\sim 1660\text{ cm}^{-1}$ in the 1-hour cured fiber was instead likely due to the presence of an impurity such as polyvinylpyrrolidone (PVP) whose amide C=O stretch modes coincides well with the peak position and shape of this band. The presence of PVP in the fibers was further supported by the NMR results, as described later.

The interior of the hollow fibers were also analyzed by ATR-IR spectroscopy in order to access the compositional uniformity of the fibers. The fibers were split length-wise to expose the interior hollow cavity and both the exterior and interior surfaces were measured by ATR-IR. An optical image of a broken fiber is displayed in the inset of Figure 61. The orange exterior surface can be seen along with a lighter colored, porous interior surface. The ATR-IR spectra collected for the exterior and interior surfaces of the 1-hour cured fiber are both shown in Figure 60. Both of the hollow fiber surfaces showed similar degrees of curing based on the intensity of the imide C=O stretches at 1776 and 1718 cm^{-1} and C-N stretch at 1370 cm^{-1} relative to the aromatic ring stretching mode at 1499 cm^{-1} . The interior surface of the fiber however did show less of the PVP contaminant than the exterior surface as evidenced by the weaker intensity of the broad amide C=O stretch at $\sim 1660\text{ cm}^{-1}$. This result suggests that PVP may be

segregating at the exterior surface. These initial studies with Gen-1 hollow fibers proved that polyimide hollow fiber membranes could be developed successfully.

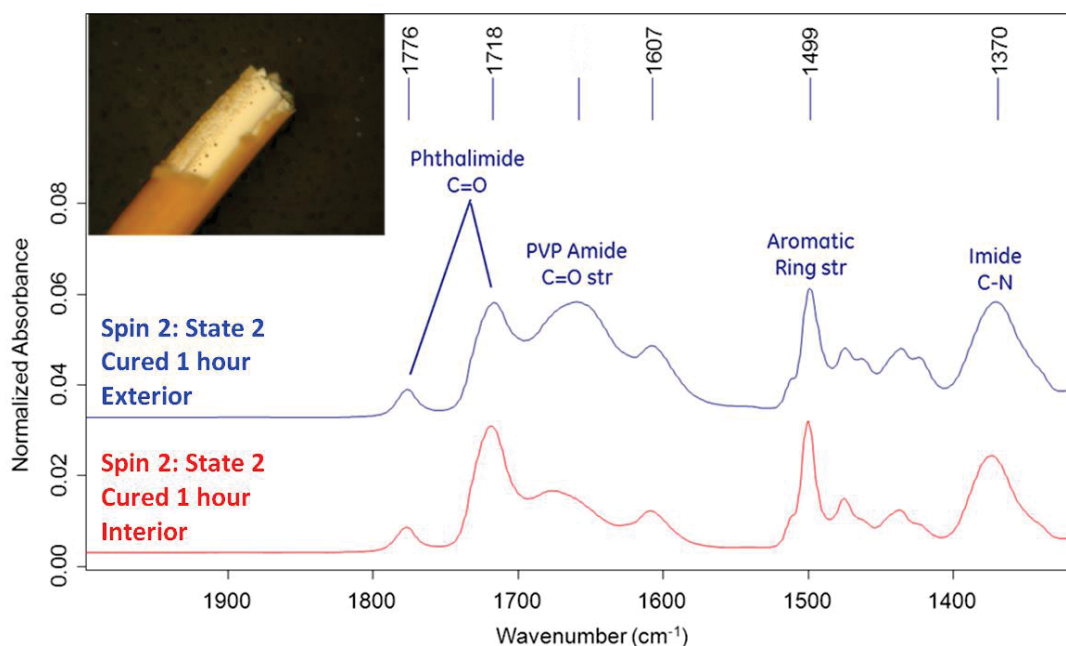


Figure 61. ATR-IR spectra of the exterior and interior surfaces of the 1-hour cured Spin 2: State 2 hollow fiber. The spectra were all normalized to the aromatic ring stretch at 1499 cm^{-1} . The inset contains an optical image of the split fiber.

The effect of curing temperature on the composition of the fibers was also examined by ATR-IR of Spin 4, state 4 hollow fibers cured at 230, 240, and 250 °C. It should be noted that the 230°C and 250°C fibers were cured for 6 hours under a 3.6 lpm nitrogen flow, while the 240°C fibers were cured for 12 hours under a 0.5 lpm nitrogen flow. Varying the cure temperature in this range did not appear to have a significant effect on the fiber curing based on the intensity of the imide modes discussed previously. The other spectral signatures of the fibers including the aromatic C=C stretches, ether C-O stretches, and aromatic out-of-plane bending modes also remain unchanged with increased curing temperature. The presence of these modes is in good agreement the polymer structure proposed based on the NMR analysis. Some additional higher frequency modes including OH or NH stretching modes near 3400 cm^{-1} and aliphatic CH stretching modes at 2,800 to $3,000\text{ cm}^{-1}$ were not expected based on the proposed poly(imide) structure. These spurious bands were likely the results of surface contaminants such as adsorbed alkanes and water species to which ATR-IR is particularly sensitive.

NMR Analysis - Poly(imide) fiber curing study as monitored by ^1H NMR

Degree of curing (imidization) of the poly(amic acid) was monitored using ^1H NMR. The presence of the amic acid COOH peak ($\sim 13\text{ ppm}$) and the amide NH peak ($\sim 10.4\text{ ppm}$) in the poly(amic acid) solution and uncured fiber, while both were absent in the cured fiber or film, indicating the condensation of COOH and amide NH into an imide group. An expansion of the aromatic region of these spectra again showed the simplicity of the cured material compared to the uncured as mentioned before. In the uncured fiber, a few high field peaks were observed. As the imidization proceeds, the polymer chain “self-heals,” resulting in the formation of the imide bonds and disappearance of the high field peaks. This agreed with our observation that the viscosity of the poly(amic acid) solution first decreased and then increased during the imidization process.

In another set of experiments, the fibers were cured at three different temperatures, 230°C, 240°C, and 250°C. As with the IR study of these fibers, it should be noted that at 230°C and 250°C fibers were

cured for 6 hours under a 3.6 lpm nitrogen flow, while the 240°C fibers were cured for 12 hours under a 0.5 lpm nitrogen flow. These fibers were only partially soluble in TCE or TCE/DMSO mixture, indicating partial cross linking. ^1H NMR spectra were collected on the soluble portions of the samples. Based on the aromatic region of the ^1H spectra, all materials seemed to be imidized almost completely. When the expanded aliphatic region was examined, some broad resonances in this region indicate that PVP was present in the fibers cured at lower temperatures, 230°C and 240°C. PVP was used as a viscosity enhancer in the fiber dopes. To further confirm the presence of PVP, solid state ^{13}C NMR spectra were collected on the fibers cured at 230°C. Clearly, PVP was present in the solid fibers, in addition to the polyimide. This study suggested that while curing at 250°C for at least 6 hours removes PVP, lower temperature curing leaves residual PVP in the fiber.

Hollow Fiber Module Development and Separation Performance Testing

Hollow Fiber Module Design

The hollow fibers must be mounted into a gas tight module assembly that allows for separate gas flows on the bore and shell side of the fibers to measure gas separation performance. A typical module is shown in Figure 62.

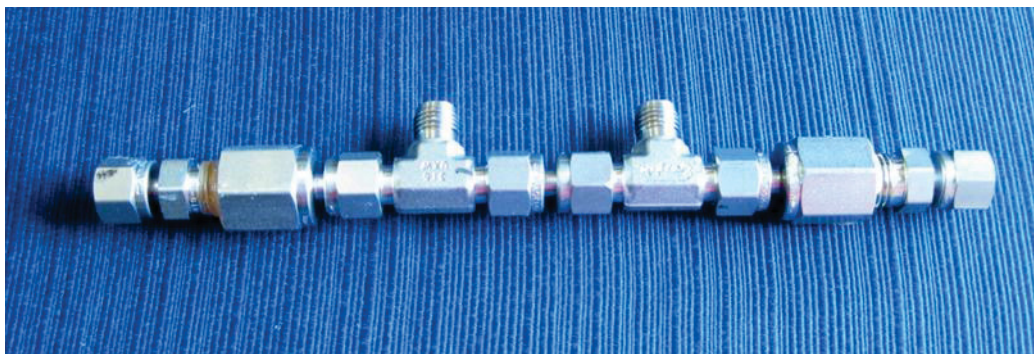


Figure 62. Typical Hollow Fiber Module Constructed from 1/4" Swagelok® Fittings.

For laboratory testing purposes, the module was typically constructed from 316 SS Swagelok® components. A module shell was constructed from 0.25 in. tube fittings, with a 0.25 in. pipe fitting on each end. The polyimide fibers were fed through the inner diameter of the fittings and held in place with a Teflon® tape plug at each end. This plug held the fibers in the center of the module and served as a barrier for a liquid potting material which was added to each end of the module. The potting material solidified as it cured and made a gas tight seal around the fiber and at the ends of the module. The potting material was typically a commercially available epoxy. After the epoxy cured, the excess epoxy was snapped off to create an open bore on each end of the potted fibers. Detailed development of hollow fiber module making technique can be found in the open literature.

Sealing Materials Selection

A critical portion of the polyimide hollow fiber membrane modules for water gas shift applications will be exposure to high temperatures (200 to 300°C). Hence, potting materials that survive thermal cycling from room temperature to 250°C and provide hermetic seals are required. Due to the low permeance of the fibers, it was important that the potting material be hermetic as well. Even a small membrane leak significantly decreases the selectivity of the membrane and increases the apparent permeance of the sample. A study of different potting materials, primarily high temperature epoxies, was conducted. Initially, three potting compounds – 3M™ Scotch-Weld™ DP100, Grace Specialty Chemicals STYCAST 2651-40, and Aremco Aremco-Bond™ 631 – were identified from literature(Zhou, 2005 #81;Koros, 2001 #82;Hassan, 1995 #83), but some of the compounds had lower than desired maximum

operating temperatures. Additional materials with similar properties but higher maximum operating temperatures were identified.

The samples were tested for leaks after curing each potting material according to its curing schedule as provided by the manufacturer. They were then heated to 180°C in a laboratory oven, cooled to room temperature, and leak tested again. The results are summarized in Table 29.

Table 29. Potting Materials Ranked by Performance.

| Material | Maximum temperature °C | Room Temperature Bench test | After 180 °C thermal cycle |
|--|------------------------|--|--|
| Dow Corning Sylard [®] 184 | 250 | Leaks at interface between steel and potting | x |
| Cotronics Durapot [™] 863 | 315 | no leak detected | no leak detected |
| Cotronics Duralco [™] 4524-IP | 260 | no leak detected | no leak detected |
| 3M [™] Scotch-Weld [™] DP100 | 180 | no leak detected | Leaks at interface between steel and potting |
| Aremco Aremco-Bond [™] 631 | 200 | no leak detected | no leak detected |
| Epoxy Technologies EPO-TEK [®] H74 | 250 | Leaks at interface between steel and potting | x |

After the thermal cycle study, only three materials did not leak: Cotronics Durapot[™] 863, Cotronics Duralco[™] 4524-IP, and Aremco-Bond[™] 631. Of these three, the Durapot[™] and Duralco[™] materials were more desirable due to a maximum operating temperature above 250°C. Despite the failure of the bench sample, EPO-TEK[®] H74 was also included in the downselect because, it had already shown itself to be hermetic in module assemblies. The main drawback of the EPO-TEK[®] H74 was that it could not be used in thermal cycling applications. However, it was kept as the fallback material if none of the other materials were leak tight at 250°C.

To identify appropriate potting/sealing materials, polyimide tubing with permeances of less than 2 GPU was used as a substitute for the hollow fibers. In all the polyimide tubing containing modules used for potting material screening, H₂ and CO₂ permeances were observed at temperatures greater than 50 °C. Of the 4 potting/sealing materials used, only the Duralco[™] 4525-IP showed no H₂ or CO₂ in the sweep stream until the temperature was above 50 °C. In addition, all of the profiles showed irregularities in the plot of H₂ permeance with temperature. If the only mechanism for H₂ and CO₂ transport to the sweep side was through the walls of the polyimide tubing, the heating and cooling permeance should show no hysteresis. All of the plots showed significant variation in permeance with temperature (Figure 63).

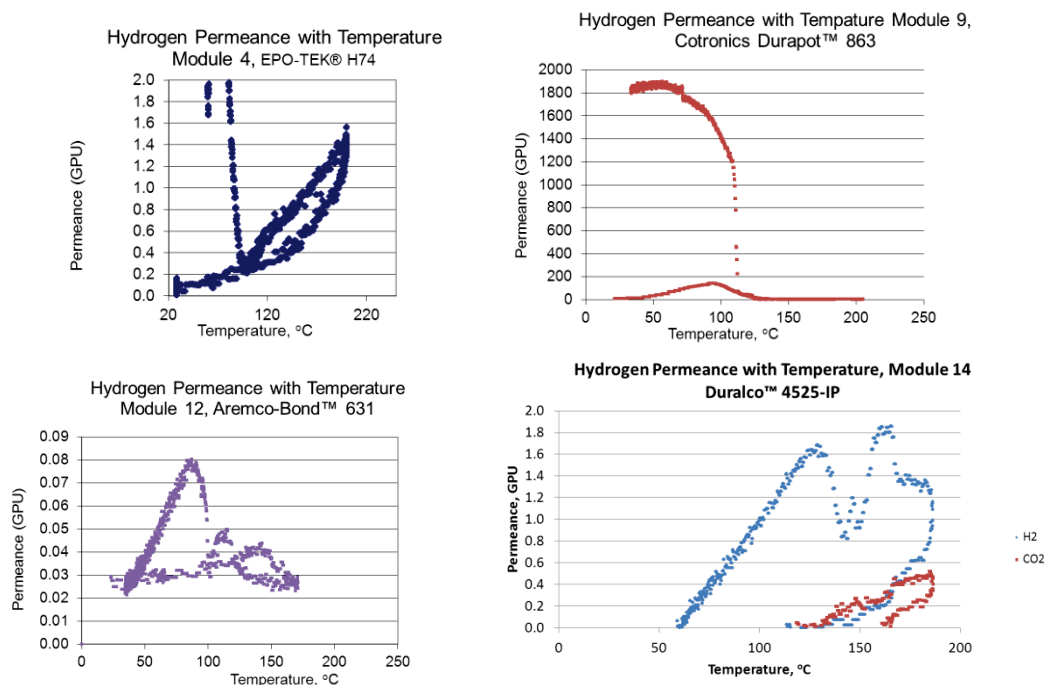


Figure 63. Gas-separation testing of polyimide tubing potted with four different potting materials. All permeances greater than ~2 GPU were assumed to be caused by potting materials leaks.

EPO-TEK® H74, Durapot™ 863, and Aremco-Bond™ 631 (maximum operating temperature of 200 °C) made a good seals at room temperature. However during cooling, a significant leak occurred when temperature dropped to 100°C. For instance, after testing, cracks were seen in the potting material around the module fittings with Durapot™ 863. The potting material was brittle, and the potting fittings could be separated, breaking the remaining epoxy seal easily (Figure 64). This material was not appropriate for sealing against the steel parts at these temperatures.



Figure 64. Cracks in Durapot™ 863 potting material after thermal cycle at 200 °C, as indicated by white circle.

Duralco™ 4525-IP showed no H₂ or CO₂ permeance below 50°C during heating or cooling. As temperature increased above 50°C, the H₂ and CO₂ permeance increased. Upon cooling, no H₂ or CO₂ permeance was observed below 50°C. Module 21 was potted with Duralco™ 4525-IP, which had a maximum operating temperature of 260°C. The material cured at room temperature, with an additional elevated temperature post-cure. The module was heated and cooled successively to 100°C, 150°C, and 200°C. At the end of cooling after 200°C heat, there was a large increase in H₂ and CO₂ permeance,

accompanied by a selectivity drop to 1, indicating a leak, and the module performance is shown in Figure 65.

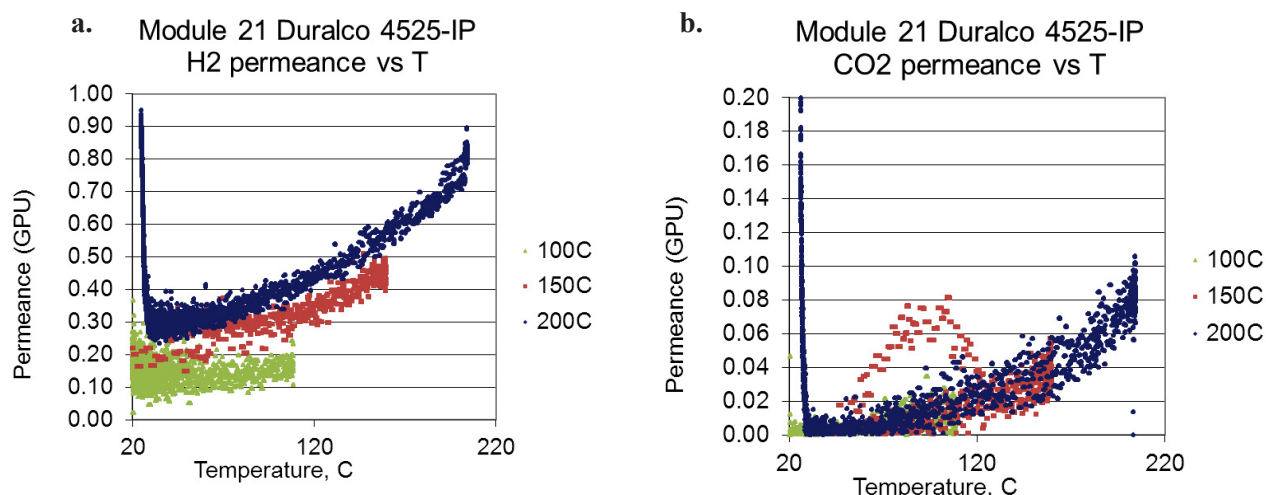


Figure 65. Permeance increase with temperature for hollow fiber module potted with Cotronics 4525-IP epoxy: (a) hydrogen, (b) carbon dioxide.

At 150°C, the H₂ permeance was 0.5 GPU with a selectivity of about 10. There was a slight increase in CO₂ permeance during cooling from 150°C, but at the end of cooling, the CO₂ permeance was zero. Additionally, the 200 °C heating and cooling cycle looks good, with no unexpected behavior until the leak at the end of cooling. The only limitation is that the module cannot survive multiple heating cycles to temperatures as high as 200°C. It is possible that some modules will be more robust than others and may survive cooling from 200°C. Conservatively, 150°C was chosen as a maximum testing limit for hollow fiber modules, so that the modules could survive multiple heating ramps. This was necessary so that modules could be tested at GEGR and then shipped to WRI for in line syngas testing.

Based on the data from these modules plus previous tests, Duralco™ 4525-IP was chosen as the potting material to be used in future testing. The studies with polyimide tubing helped to decouple the gas leakage from the hollow fiber and potting material. Using dense polyimide tubing, the defects in the hollow fibers were eliminated and appropriate epoxy sealing materials were selected.

Hollow Fiber Membrane Module Fabrication and Testing

Module Assembly

Module testing showed that fiber to fiber quality varied widely. The first modules were made with fibers that had passed only a visual inspection after imidization. After assembled modules showed leaks during bench screening (N₂ permeance measurement) or mixed gas testing, it was decided to more carefully screen the fiber bundles prior to module assembly. Furthermore after screening several fiber bundles and continuing to find leaks, it was determined that the VTEC hollow fiber membranes needed to be individually screened. While the system sensitivity was limited, it could detect N₂ permeance of 10 GPU or higher. If a fiber did not show a detectable leak (N₂ permeance less than 10 GPU), the fiber was considered a pass.

Polyimide hollow fibers were grouped into bundles of 1-10 fibers and assembled into modules to be tested for H₂ and CO₂ gas separation performance. The bundle of fibers were inserted into a stainless steel shell and potted on both ends with an epoxy or other suitable material to make a hermetic seal between the module and the fibers. The module was then tested in the H₂/CO₂ test system. The assembly and potting of a module was a time consuming process. In addition, leaks may develop either at the potting

material or within the fibers themselves during module assembly. The screening of the polyimide fibers prior to module assembly was an important step to ensure that only good fibers were being incorporated into modules and to determine if damage to the fibers was occurring during module assembly or potting. This preliminary screening test resulted in time and module parts saved and increased experimental clarity about when leaks were occurring in the system, if there were any leaks (see Appendices G and H).

H₂/CO₂ Hollow Fiver Gas Permeability Testing

Four modules were assembled with VTECTM polyimide fibers (Spin 4, states 1 and 7 and Spin 5, state 4) that had been tested to verify that they were free of large viscous defects. Based on the N₂ permeance testing results, all of the fibers were expected to have dense outer skins. This was supported by microstructural evaluation in the SEM. Each module was filled with 5 fibers and potted with Cotronics epoxy. A cross section of potted fibers is shown in Figure 66.

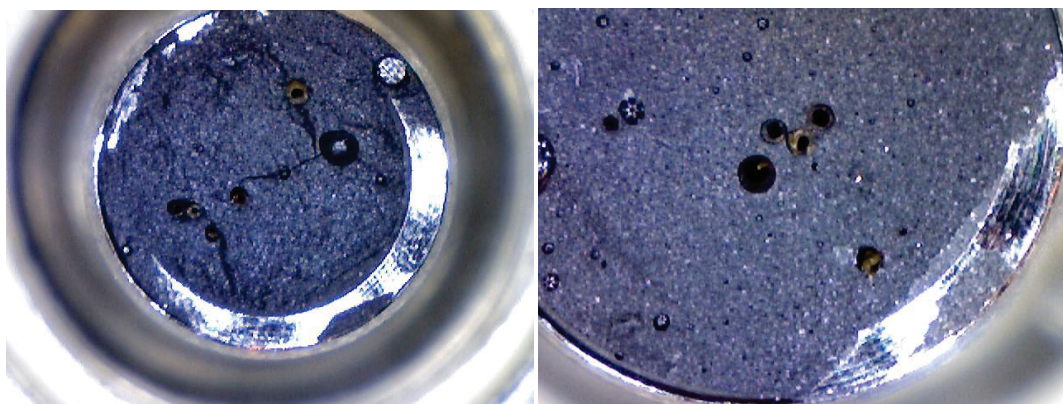


Figure 66. Cross section of potted VTEC fibers potted in module with DuralcoTM 4525-IP.

The modules were heated to 150°C in ideal syngas (50 vol.% H₂ / 50 vol.% CO₂) to measure permeance of H₂ and CO₂ and H₂/CO₂ selectivity. The modules showed similar performance to each other and similar permeance to polyimide tubing, confirming that the fibers were dense. All of the modules survived heating to 150 °C and cooling to back to room temperature. The H₂/CO₂ selectivity values ranged from 4–15. The range of selectivities measured was wide due to noise in the mass spectrometer signal and was attributed to low CO₂ concentrations (Appendix H).

The behavior of permeance with temperature was the same for heating and cooling for both H₂ and CO₂, indicated no leaks or changes in the fibers during the heating cycle. The values were on the same order of magnitude as the values measured for polyimide tubing, emphasizing that the fibers must be dense. The H₂ and CO₂ permeance values of the fibers seem slightly lower than the tubing, which may be within the experimental error of the measurement or due to a slightly greater wall thickness than the tubing. Two modules, 23 and 25 were sent to WRI for syngas testing. (see Appendix H).

Summary of Hollow Fiber Membrane Module Testing

Module 23 contained 5 VTECTM fibers potted with Cotronics DuralcoTM 4524-IP. The module was initially tested at GEGR in 50 % H₂ / 50% CO₂. The module was heated to 150°C and cooled back to room temperature. There was no sign of module leaks during the initial testing. At 150°C, H₂ permeance was 0.2 GPU and H₂/CO₂ selectivity was 8. The results were summarized in Table 30.

Table 30. Summary of Permeability Testing: Hollow Fiber Module 23.

| Hollow Fiber Module 23 | | | Average values | | |
|------------------------|----------------|---------------------------------|----------------|-----------------|---------------------------------|
| | Feed Pressure, | | H ₂ | CO ₂ | |
| | | | permeance | permeance | |
| Temp, °C | psig | Gas | GPU | GPU | H ₂ /CO ₂ |
| 150 | 4 | H ₂ /CO ₂ | 0.19 | 0.02 | 8.2 |

Module 25 contained 5 VTEC™ fibers potted with Cotronics Duralco™ 4524-IP, and initially tested in 50% H₂/50% CO₂. The module was heated to 150°C and cooled back to room temperature. There was no sign of module leaks during the initial testing. At 150°C, H₂ permeance was 0.1 GPU and H₂/CO₂ selectivity was around 11. The results were summarized in Table 31.

Table 31. Summary of Permeability Testing: Hollow Fiber Module 25.

| Hollow Fiber Module 25 | | | Average values | | |
|------------------------|----------------|---------------------------------|----------------|-----------------|---------------------------------|
| | Feed Pressure, | | H ₂ | CO ₂ | |
| | | | permeance | permeance | |
| Temp, °C | psig | Gas | GPU | GPU | H ₂ /CO ₂ |
| 150 | 4 | H ₂ /CO ₂ | 0.11 | 0.01 | 11.0 |

H₂/CO₂ Gas Permeability Testing

At WRI, the module was initially heated to 150°C in pure H₂ and held for 100 hrs. The H₂ permeance was 0.35 GPU, which is in good agreement with the GEGR mixed gas data. The process was then changed to 60.7 vol. % H₂ / 38.3 vol. % CO₂ / 0.98 vol. % CO and the module was held at temperature for 200 hours. The H₂ permeance did not change, and CO₂ permeance was measured as 0.03 GPU, with H₂/CO₂ of 10. After 200 hours the temperature was increased to 200°C and held for 200 hours. The H₂/CO₂ selectivity remained stable, and the H₂ permeance increased to 0.6 GPU. The results are summarized in Table 32, and Figures 67 and 68.

Table 32. Summary of Permeability Testing: Hollow Fiber Module 23.

| Hollow Fiber Module 23 | | | | Average values | | |
|------------------------|----------|----------------|---------------------|----------------|-----------------|---------------------------------|
| | | Feed Pressure, | | H ₂ | CO ₂ | |
| | | | | permeance | permeance | |
| Hrs. | Temp, °C | psig | Gas | GPU | GPU | H ₂ /CO ₂ |
| 100 | 150 | 5 | Pure H ₂ | 0.35 | x | x |
| 200 | 150 | 5 | NETL | 0.35 | 0.03 | 10.3 |
| 200 | 200 | 5 | NETL | 0.61 | 0.07 | 9.0 |

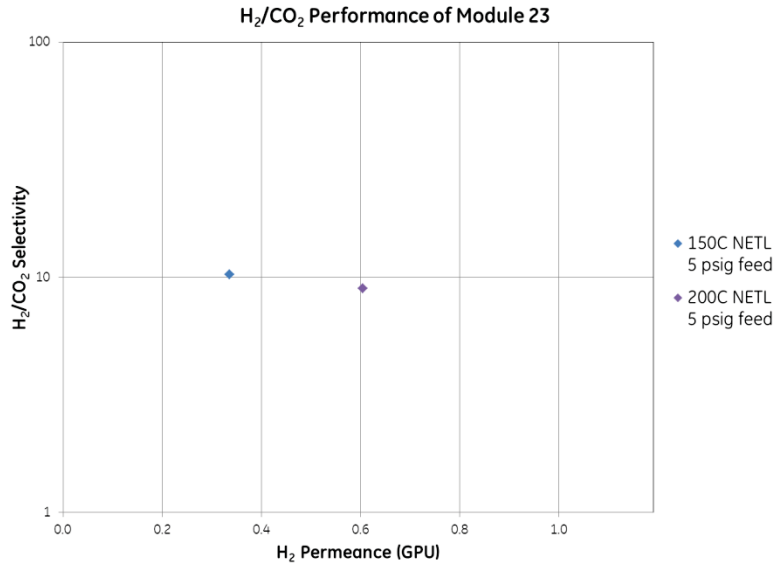


Figure 67. H₂/CO₂ selectivity performance of Module 23.

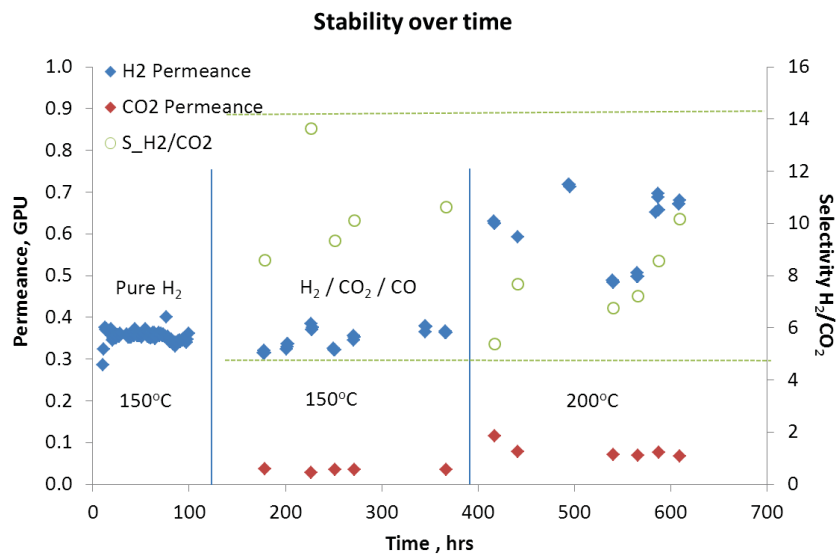


Figure 68. Gas-separation performance of Module 23 over time.

After 200 hours, the module developed a leak. It was cooled back to room temperature and returned to GEGR for evaluation. The module was pressurized with nitrogen on the shell side and a bubble test was used to determine the leak site. Two leaks were observed: (1) a leak at one of the hollow fibers and (2) a leak on both ends between the potting material OD and the ID of the steel module. Based on experience with previous modules, the leak that developed at temperature was probably due to a damaged fiber not potting material failure. As the module was cooling from 200 °C, the leak between the potting material and the module shell probably developed due to differential thermal contraction of the polymer and metal housing.

Images of the module bore side ends before and after testing are shown in Figure 69.

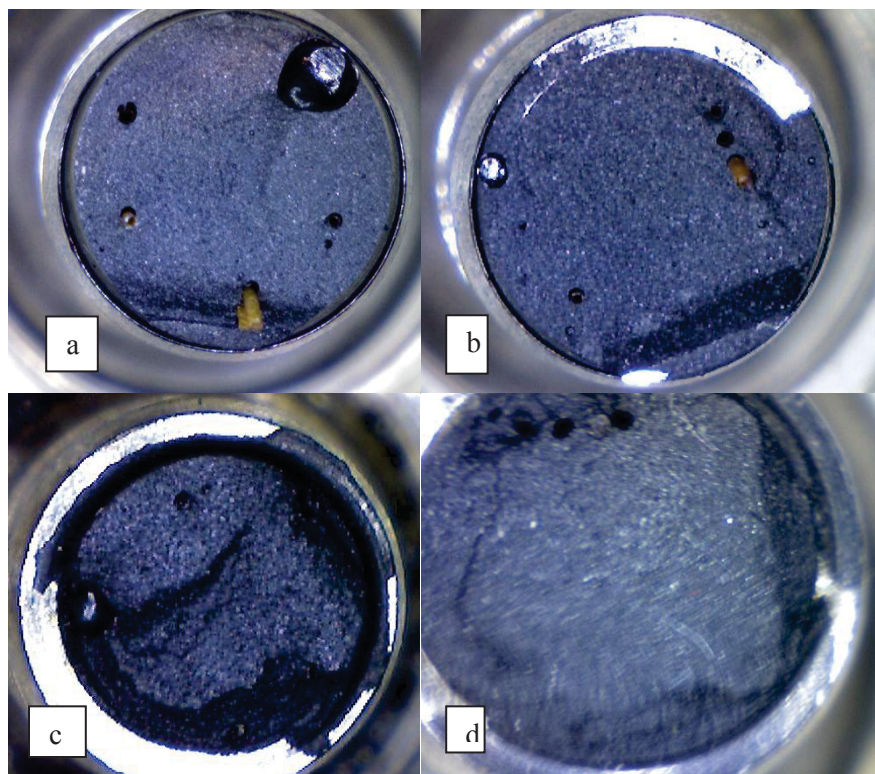


Figure 69. Ends of Module 23 before and after testing at WRI, showing potting material changes: (a) end 1 before testing (b) end 2 before testing (c) end 1 after testing (d) end 2 after testing.

Before testing, the epoxy surface was smooth with no cracks or raised features other than a fracture feature from when the excess epoxy was removed after potting. After testing, the epoxy surface is rough and protrudes slightly from the end of the Swagelok[®] fitting.

Summary

The curing process for the VTEC poly(amic acid) based hollow fibers was analyzed with a variety of characterization techniques and modified as appropriate. Further analyses are needed to determine the mechanisms that result in the densification of the porous bulk of the hollow fibers which leads to a significant drop in the fiber permeance. Imidization of the fibers is affected by a number of factors including: the type of atmosphere, amount of water present, solvents/byproducts removal rate, heating rates, and temperatures and soak times. Due to time constraints, a thorough examination of these factors was not possible. However, some optimization of the curing process was made possible by thermogravimetric (TGA) analysis, nuclear magnetic resonance (NMR) spectroscopy, infrared (IR) spectroscopy, and scanning electron microscopy (SEM) studies. A bench-scale fiber curing oven was designed and fabricated to scale-up the curing protocol allowing imidization of multiple polyamic acid hollow fiber strands of up to 1 m in length.

The Team screened a variety of commercial epoxy materials for creation of a hermetic seal between the hollow fibers and the module housing at high temperatures (200-250 °C) while with standing thermal cycling (from room temperature to 200 °C). Cracking of the epoxies and delamination of the seal due to CTE mismatch of fibers/epoxy/module wall were the key issues during thermal cycling. Future work will require development of carefully tuned epoxy or other polymer formulations to allow durable hermetic seal formation. Based on the data from these modules plus previous tests, Duralco™ 4525-IP was chosen as the potting material to be used. The studies with polyimide tubing helped to decouple the gas leakage from the hollow fiber and potting material. Using dense polyimide tubing, the defects in the hollow fibers

were eliminated and appropriate epoxy sealing materials were selected. The behavior of permeance with temperature was the same for heating and cooling for both H₂ and CO₂, indicated no leaks or changes in the fibers during the heating cycle. The values were on the same order of magnitude as the values measured for polyimide tubing, emphasizing that the fibers must be dense. The H₂ and CO₂ permeance values of the fibers seem slightly lower than the tubing, which may be within the experimental error of the measurement or due to a slightly greater wall thickness than the tubing.

The hollow fiber modules were initially heated to 150°C in pure H₂ and held for 100 hrs. The H₂ permeance was 0.35 GPU, which is in good agreement with previous mixed gas data. The process was then changed to 60.7 vol. % H₂ / 38.3 vol. % CO₂ / 0.98 vol. % CO and the module was held at temperature for 200 hours. The H₂ permeance did not change, and CO₂ permeance was measured as 0.03 GPU, with H₂/CO₂ of 10. After 200 hours the temperature was increased to 200°C and held for 200 hours. The H₂/CO₂ selectivity remained stable, and the H₂ permeance increased to 0.6 GPU. Overall, this data shows that the hollow fiber format is a viable answer for these demanding conditions using VTEC polymers. In the future, it is possible that the hollow fiber processing and module assembly can be refined further to accommodate the aggressive humidified gas streams at high temperatures.

BENEFITS ASSESSMENT

The benefits of WGS–MRs are related to driving the equilibrium reaction in the forward direction to get higher CO conversion at medium temperatures (280 to 420°C) and lower H₂O/CO (1 to 4.5) ratios because H₂ is being removed continuously in the membrane. For this process, N₂ sweep is used. Specifically, when the WGS–MR is used for coal-to-ammonia process, a number of benefits are seen: (1) a smaller methanator, (2) a smaller CO₂ separator, and (3) an integrated system/improved efficiency. These benefits, based upon an analysis performed in 2010, translate to a lower capital expenditure (CAPEX) and lower ammonia-production costs. The Team has shown that CAPEX is reduced from \$747MM to \$668MM for a 2000 TPD ammonia plant. The price of coal used for the study was assumed to be 24\$/ton. The production-cost decreases from ~320\$/ton to ~290\$/ton. However, by 2010, unanticipated energy market shifts due to abundant supplies of natural gas created a real shift away from use of syngas for virtually any application until the natural gas supply tightens up again.

COMMERCIALIZATION

GEGR has a long history of taking technologies from the conceptual/laboratory stage to commercial products. GEGR anticipates technology penetration into existing syngas facilities through retrofitting of existing reactors. In particular, ammonia production requires a mixture of high pressure H₂ and N₂ and is a strong fit for this technology which matches WGS-MR output.

Due to the very large opportunity space, the growing installed base of gasification systems in the U.S. and globally, and the widespread use of WGS technology in the chemical industry, we anticipate that this technology will contribute substantially to AMO's energy use reduction targets of 25% total by 2017 and 30% by 2020 through substantial savings over a large number of units.

- **Prototype demonstration.** The Team has developed a promising membrane material that can be integrated with a WGS reactor. Due to falling natural gas prices, the WGS Membrane reactor will be developed however at a much slower rate than originally envisioned. This project has succeeded in bringing the elements for a successful commercialization of the WGS-MR unit. This project has brought understanding of the risks associated with scale-up, lifetime, and durability of the membrane material, integrity of the membrane-reactor module, impact of impurities in the feed, impact of system variants, etc. Industry is reluctant to accept new technologies or processes unless their benefits can be demonstrated on a relatively large scale using industrial solutions.

GE's strategy for the WGS membrane reactor directly addresses this issue by:

- Building pilot equipment and small prototypes illustrating and verifying the new concepts

- Performing continuous operation on pilot equipment.

To address these risks this Team has designed and fabricated an intermediate scale prototype unit and tested it at GEGR and simulated syngas conditions and under coal conditions at WRI. The operational space for the WGS-MR continues to be developed through the systematic design of experiments based on six sigma methodology. While fabricating the prototype unit, the Team has identified partners for commercial production of membrane material and the module.

Identify business/partners for bulk production of membrane material and module fabrication.

GEGR has extensive experience in development and commercialization of membrane modules. GEGR is one of the world's largest manufacturers of integrated membrane-based water treatment systems for industry and is a global leader in the use of membrane filtration for waste prevention. GEGR's membranes are used in a wide range of applications, from purifying water for soft drinks to removing harmful chemicals from wastewater. The use of GEGR process membranes by GEGR's major customers has eliminated more than 16 billion gallons of industrial wastewater per year, reducing the burden on treatment plants and conserving clean water for domestic and agricultural needs (GE Ecomagination, 2012). In addition, GEGR is one of the world's leading providers of both gasification and power generation technologies. There are over 60 commercial sites worldwide using GEGR gasification technologies. GE Oil & Gas manufactures heavy wall reactors for refineries, tubular reactors, special vessels for petrochemical production plants, and large high-pressure heat exchangers.

Research programs supporting commercial development. INL and GEGR are continuing to carry out research programs to improve the WGS-MR performance further during the development stage. The materials development experts from both INL and GEGR will continue to further optimize the performance of the membrane module through focused research programs.

Adjacent Market Opportunities

The integrated WGS-MR product continues to have a huge potential for wider adoption in industries other than ammonia production, however the low cost of natural gas at this time will cause a lengthened schedule for further development and deployment. The gasification based plants can use the integrated WGS-MR reactor to reduce the energy usage in the plant and improve H₂ generation efficiency. New power generation plants based on IGCC with CO₂ capture would benefit significantly from the WGS-MR technology as it would reduce the CAPEX and footprint and increase the overall plant efficiency compared to the conventional shift followed by the Selexol approach. Further, the existing chemicals/fertilizer plants based on gasification can be retrofitted with the WGS-MR reactor to reduce the steam usage in conventional CO₂ capture. The gasification based market is simply not growing as rapidly all over the world including the USA as was originally anticipated. The U.S. currently has a syngas capacity of 7,722 MW_{th}, a 14% share of the world total. We continue to expect that the WGS-MR product will make considerable market penetration by 2040.

Further, the hydrogen production plants based on steam methane reforming can also benefit from the integrated membrane reactor technologies. The U.S. hydrogen industry currently produces nine million tons of hydrogen per year for use in chemicals production, petroleum refining, metals treating, and electrical applications (Department, 2002, National Hydrogen Energy Roadmap) Steam methane reforming accounts for 95% of the hydrogen produced in the U.S. Integration of the hydrogen selective membrane with the WGS reactor can reduce the footprint and CAPEX and improve the hydrogen conversion efficiency. The hydrogen production in the U.S. alone is expected to grow to 40 million tons of hydrogen per year during the next 20-30 years. The integrated WGS-MR product is expected to make substantial market penetration of this market.

The success of this program is having many cross-cutting benefits for other membrane development efforts. Advances in the manufacturability of inorganic supports are being applied to improve the economics of metal or microporous ceramic membranes, for the production of high purity hydrogen. Such

membranes can be further integrated with high temperature reactors, such as reformer or gasifiers opening up new markets.

Corporate Commitment

GEGR has continuously committed significant internal resources to developing a range of technologies for sustainable energy production, including reforming technologies and advanced cycles for energy production in a carbon constrained world. In May 2005, GEGR launched a company-wide ecomagination initiative to develop products that significantly and measurably increase both customer's environmental performance and operating performance. The effort has more than doubled the product portfolio by driving ecomagination into R&D, including the support of programs such as this one. In August 2002, GEGR initiated a Sustainable Energy Advanced Technology program at the corporate level with multi-million dollar funding. In addition, GE, ExxonMobil, Schlumberger, and Toyota are collaborating and making a 10-year investment in the Stanford University Global Climate and Energy Project (<http://gcep.stanford.edu/>) to address long-range sustainable energy technologies including CO₂ separation and sequestration. Such a long-term corporate level commitment is crucial for developing technologies for long-range markets.

ACCOMPLISHMENTS

Journal Articles

Klaehn, J.R.; Orme, C. J.; Stewart, F. F.; Peterson, E. S. "Humidified Gas Stream Separations at High Temperatures using Matrimid 5218," *Separation Science and Technology*, ASAP 2012.

Klaehn, J. R.; Peterson, E. S.; Orme, C. J.; Stewart, F. F.; Urban-Klaehn, J. M., Title: "High Temperature Gas Separations Using High Performance Polymers," In *Inorganic, Polymeric and Composite Membranes: Structure-Function and Other Correlations – Series: Membrane Science and Technology*, Eds: Oyama S.T.; Stagg-Williams, S.M. Publisher: Elsevier B.V., 2011.

Presentations

Klaehn, J. R.; Orme, C. J.; Stewart, F.F.; Peterson, E. S., "Humidified High Temperature Gas Separations," *Gordon Research Conference on Membranes: Materials & Processes*, 2012 GRC on Membranes: Materials & Processes, 2012.

Klaehn, J. R.; Orme, C. J.; Peterson, E. S.; Stewart F.F. "Water Containing Gas Stream Separations at High Temperature" 17th Symposium on Separation Science and Technology for Energy; 2011.

Klaehn, J. R.; Orme, C. J.; Peterson, E. S.; Quarles, C.A. "Blended polyimides for high temperature gas separations" North American Membrane Society (NAMS) NAMS 2011 Meeting; Gas Separations; 2011.

Klaehn, J. R.; Orme, C. J.; Peterson, E. S.; Quarles, C.A., "Correlations of polyimides and blended polyimides for high temperature gas separations," *ACS Division of Fuel and Petroleum Chemistry: Advances in Membrane Reactors*, ACS 241th 2011 Spring National Meeting, 2011.

Publications

Kimberly Polishchuk, Polyimide Membranes: Mechanical Constraint and Thickness Effects on Gas-Separation Performance; MS thesis in Materials Science and Engineering (advisor Dr. S. Pilgrim) 2011, Alfred University, NY.

Patent Activitie

Table 33 shows the patent activities that have taken place with the project as of January, 2013.

Table 33. A list of the project's patent activities.

| | Filing | Country | Title | Filing Desc | Application | App Date |
|--------|---------------|----------------|---|---------------------------|--------------------|-----------------|
| 249634 | 1 | US | Boehmite Bond-coat for Polyimide Membranes | PRI-Priority Application | 13/221657 | 30-Aug-11 |
| 249634 | 2 | CN | Boehmite Bond-coat for Polyimide Membranes | ORD-Utility Patent Filing | 201210314296.5 | 30-Aug-12 |
| 249634 | 3 | EP | Boehmite Bond-coat for Polyimide Membranes | ORD-Utility Patent Filing | 12181251.5 | 21-Aug-12 |
| 249634 | 4 | JP | Boehmite Bond-coat for Polyimide Membranes | ORD-Utility Patent Filing | 2012-187107 | 28-Aug-12 |
| 249634 | 5 | RU | Boehmite Bond-coat for Polyimide Membranes | ORD-Utility Patent Filing | 2012136870 | 29-Aug-12 |
| 259465 | NA | NA | Layered Membrane Module for Hydrogen Separation | NA | NA | NA |
| 259552 | 1 | US | Robust Polyimide Membranes and Method of Production | PRO-Provisional | 61/728419 | 20-Nov-12 |
| 259552 | 2 | US | Robust Polyimide Membranes and Method of Production | ORD-Utility Patent Filing | 13/730498 | 28-Dec-12 |
| 259566 | 1 | US | System for Ammonia Production from Coal | PRI-Priority Application | 13/665370 | 31-Oct-12 |

TECHNICAL ACCOMPLISHMENTS

The initial technical goals for this program were met (Appendix I). The analysis of the gas transport, mechanical, and economic constraints for the membrane were continually updated to determine optimal microstructural and performance targets for the intermediate and external separatory layers. The key membrane performance accomplishments relevant physical constraints, and resulting (measurable) intermediate and top coat layers performance targets are listed in Table 34.

Table 34. Membrane Performance Accomplishments.

| Parameter | Physical Constraint | Target (measurable) | Project Status |
|------------------|---|--|-----------------------|
| Selectivity | Overall membrane permeance and selectivity were controlled by polymer layer | Intermediate layer permeance > 5000 gas permeation unit (GPU) | Completed |
| | Bypass flow through pinhole defects contributes less than 1% of total flow | Ultrafiltration rate: < 5% tracer pass-through; Intermediate layer selectivity ~ Knudsen | Completed |
| Permeance | Low surface roughness to allow coating of continuous 100 nm polymer layer | Intermediate layer RMS roughness < 30 nm | Completed |
| | Intermediate layer pore size was smaller than solvated polymer coil size to avoid infiltration during coating | Intermediate layer pore size < 30 nm | Completed |

| Parameter | Physical Constraint | Target (measurable) | Project Status |
|-----------|---|---|----------------|
| Stability | Chemical compatibility with syngas components at realistic operating temperatures and pressures | No reaction upon 100 h slipstream exposure | Completed |
| | No delamination or thermal stress-driven cracking of polymer layer due to coefficient of thermal expansion (CTE) mismatch | | Completed |
| Economics | Cost per unit H ₂ from the membrane system was less than baseline SMR technology | Cost of H ₂ (membrane) < Cost of H ₂ (baseline) | Completed |

The Team, Idaho National Laboratory (INL), in conjunction with GE Global Research (GEGR) and Western Research Institute (WRI) (The Team), produced successful hydrogen-selective membranes for water-gas-shift (WGS) membrane reactors that give high-pressure hydrogen product streams. Several high performance (HP) polymer membranes were investigated for their gas separation performance in a simulated (mixed gas) and actual syngas conditions. To enable optimal system performance, membranes with high hydrogen (H₂) selectivity, permeance, and stability under WGS conditions are needed. The Team concluded that the VTEC PI 80-051 and VTEC PI 1388 (polyimide from Richard Blaine International, Inc.) are the leading candidates for the H₂ gas separations at operating temperatures (~200°C). Due to difficulties in polymer processing with VTEC PI 1388, VTEC PI 80-051 was thoroughly analyzed for its H₂ separations in syngas conditions using various membrane formats: flat sheets, tube modules, and hollow fibers. Each membrane format has shown that the selected VTEC material is capable of providing highly selective H₂/CO₂ separation ($\alpha = 7-9$) and H₂/CO separation ($\alpha = 40-80$). In addition, the VTEC polymer membranes are resilient to syngas conditions (WRI coal gasification) at 200°C for over 1,500 hours. We observed that the maximum differential pressure across the membrane was 30 bar which is similar to the conditions desired in actual WGS-MR operations.

VTEC PI polyimides are high temperature gas separation membrane materials that The Team has developed film casting methodologies for many different high performance polymers and their blends. Water is an issue for gas testing, especially at ambient conditions, possibly up to 150°C. The mixed gas permeability apparatus was modified for high temperature (> 200°C), and water-containing streams. Several different polyimides (e.g., Matrimid) were tested and analyzed with this apparatus to evaluate and quantify water's influence to the polymers. These preliminary results were successful at showing water not being an issue for humidified, high temperature gas separations. The Team's gas separation performance testing of the VTEC PI polyimide polymers demonstrates the following: H₂/CO₂ separation factor (alpha) up to 9, even at 250°C; H₂/CO₂ separation factor (alpha) up to 8, at 200°C with gas streams containing 2-4% water content; and survives syngas conditions at 250°C for 168 hours without adhesion or deformation issues.

A major technical accomplishment for this program is The Team's development of manufacturing technology for both porous steel tubes and hollow fibers—an unexpected result of the program. The Team found that coating the porous steel tubes required great care both in developing the intermediate ceramic layers that prevented the polymer solutions from penetrating too deeply into the matrix as well as getting a good quality coating on the surfaces of the ceramic intermediate layer. Both challenges were overcome and methods used were proven for larger scale tube products.

As indicated above, another significant accomplishment for The Team was development of hollow fiber membranes. Spinning techniques, dope formulations, curing conditions, and hollow fiber membrane module potting/sealing methodologies were developed and proven. The program proved that the techniques developed are transferable to larger/commercial scale manufacturing implementation.

Conclusions

Based upon the modeling studies, an H_2 selective membrane-based WGS–MR model was developed by The Team. This model provides a detailed account of the mass and energy balance for the hydrogen-separation process in this reactor. As experimental data on membrane performance become available, the integrated model will be updated to provide more accurate reactor sizing and separation-performance projection. At the same time, the integrated model can be used to explore trade-offs between various membrane-performance parameters, such as selectivity, permeability, pressure drop, etc. Such a trade-off provides important information about future research directions while setting material development targets.

The benefits of WGS–MRs are related to driving the equilibrium reaction in the forward direction to get higher CO conversion at medium temperatures (280 to 420°C) and lower H_2O/CO (1 to 4.5) ratios because H_2 is being removed continuously in the membrane. For this process, N_2 sweep is used. Specifically, when the WGS–MR is used for coal-to-ammonia process, a number of benefits are seen: (1) a smaller methanator, (2) a smaller CO_2 separator, and (3) an integrated system/improved efficiency. These benefits, based upon an analysis performed in 2010, translate to a lower capital expenditure (CAPEX) and lower ammonia-production costs. The Team has shown that CAPEX is reduced from \$747MM to \$668MM for a 2000 TPD ammonia plant. The price of coal used for the study was assumed to be 24\$/ton. The production-cost decreases from ~320\$/ton to ~290\$/ton.

The Team's polymer development efforts resulted in a product for a WGS–MR prototype. The project developed a method to obtain consistent gas permeability data from HP polymers for high-temperature mixed-gas analysis. The selected HP polymers are two polyimides, named VTEC PI 80-051 and VTEC PI 1388 (RBI, Inc.). These polyimides were chosen due to their ease of casting films and thermal processing of these films. The Team studied various HP polymers for several years and investigated their gas permeabilities and separations using a mixed-gas stream from ambient temperatures to 250°C. It was found that the VTEC polymers were excellent at handling extreme temperatures, 300°C or greater, and delivering high H_2/CO_2 gas pair separations (H_2/CO_2 separation factor = 7–9) at 250°C. These polymers performed for the project's desired gas separations, which are beyond those of many other HP polymers currently in use. Also, preliminary tests with elevated concentrations of CO_2 (>10 vol%) with the VTEC membrane remained stable at temperatures ranging from ambient to 200°C. Therefore, these two VTEC polymers were tested under simulated conditions for a syngas stream (humidified) and their performances were determined at very small laboratory scale and somewhat larger bench scale.

Water is a common component in many industrial gas mixtures. The literature is very limited regarding humidified gas streams, and no articles analyze water vapor at temperatures beyond 100°C. Due to water vapor's high condensability and small kinetic gas diameter, water vapor can be aggressive and has the potential to destroy polymer membranes. Therefore, new system designs were needed and developed by The Team to analyze for water–vapor-containing gas streams. The modified gas-permeability apparatus at INL, GE, and WRI are capable of analyzing water vapor along with other gaseous components in a mixed-gas stream simultaneously at high temperatures.

A series of gas permeation tests (dry pure gas, dry mixed gas and humidified mixed gas) were performed using a proxy polyimide, Matrimid 5218, which has been studied extensively in the literature. The literature data were used to compare and evaluate the data developed by The Team. Our initial studies showed that Matrimid 5218 membranes were found to be both chemically and dimensionally stable at temperature in the presence of water. The permanent gases CO_2 and water vapor encompassed a range of kinetic gas diameters and critical temperatures (condensability). Across the temperature range, permeability of all components was observed to increase with increasing temperature. Addition of water into the feed stream resulted in an increase in permeability for all gases with a slight loss in selectivity. This observation was made at both 30°C and 150°C. Increases in permeability with membrane hydration were greatest for CO_2 , suggesting that water-induced plasticization of the polymer plays a role in

transport. The data suggest that humidified-gas separation processes are possible if the humidified gas stream is kept at high temperatures at which water will remain a vapor and the polymer membrane will remain stable.

Several different HP polymers were analyzed for their gas permeation characteristics using three common gases (H_2 , CO_2 , and CH_4) at temperatures ranging from 30°C to 200°C, both with and without added humidity. From these initial gas-permeability data, VTEC PI 80-051 and VTEC PI 1388 membranes were found not to perform consistently at ambient temperatures (up to 100–150°C), but they do work much better with increasing temperature ($>150^\circ C$). As stated previously, water is possibly plasticizing these polymer membranes, thus changing their permeabilities and selectivities. However, free-standing films of VTEC polyimides demonstrate that they have exceptional physical stability towards water-vapor-containing gas streams for long durations. A long term study was done with the VTEC polyimides that were tested in a mixed-gas stream at 200°C in the presence of humidity (2–4 vol%). Remarkably, both VTEC polyimides showed excellent separations (H_2/CO_2 separation = 7–8) for over 80hrs. The Team has demonstrated that the VTEC PI polymer family is an excellent candidate for the syngas experiments that were pursued during this project.

Development of two types of membrane separator and direct comparison of each of them has proven quite useful. While the steel tubular membrane systems have their place in very high temperature applications where cost is not of concern, generally they are cost prohibitive when compared to hollow fiber systems that can withstand the operational conditions.

OVERALL SUMMARY AND CONCLUSION

Overall, the data obtained by The Team are the first known experiments which provide conclusive evidence, from several independent sources (INL, GEGR, and WRI), that the VTEC PI polymers will not only survive syngas conditions but perform at industrially significant levels while following the modeled behaviors, and give effective hydrogen versus carbon dioxide separations at elevated temperatures for extended periods without issues. The Team has moved the WGS-MR technology from Technology Readiness Level (TRL) 2 to TRL 4, as promised in the proposal. The Team also has extended the research and development work to include the hollow fiber membrane format that enables these technologies to be implemented into commercial industrial gas processing at a reasonable cost. However, further development of the hollow fibers (currently estimated at TRL 2) is required to realize the full potential of large scale gas applications. The results from this project have it ready to go into GE's product development cycle, when economics for the process are determined appropriate.

Recommendations and Future Work

This research has demonstrated the efficacy, in terms of cost and performance, of high temperature stable hydrogen separation membranes in WGS modules. Continued support of this effort within the following areas will provide necessary stimulus to deploy and improve this technology.

Coated tube platform

1. Experimental studies with 0.5 in. button samples indicated that the boehmite bond-coat or secondary intermediate layer showed ageing resulting in reductions in gas permeance. For very thin membrane layers (≈ 100 nm thickness) the permeance of the membrane may approach that of the boehmite layer, resulting in a decrease in membrane performance. The membrane modules produced for this body of work were sufficiently thick (1-5 μm), such that this was not an issue. Future work should focus on evaluating other bond coat layer materials to allow further reductions in membrane thicknesses.
2. The Team's primary goal was to successfully create a H_2/CO_2 selective, defect-free 20 cm VTEC polyimide coated membrane and sealing methods to enable high temperature, high Δp module testing under coal syn gas conditions. However, the membrane coating layer was thick (1-5 μm) with a H_2 permeance ≈ 10 GPU. The target membrane H_2 permeance for the coal-to-ammonia process was

estimated to be between 500-1000 GPU. The Team has successfully demonstrated on ½” button samples that defect-free performance with high permeance can be achieved. Future work must focus on transitioning the bond-coat or secondary intermediate layer formation on tubular structures to achieve thinner membrane coatings leading to higher permeances.

3. The Team successfully demonstrated performance of 20 cm H₂ selective tubular membrane inside a module. Future work should focus on the scale up of the process to full scale modules (1 meter or greater) and employing multiple coated tubes in a module.

Hollow fiber platform

1. The curing process for the VTEC poly(amic acid) based hollow fibers was analyzed with a variety of characterization techniques and modified as appropriate. Further analyses are needed to determine the mechanisms that result in the densification of the porous bulk of the hollow fibers which leads to a significant drop in the fiber permeance.
2. The Team screened a variety of commercial epoxy materials for creation of a hermetic seal between the hollow fibers and the module housing at high temperatures (200-250 °C) while with standing thermal cycling (from room temperature to 200 °C). Cracking of the epoxies and delamination of the seal due to CTE mismatch of fibers/epoxy/module wall were the key issues during thermal cycling. Future work will require development of carefully tuned epoxy or other polymer formulations to allow durable hermetic seal formation.

For the overall area of high temperature membrane separators, The Team feels that it is important to further develop a robust economic model that is broadly applicable for the important area of high performance polymer membrane separators. This model will need to be sensitive to costing of the competing energy sources (in this case specifically natural gas costing that dropped significantly during the course of the project).

Finally future work should address advancement of this area by developing industrial scale-up and pilot plant demonstrations of the technology—taking this very successful work from Technology Readiness Level (TRL) 4 to TRL 6 or beyond.

BIBLIOGRAPHY

- Adhikari, S., & Fernando, S. (2006). Hydrogen Membrane Separation Techniques. *Ind. Eng. Chem. Res.*, 45, 875-881.
- Al-Masri., M., Kricheldorf., H. R., & Fritsch., D. (1999). New Polyimides for Gas Separation. *Macromolecules*, 32, 7853-7858.
- An Installer's Pocket Guide to Swagelok(r) Tube Fittings. (2011). Swagelok Company.
- Ayala, D., Lozano, A., de Abajo, J., Garcia-Perez, C., de la Campa, J., & Peinemann, K. (2003). Relation of gas permeability with structure of aromatic polyimides. *Journal of Membrane Science*, 215, 61-73.
- Bernardo, P., Drioli, E., & Golemme, G. (2009). Membrane Gas Separation: A Review/State of the Art. *Industrial & Engineering Chemistry Research*, 48(10), 4638-4663.
- Bersa, L., & Liu, M. (2007). A review on fundamentals and applications of electrophoretic deposition. *Progress in Materials Science*, 52(1), 1-61.
- Bhandari, D., Polishchuk, K., Narang, K., Wickersham, P., Davis, R., Zhang, T., et al. (2012). Polyimide Hollow Fiber Membranes for Gas-Separation: GE Global Research TISCAT. In progress.
- Biesheuvel, P., & Verweij, H. (1999). Design of Ceramic Membrane Supports: Permeability, Tensile Strength and Stress. *Journal of Membrane Science*, 156(1), 141-152.
- Bischoff, B., Judkins, R., Adcock, K., & Powell, L. (2005). *19th Annual Conference on Fossil Energy Materials*.
- Bonekamp, B. (1996). Chapter 6 Preparaton of Asymmetric Ceramic Membrane Supports by Dip-Coating. In A. J. B. a. L. C. Elsevier (Ed.), *Membrane Science and Technology* (pp. 141-255).
- Breck, D. (1974). *Zeolite Molecular Sieves: Structure, Chemistry and Use: Zeolite Molecular Sieves: Structure, Chemistry and Use*.
- Brinker, C., & Scherer, G. (1990). The physics and chemistry of Sol-Gel Processing. *Academic Press, San Diego*.
- Brunetti, A., Scura, F., Barbieri, G., & Drioli, E. (2010). Membrane technologies for CO2 separation. *Journal of Membrane Science*, 359(1-2), 115-125.
- Chan, H. (1997). Layered Ceramics: Processing and Mechanical Behavior. *Annual Review of Materials Science*, 27, 249-282.
- Chen, G., Scholes, C., Qiao, G., & Kentish, S. (2011). Water vapor permeation in polyimide membranes. *Journal of Membrane Science*, 379, 479-487.
- Chiesa, P., Consonni, S., Kreutz, T., & Williams, R. Co-production of hydrogen, electricity and CO2 from coal with commercially ready technology. *International Journal of Hydrogen Energy*, 30(7), 747-767.
- Company, G. E. (2012). Products & Services: Oil and Gas. from http://www.ge-energy.com/products_and_services/products/oil_and_gas_reducing_and_metering_systems/index.jsp
- Criscuoli, A., Basile, A., & Loiacono, O. (2001). An economic feasibility study for water gas shift membrane reactor. *Journal of Membrane Science*, 181(1), 21-27.
- Energy and Environment Profile of the U.S. Chemical Industry*. (2000).
- Energy, D. o. (2002). *National Hydrogen Energy Roadmap*. Retrieved from http://www.netl.doe.gov/technologies/hydrogen_clean_fuels/refshelf/The%20National%20Hydrogen%20Roadmap.pdf

Estimate for H₂O:CO ratio required for the membrane reactor is based on an internal analysis by GE.

Evaluation of Alternate Technologies for Ethylene, Caustic-Chlorine, Ethylene Oxide, Ammonia and Terephthalic Acid. Prepared for DOE-ITP by JVP International, Inc. 2007.
http://www1.eere.energy.gov/industry/chemicals/pdfs/alt_tech_pub.pdf.

Fink, J. (2008). Polyimides: in Plastics Design Library. High Performance Polymers. In M. Willaim Andrew, Austria. (Ed.).

Freeman, B. (1999). Basis of Permeability/Selectivity Tradeoff Relations in Polymeric Gas Separation membranes. *American Chemical Society*, 32(2), 375-380.

Gasification World Database: Current Industry Status: Robust Growth Forecast. (2007). Retrieved from http://www.netl.doe.gov/technologies/coalpower/gasification/database/Gasification2007_web.pdf.

GE. from <http://ge.ecomagination.com/site/products/admt.html>

Gorgojo, P., Zornoza, B., Uriel, S., Tellez, C., & Coronas, J. (2008). Mixed Matrix Membranes from Nanostructured Materials for Gas Separation (Vol. 174, pp. 653-656): *Stud. Surf. Sci. Catal.*

Heaven, D., Mak, J., Clark, M., & Sharp, C. (2004). *Synthesis Gas Purification in Gasification to Ammonia/Urea Complex*. Paper presented at the Gasification Technology Conference.

Hirayama, Y., Yoshinaga, T., Kusuki, T., Ninomiya, Y., Sakakibara, T., & Tamari, T. (1996). Relation of gas permeability with structure of aromatic polyimides I. *Journal of Membrane Science*, 111(169-182).

Hosseini, S., Teoh, M., & Chung, T. (2008). Hydrogen Separation and Purification in Membranes of Miscible Polymer Blends with Interpenetration Networks. *Polymer*, 49(6), 1594-1603.

Hwang, S., & Kammermeyer, K. (1984). *Membranes in Separations*. Malabar, FL: Robert E. Kreiger Publishing Company, Inc.,.

Hydrogen from Coal Program: Research, Development and Demonstration Plan for the period 2007 to 2016. (2010). Retrieved from http://fossil.energy.gov/programs/fuels/hydrogen/2010_Draft_H2fromCoal_RDD_final.pdf.

Hydrogen Fuel Cells, and Infrastructure Technologies Multi-year RD&D Plan. (2007).

Intro to Ammonia Manufacturing. Syntex. <http://www.diquima.upm.es/docencia/tqi/docs/ammonia.pdf>.

JVP International, I. (2007). *Evaluation of Alternate Technologies for Ethylene, Caustic-Chlorine, Ethylene Oxide, Ammonia and Terephthalic Acid*. Retrieved from http://www1.eere.energy.gov/manufacturing/industries_technologies/chemicals/pdfs/alt_tech_pub.pdf

Kapton Product Sheet. (2010). 2010, from http://www2.dupont.com/Kapton/en_US/

Kaya, C., Boccaccini, A., & Trusty, P.

Kaya, C., Boccaccini, A., & Trusty, P. (1999). Processing and Characterization fo 2-D Woven Metal Fibre-Reinforced Multilayer Silica Matrix Composites Using Electrophoretic Deposition and Pressure Filtration. *Journal of European Ceramic Society*, 52(1), 1-61.

Klaehn, J., Orme, C., Luther, T., Jones, M., Wertsching, A., & Peterson, E. (2007a). 772872.

Klaehn, J., Orme, C., Luther, T., Jones, M., Wertsching, A., & Peterson, E. (2007b). 7772361.

Klaehn, J., Orme, C., Luther, T., Jones, M., Wertsching, A., & Peterson, E. (2007c). US Patent No. 7,259,230.

Klaehn, J., Orme, C., Luther, T., Jones, M., Wertsching, A., & Peterson, E. (2007d). Soluble N-Substituted Organosilane Polybenzimidazoles. *Macromolecules*, 40(21), 7487-7492.

- Klaehn, J., Orme, C., Luther, T., Jones, M., Wertsching, A., Peterson, E., et al. (2007). 7,309,758.
- Klaehn, J., Orme, C., Luther, T., Jones, M., Wertsching, A., Trowbridge, T., et al. (2007a).
- Klaehn, J., Orme, C., Luther, T., Jones, M., Wertsching, A., Trowbridge, T., et al. (2007b). 933604.
- Klaehn, J., Orme, C., Luther, T., Peterson, E., & Urban-Klaehn, J. (2007). *Polyimides and Their Derivatives for Gas Separation Applications*. Paper presented at the 234th Annual ACS National Meeting.
- Klaehn, J., Orme, C., Peterson, E., Luther, T., Jones, M., & Wertsching, A. (2008). *CO₂ Separation Using Thermally Optimized Membranes: A Comprehensive Project Report*.: Idaho National Laboratory.
- Klaehn, J., Orme, C., Peterson, E., Luther, T., Jones, M., Wertsching, A., et al. (2007).
- Klaehn, J., Peterson, E., Orme, C., Stewart, F., & Urban-Klaehn, J. (2011). High Temperature Gas Separations Using High Performance Polymers, In Inorganic, Polymeric and Composite Membranes: Structure, Function and other Correlations, Eds. In Elsevier (Ed.), (pp. 295-309).
- Koros, W., & Fleming, G. (1993). Membrane-based gas separation. *Journal of Membrane Science*, 83, 1-80.
- Kreutz, e. a. (2005). *Int J of H₂ Energy*, 30, 769.
- Kreutz, T., Williams, R., Consonni, S., & Chieasa, P. (2005). Co-production of hydrogen, electricity, and CO₂ from coal with commercially ready technology. Part B: Economic analysis. *International Journal of Hydrogen Energy*, 30(7), 769-784.
- Kunjunny, A., Patel, M., & Nath, N. Revamping CO₂ Removal Section in Ammonia Plant at IFFCO Kalol.
- Lee, B. (2007). *Polyimides*: A.A. Tracton. CRC Press, USA.
- Lide, D. (2004). *CRC handbook of chemistry and physics: a ready-reference book of chemical and physical data*: CRC Press.
- Liu, Y., Wang, R., & Chung, T. (2001). Chemical cross-linking modification of polyimide membranes for gas separation. *Journal of Membrane Science*, 189, 231-239.
- Nakagawa, T. (1994). *Industrial Applications of Membranes for Gas Separation in Japan*. London: CRC Press.
- Polischuk, P. (2011). *Polyimide Membranes: Mechanical Constraint and Thickness Effects on Gas-Separation Properties*., Alfred University.
- Potreck, J., Nijmeijer, K., Kosinski, T., & Wessling, M. (2009). Mixed water vapor/gas transport through the rubbery polymer PEBAX-1074. *Journal of Membrane Science*, 338, 11-16.
- Powell, C., & Qiao, G. (2006). Polymeric CO₂/N₂ gas separation membranes for the capture of carbon dioxide from power plant flue gases. *Journal of Membrane Science*, 279, 1-49.
- Qi, X., Akin, F., & Lin, Y. (2001). Ceramic-Glass Composite High Temperature Seals for Dense Ionic-Conducting Ceramic Membranes. *Journal of Membrane Science*, 193(2), 185-193.
- Reijerkerk, S., Nijmeijer, K., C., R., Freeman, B., & Wessling, M. (2011). On the effects of plasticization in CO₂/light gas separation using polymeric solubility selective membranes. *Journal of Membrane Science*, 367, 33-34.
- Robeson, L. (1991). Correlation of Separation Factor Versus Permeability for Polymeric Membranes. *J. Membr. Sci.*, 62(2), 165-185.

- Robeson, L. (1991). Correlation of separation factor versus permeability for polymeric membrane. *Journal of Membrane Science*, 62(2), 165-185.
- Robeson, L. (1999). Polymer membranes for gas separation. *Current Opinion in Solid State and Materials Science*, 4, 459-552.
- Robeson, L. (2008). The upper bound revisited. *Journal of Membrane Science*, 320, 390-400.
- Roman, P., Detlev, F., Thomas, K., & Klaus-Viktor, P. (2011). Gas permeation measurement under defined humidity via constant volume/variable pressure method. *Journal of Membrane Science*.
- Shishatskiy, S., Nistor, C., Popa, M., Nunes, S., & Peinemann, K. (2006). Polyimide Asymmetric Membranes for Hydrogen Separation: Influence of Formation Conditions on Gas Transport Properties. *Advanced Engineering Materials*, 8, 390-397.
- Sijbesma, H., Nymeijer, K., van Marwijk, R., Heijboer, R., Potreck, J., & Wessling, M. (2008). Flue gas dehydration using polymer membranes. *Journal of Membrane Science*, 313, 263-276.
- Sridhar, S., Smitha, B., & Aminabhavi, T. (2007). Separation of Carbon Dioxide from Natural Gas Mixtures through Polymeric Membranes - A Review. *Separation & Purification Reviews*, 36(113).
- Syntex. Intro to Ammonia Manufacturing. from <http://www.diquima.upm.es/docencia/tqi/docs/ammonia.pdf>
- Tenison, S. (2000). Current Hurdles in the Commercial Development of Inorganic Membrane Reactors. *Membrane Technology*, 128, 4-9.
- Tin, P. C. T., Wang, Y., Liu, R., & Pramoda, K. (2003). Effects of cross-linking modification on gas separation performance of Matrimid membranes. *Journal of Membrane Science*, 225, 77-90.
- Tock, R. (1983). Permeabilities and water vapor transmission rates for commercial polymer films. *Advances in Polymer Technology*, 3, 223-231.
- Trembly, J., Gemmen, R., & Bayless, D. (2007). The Effect of Igfc Warm Gas Cleanup System Conditions on the Gas-Solid Partitioning and From the Trace Species in Coal Syngas and Their Interaction with Sofc Anodes. *Journal of Power Sources*, 163(2), 986-996.
- van der Drift, A., van Ree, R., Boerrigter, H., & Hemmes, K. (2004). *Bio-syngas: key intermediate for large scale production of green fuels and chemicals*. Paper presented at the The 2nd World Conference on Biomass for Energy, Industry, and Climate Protection. Retrieved from <http://www.kmitl.ac.th/emc/web%20trm/Energy%20%20in%20project%20group/2/Global/2.2.2%20return%20Energy/biomass%20market%20trend/Biomass%20world%20market%20trend%202004.pdf>
- Verweij, H., Lin, Y., & Dong, J. (2006). Microporous Silica and Zeolite Membranes for Hydrogen Purification. *MRS Bulletin*, 31(10), 756-764.
- Vos, R., & Verweij, H. (1998). High-Selectivity, High-Flux Silica Membranes for Gas Separation. *Science*, 279(5357), 1710-1711.
- VTEC PI Polyimide Data Sheet. (2010). from http://www.vtecpi.com/pdf/VTEC_Polyimide_SI_Units.pdf
- Weil, K., Hardy, J., Rice, J., & Kim, J. (2006). Brazing as a Means of Sealing Ceramic Membranes for Use in Advanced Coal Gasification Processes. *Fuel*, 85(2), 156-162.
- White, L., Blinka, A., Kloczewski, H., & Wang, I. (1995). Properties of a Polyimide Gas Separation. *J. Membr. Sci.*, 103(1-2), 73-82.

- Xiao, Y., Low, B., Hosseini, S., Chung, T., & Paul, D. (2009a). The Strategies of Molecular Architecture and Modification of Polyimide-Based Membranes for CO₂ Removal from Natural Gas: A Review. *Progress in Polymer Science*, 34(6), 561-580.
- Xiao, Y., Low, B., Hosseini, S., Chung, T., & Paul, D. (2009b). The Strategies of Molecular Architecture and Modification of Polyimide-Based Membranes for CO₂ Removal from Natural Gas: A Review. *Prog. Polym. Sci.*, 34(6), 561-581.
- Zhao, H., Cao, Y., Zhou, M., & Yuan, Q. (2008). Effects of cross-linkers with different molecular weights in cross-linked Matrimid 5218 and test temperature on gas transport properties. *Journal of Membrane Science*, 323, 176-184.

Appendices

Appendix A. Dry Permeability Gas Analysis

Pure gas permeability results were obtained using the pressure-rise time-lag method. Membranes were exposed to three individual gases: H₂, CH₄ and CO₂. The membrane cell area was 13.8 cm² using a circular flat sheet 47 mm modified filtration cell obtained from Millipore, Inc. Membrane thicknesses were determined by direct caliper measurement and ranged from 40 to 80 µm. The test gas pressure was 30 psi and temperatures were varied from 20°C to 70°C.

Dry mixed gas experiments have been carried out using a method previously described in the literature [1-8]. In the mixed gas procedure, permeation is determined analytically by gas chromatography. The feed gas was a mixture of gases (3% by volume) for H₂, CH₄ and CO₂ with helium making up the balance gas and was obtained from Scott Specialty Gases, Inc. Dry gas permeabilities for Matrimid 5218 were determined over a temperature range of 30°C to 200°C with a feed gas pressure of 30 psi.

References

1. Barrer, RM and Rideal, EK (1939). Permeation, diffusion and solution of gases in organic polymers. *Trans. Faraday Soc.* **35**: 628-643.
2. Wijmans, JG and Baker, RW (1995). The solution-diffusion model: a review. *Journal of Membrane Science* **107**: 1-21.
3. Rogers, C, Meyer, JA, Stannett, V and Szwarc, M (1956). Studies in the gas and vapor permeability of plastic films and coated papers, Parts I and II. *TAPPI* **39**: 737.
4. Van Amerongen, GJ (1946). The Permeability of Different Rubbers to Gases and Its Relation to Diffusivity and Solubility. *Journal of Applied Physics* **17**: 972.
5. Koros, WJ, Chern, RT, Stannett, V and Hopfenberg, HB (1981). A model for permeation of mixed gases and vapors in glassy polymers. *Journal of Polymer Science: Polymer Physics Edition* **19**: 1513-1530.
6. Costello, LM and Koros, WJ (1993). Comparison of pure and mixed gas carbon dioxide and methane permeabilities in polycarbonate: effect of temperature. *Ind. Eng. Chem. Res.* **32**: 2277-2280.
7. Merkel, T., Gupta, R., Turk, B. and Freeman, B. (2001). Mixed-gas permeation of syngas components in poly(dimethylsiloxane) and poly(1-trimethylsilyl-1-propyne) at elevated temperatures. *Journal of Membrane Science* **191**: 85-94.
8. O'Brien, KC, Koros, WJ, Barbari, TA and Sanders, ES (1986). A new technique for the measurement of multicomponent gas transport through polymeric films. *Journal of Membrane Science* **29**: 229-238.

Appendix B. Mixed Gas Separation Apparatus Description

The literature is lacking experimental guidance on methods to study and characterize polymeric membranes at temperatures beyond 150°C in the presence of steam. This is a new area for gas transport measurement, and new equipment designs coupled with experimental procedures are currently evolving for these types of industrially focused applications. INL has developed a gas permeability testing apparatus that is able to analyze mixed gas streams containing gaseous water at high temperatures, Figure B-1.



Figure B-1. High Temperature gas testing facility, note the 140 cm stainless steel 0.125 inch tubing coil within the hot zone on the feed end of the cell.

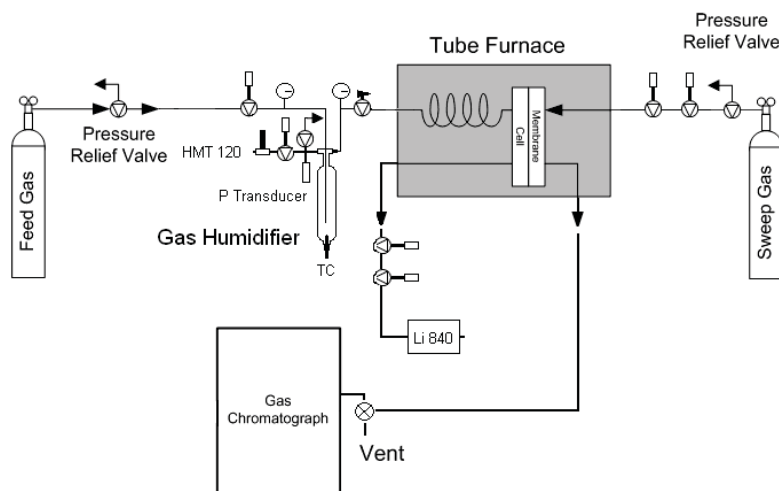


Figure B-2. Humidified Mix Gas Testing System.

Figure B-2 illustrates, the mixed gas permeability apparatus used to make measurements on H_2 and CO_2 containing streams resulting in selectivity determinations of H_2/CO_2 using a highly humidified feed gas stream up to 200°C. The feed gas is humidified and flowed across one side of the membrane at a rate of 10 ml/min. Adjustments among a series of needle valves positioned outside of the 200 °C hot zone

were used to set the pressure and gas flow passed across the feed side of the membrane. The feed gas pressure for these experiments was fixed at 226 KPa (43 Psia).

Permeate gases were swept using a helium gas stream. The permeate sweep gas flow was also controlled by a series of needle valves and the sweep flow was initially set to 5 ml/ min for each test. No accounting was made for potential helium back diffusion since it was considered minimal and would have no significant effect on the obtained data. High water permeation was noted that prevented reliable analysis of the permeate stream, so the helium sweep flow was increased to 20 ml/min to prevent condensation.

The total permeate flow during testing was measured directly with an electronic soap bubble meter. The permeate flow was directed through a gas chromatograph (GC) for analysis. The retentate line was plumbed to the Li-Cor[®], Li 840 infrared detector (IR) to verify that the flow passed the membrane was saturated with water vapor. Both the retentate and permeate lines outside of the 200 °C hot zone were maintained above 100 °C using heat tape. Inside the hot zone, a 140 cm coiled 0.125 in. stainless steel line assured thorough heating of the feed gas stream prior to introduction to the membrane cell. The membrane cell was housed in a tube furnace to maintain a constant temperature of 200 °C. The test membranes were maintained at temperature for 2 hrs while exposed to the humidified feed gas prior to data acquisition.

GC analyses of H₂, CO₂, and CH₄ were completed using a SRI Multiple Gas Analyzer #2 GC equipped with both a thermal conductivity detector (TCD) and a Helium Ionization Detector (HID). Two different GC columns were used in this analysis: 1) a SRI Molecular Sieve 13X Column and 2) a SRI Hayesep-D column. The GC injection valves were conditioned with dry instrument air prior to testing and periodically flushed during testing to eliminate any water build up in the injection valves.

Appendix C. Gas Humidification Procedure

A certified 3% by volume H_2 , CO_2 , CH_4 , in Helium gas mixture was purchased from Scott Specialty Gas. This gas mixture was humidified prior to its introduction to the membrane test system using the humidification apparatus illustrated in Figure C-1. The Humidified feed gas stream was produced by placing a 50 ml volume of Nano-Pure filtered water in the humidifier for each set of tests. The gas humidifier was then held at 60 °C to produce the desired water vapor concentration. Temperature control and stability were maintained by heat tape and foil insulation. The pre-membrane feed water vapor concentration was verified by flowing 10 ml/min of feed gas through a fixture fitted with a VAISALA humidity and temperature probe, model HMT 120. The membrane exposure humidity (RH) ranged from 70 to 90% at 60 °C.

Addition of water to the mixed gas feed stream was performed first by passing the gas through a water filled chamber and then through an empty demisting chamber that provided a water vapor concentration of 2-4% by volume. The water vapor concentration was verified using an IR detector (LI-COR, model LI-840). As with the dry experiments, permeability in the humidified mixed gas tests was determined by gas chromatography.

Humidified gas permeabilities for the various polyimides were determined over the same test conditions as the dry gas permeabilities. Variable temperature data was treated with an Arrhenius type analysis to yield activation energies of permeation (E_p).

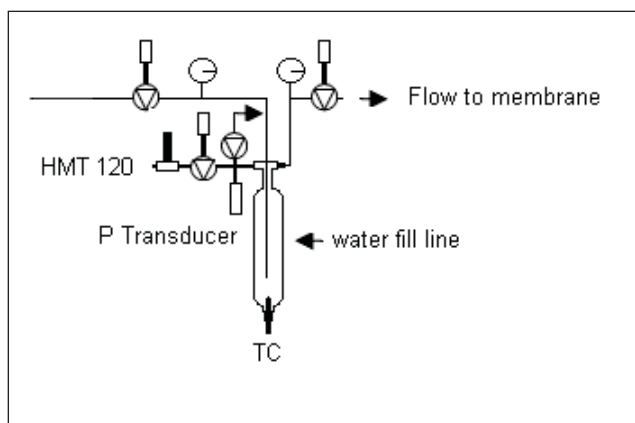


Figure C-1. Gas humidification apparatus.

Appendix D. Permeability Calculations

Permeability values were calculated using Equation 1 where $\Delta V/\Delta t$ is the total flow through the membrane, $T_{\text{exp}} P_{\text{stp}} / T_{\text{stp}} P_{\text{exp}}$ corrects to standard temperature and pressure, l is the membrane thickness, A is the membrane area, and Δp_1 is pressure differential taken from the feed pressure and concentration determined from the gas chromatography (GC). Permeabilities of each component gas were then used to calculate the separation factors for H_2/CO_2 .

$$p = \frac{\Delta V}{\Delta t} \frac{T_{\text{exp}} P_{\text{stp}}}{P_{\text{exp}} T_{\text{stp}}} \frac{l}{A \Delta p_1}$$

Equation 1. Calculation of membrane permeabilities for a dynamic (flowing) mixed gas stream.

Humidified gas permeabilities for the various polyimides were determined over the same test conditions as the dry gas permeabilities. Variable temperature data was treated with an Arrhenius type analysis to yield activation energies of permeation (E_p).

Appendix E. Thermal Analysis

Thermogravimetric Analysis (TGA) and Dynamic Mechanical Analysis (DMA) measurements were obtained using TA Instruments Q500 TGA and Q800 DMA, respectively.

Appendix F. High Performance Polymers on Porous Supports

For VTEC PI Polyimide Coatings on Ceramic and Porous Metal Discs

When coating the porous supports, it was found that the VTEC PI 1388 stock solution needed to be diluted with N,N-dimethylacetamide (DMAc) before coating the discs, because the resulting 1388 films show “stress” fracturing on the alumina discs. A 1:1 dilution of VTEC PI 1388 and DMAc did not show this behavior. The casting solutions for the porous supports used the VTEC PI 80-051 stock solution and a 1:1 dilution with DMAc and VTEC PI 1388. These polymer solutions did not penetrate into porous alumina or metal supports, when observed by an optical microscope. After coating, these discs required that the VTEC polymers to be thermally processed before they could be tested at WRI. All of the VTEC polymer laminated discs were processed in a vacuum oven at 150°C for 24 hours and then at 250°C for 24 hours.

An example of these polymer coatings is illustrated for VTEC PI 1388 (Figure F-1). These pictures are the γ -alumina on Inconel during the stages of polymer processing for these discs: plain discs (top left picture; **A**); polymer casting on to the discs (bottom left picture; **B**); DMAc removal using low heating on the hot plate (top right picture; **C**); polymer processing at 150°C (middle right picture; **D**); and final polymer processing at 250°C (bottom right picture; **E**). These polymer coatings were thin, and they did not show any cracking or fissure issues. From this set of discs, the polymers were successfully coated on to the disc surface.

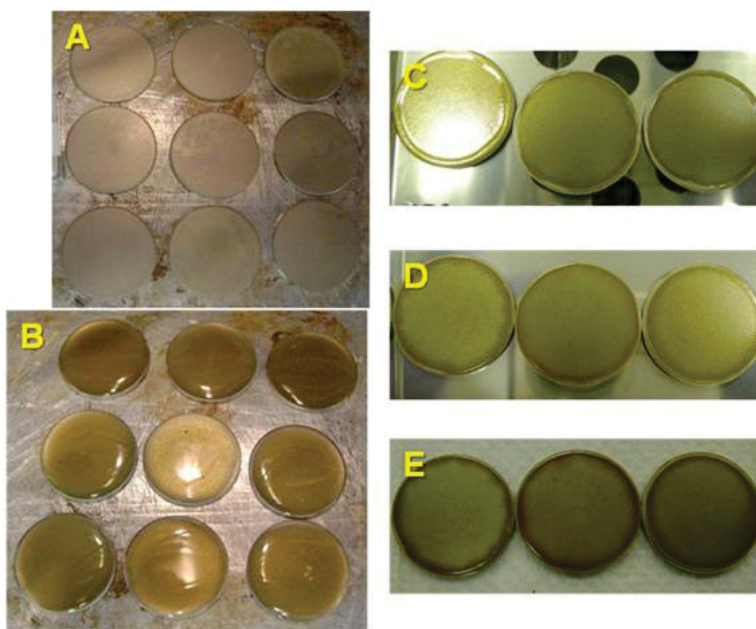


Figure F-1. Various stages of VTEC PI 1388 polymer processing with γ -alumina on Inconel discs.

High Performance Polymers on Porous Supports For Process Development of Porous Metal Tube Support

Porous Metal Support Layer Selection

The porous tubes used for the membrane support were seamless stainless steel sintered tubes manufactured by the Mott Corporation. The specifications for these tubes were as follows:

- OD=0.5 in. Nominal
- ID=0.375 in. +/-0.020 in.
- Length=8.0 in.+/-0.040 in.
- 0.2 micron media grade
- Material: 316L SS

Best Practice for Fabricating Steel Supported Polyimide Membranes

1. Support Preparation

- **Porous Stainless Steel Tubes** (Mott Corporation, NRE-2300 Series, 316L SS, 0.5 in. nominal O.D., 0.375 in. \pm 0.020 in. I.D., 0.2 μ m media grade, 6 in. – 8 in. length)
- **Modification:** Dense metal tube welded onto ends of porous tube for fixturing

2. Intermediate Layer

- Batch Slurry
 - 33 wt% Versal Alumina Slurry (Versal V250 γ -alumina milled in water at 28 wt% solids, pH adjusted to 4.5-5.0 with nitric acid, milled to 1.5 μ m)
 - 15 wt% Sasol Alumina Slurry (Sasol alumina milled in water at 50 wt% solids to 2.5 μ m)
 - 46 wt% Boehmite Sol (Hydrolysis and condensation of ATSB to form a 1.1 wt% solution of 230 nm boehmite colloids)
 - 6 wt% PVA Solution (14.5% poly(vinyl alcohol) in water)
- **Coat Slurry** (10 psid, 2 minute soak)
- **Controlled Drying** (80% RH, 25°C, 3 days, tubes held in vertical position and resting on sponges)
- **Sintering** (Thermolyne box furnace)
 - 2°C/min to 350°C, hold 2 hrs
 - 2°C/min to 400°C, hold 0.5 hrs
 - 2°C/min to room temperature

3. Polymer Coating

- Coating Solution
 - RBI, VTEC 080-051 poly(amic acid) solution: diluted to 10 wt% polymer in NMP
 - Tubes filled with 1-5 g of coating solution, rotated by hand to coat entire ID, immediately put into rotating oven
- **Thermally Imidize** (0.5 lpm Nitrogen flow rate, 3 rpm rotation)
 - 2°C/min to 65°C, hold 6 hrs
 - 2°C/min to 250°C, hold 6 hrs

- 2°C/min to room temperature

Process Development of Intermediate Layer Selection for Metal Porous Supports

Based on the above described down selection matrix, slurry casting process based on a multicomponent inorganic precursor suspension was shortlisted for further development and coating onto porous metallic support. The coating process involved four discrete steps: 1. Slurry preparation, 2. Coating, 3. Drying, and 4. Firing which are covered in detail in the subsequent sections.

Slurry Preparation

In this process an aqueous slurry was used. The components of the slurry were alumina particles, inorganic and organic binders, and viscosity modifiers. The particle size, surface charge, and mass loading in the slurry were key factors that set the primary structure of the deposited intermediate layer. Inorganic and organic binders were added to maintain the integrity of the coating. Viscosity modifiers were used to adjust the flow properties of the slurry to ensure continuous layers.

The intermediate layer slurry was prepared using the procedure outlined in Figure F-2. The slurry was an aqueous solution of: a γ -alumina powder (Versal V250 from UOP LLC), an α -alumina powder (from Sasol), a boehmite sol, and a polyvinyl alcohol (PVA) binder (Evanol 7515 PVA from Dupont). Each component was prepared separately and mixed together directly prior to the coating process.

The γ -alumina powder has an average particle size of approximately 20 μm as received. This was reduced to 1.5 μm via ball milling for approximately 15 hours. 29.7 wt% Versal V250 powder was slowly added to 18M Ω water with a 60 vol% charge of 5 mm TZP zirconia grinding media. Nitric acid was added periodically during the milling process to keep the pH of the slurry around 5 (10-12 mL of nitric acid in total). The final solid loading was determined by loss on ignition (LOI).

The α -alumina powder was ball milled at 50 wt% solid loading in 18M Ω water for 2 hours. Teflon milling media was added to disperse the powder and break up soft agglomerates. The final average particle size was 2.4 μm .

The boehmite sol was made via the hydrolysis and condensation of aluminum-tri-sec-butoxide (ATSB). 82 mL of ATSB was added to 630 mL of 18M Ω water in a 1L flask with a magnetic stirrer. The solution was heated to 92°C under reflux conditions. 70-80 mL of butanol was distilled out and 0.1 N nitric acid was added. The solution was kept at 92°C and 250 rpm stirring for 24 hours. The solution was allowed to cool to room temperature and then centrifuged for 2 hours at 2800 rpm. The supernatant was decanted and stored in a laboratory refrigerator. The particle size was measured by dynamic light scattering (DLS) and should be approximately 230 nm.

The PVA solution was made by slowly adding 14.5 wt% Evanol 7515 PVA to 18M Ω water at 120°C under refluxing conditions. Once all the PVA had dissolved into solution, the mixture was slowly cooled to room temperature.

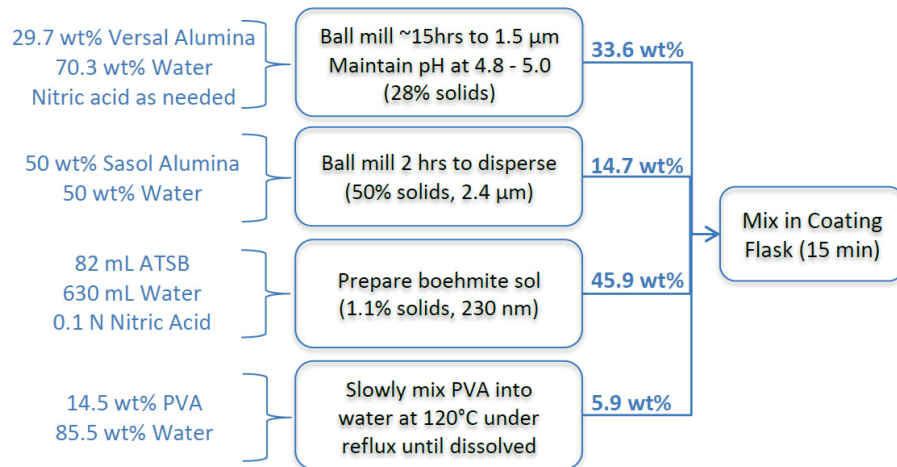


Figure F-2. Process for preparing alumina slurry for intermediate layer.

Coating

The coating process involved circulation of the slurry, under pressure, through the interior of the porous metal support. The slurry was pumped through three tubes in parallel, as shown in Figure F-3. Once the slurry had completely filled the tubes from the bottom to the top, the pressure was increased to 10-11 psi and the slurry continued to circulate for 2-3 minutes. The slurry was then drained from the tubes by opening vacuum and vent valves. Each tube was removed and excess slurry was absorbed from the ends with a sponge. The tubes were immediately placed in a controlled humidity box for drying.

The thickness of the coating could be controlled by increasing the pressure or duration of the coating process, or by applying multiple coats. While one coat was usually sufficient to create a continuous intermediate layer, two or more coats were desired for defect repair. Intermediate layer thicknesses of 2-6 μm was desired to ensure complete coverage of the pores in the metal support, while still being thin enough to have sufficient permeance.

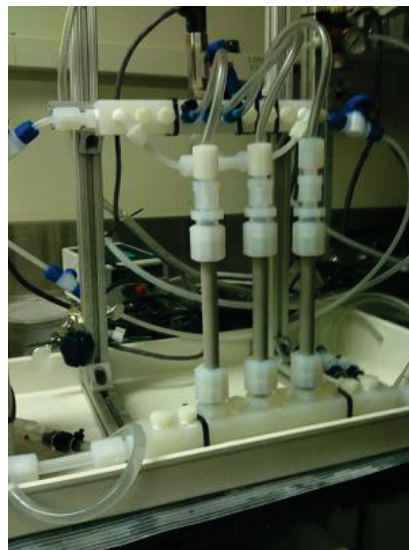


Figure F-3. Coating rig for applying intermediate layer coatings to steel tubes.

Controlled Drying

The coated tubes were dried vertically in a controlled humidity chamber at 80% relative humidity for a minimum of 3 days. The high humidity ensured that the water evaporated slowly and evenly from the coating, preventing the formation of drying cracks. However, this also led to long drying times. The drying step could be shortened by increasing the temperature of the chamber.

Firing

Samples were subjected to a thermal treatment step to consolidate the ceramic structure and improve adhesion of the intermediate layer to the support. A key challenge for the alumina intermediate layer has been the sintering cycle. The ideal sintering method would burnout all of the organics in the coating, sinter the alumina without densifying or reducing it, and not oxidize the steel. Unfortunately, the temperatures desired for sintering the alumina intermediate layer (400-600°C) were high enough to cause oxidation in stainless steel, as shown in Figure F-4. At 400°C, the chromium in the stainless steel oxidizes, causing the steel to appear orange in color. By 600°C, the iron in the steel oxidized, creating the red color of rust. The chromium oxide was not detrimental to the intermediate layer or the support and can be tolerated in membrane samples. However, the formation of iron oxide should be avoided as this will continue to degrade the steel support structure.

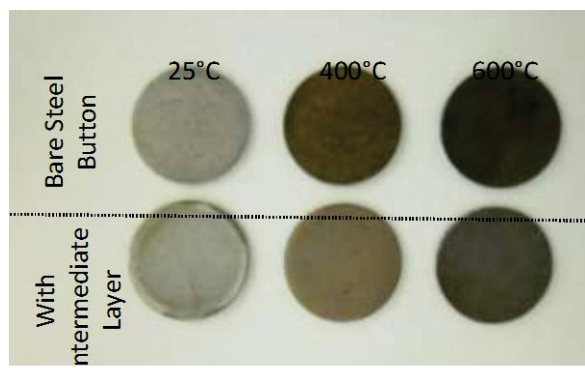


Figure F-4. Steel buttons with and without intermediate layer coatings, in the unfired state (25°C) and after being fired in air to 400°C or to 600°C.

If multiple coats of intermediate layer were being applied, then the first coats can be sintered at a lower temperature to avoid oxidizing the steel, with a higher temperature firing done on the final coat to fully sinter the entire intermediate layer. The current method involves a 2 hour soak at 350°C for the preliminary intermediate layer coatings, as shown in Table , and an additional 30 minute soak at 400°C for the final coating, as shown in Table F-2. This 400°C firing was sufficient to sinter the alumina, but oxidizes significant amounts of chromium in the steel and can occasionally cause rust spots. While the chromium oxide itself was not detrimental, the formation of iron oxide is.

Table F-1. Intermediate Layer Firing Cycle (Preliminary Coats)

| Ramp Rate (°C/min) | Hold Temp (°C) | Hold Time (hrs) |
|-----------------------|-------------------|--------------------|
| 2 | 350 | 2 |
| 2 | 25 | -- |

Table F-2. Intermediate Layer Firing Cycle (Final Coat)

| Ramp Rate (°C/min) | Hold Temp (°C) | Hold Time (hrs) |
|-----------------------|-------------------|--------------------|
| 2 | 350 | 2 |
| 2 | 400 | 0.5 |
| 2 | 25 | -- |

With this in mind, a steel button coated with the alumina slurry was sintered at 400°C for two hours in an inert gas. The steel appeared un-oxidized, but the alumina appeared slightly grey in color indicating trace levels of aluminum metal. Heating the button up to 350°C in air was sufficient to fully oxidize the alumina without oxidizing the steel. Further optimization of the sintering process was recommended. Specifically, experiments with low partial pressure oxygen firings could lead to the development of a firing cycle that would prevent the reduction of the alumina without oxidizing the stainless steel.

Boehmite Bond Coat Layer

The original intermediate layer compositions was coated onto a porous stainless steel tube, sintered, and then coated with a polymer membrane layer. An SEM image of this sample is shown in Figure F-5. Key observations include:

1. The intermediate layer was sufficient to seal over pores in the steel tube.
2. The intermediate layer was fairly porous.
3. No contiguous polymer membrane layer observed.

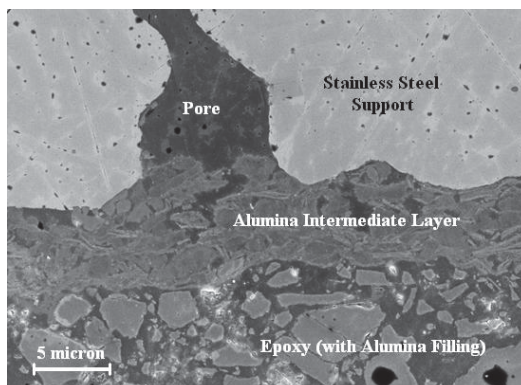


Figure F-5. Porous stainless steel tube coated with an alumina intermediate layer and potted in epoxy containing alumina filler material. No polymer membrane coating was visible.

It was hypothesized that the intermediate layer was too porous and allowed the polymer coating solution to infiltrate into the support, which would explain the lack of a continuous polymer layer. These observations led to experiments with a second intermediate layer formed from a boehmite sol. This coat would further reduce the pore size and surface roughness in order to prevent infiltration and facilitate film formation of the polymer solution.

A 50 nm boehmite sol was produced via the hydrolysis and condensation of alumina tri-sec-butoxide (ATSB) in acidic water, as described. In the case of tube samples, the boehmite sol was poured into the tube until the tube was full, then after approximately 10 seconds the boehmite sol was poured out of the tube. The tube was then dried and fired according to the same procedures as for an intermediate layer

coating (dried at room temperature and 80% relative humidity for 3 days then fired at 2°C/min to 350°C for 2 hours in air).

The initial coatings of boehmite were found to flake off in certain areas, creating defects. To prevent this, poly(vinyl alcohol) was added to aid in film formation and act as a binder. The same 14.5 wt% PVA solution used to make the intermediate layer coating was used. The 50 nm boehmite sol, the 14.5 wt% PVA solution, and distilled water were mixed together in the weight percentages given in Table F-3. The coating, drying, and firing procedures were not changed.

Table F-3. Boehmite Coating

| Boehmite Diameter | PVA Solution Concentration | Boehmite Sol Wt % | PVA Solution Wt % | Water Wt % |
|--------------------------|-----------------------------------|--------------------------|--------------------------|-------------------|
| 50 nm | 14.5 wt% | 75.0% | 3.5% | 21.5% |

Some experimental work with button samples has indicated that the boehmite layer may continue to densify over time, resulting in reductions in permeance. For very thin membrane layers (<100 nm thick) the permeance of the membrane may approach that of the boehmite layer, resulting in a decrease in membrane performance. The membrane modules produced for this body of work were sufficiently thick, such that this was not an issue. However, the necessity of the bond-coat or secondary intermediate layer should be reevaluated to allow for future reductions in membrane thicknesses.

Standard Work Procedure for Boehmite Sol

An 82 mL aliquot of ATSB was pipetted in a nitrogen box to prevent premature hydrolysis. The ATSB was added drop-wise to 630 mL of deionized water in the 2 liter flask. A condenser was placed on the flask to prevent loss of water from evaporation. The solution was heated to 86°C. Once the solution reached temperature, vacuum was applied through a second condenser so that a slow boil was maintained. Approximately 75 mL of butanol, resulting from the hydrolysis of the ATSB, was collected and discarded. A 2N solution of nitric acid was prepared and 15 mL added to the solution. The solution was heated to 92°C for 20 hours with a stir bar set to 250 rpm. The sol was allowed to cool to room temperature then centrifuged for 2 hours at 2300 rpm. The supernatant was collected and filtered through a 450 nm filter.

The nominal particle size was taken as the hydrodynamic diameter as measured by dynamic light scattering (DLS). A Brookfield ZetaPALS instrument with a 657 nm laser positioned 90° to the detector was used. The sample temperature was controlled at 25°C and the boehmite particles' refractive index was assumed to be 1.65. The quadratic model was used to determine the hydrodynamic diameter of the sol. The boehmite sol was found to have a mean diameter of 49 nm.

High Performance Polymers on Porous Supports For Membrane Layer Preparation for Porous Supports

Coating & Curing Process

The original tube coating procedure used the simple experimental setup shown in Figure F-6. The porous metal support tube was plugged at the bottom and filled with polymer solution, usually a 10 wt% solution of VTEC 080-051 polyimide in N-Methyl-2-pyrrolidone (NMP). After about 10 seconds, the clamp would be removed from the plug and the tube allowed to drain into a beaker. The silicone tube from the flowmeter would then be attached to the top of the tube and the nitrogen flow slowly increased (~ 5 mm/sec) to the desired maximum flow rate, typically 100 mm/s. The flow would then be slowly decreased to zero and the tube removed from the apparatus. Tubes were left in the vertical position to finish drying, which typically took about a minute.

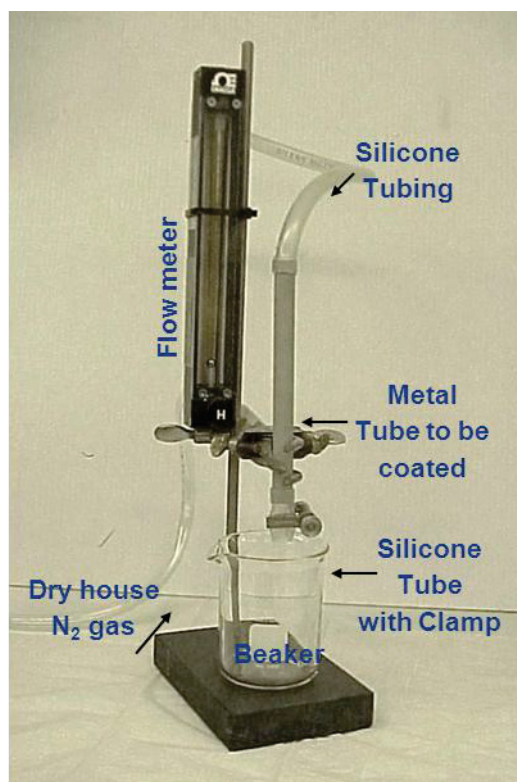


Figure F-6. Tube coating apparatus.

Initially, polymer coatings were formed by filling the tube with polymer solution, draining the excess solution, and allowing the tube to dry vertically overnight. A uniform coating of highly viscous polymer would result. The tubes would then be cured horizontally in an oven. The tubes appeared orange-brown in color afterwards, suggesting complete coverage of the polymer. However, it was later discovered that the polymer coating became significantly more fluid during the thermal treatment, resulting in most of the polymer to be deposited on one side of the tube. The orange-brown coloration was thought to be residue and not a continuous coating. To eliminate this problem, a rotating oven was designed and built, as shown in Figure F-7. It could accommodate three 20 cm (6 in.) long tubes, which were rotated continuously during the thermal treatment.

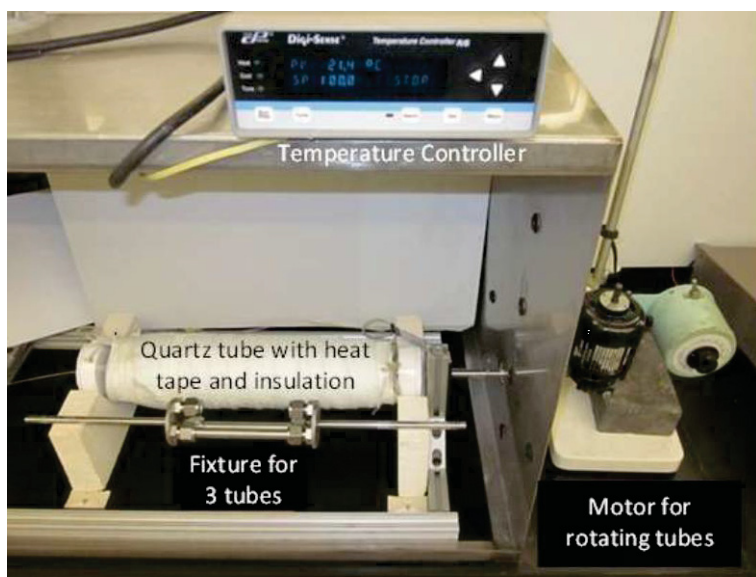


Figure F-7. Gen 1 rotating oven for curing polymer coated tubes.

Nitrogen purge capabilities were later added to the rotating oven set-up used to dry and cure the polymer membrane layer. Originally, the ends of the tubes were plugged to force solvent to evaporate through the porous walls of the steel tube. This was done in an effort to create more uniform coatings. However, tubes cured this way were found to cure improperly. The polymer coatings near the ends of the tubes were cracked and brittle in appearance, as shown in Figure F-8b. By comparison, the polymer coating on tubes that were cured in the box furnace with open ends appeared smooth and ductile, as demonstrated in Figure F-8a by the appearance of polymer chains bringing the gap created by a small crack in the coating. It was concluded that excessive solvent residue left in the tube during curing resulted in a brittle membrane.

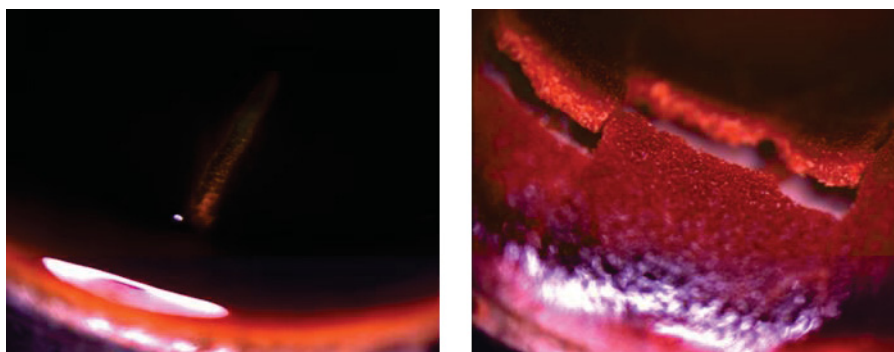


Figure F-8. Tubes cured in stagnant air in a) box furnace, and b) the rotating oven with plugged ends.

The addition of a 2 slpm N_2 gas flow through the interior of the tubes was found to be sufficient to remove the evaporating solvent during the curing process. A high flow rate allowed uniform removal of NMP solvent reducing the time required for the drying step to less than 1 hour and resulted in proper curing of the polyimide. Optimization of the thermal treatment parameters (temperatures, times, rotation speed, and purge flow rate) was performed on glass tubes to enable quick visual inspections of film uniformity and coverage. The optimized procedure was then transitioned to the porous metal tube supports with alumina intermediate layers.

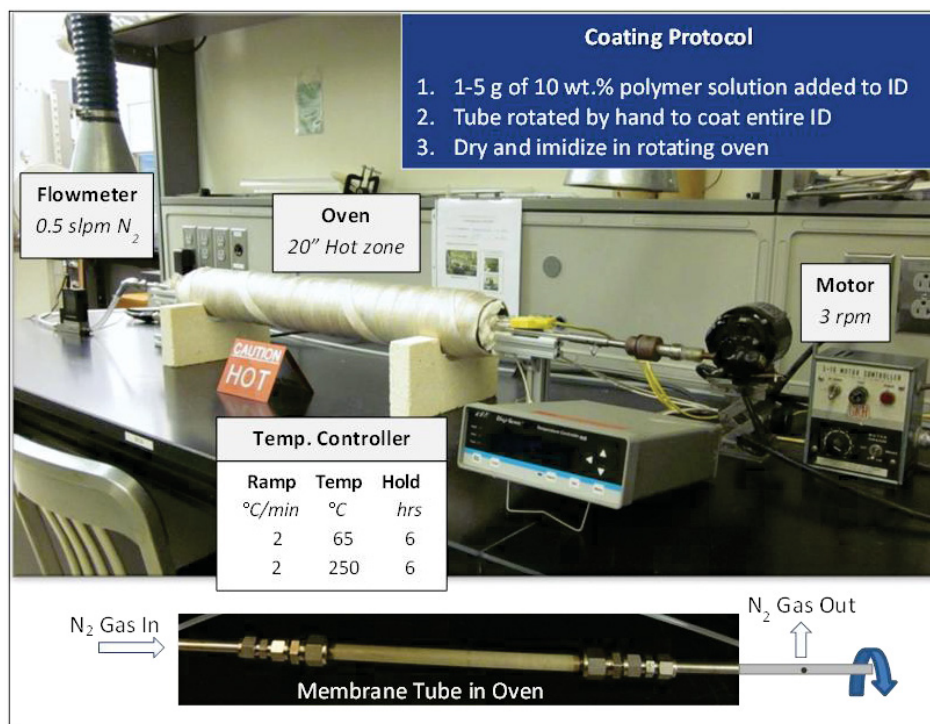


Figure F-9. Gen 2 rotating oven for coating polymer coated tubes

The GEN 2 Rotating Oven (Figure F-9) was developed and built for the polymer curing process based on the observations and results from polymer coating and curing process development described earlier. This oven consisted of a steel tube wrapped with heat tape and insulation and was twice the length of the previous model (GEN 1). There were attachments to enable sample rotation (0 - 3.5 rpm) and nitrogen purges (0 - 10 slpm). Multistep ramp-soak temperature profiles could be programmed and run autonomously. The GEN 2 oven was suitable for curing both hollow fibers and 0.5 in. tubular membranes up to 35 cm in length.

The drying and curing processing steps were optimized to produce continuous, uniform polymer coatings for the 20 cm tubular porous metal-supports with an intermediate layer coating. Maintaining a relatively high viscosity during the drying step was found to be a key factor in producing uniform coatings. The high viscosity, along with proper rotation, helped to ensure that the polymer coating did not slump or delaminate from the ceramic intermediate layer during the drying or curing step. Viscosity during the drying stage was increased by reducing the drying temperature from 150°C to 100°C. This resulted in an increase in drying time, however; increasing the nitrogen purge through the tube significantly decreased drying times, resulting in a net decrease in drying time to 1 hour. High nitrogen flow rates were ideal for solvent removal during drying, and the water removal generated during the imidization or curing step. However, increasing the nitrogen purge caused a shift in the hot zone, leading to non-uniform imidization. Pretreated N_2 could be used as a potential next step for eliminating this issue.

Characterization of Polymer Coated, Metal Tube Porous Supports

Thermogravimetric analysis (TGA), infra-red spectroscopy (IR), and nuclear magnetic resonance spectroscopy (NMR) were used to characterize the polyimide fibers and films made from the VTEC 080-051 poly(amic acid) precursor. These characterization studies were performed on polymeric hollow fiber membranes due to difficulties in characterizing a multi-layer membrane structure comprising of a porous metal, alumina intermediate layer and polyimide selective membrane layer vs. a hollow fiber membrane

with an asymmetric structure comprising entirely of polymer. The results of these characterization techniques are covered in a separate report on hollow fibers.

The membrane layer applied to the inner diameter of the stainless steel tubes was imaged by scanning electron microscopy (SEM) to determine thickness, uniformity, and continuity. The ductility of the polymer, the porosity of the support, and the difference in compliance between each layer made sample preparation difficult.

Initially, tubes were cross-sectioned, mounted in epoxy, and polished for analysis. Each cross-section was sputter coated at 20 mA for 20 seconds with platinum. A Zeiss Supra 55VP Field Emission SEM was used to image the cross-sections (see Figure F-10a). However, it was discovered that the standard epoxy caused the polymer layer to swell and appear up to twice as thick as expected.

To avoid swelling the polymer membrane, Fast Ion Beam (FIB) etching was used to expose a cross-sectional surface. A FEI Helios NanLab dual beam FIB/SEM was used to ion mill and to image the samples. A small section of the tube was cut out and the top of the polymer surface was sputter coated with a thick layer of platinum to make it conductive. The sample was mounted and positioned orthogonal to the ion beam in the FIB/SEM. A gallium ion beam was used to mill through the surface and expose the cross-section of the polymer and intermediate layers. The electron beam used to image the samples was oriented at a 52° angle relative to the milled surface.

Since the milled cross-section was not coated with a conductive layer, this technique lacked the detail seen in the freeze fractured samples. The polymer, being highly insulating, does not appear directly in the micrographs, as shown in Figure F-10b, but can be located by its interfaces with the platinum coating and the ceramic intermediate layer. This technique was found to produce distinct interfacial boundaries necessary for thickness measurements, but lacked some of the microstructural details seen in traditionally mounted and polished samples.

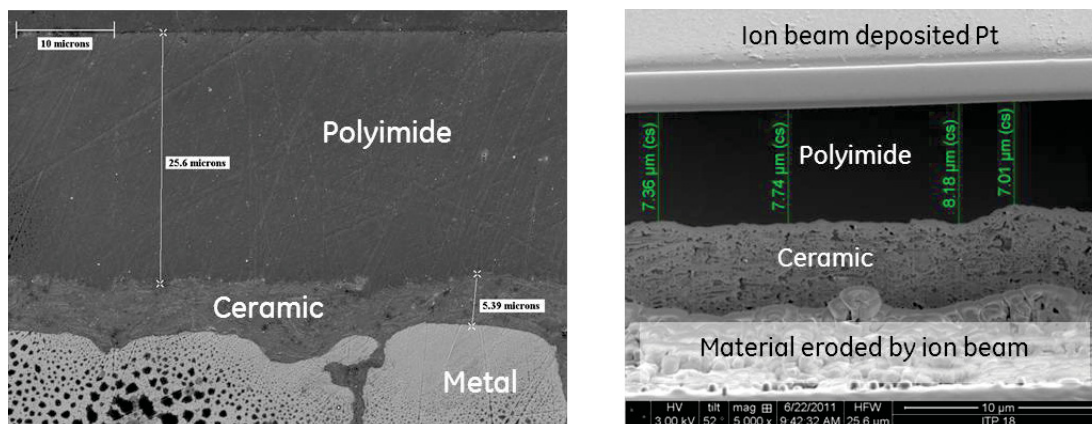


Figure F-10. SEM images of a porous steel tube with an alumina intermediate layer and a polyimide membrane layer prepared by a) mounting and polishing, and b) FIB etching.

High Performance Polymers on Porous Supports Porous Support Module Prototypes

Sealing Methods

High Temperature Epoxy Sealing Technique

Membrane tubes were sealed into modified Swagelok[®] fittings for integration into test fixtures using Epoxy Technologies EPO-TEK[®] H74 epoxy. H74 was a two component, thermally conductive epoxy designed for providing a hermetic or near hermetic seal. This epoxy was chosen for its room temperature viscosity, lengthy working time, fast cure time and maximum continuous operating temperature of 250°C.

H74 can be cured at temperatures of 100 to 150°C in 1 hour or less depending on epoxy bond line thickness.

The membrane sample consists of a nominal 0.5 in. outer diameter porous metal tube that may have one or more coating layers applied to the inner diameter. There were two seals to be made on the sample: (1) an end seal and (2) a bond of the sample to a standard tube fitting. The end seal was made at the end of the tube and along the inner diameter where the coating may be defective or nonexistent. The purpose of the end seal was to prevent leak paths through the porous tube body that bypass the selective coating. The purpose of the seal to the standard tube fitting was to integrate the sample with any testing system and/or module housing.

For all seals, the epoxy was mixed according to data sheet specifications: 100 parts A to 3 parts B (hardener) by weight. The epoxy was mixed by hand until the mixture was visually uniform, about 1 minute of stirring. For the end seal, the sample was pre-heated to a minimum temperature of 100 °C and dipped in the epoxy to apply a solid coating over all surfaces of the tube. After the tube was withdrawn from the epoxy, the sample was placed vertically in an oven at 100°C for one hour to cure the epoxy. The epoxy became less viscous at elevated temperature, so excess material drips out of the tube, leaving the inner diameter open. Upon curing, the epoxy undergoes a color change from tan to reddish brown. A fully cured end seal is shown in **Error! Reference source not found..**



Figure F-11. End seal of porous metal tube with EPO-TEK[®] H74, after curing.

The end sealed tube was then potted into a Swagelok[®] reducing union. The same curing schedule was used as for the end seals. Prior to joining, the fitting was prepared by roughening the inside walls (typically using a sand or grit blaster) and degreasing thoroughly by sonication in solvent to maximize the adhesion of the epoxy to the metal surface. A potted tube is shown in Figure F-12.

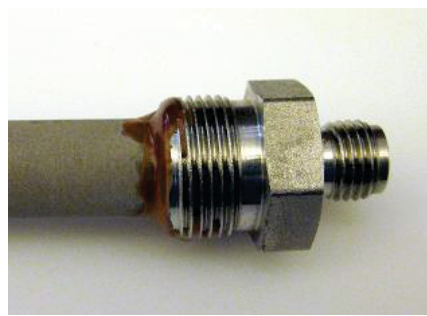


Figure F-12. Porous metal tube potted into fitting, after curing.

The epoxy seals were evaluated by sealing a dense steel tube to a fitting and testing it in the same way that a membrane would be tested. Since there will be no gas flow through the walls of the dense tube, any gas flow detected through the part represents a seal leak. The tube was pressurized up to 50 psig at room temperature and found to be leak tight. The seal was heated from room temperature to 250°C while being pressurized on the inside with a mixture of H₂/CO₂. No leak could be detected through the seal by mass spectrometer. However, upon cooling, a leak developed between the epoxy and the inner diameter of the Swagelok® fitting.

The behavior was reproducible and occurred at temperatures between 120 and 70°C during the cooling cycle. The leak was attributed to a combination of CTE mismatch and behavior of the epoxy as its temperature dropped below its glass transition temperature, T_g, which was stated by the manufacturer to be > 100°C.

H74 epoxy was chosen because it had been successfully used for membrane sealing in other systems that cycled to temperatures as high as 250°C and exhibited no leaks during heating or cooling. It was shown to maintain its adherence between a ceramic part and a steel surface during thermal cycling, but in a different geometry than was used to seal a tube into a fitting.

For the tube seal, the leak that occurred upon cooling was a failure in the adhesion of the epoxy to the stainless steel fitting that contained it, as shown in Figure F-13.



Figure F-13. Leak site at interface between epoxy potting and stainless steel end fitting.

Several factors were considered to see if the epoxy failure upon cooling could be prevented, including seal geometry, surface preparation, epoxy cure temperature and system cooling temperature. Additional epoxies were also tested. Test parts were made using steel tubing in place of the porous steel membrane substrate. Test parts were sealed with epoxy and subjected to thermal cycling to 200°C. After heating and cooling, the parts were checked for leaks.

The standard tube-in-fitting geometry was compared against a flat butt joint and a modified butt joint that mimicked sealing the flat end of the steel tube to a flat disk. The modified butt joint geometry was included based on previous experience with H74 epoxy at high temperature. Pictures and schematics of the joints are shown in Figure F-14.

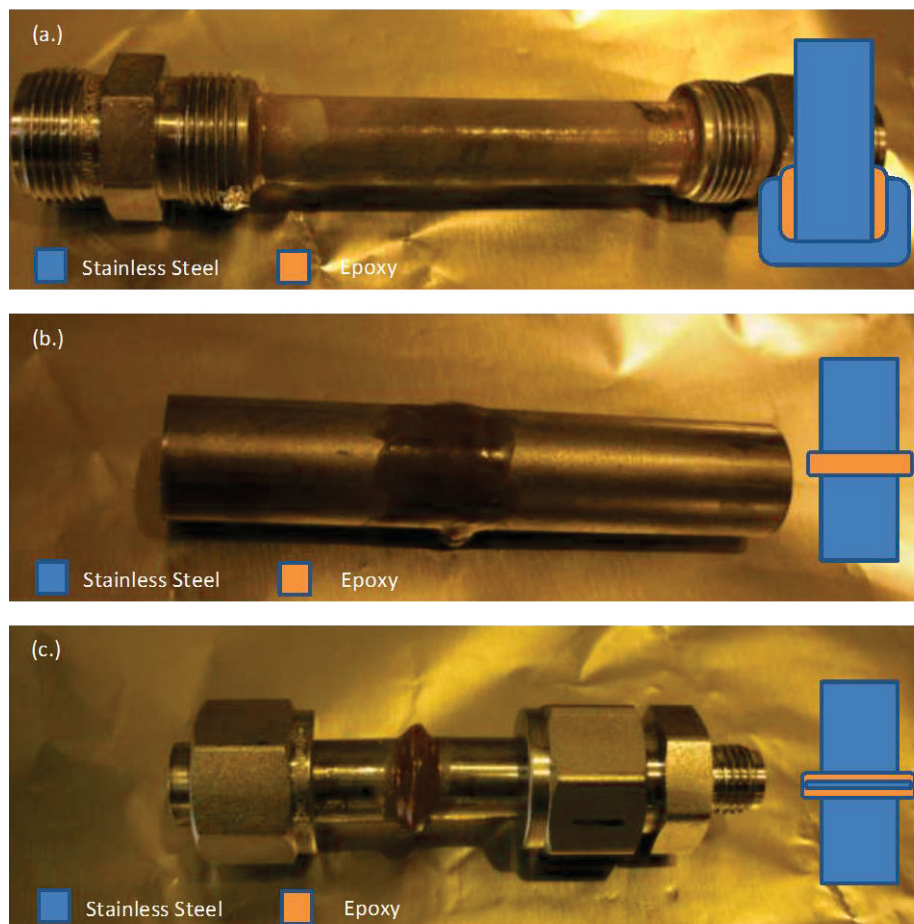


Figure F-14. (a) Standard tube in fitting geometry, (b) butt joint, and (c) modified butt joint that mimics seal to flat disk.

Prior to assembly, the metal tube surfaces were cleaned by wiping with solvent and roughened slightly with a metal file. Parts were assembled in each geometry, and H74 epoxy was applied and cured according to manufacturer's specifications. After the samples were sealed, they were tested for leaks at room temperature. Since no leaks were found, the samples were then heated to 200-250°C and allowed to free cool after a soak at temperature of at least 2 hours. The samples were then retested for leaks. All parts showed leaks at the epoxy – steel interface.

In order to improve the adhesion of the epoxy to the steel, the surface preparation of the metal parts was modified. The standard tube-in-fitting geometry was used, since no benefit was seen from geometry modifications. The surface of the steel that was to contact epoxy was roughened by sand blasting. An as-received part and sand blasted part are shown in Figure F-15.



Figure F-15. Steel fittings as received (left) and after surface treatment (right).

After sandblasting, the parts were ultrasonically cleaned in solvent to remove any residue from the surface. After this surface preparation, several samples were assembled, epoxied, and tested. Out of several samples tested, most showed leaks but one or two samples did not show leaks after one thermal cycle. Additionally, the amount of force required to break the epoxy seal was found to be greater than for a sample without pre-roughened surfaces.

Based on a discussion with a representative from Epotek, the epoxy curing temperature was raised from 150 to 200°C and thermal cycling tests were repeated. An additional soak at 100°C was added to the curing profile, to allow the epoxy to stabilize before raising the temperature to 200°C and allowing the epoxy to cure overnight (Figure F-16). A significant change in leak performance was not seen with the modified curing profile. System cooling rate was reduced greatly to see if a more gradual temperature change might alleviate the leak. The cooling rate was reduced from 4°C/min to 1°C/min. Epoxy leaks were still seen upon cooling at the same location.

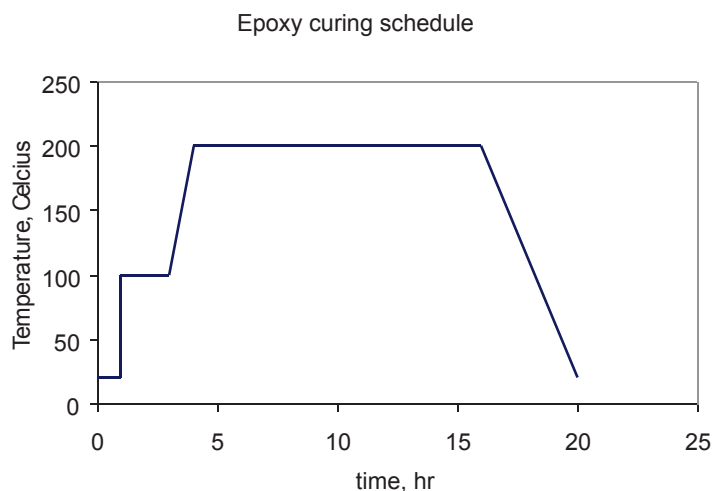


Figure F-16. Epoxy cure schedule, increased time and temperature.

Two other high temperature epoxies were considered: Cotronics Duralco™ 4525-IP and Aremco-Bond™ 526N-ALOX-BL. Test parts were assembled with these epoxies, utilizing the improved surface preparation and the modified curing schedule. These epoxies showed a leak at the same interface between the epoxy and the steel fitting. A more exhaustive survey of epoxies would be necessary to identify a better candidate for thermal cycling. It was decided to keep using the H74 epoxy with the understanding that samples could be heated only one time. This was used as an intermediate sealing method that allowed samples to be tested while developing membrane samples with welded steel ends.

Machined End Tubes

One of the methods attempted for sealing the ends of the porous stainless steel Mott tubes was to machine the ends on a lathe. During the machining process the lathe cutting tool shears and presses the metal particles together, filling in the gaps between them. Figure F-17 shows a close-up of a tube with a machined end followed by one that has been machined and then swaged on both ends. To test the method an entire tube was turned on the lathe, swaged on both ends, capped on one end, pressurized with hydrogen, and then valved off on the other end. Pressure was measured over a period of ten minutes. Approximately ten different samples were tested in this manner. In two cases the tubes were found to be leak free (i.e. no detectable drop in pressure) at 40 psig of hydrogen for ten minutes. In all other cases leaks were found. No systematic study was performed to determine the optimal machining parameters that result in a good seal since other sealing options were available as described later.

One important lesson learned was that swaging torque was a critical parameter. These sintered porous tubes were much more deformable than their solid stainless steel counterparts. Swaging has the effect of deforming the tube and reopening some of the pores near the ferrule. Additionally, too much deformation will result in a compromised ferrule to tube seal. This was shown to be the case by performing “snoop” leak testing on one of the tubes while tightening. Initially there were no leaks near the ferrule, but after a critical amount of tightening was performed bubbles began to form. As the ferrule was tightened further, bubbling became more vigorous indicating that the leak rate was getting worse. It was discovered that using nylon ferrules resulted in far fewer leaks near the ferrules than stainless ferrules since less torque need be applied. However in most cases where nylon ferrules were used leaks were found elsewhere on the machined surface.



Figure F-17. Close-up of a tube with a machined end (above) followed by one that has been machined and then swaged on both ends (below).

Welded Steel End Seals

The most reliable and scalable sealing solution was to have solid steel tubing welded to porous substrates prior to coating. Tubes of this sort were acquired from two sources: (1) supplied directly from the substrate manufacturer and (2) fabricated on site using existing porous substrates and standard seamless tubing. In both cases, the tubing was welded to the substrate and machined as necessary to provide a smooth interface between the porous and solid tube. There was no performance difference noted between the two types of tubes.

Prior to coating, on each end of the porous tubes a 1 in. long solid SST tube with a 0.5 in. OD was welded and machined such that there was a smooth, gap-free transition on the ID. The smooth transition was necessary to assure that the intermediate and polymer coatings could be applied without any discontinuities. The dense end addition was originally done by the manufacturer (Mott), and then later developed in-house. It was found that the best way to do this was to machine a small step in both the porous and dense tubes, fit them together, and then TIG weld the OD. Surface finish for the 1 in. extensions was specified at 20Ra. After coating the ID with the polyimide, the tubes were swaged for gas testing.

For laboratory testing, a standard compression seal to each end of the tube was used so that the module shell and test fixture could be reused for successive samples. In commercial practice, the tube would likely be welded into place. For leak tight compression seals, the tubing used must be close to the nominal diameter 0.500 in., not out-of-round and have a significantly smooth outer surface. According to Swagelok® Company, “tubing with any kind of depression, scratch, raised portion, or other surface defect will be difficult to seal, particularly in gas service.” Surface roughness along the tube provided a leak path for gas molecules between the ferrule and the tube wall. Several of the substrate tubes received had unacceptably rough surface finishes on the solid ends that had to be machined smooth to permit compression sealing. The surface machining required material removal, reducing the outer diameter of some tubes by as much as two thousandths of an inch.

In order to compensate for surface roughness and slightly reduced diameter, the performance of several different ferrule materials was tested. The ferrule seal was required to be substantially hermetic during thermal cycling from room temperature to 250°C while containing an internal pressure of at least 15 psig. Swagelok® tube fittings were tested using two piece ferrules of three different materials: 316 stainless steel, Teflon®, and graphite. In addition, a Parker CPITM fitting utilizing a single 316 stainless steel ferrule was tested.

A nonporous stainless steel tube (same type as the dense ends) was sealed to the membrane test fixture using each ferrule type. Each sample was pressurized to 15 psig with an equimolar mixture of H₂ and CO₂. An inert sweep gas stream flowed through the surrounding shell past the sample and to a mass spectrometer. The concentration of H₂ and CO₂ in the sweep gas stream were measured to determine the leak rate from the process side. Any detectable leak was attributed to the compression seal to the sample tube. The system was heated to 200- 250°C, held at temperature, and cooled back to room temperature.

The results of the ferrule material tests are shown in Figure F-18 and compared to the permeance measured through a typical coated tube. The leak through the seals needs to be at least an order of magnitude lower than the tube permeance so that the gas selectivity performance of the coating was not compromised by poor seals. The Teflon® ferrule leaked initially, but the leak decreased as the sample was heated. Upon cooling to room temperature, the leak was evident again, making the Teflon® unsuitable for thermal cycling.

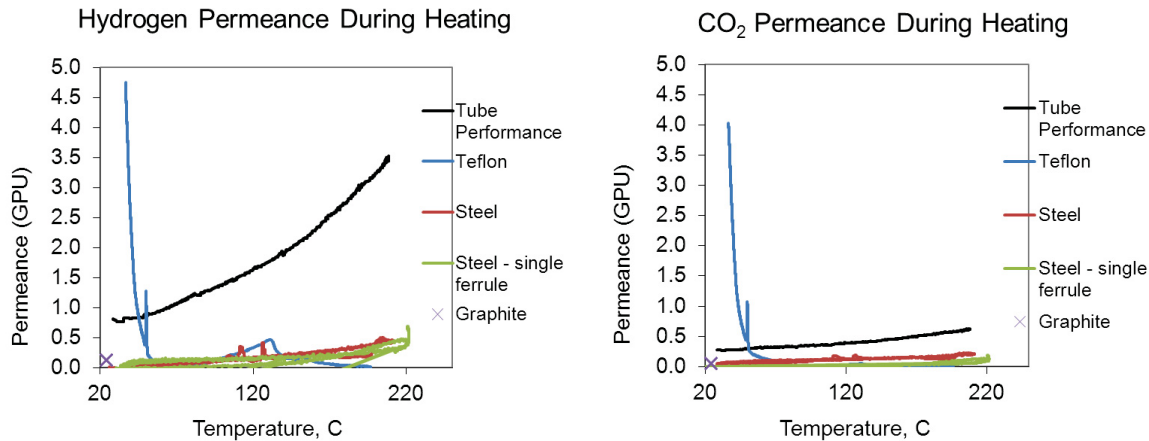


Figure F-18. Performance of ferrule materials during thermal cycle to 250°C.

Both the single and double stainless steel ferrules showed a permeance that was much less than the permeance of a coated tube (~ 10% at temperature), and both types of ferrules showed no detrimental effects from thermal cycling. The graphite ferrule had a higher leak rate than the steel ferrules at room temperature and was not heated. Of the two steel ferrule types, the single ferrule showed a lower CO₂ permeance than the two piece ferrule. The ParkerCPITM fitting with the single ferrule design was chosen to seal membrane tubes with solid ends to the test fixture.

Laser Welding of Tubes

There was concern that the heat generated by the welding process would compromise the coating, so to mitigate this risk we decided to use laser welding to attach the fittings to the dense ends. Because the laser energy can be precisely controlled and the weld can be precisely located, it was possible to create welds without generating large amounts of excess heat. However due to the precise nature of the weld, some additional prep work was needed. Before welding, the tube ends were turned on a lathe so that their OD matched that of the weld-on fitting. It was also necessary to machine the ends flat (also on the lathe) to assure a good mate between the pieces.

The laser welder uses an 80 Watt pulsed YAG 1064nm laser. The weld type was a seam weld with butt joint. Pulse energy was around 3.6 Joules per pulse. The laser was stationary and the workpiece was held in a rotating fixture. Rotational speed was 18 degrees per second, and the piece rotates one full turn (360°) with 10° overlap to ensure no gaps in the weld. Argon was used as the shield gas and the flow rate was 18 CFH.

Laser welding was attempted a total of 6 times and 2 out of the 6 joints were found to be leak free. Samples were leak tested by pressurizing with Helium to 50 psig and applying Snoop to the weld. Examples of a successful and unsuccessful weld are shown in Figure F-19 below. Even though the yield rate was only 33%, this was sufficient to prove that the laser welding method can be successfully implemented. There were a number of parameters that can be adjusted for this process such as pulse energy, laser focus, part rotation, fixture alignment, etc. Parameter optimization would be required in order to improve the yield rate above 33%. With optimization, we would expect close to a 100% yield rate.

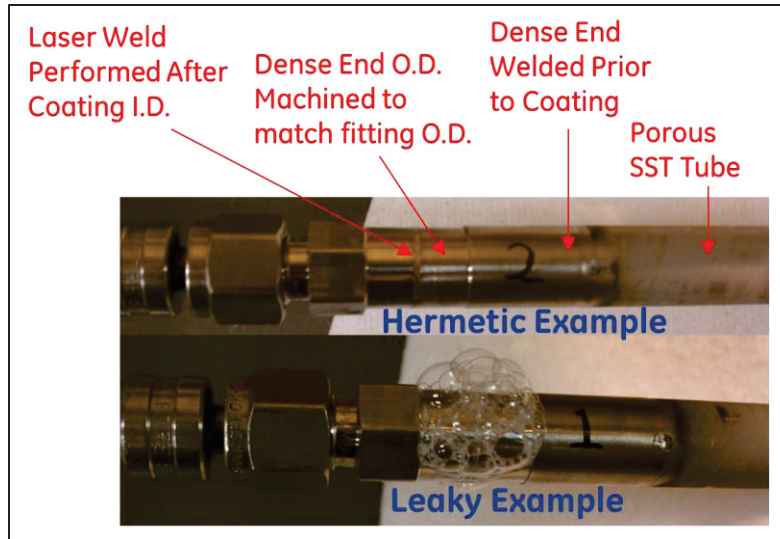


Figure F-19. Sample Laser Weld Results.

Porous Support Module Housing

The membrane tube was joined to Swagelok® tube fittings on either end using an epoxy seal or a compression seal onto dense ends, as previously described. This allowed the process gas to flow through the inner diameter of the membrane tube. One end was connected to the process gas delivery system and the other to exhaust (Figure F-20). A small segment of flexible hose was used in the process line to help with assembly and alignment of the tube into the module shell.

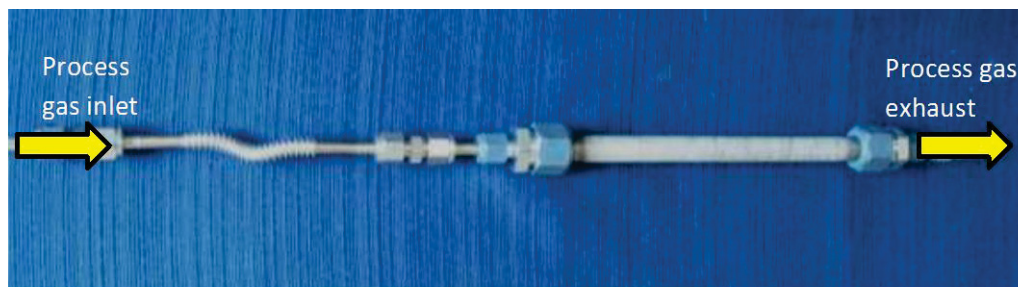


Figure F-20. Membrane tube with welded ends connected to process gas piping, using standard compression fittings.

The tube was surrounded by an outer housing constructed from 304 stainless steel components (1 nipple and 2 tees) with NW40 flanges on each end. The NW40 flange ends were held together by an aluminum clamp which compresses a centering ring assembly. The centering ring assembly was comprised of an overpressure ring, a silicone o-ring, and a stainless steel centering ring. The tube components passed through the end flanges and the inner diameter of the housing (Figure F-21). Sweep gas flow was allowed through the housing, countercurrent to the process gas flow.



Figure F-21. Membrane tube module. (a) Membrane connected to process gas plumbing and inserted into module housing. (b) Module housing encloses process line.

The maximum temperature of the test module was rated at 200°C, due to the silicone seals on the module shell components. In practice, the silicone o-rings can be taken as high as 220°C. The maximum temperature could be increased by replacing the silicone o-rings with Kalrez[®] 4059 o-rings, which have a maximum operating temperature of 327°C. Temperature was measured by a type K thermocouple inserted into the sweep gas and positioned near the center of the membrane. The maximum pressure of the test module shell was rated to 75 psig, also limited by the elastomer seals. The process side of the module was constructed of Swagelok[®] compression fittings, 0.5 in. steel tubing, and the seal to the membrane tube. In the case of a membrane tube with welded metal ends and compression fittings, the process side can be pressurized up to 1000 psig, limited by pressure rating of the Swagelok[®] fittings at temperature.

High Performance Polymers on Porous Supports Bench Gas Permeability Testing for Metal Tube Porous Supports

After coated tubes were produced, the first tests performed were bench tests designed to quickly determine if the coating and end seals were substantially free of large defects or leaks. Single gas permeance testing was used to screen sample quality prior to sample measurement with the mass spectrometer. An approximate single gas permeance as a function of applied pressure could be determined for samples with flows > 0.1 sccm. It took < 1 hour to bench test a sample compared to the minimum 2 hours to measure a sample in the mixed gas rig. This test was typically conducted with nitrogen, so it was typically referred to as the nitrogen permeance test. Bubble testing was performed at the same time to ensure that there were no leaks present around the seals. Figure F-22 shows the test set-up used for bench testing.



Figure F-22. Nitrogen permeance test of a composite membrane tube.

The test-set up consisted of a gas source (house plumbing or cylinder), a 0-100 sccm mass flow controller which could measure pressure, and appropriate fixturing to connect a mounted sample to the system. System measurement capability could be expanded by using additional MFCs with higher or lower flow ranges.

The end sealed sample was connected to the MFC via Swagelok® connection. The other end of the sample was sealed with a cap. In order to calculate the sample permeance, the following parameters were needed:

1. Atmospheric pressure - The MFC that was used displayed pressure and temperature. The reading on the instrument prior to connecting the sample was used as the atmospheric pressure.
2. Sample area – The unsealed length of the sample was used to calculate sample area.
3. Flow rate – This was the flow that was delivered by the MFC into the sample. The flow rate was set on the MFC prior to the measurement.
4. Pressure - At a given flow rate, the pressure inside the sample could be read from the MFC display.

Gas was delivered to the sample, starting at the lowest possible flow rate 0.1 sccm. If the pressure in the sample increased to greater than atmospheric pressure, the pressure was allowed to stabilize and the first data point was taken at this flow rate. Otherwise, the flow rate was increased until the pressure in the sample was greater than atmospheric pressure. The pressure was allowed to stabilize. In some cases, at low flow rates, this could take more than 30 min. The flow rate and pressure were recorded when they were stable. From this information, the permeance of the sample could be calculated. This calculation assumed that the sample was being pressurized with nitrogen and that the atmosphere outside the tube was air. A sample calculation is shown in Table F-4.

Table F-4. Calculations of ΔP , flux and permeance from flow rate and sample pressure.

| | | |
|---------------------|-----------------------|----------------|
| Sample area | m ² | 0.003506 |
| Gas | - | N ₂ |
| P _{sample} | PSIA | 14.81 |
| P _{atm} | PSIA | 14.78 |
| T | C | 22.34 |
| Flow | sccm | 2 |
| ΔP | PSID | 0.03 |
| J flux | mol/m ² /s | 0.000424 |
| Permeance | GPU | 57 |

The pressure gradient $\Delta P = P_{\text{sample}} - P_{\text{atm}}$. This was the total pressure difference between the pressure inside and outside the tube. The flow rate of nitrogen into the sample was converted to flux:

$$J = \frac{f}{A} \left(\frac{1L}{1000cc} \right) \left(\frac{1 \text{ min}}{60 \text{ s}} \right) \frac{1 \text{ mol}}{22.4 \text{ L}}$$

where,

J = flux in mol/m²/s

f = flow rate into sample, sccm

The nitrogen permeance of the sample was calculated by dividing the flux by the pressure gradient of nitrogen across the membrane.

Table F-5. Data set from nitrogen permeance bench test.

| Gas | P [PSIA] | Patm | DP [PSID] | T [C] | Flow sccm | J [mol/m ² /s] | Perm [GPU] |
|-----|----------|-------|-----------|-------|-----------|---------------------------|------------|
| N2 | 14.81 | 14.78 | 0.03 | 22.34 | 2.0 | 0.000424 | 12.6 |
| N2 | 15.01 | 14.78 | 0.23 | 22.37 | 20.0 | 0.004244 | 124.3 |
| N2 | 15.82 | 14.78 | 1.04 | 22.41 | 50.0 | 0.010611 | 294.8 |
| N2 | 16.34 | 14.78 | 1.56 | 22.51 | 75.0 | 0.015916 | 428.1 |
| N2 | 16.85 | 14.78 | 2.07 | 22.59 | 100.0 | 0.021222 | 553.5 |

From this data set, the permeance can be plotted as a function of ΔP (Figure F-23).

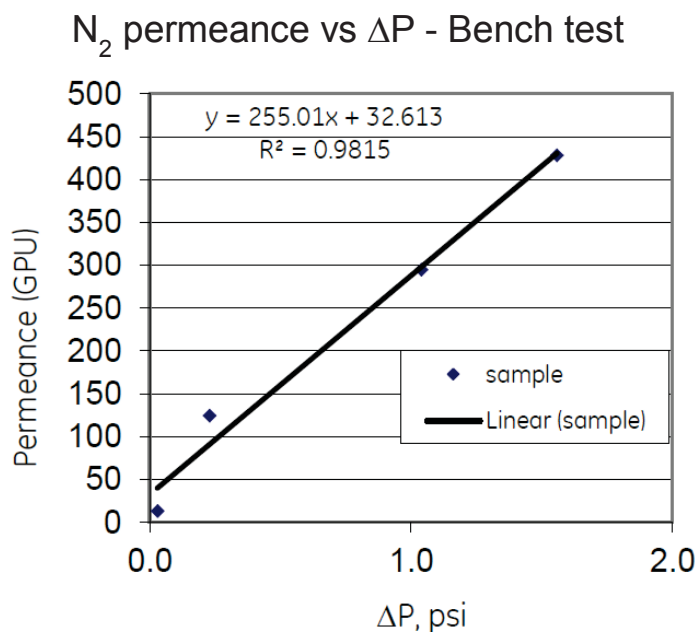


Figure F-23. Plot of nitrogen permeance with increasing pressure gradient.

From the graph (Figure F-23), the slope and intercept of the permeance values were obtained and used to compare samples. The slope was found to increase due to the increase of viscous flow through the sample as pressure was increased. Higher slope was found to increase due to the higher viscous flow through the sample, possibly due to either a seal leak or large defective areas in the coating. Since the flux through the defect-free polyimide coatings was small (on the order of 0.1 sccm) due to a 1-5 μm thick coating layer, a sample was considered to have passed the nitrogen permeance test if pressure inside the sample increased to greater than 30 psia at 0.1 sccm of N_2 flow to the sample.

Following the estimation of permeance from the data, a bubble test was performed while the sample was still pressurized with nitrogen. The sample coating and seals were then qualitatively evaluated for large leaks or defects by bubble testing with a soap solution such as Snoop. The sample was internally pressurized to 15 psig with nitrogen. The flow rate into the sample was then adjusted to hold sample pressure ~ 15 psig, while the sample was wet with soap solution, and the bubble locations were noted as shown in Figure F-24. This test was typically performed on samples that had high viscous flows and were considered poor quality samples. If bubbles were seen during this test the samples were rejected since it would not show any H_2/CO_2 selectivity during testing due to the presence of large defects causing leaks.

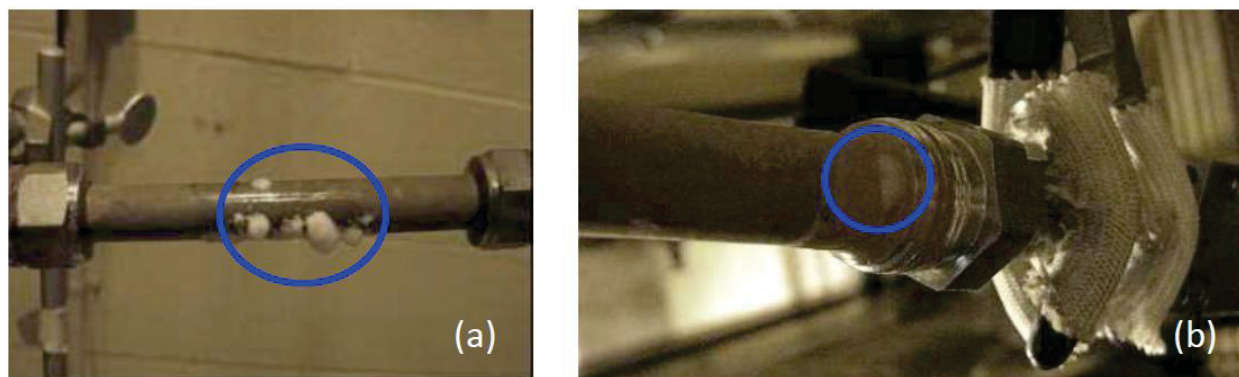


Figure F-24. Leaks indicated by bubble test at (a) coating and (b) seal.

H_2/CO_2 Testing at GEGR

The membrane test facility at GEGR can measure the flow performance and separation capability of gas separation membranes. Membranes can be tested in two geometries: flat samples up to 1 in. across and tubular samples up to 1 in. diameter. The samples can be tested using pre-mixed bottle gases or using the gas mixing system to blend the desired ratio of H_2 , CO_2 , and N_2 . Additionally, the gas mixing system was designed to allow for gas mixtures containing H_2S and CO . Steam could be generated within this system and added to the process gas stream.

The membrane test facility consisted of a gas blending system that delivered a pre-mixed gas stream to the feed side of a separation device, which was mounted inside a furnace for heating, along with backpressure regulation systems, gas composition measurement devices, and additional instrumentation for control and recording of process conditions. The experiment was housed inside an enclosure with a dedicated fan and toxic/hazardous gas monitoring system and was fully automated and designed for unattended operation. Control of the system and data acquisition was performed with National Instruments compact Fieldpoint Modules connected to a PC running LabView software. Figure F-15 shows the experimental rig.



Figure F-15. Membrane test facility.

The gas blends can include some or all of the following constituents: hydrogen (H_2), carbon dioxide (CO_2), nitrogen (N_2), carbon monoxide (CO), hydrogen sulfide (H_2S), and water/steam (H_2O). Hydrogen, carbon dioxide, and nitrogen were supplied from high pressure gas cylinders piped around the perimeter of the lab and into the enclosure. Hydrogen sulfide and carbon monoxide (if used) could be supplied from small gas bottles stored inside the enclosure. All gases were metered into the flow loop using electronic mass flow controllers. The constituent gases passed through regulators capable of supplying up to 100 psig gas pressure. The gases would then flow into the mass flow controllers (MFCs) and the gas mixture(s) would then flow through the membrane module, which was mounted in a temperature controlled furnace.

Downstream of the module the feed and sweep gases would exit the furnace through the backpressure regulators to the mass spectrometer. The gases were then vent into the exhaust line.

The gases that permeate through the membrane were carried by an inert sweep gas stream. The pressure gradient across the sample was measured by a differential pressure transducer which measured the pressure difference between the process gas and sweep gas outlets in the system. From this data, the permeance and selectivity of a sample could be evaluated at temperatures from room temperature to $250^\circ C$.

For testing polyimide membranes, equimolar H_2/CO_2 was used as an ideal syngas mixture. The membrane was mounted and enclosed in a stainless steel module housing. H_2/CO_2 mixture was fed inside the tube at a flow rate of 1 slpm. A countercurrent flow of 1 slpm N_2 sweep was fed through the shell as a sweep gas to carry the permeate out of the system. The concentration of H_2 and CO_2 in the sweep stream was measured and the permeance values were calculated.

Permeance of a component gas was calculated from the flow rate of gas through the membrane, divided by membrane area and the partial pressure gradient of that gas across the membrane.

$$\text{Permeance} = F / A \Delta P$$

where, F = flow in mol/s of component i through the membrane

A = membrane area, m^2

$\Delta P_i = P_{\text{feed}} - P_{\text{sweep}}$ for component i , Pa

$$\text{Permeance}_i = \frac{F_i}{A \Delta P_i} = \frac{\text{mol}}{\text{m}^2 \text{ Pa s}}$$

$$\text{Permeance} = \frac{\text{Gas Signal (torr)} * \text{Signal to Flow rate conversion based on calibration (cc/s/torr)}}{\text{Membrane Area (m}^2\text{)} * 22400 \text{ (conversion to mol)} * \text{Partial pressure gas in feed (Pa)}}$$

Permeance was reported in Gas Permeation Units or GPU ($1 \text{ GPU} = 10^{-6} \cdot \text{cm}^3(\text{STP}) / \text{cm}^2 \cdot \text{s} \cdot \text{cmHg}$), which was the value above divided by 3.3×10^{-10} . Mixed gas selectivity of one gas with respect to another was calculated from the relative flows of gas through the membrane.

$$\text{Selectivity (gas}_1\text{/gas}_2\text{)} = \frac{\text{Gas}_1 \text{ Permeance}}{\text{Gas}_2 \text{ Permeance}}$$

H_2/CO_2 testing was typically reserved for samples that have passed both the nitrogen permeance test and the bubble test. The first mixed gas test performed was a room temperature pressure sweep. The pressure across the membrane was increased from 0 -15 psid, and the gas separation performance was measured at a minimum of three points. This test provided information about membrane defects, permeance, and selectivity. The H_2 and CO_2 permeance and H_2/CO_2 selectivity with no pressure gradient across the membrane represented the material performance with no contribution from defects large enough to permit viscous flow. In the case of H_2/CO_2 , Knudsen flow was expected to dominate at pore sizes less than 20 nm with a H_2/CO_2 selectivity for Knudsen flow of 4.7. Pores larger than 20 nm would typically allow non-selective viscous flow. As the pressure was increased, if there was a pathway for viscous flow, the permeance values would increase and H_2/CO_2 selectivity would decrease close to 1 indicating no separation capabilities of the membrane.

If the selectivity at increased pressure gradient did not decrease below the Knudsen selectivity of 4.7, the sample was heated to 200°C . At elevated temperature, the H_2 permeance of the polyimide increased significantly. By contrast, Knudsen flow decreased as a function of temperature. After a soak at 200°C , the membrane was cooled back to room temperature by natural convection. If the permeance increased during cooling or did not decrease upon return to room temperature, the membrane may have developed a leak during testing possibly due to damage to the coating or gas bypass through a seal.

Appendix G. High Performance Polymers on Porous Supports Polyimide Hollow Fiber Membranes for Gas-Separation

Hollow Fiber Membrane Fabrication Process

For spin dope preparation, a measured amount of polyamic acid solution was added to the 1000 mL glass jar (Quorpak, Bridgeville, PA), followed by the addition of desired quantities of solvents (THF), non-solvents (ethanol) and additive (PVP) to get the desired composition. The dope was sealed and put on a roller at room temperature (gen-1 dopes) or heated to 40 - 50°C (Gen-2 dopes) with the help of an IR lamp, until complete additive dissolution and dope uniformity was observed. The spin dope and bore fluid were then poured into syringe pumps (Model: 500 DM, Teledyne Isco, Lincoln, NE) for spinning and kept undisturbed for about 12 h to ensure complete degassing of the dope solution.

Hollow fiber membranes were made by the dry jet-wet quench solution spinning technique. Figure G-1 shows a schematic representation and a photograph of the fiber spinning apparatus. Figure G-2 shows the side and front section view of the dual compartment hollow fiber nozzle used in this work.

Table G-1 summarizes the various spinning parameters used in the project with their typical range. Polymer solution or dope was fed to the outer compartment, and simultaneously; the bore fluid (or internal coagulant) was fed into the inner compartment. The core dope flow rate was varied between 180-1000 mL/hr, while, the bore layer flow rate was varied between 0.3-0.5 times the core flow rate. The bore fluid and the core dope were filtered through 15 μm and 40 μm mesh size in-line filters to remove any impurities or insoluble particles before entering the nozzle channels. Spinning temperatures (spinneret, pumps and transfer lines temperature) of 25°C and 40°C were studied.

The extruded nascent fiber then passed through an adjustable air gap (dry jet) varied between 0-15 cm before entering the external coagulant or quench bath (wet quench) where it phase separates and vitrifies. In the air gap, volatile solvents (THF) and non-solvents (ethanol) leave the dope, thereby driving the outer surface composition close to the vitrified region and forming the skin layer. Tap water was used as an environmentally friendly and easily available quench bath (1 m deep) medium. A rotating water wheel located in the coagulation bath was used to maintain uniform mixing and bath temperature. Quench bath temperatures of 30°C and 50°C were studied. In the quench bath, ingress of the non-solvent (water) and outflow of the solvents drive the composition of the region below the skin layer into the two-phase region, thereby forming the substructure. In this way, spinning through both the air gap and entering the quench bath results in the desirable asymmetric morphology. The fiber passes under two Teflon[®] guides located in the quench bath and is either collected by a free-fall mechanism into a collection bath filled with DI water or onto a 25 cm (Gen-1 fibers) or a 75 cm (Gen-2 fibers) circumference rotating take-up drum continuously replenished with fresh DI water (Figure G-1). The take-up rate was also a variable factor with typical speeds up to 30 m/min used in the study with a maximum take-up speed of 70 m/min achieved in the runs. Once collected, each state was allowed to rotate on the drum at speed of around (<10 m/min) for about 15 min to allow complete phase separation and vitrification.

Fibers spun under identical conditions (called a 'spin state') comprising 10-20 fibers, 75 cm in length, were removed from the take-up drum and tied together. By manipulating various spinning parameters, several spin states were collected and analyzed. Each spin state was individually soaked in 1 m long, 1 inch diameter solvent exchange tubes to prevent curling and entanglement of the fibers (Figure G-3). The fibers were soaked in de-ionized (DI) water for up to 3-5 days changing with fresh DI water daily. The exchange with fresh DI water helped in leaching out residual solvents and non-solvents from the fiber substructure. The PVP additive was also leached out owing to its solubility in water. Removal of PVP helps in formation of a more open and porous fiber substructure. The water present in the fiber sub-

structure was then solvent exchanged by immersion of spin states for 30 minutes each in three batches of fresh methanol followed by three batches of fresh hexane. To remove the residual hexane, fibers were hung in a fume hood at room temperature for 1 hour and stored for further characterization.

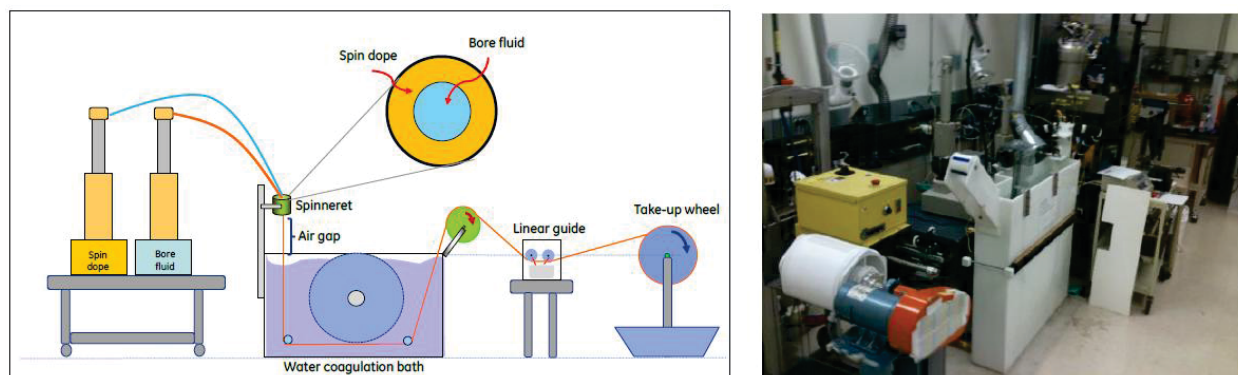


Figure G-1. (left) Schematic representation of the hollow fiber fabrication setup; (right) Photograph of the hollow fiber fabrication setup.

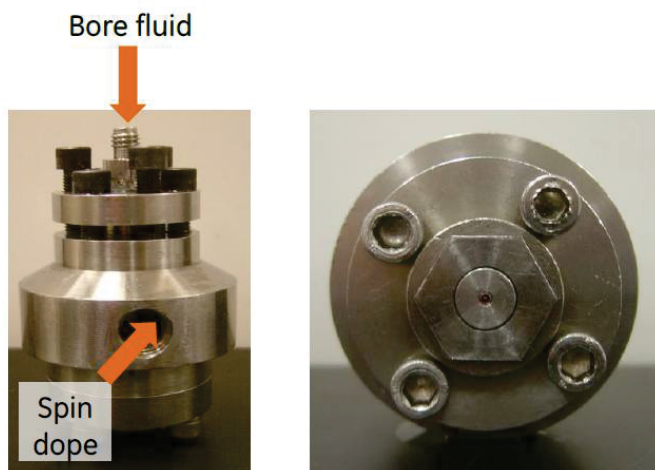


Figure G-2. Front and cross section view of the dual compartment hollow fiber nozzle used in this work

Table G-1. Spinning conditions for dual layer fiber sorbents.

| | |
|-----------------------|---|
| Dope (Core) | |
| Pump temperature | 40°C (gen-1, Gen-2), 25°C (gen-2) |
| In-line temperature | 40°C (gen-1, Gen-2), 25°C (gen-2) |
| Flow rate | 180 to 1000 mL/h (typically 180 to 300 mL/hr) |
| Bore fluid | |
| Composition | NMP:Water = 95:5 wt.% (gen-1), 70:30 (gen-2) |
| Temperature | Room temperature |
| Flow rate | 60-500 mL/h (0.3-0.5 of core flow rate) |
| Spinneret temperature | 40°C (gen-1, Gen-2) and 25°C (gen-2) |
| Air temperature | Room temperature ($\approx 25^{\circ}\text{C}$) |
| Air-gap | 0-15 cm (typically 10 cm) |
| Quench bath | |

| | |
|----------------------------------|----------------------------------|
| Media | Tap water |
| Depth | 1 m |
| Temperature, T_{quench} | 30°C and 50°C (typically 30 °C) |
| Take-up rate | 15-70 m/min (typically 30 m/min) |



Figure G-3. Extruded polyamic acid hollow fibers in a solvent exchange tube filled with DI water.

Gen-1 polyamic acid hollow fiber fabrication

Cloud point technique was utilized to formulate the Gen-1 spin dope and bore fluid compositions as described in Table G-2 and Table G-3 respectively. A dope temperature of 40°C and a quench bath at temperature $\approx 30^\circ\text{C}$ were used.

Table G-2. Spin dope compositions identified for hollow fiber membrane creation (units in wt. %).

| ID | Polyamic acid solution | THF | PVP | Ethanol |
|-------|------------------------|------|-----|---------|
| Gen-1 | 80.1 | 10.9 | 6 | 3 |
| Gen-2 | 89 | 0 | 8 | 3 |

Table G-3. Summary of bore fluid compositions (units in wt. %).

| Bore Fluid | NMP | Water |
|------------|-----|-------|
| Gen-1 | 75 | 25 |
| Gen-2 | 70 | 30 |

The dope was found to have a low viscosity and slow phase separation rate possibly due to high dope temperature (40°C). The slow phase separation could be attributed to the experimental binodal curve determined at room temperature shifting at higher process temperatures. This could have led to a slower phase separation of the nascent fiber in the non-solvent water coagulation bath. Take up rates of 15 m/min were feasible, with higher take-up rates leading to fiber strand breakage. THF was found to be a swelling agent for the dope and caused the nascent fiber to stick to the guide roles causing inability to be drawn onto the take-up drum. The fibers were solvent-exchanged using the protocol described earlier. The

polyamic acid fibers were found to be stable even upon prolonged exposures of soaking (3-5 days) in the solvent exchange bath.

Figure G-4 shows the SEM images of the as-spun Gen-1 hollow fibers (GE ID: Spin 2). Finger-shaped macrovoids were observed in the outer part of the hollow fiber. Macrovoids can be attributed to the low viscosity of the spin dope and can be reduced or eliminated by increasing the dope viscosity which delays the diffusion of solvent into the polymer-lean phase that causes the growth of macrovoids.

Typical water-gas shift operations involving H_2/CO_2 separations are conducted at gas pressures of up to a maximum of 30 bar (450 psi). Macrovoids can reduce the mechanical strength of the fiber causing it to burst or collapse at high trans-membrane pressures. Macrovoids can also cause non-selective pathways for gas/water vapor flow rendering the thin-selective layer ineffective.

The hollow fiber membranes were observed to have a tear drop-shaped bore structure possibly due to slow phase separation rate in the air-gap and the water coagulation bath before it hit the first guide role. The slow phase separation rate could be attributed to the high NMP (solvent) content in the bore fluid. A reduction in the solvent content of the bore fluid can lead to a faster phase separation of the bore giving it the circular, uniform structure. One spin run (Spin 2) was completed using Gen-1 spin dope and bore fluids compositions. To reduce or eliminate the formation of macrovoids in the fiber wall and formation of uniform circular bore layer, Gen-2 spin dopes and bore fluid compositions were developed.

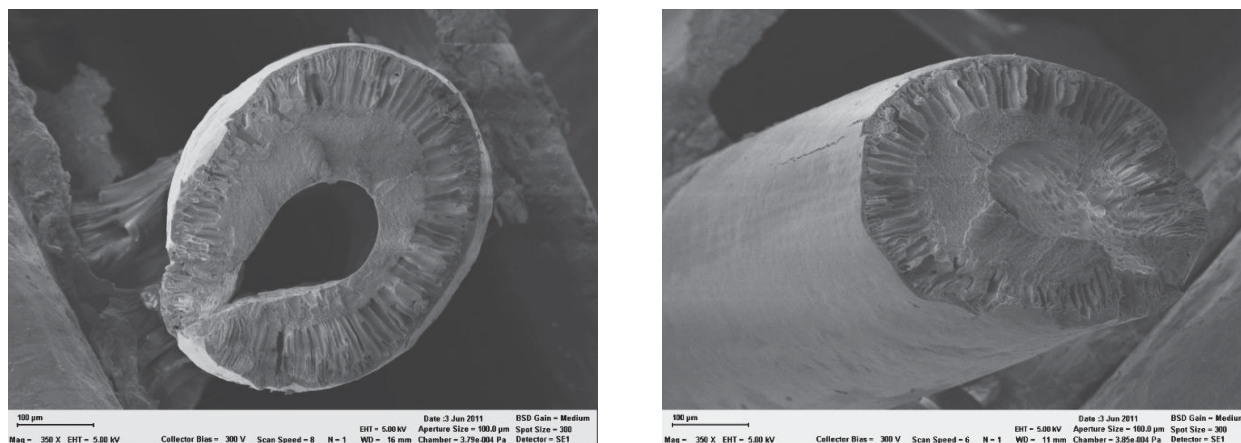


Figure G-4. (left to right). (a) Cross-section SEM image of the as-spun Gen-1 hollow fibers (b) Horizontal SEM image of the as-spun Gen-1 hollow fiber membranes (GE ID: Spin 2).

Gen-2 polyamic acid hollow fiber fabrication

Cloud point technique was used to modify the dope composition based on the learnings from Gen-1 hollow fiber fabrication. The modified dope composition is summarized in Table G-2. The PVP additive content was increased from 6 to 8 wt. % to increase the dope viscosity and THF (high volatility solvent) was removed. The ethanol (high volatility non-solvent) content was kept the same. The bore fluid composition was modified to a 70:30 wt.% NMP:Water to give a neutral bore fluid. Spinning temperatures (spinneret, pumps and transfer lines temperature) of 25°C, 40°C were studied.

The dope viscosity was found to be appropriate for fiber spinning as shown in viscosity measurements in Figure G-5. The spin dope indicated a viscoelastic behavior with shear thinning behavior observed at higher shear rates. The dope viscosity was found to reduce at higher temperature, as expected. In the first run with Gen-2 spin dope a dope temperature of 25°C was used. The viscosity of the spin dope led to a high pressure build-up in the nozzle dope compartment, leading to possible misalignment of the nozzle. The high viscosity led to a large die swell at the nozzle annulus and the bore needle misalignment lead to the bore fluid flowing through the side of the nascent fiber. This undesired

phenomenon led to formation of a solid fiber with a semi-circular structure (GE ID - Spin 3), with a porous flat-region possibly caused by the bore fluid flow as shown in Figure G-6.

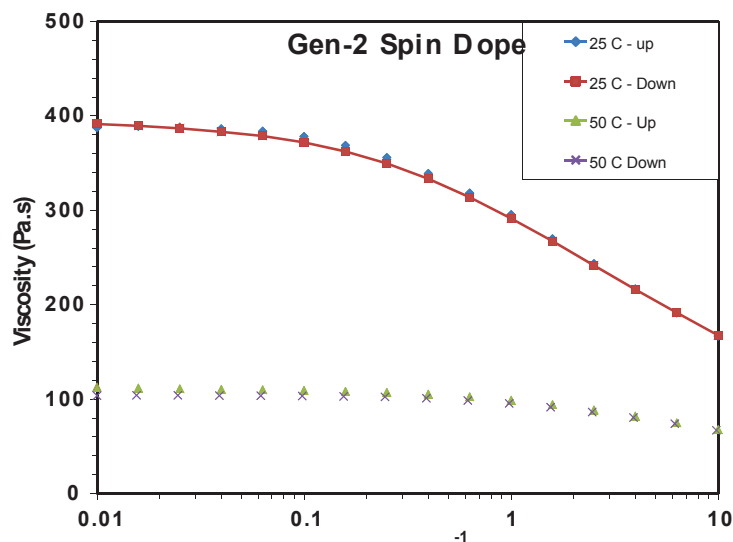


Figure G-5. Viscosity measurement of Gen-2 spin dopes.

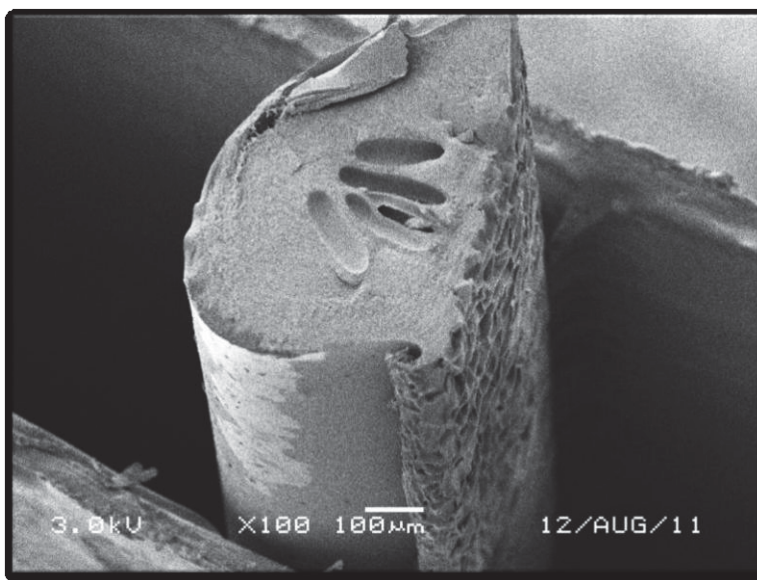


Figure G-6. Cross-section SEM image of undesired hollow fiber morphology caused by high viscosity spin dope fluid leading to nozzle misalignment (GE ID: Spin 3).

Viscosity measurements

Viscosities of Gen-2 dopes were measured to augment the observations from the cloud point technique. TA instruments rheometer, Model ARG2 fitted with a cup-bob fixture at a sweep rate from 0.01 s^{-1} to 10 s^{-1} was used. The dope viscosity was measured at 25 and 50°C respectively. The viscosity measured at very low shear rates (0.01 s^{-1}) can be used to approximate the dope viscosity in the binodal diagram, while the viscosity at high shear rate (10 s^{-1}), can be approximated as the dope viscosity at the nozzle annulus during the fiber spinning process.

Scanning electron microscopy (SEM)

The surfaces and cross-sections of hollow fibers were examined by optical microscopy and scanning electron microscopy (SEM). The cross-sections of fibers were prepared by freeze fracturing the fiber in liquid nitrogen. SEM samples underwent further preparation by mounting on copper SEM tape and sputter-coating with gold. The morphology of the fibers, as observed in the microscopy images, led to changes in spinning process parameters.

TGA Study

Spin 4, state-4 fibers were analyzed in platinum sample pans with Inconel capped bale wires using a TA Instruments Q5000 TGA (Serial #: 5000-0108) under nitrogen flow, with a purge rate of 10 mL/min in the balance chamber. Calibration verification was performed using alumel and nickel with expected Curie point transitions of 154°C and 358°C. The experimental values were found to be within 5°C of the expected values when analyzed at a ramp rate of 2°C/min under a nitrogen purge of 50 mL/min. The 30 minute hold at the beginning of the run allowed time for room air to exchange with nitrogen purge before the start of the heating run.

Three TGA runs were performed using the conditions specified in Table G-4 through Table G-6. The ‘baseline’ protocol replicated the protocol developed by INL, while, the other two protocols explored the effect of reducing the time taken and the gas flow rate for the imidization process (Figure G-7).

Table G-4. Conditions for TGA — “Baseline”

| Hold Temperature (°C) | Hold Time (hrs) | Temp Ramp Rate | (°C/min) | 2 |
|---------------------------|--------------------|---------------------------------|------------|---------|
| RT | 0.5 | N ₂ Flow Rate | (mL/min) | 50 |
| 100 | 1 | N ₂ Exchange Rate | (per min.) | 10 est. |
| 150 | 24 | | | |
| 250 | 24 | | | |

Table G-5. Conditions for TGA — “Short Run”

| Hold Temperature (°C) | Hold Time (hrs) | Temp Ramp Rate | (°C/min) | 2 |
|---------------------------|--------------------|---------------------------------|------------|--------|
| RT | 0.5 | N ₂ Flow Rate | (mL/min) | 50 |
| 100 | 0 | N ₂ Exchange Rate | (per min.) | 1 est. |
| 150 | 6 | | | |
| 250 | 6 | | | |

Table G-6. Conditions for TGA — “Low Flow”

| Hold Temperature (°C) | Hold Time (hrs) | Temp Ramp Rate | (°C/min) | 2 |
|---------------------------|--------------------|---------------------------------|------------|--------|
| RT | 0.5 | N ₂ Flow Rate | (mL/min) | 5 |
| 100 | 0 | N ₂ Exchange Rate | (per min.) | 1 est. |
| 150 | 6 | | | |
| 250 | 6 | | | |

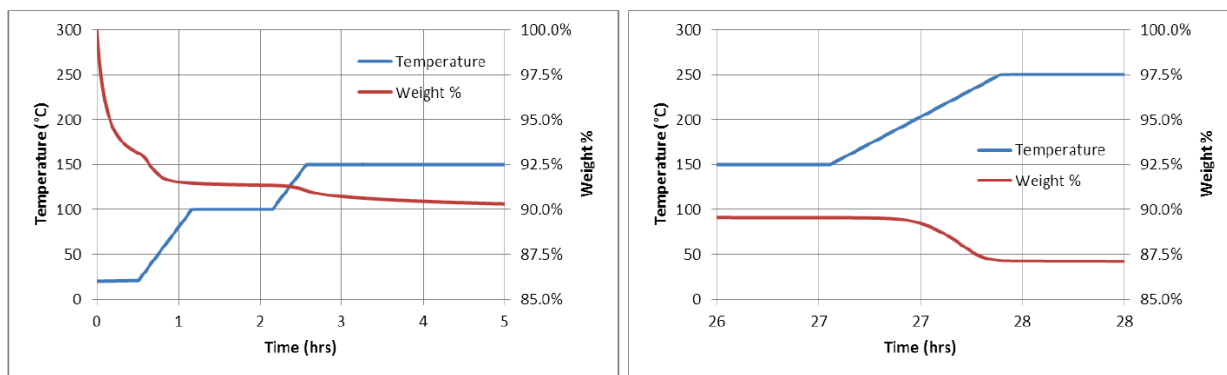


Figure G-7. Detail sections of the TGA profile, where the left graph shows the evaporation of physisorbed molecules and the right graph shows the water loss associated with the imidization reaction.

The fibers lost approximately 6.7% of their weight during the 30 minute hold at room temperature. This accounts for more than half of the total weight loss during the TGA run. The fibers were stored in a plastic bag (stagnant air) prior to the TGA run. Therefore, this large weight loss could be physisorbed water or excess hexane which came off in the dry nitrogen stream. The desorption of these components was mostly completed by 80°C, with an additional 1.8% weight loss.

The one hour hold at 100°C proved to be unnecessary, as no significant weight loss occurred. The sample lost an additional 2 wt% by the end of the 150°C hold, with the majority (75%) of this weight loss occurring in the first six hours of the hold. This is expected to be from trace NMP and PVP removal.

The next significant weight loss was during the ramp from 150°C to 250°C, with the highest rate of weight loss occurring at 227°C. The sample lost 2.4 wt% during this ramp. This weight loss could be associated with imidization of the poly(amic acid) to form the polyimide structure with water as a byproduct. The imidization process appears to be completed by the time the sample reached 250°C. The hold at 250°C was largely unnecessary given that it only resulted in a 0.2% weight loss. These weight losses are summarized in Table G-7, along with possible sources for each weight loss.

Table G-7. Summary of TGA Weight Losses in “Baseline” Run

| Step | Weight Loss (%) | Potential Source |
|---------------|-----------------|--------------------------------------|
| RT Hold | 6.7% | Physisorbed H ₂ O, Hexane |
| RT to 100°C | 1.8% | Physisorbed H ₂ O, Hexane |
| 150°C Hold | 2.0% | Trace NMP / PVP |
| 150°C - 250°C | 2.4% | Imidization (H ₂ O) |
| 250°C Hold | 0.2% | Imidization (H ₂ O) |

The rates of weight loss during the TGA run were analyzed by plotting the first derivatives of the TGA data. The first derivative of the weight loss with respect to temperature is shown in Figure . The isothermal holds were removed from this data and all temperature ramp rates were 2°C/min during the run. The first derivative of the weight loss with respect to time is shown in Figure . This graph includes all of the run data after the 30 minute hold at room temperature.

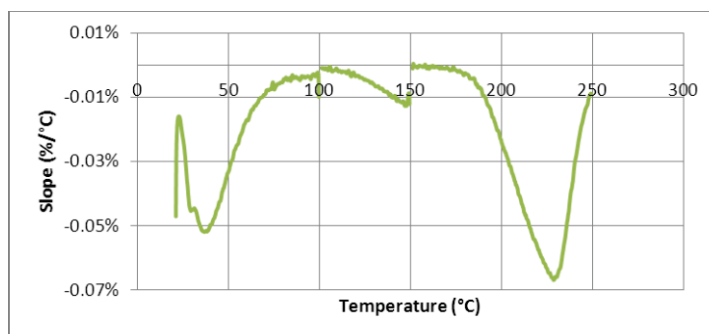


Figure G-8. First derivative of the weight loss in the “Baseline” TGA run with respect to temperature.

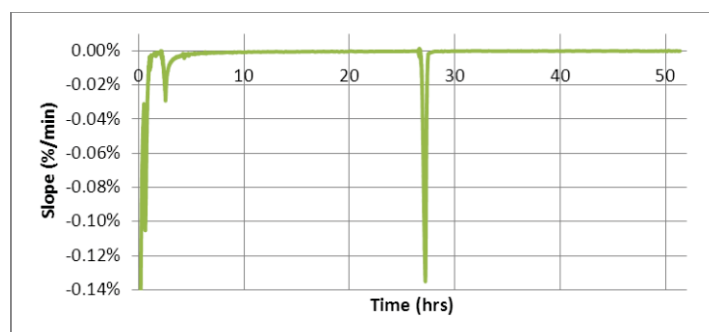


Figure G-9. First derivative of the weight loss in the “Baseline” TGA run with respect to time.

The fastest rate of weight loss in the hollow fibers occurred in the beginning of the 30 minute nitrogen sweep at room temperature. The rate of weight loss in the first 2 minutes was around 1.0 wt %/min, but quickly dropped off to less than 0.1 wt%/min after 16 minutes under nitrogen purge. There were three peaks in the rate of weight loss: 1) 37°C, 2) 147°C, and 3) 226°C. Since the second peak was very close to an isothermal hold, it is difficult to determine whether this weight loss rate would have kept increasing without the hold, to peak at a higher temperature. Regardless, the two 24 hour holds at 150°C and 250°C were significantly longer than necessary, as evident by the negligible rates of weight loss between 8 and 26 hours and 28 and 51 hours in Figure G-9. Hence, a modified “Short Run” protocol was developed and TGA studies were conducted to verify if results similar to “Baseline” TGA studies were obtained.

The TGA results from the “Short Run” were very similar to the “Baseline” TGA data. This was to be expected, since the only change was to eliminate the isothermal sections with minimal weight loss (i.e. eliminate the 100°C hold and significantly reduce the 150°C and 250°C holds). The summary of weight losses during the “Short Run” is shown in Table G-8, with the profile for the run shown in Figure G-10.

Table G-8. Summary of TGA Weight Losses in the “Short Run”.

| Step | Weight Loss (%) | Potential Source |
|---------------|-----------------|--------------------------------------|
| RT Hold | 5.0% | Physisorbed H ₂ O, Hexane |
| RT to 150°C | 2.0% | Physisorbed H ₂ O, Hexane |
| 150°C Hold | 1.9% | Trace NMP / PVP |
| 150°C - 250°C | 2.0% | Imidization (H ₂ O) |
| 250°C Hold | 0.3% | Imidization (H ₂ O) |

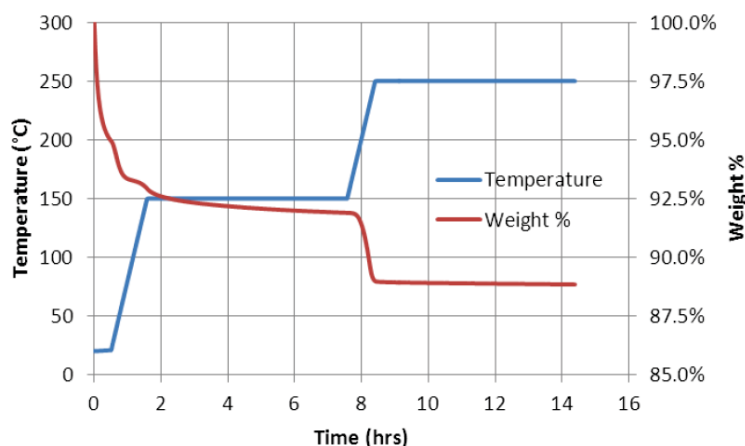


Figure G-10. "Short Run" TGA profile for poly(amic acid) hollow fibers.

In order to study the effect of the purge gas environment, TGA studies were conducted with lower flow rate of purge gas. The results from the "Low Flow" run were found to be significantly different from the previous two runs. The fibers did not fully imidize during this run and remained whitish in color, compared to the orange color that imidized fibers take on. The profile for the "Low Flow" TGA run is shown in Figure G-11.

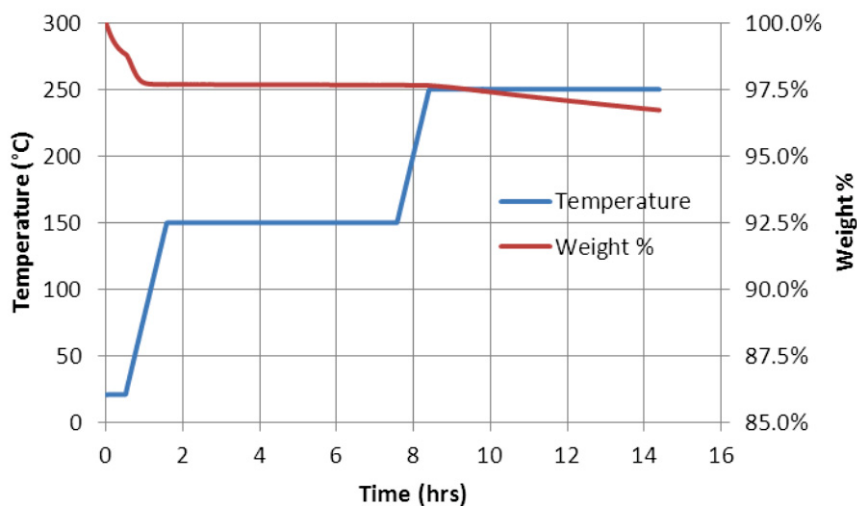


Figure G-11. "Low Flow" TGA profile for poly(amic acid) hollow fibers.

Another interesting factor was that the fibers were not losing the residual solvents prior to reaching the imidization temperature. The imidization temperature appeared to be shifted to above 250°C, with some limited reaction started to occur at 250°C. The presence of water, which would have otherwise been removed by a higher flow rate of gases, appeared to retard the imidization process.

Table G-9. Summary of TGA Weight Losses in the “Low N₂ Flow” Run.

| Step | Weight Loss (%) | Potential Source |
|---------------|-----------------|--------------------------------------|
| RT Hold | 1.2% | Physisorbed H ₂ O, Hexane |
| RT to 150°C | 1.1% | Physisorbed H ₂ O, Hexane |
| 150°C Hold | 0.0% | -- |
| 150°C – 250°C | 0.0% | -- |
| 250°C Hold | 0.9% | Imidization (H ₂ O) |

Using the TGA results (TableG- 9), the thermal cycle required to imidize the VTEC 080-051 poly(amic acid) hollow fibers from Spin 4 was significantly reduced from 2 days to 15 hours. The importance of maintaining high nitrogen flow rates was also realized. TGA studies helped develop an imidization protocol which was significantly shorter than the baseline protocol developed for flat sheet membrane films by INL. With the studies conducted on small fiber strands it was desired to develop an experimental setup which would allow scale-up the imidization protocol developed using TGA.

Infrared (IR) Analysis

Attenuated total reflectance (ATR) IR spectra were obtained on a Bruker Optics, Vertex 70 FTIR. The Vertex 70 was configured with a liquid nitrogen-cooled, wide-band MCT detector and KBr beamsplitter. For ATR-IR measurements, the FT-IR was fitted with an ASI, diamond ATR accessory. A total of 64 interferograms were collected for each spectrum prior to the Fourier transform. A background spectrum was obtained from the bare diamond crystal. Spectra were baseline corrected to eliminate slopes and Gentle curves. The region around 2100 wavenumbers may be obscured by the strong diamond absorbance in this region. A minimum of 5 spectra collected at different points along the fiber and then averaged to obtain a representative spectrum for each sample.

NMR Analysis

All solution state ¹H and ²D spectra were obtained on a Varian NMRS 600 spectrometer using a 5 mm “indirect detection triple-axis” gradient probe, and ¹³C spectra were obtained on a Varian INOVA 600 spectrometer using a 10 mm broadband probe.

For ¹H-NMR samples, the poly(amic acid) solution (20-25mg) was mixed with dimethyl sulfoxide (DMSO), the fibers were dissolved in either dimethyl sulfoxide (DMSO) at RT or tetrachloroethane (TCE) or a mixture of the two ~100°C, depending on the degree of imidization. Usually 16 or 32 transients were collected using a total acquisition cycle time of 15 sec. For ¹³C samples, 100-200mg of material was usually dissolved in 3.2mL of DMSO or TCE with 0.5wt% Cr(AcAc)₃, and at least 6400 scans were collected in an overnight run with a total cycle time of 10s. Residual solvent resonances from DMSO or TCE were used as chemical shift standards (7.26 ppm for CHCl₃, 2.49ppm for DMSO and 5.9 ppm for TCE on ¹H, and 77ppm for CHCl₃, 40 ppm for DMSO and 74 ppm for TCE on ¹³C).

Solid state ¹³C spectra were collected on a Bruker Avance 300 spectrometer using a 4 mm MAS probe. Fibers were simply cut into bead-sized particles and ~100 mg of sample was spun at 11.0 kHz. A 2.5 ms cross-polarization contact at 55 kHz field strength was used to develop ¹³C magnetization. A total of 6816 scans were accumulated with a relaxation delay of 2 sec. The chemical shift offset was estimated by reference to an external standard, hexamethylbenzene.

Data processing was carried out using the NetNMR software developed at GE Global Research.

Curing Test Rig Design and Development

To scale-up the thermal imidization protocol a custom built oven shown in Figure G-12 was designed and fabricated. The oven consisted of a steel tube wrapped with heating tape (BriskHeat, 1 in. x96 in., 830W, 120V), and insulating tape (Glaspun, 2 in. x0.03 in. x100 ft.). The heating tape was controlled by a Digi-Sense® Temperature Controller R/S with a thermocouple positioned in the middle of the tube within a few millimeters of the fibers. If desired, a nitrogen atmosphere could be maintained via nitrogen being feed into the oven and controlled with a flow meter. Fibers were cured on either a graphite shelf or a quartz tray positioned near the middle of the oven. The graphite shelf consisted of 20 mil graphite sheet. However, it was found that the fibers tend to stick together if they were in direct contact with each other during imidization. The quartz tray had five 3 mm grooves to place individual fibers, which helped in eliminating this problem. Fibers which did become stuck together during storage could be easily separated, however, there was a high risk of creating defects in the hollow fiber skin-layer. The effects of temperature and atmosphere on the porosity, surface roughness, and densification of the hollow fibers were studied.

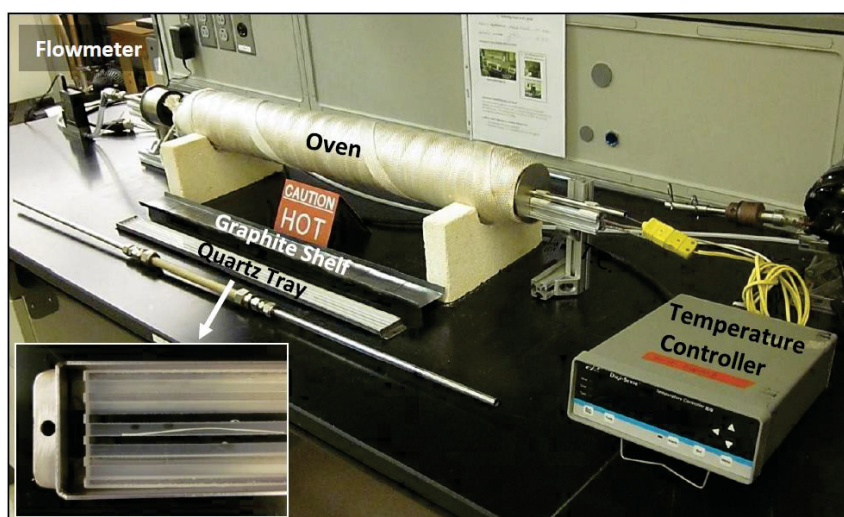


Figure G-12. Oven for curing polyimide hollow fibers. Close-up of quartz tray shown in detail.

Hollow Fiber Module Development and Separation Performance Testing

Sealing Materials Selection

Polyimide hollow fiber membrane modules for water gas shift applications will be exposed to temperatures in the range of 200-300°C. Hence, potting materials that could survive thermal cycling from room temperature to 250°C and provide hermetic seals are required. Due to the low permeance of the fibers, it was important that the potting material be hermetic. Even a small amount of leak could significantly decrease the selectivity of the membrane and increase the total permeance of the sample due to potential leak paths.

A study of different potting materials, primarily high temperature epoxies, was conducted. Initially, 3 potting compounds – 3M™ Scotch-Weld™ DP100, Grace Specialty Chemicals STYCAST 2651-40, and Aremco Aremco-Bond™ 631 – were identified from literature, but some of the compounds had lower than desired maximum operating temperatures. Additional materials with similar properties but higher maximum operating temperatures were identified (Figure G-13).

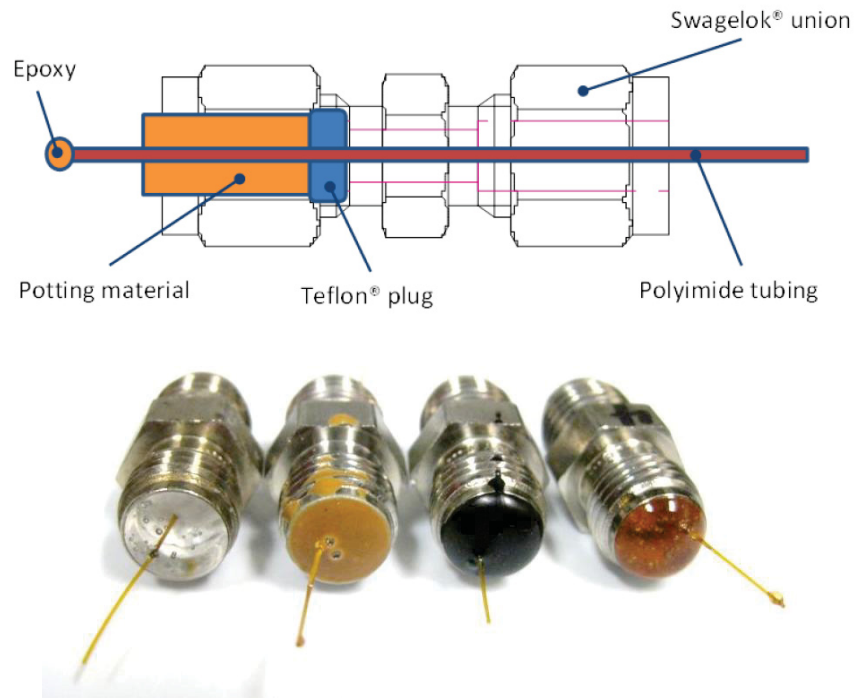


Figure G-13. Potting material test samples, drawing from www.swagelok.com.

A sealing material screening process identified several candidates for heating to 180 – 200°C. Bench testing was done using these potting materials to pot dense polyimide tubing. The goal was to identify a material that remained leak tight after thermal cycling. The leak site was typically between the ID of the steel module and the OD of the potting material. This area is shown in Figure G-14. Leaks were also been seen through cracks or pinholes in the potting material.

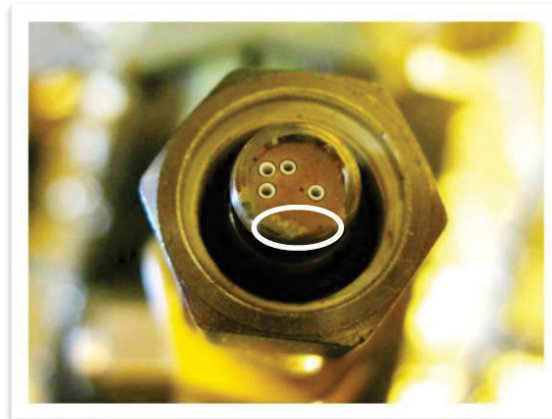


Figure G-14. Leak site between inner wall of steel tube and potting material, as indicated by white circle.

After assembly and curing, the modules were pressurized on the bore side with N₂ to 15 psig and held for 15 minutes to look for any pressure drop due to leaks. Any leaks seen would be due to gas leak from the polyimide tubing or the potting material. Leaks from the polyimide tubing were unlikely unless the tubing was damaged during the module potting assembly or potting process. Leaks from the potting material could be through the bulk of the potting material through cracks or pinholes, at the interface of the potting material and the fiber OD, or at the interface of the potting material OD and steel module ID. None of the modules showed leaks at room temperature.

After testing with N₂, the bore side of the module was pressurized to 0 - 15 psid with an equimolar mixture of H₂ and CO₂. An Argon sweep gas stream flowed through the surrounding shell past the sample and to a mass spectrometer. The concentration of H₂ and CO₂ in the sweep gas stream was measured to determine the leak rate from the process side. Since no leaks were seen from a pressure test with N₂ at room temperature, there should be no H₂ or CO₂ seen at room temperature.

The system was heated to 200–250°C, held at temperature, and cooled back to room temperature, while continuously measuring H₂ and CO₂ concentration in the permeate. As the temperature of the system was increased to temperatures > 100°C, any H₂ or CO₂ measured on the sweep side could be due H₂ and CO₂ permeating through the polyimide, a leak in the polyimide tubing, or a leak in the potting material. Based on data reported by INL, the H₂ permeance of VTEC PI 80-851 at 250°C was expected to be around 80 barrer with H₂/CO₂ selectivity around 8. This data can be used as a guideline for expected polyimide permeance, although the exact composition of the polyimide tubing is unknown. During the elevated temperature potting material tests, if the H₂ permeance measured was significantly higher than this value, coupled with a low H₂/CO₂ selectivity, it can be assumed that the potting material was leaking.

In all the modules used for potting material screening, H₂ and CO₂ permeance was seen at temperatures greater than 50°C. Of the 4 materials used, only the Duralco™ 4525-IP showed no H₂ or CO₂ in the sweep stream until the temperature was above 50°C. In addition, all of the profiles showed irregularities in the plot of H₂ permeance with temperature. If the only mechanism for H₂ and CO₂ transport to the sweep side was through the walls of the polyimide tubing, the heating and cooling permeance should show no hysteresis. All of the plots showed significant variation in permeance with temperature (Figure G-15).

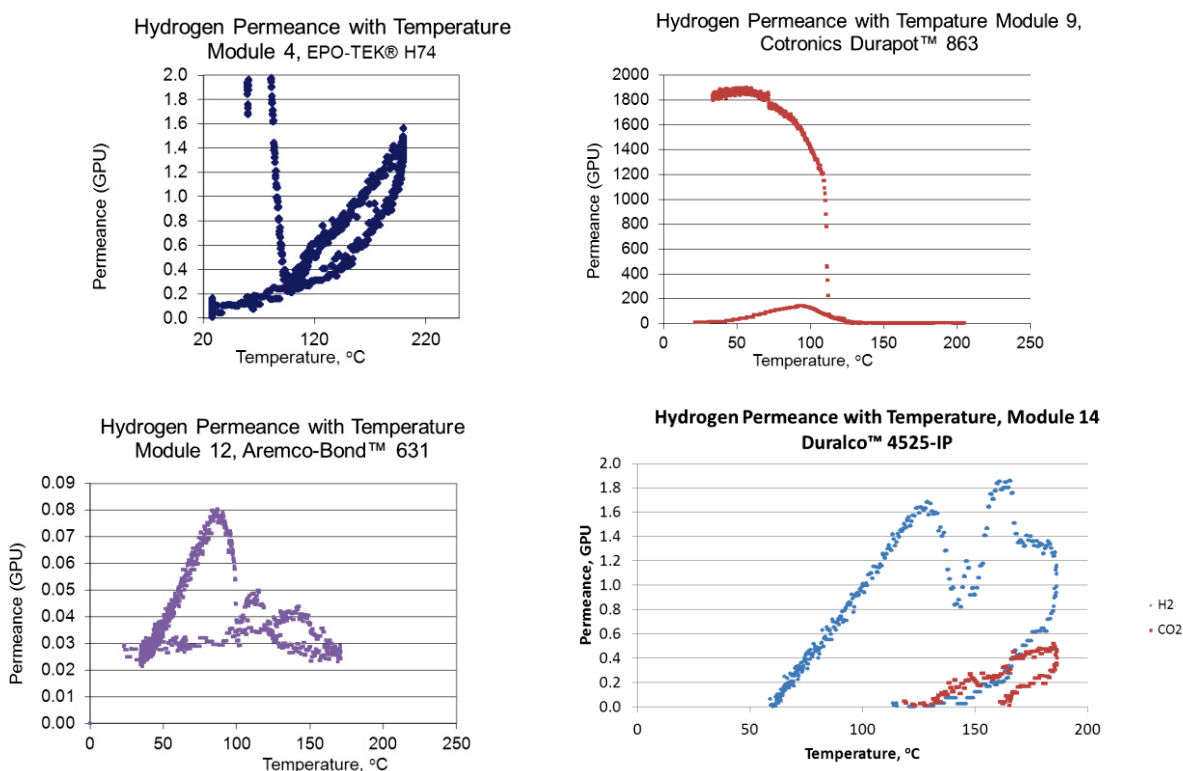


Figure G-15. Gas-separation testing of polyimide tubing potted with four different potting materials. All permeances greater than ~2 GPU were assumed to be caused by potting materials leaks.

The EPO-TEK® H74 made a good seal at room temperature. The module showed little or no H₂ permeance at room temperature and no CO₂ permeance until the module was heated to 100°C. The H74

epoxy showed stable behavior at a temperature of 200°C, with H₂ permeance 1 – 3 GPU and H₂/CO₂ selectivity close to Knudsen selectivity (=4.7). In the case of H₂/CO₂, Knudsen flow was expected to dominate at pore sizes less than 20 nm. Pores larger than 20 nm will allow non-selective viscous flow. As the pressure was increased, if there was a pathway for viscous flow, the permeance values will increase and H₂/CO₂ selectivity will decrease. If the H₂/CO₂ selectivity was Knudsen or greater, a leak from the potting material was not detected.

During cooling, a significant leak occurred when temperature dropped to around 100°C. As shown in the plot of hydrogen permeance with temperature for GE ID-module 4, the leak upon cooling was sudden and pronounced. At the time of leak, H₂/CO₂ selectivity immediately dropped to 1, meaning the flow was completely viscous. This behavior was repeated over several modules. Based on this performance, H74 could be used to make a module for long term testing at 200°C, with no thermal cycles, but the module would develop a leak as soon as it was cooled (Figure G-16).

The module potted with Durapot™ 863 showed a low non-selective H₂ and CO₂ permeance at room temperature. As the module was heated, the H₂ and CO₂ permeance continued to increase until the temperature reached about 100°C. At temperatures greater than 100°C, the permeance of both H₂ and CO₂ began to decrease until it was even lower than the initial room temperature values, with a slight H₂/CO₂ selectivity of 2. This behavior may be related to additional heat curing of the potting material. The sample reached a maximum temperature of 200°C and remained stable until cooling. During cooling from 200°C, a large leak occurred around 100°C. After testing, cracks were seen in the potting material around the module fittings. The potting material was brittle, and the potting fittings could be separated, breaking the remaining epoxy seal easily. This material was not appropriate for sealing against the steel parts at these temperatures.



Figure G-16. Cracks in Durapot™ 863 potting material after thermal cycle at 200°C, as indicated by white circle.

Aremco-Bond™ 631, while limited by a maximum operating temperature of 200°C, survived being heated in a module made with polyimide tubing at a pressure gradient of around 25 psi. At a temperature of 200°C, H₂ permeance was 0.3 GPU and selectivity was close to 3. During cooling, there was a slight leak at 100°C. When the sample returned to room temperature, the H₂ and CO₂ permeance matched starting values. Aremco-Bond™ 631 survived a complete thermal cycle to 200°C without any large leaks. An advantage of this material was a shorter curing time than EPO-TEK® H74 or Duralco™ 4525-IP. The disadvantage was the lower maximum operating temperature of 200°C.

Duralco™ 4525-IP showed no H₂ or CO₂ permeance below 50°C during heating or cooling. As temperature increased above 50°C, the H₂ and CO₂ permeance increased. Upon cooling, no H₂ or CO₂ permeance was seen below 50°C. However between 50–180°C, there was noticeable hysteresis between the heating and cooling lines. During this test, the feed inlet pressure rose from a starting value ~ 20 psig up to 40 psig and did not decrease until the feed gas flow rate was reduced (Figure G-17).

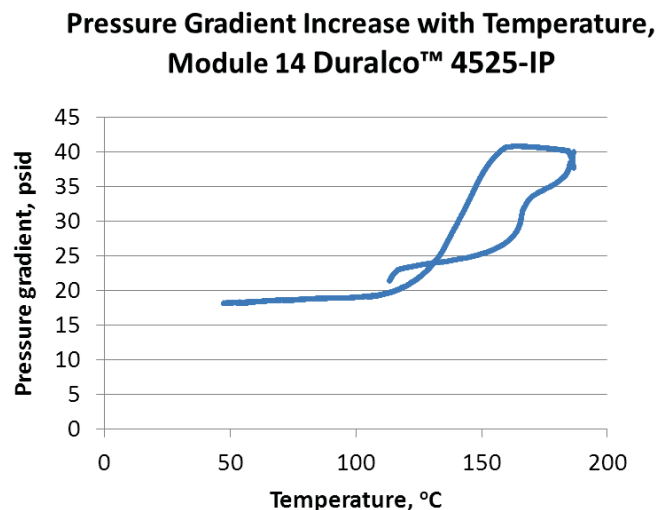


Figure G-17. Increase of pressure gradient as Module 14 is heated, due to increase in feed pressure.

This increase in feed pressure was observed in multiple modules. The cause of this pressure build-up was unclear. It was thought to be due to heating and possible compression or blockage of the polyimide tubing from the epoxy. A large difference was noticeable between the process pressure at the module inlet and the pressure at the module outlet. In order to negate this back pressure effect, modules were assembled with larger diameter polyimide tubing.

The tubing OD was increased from 0.014 to 0.07 inches and new modules were made using Aremco-Bond™ 631 and Duralco™ 4525-IP. The Aremco-Bond™ 631 was cured at room temperature, with a 24 hour soak. The Duralco™ 4525-IP cured at room temperature with a 24 hour soak, followed by an elevated temperature post cure: 1 hour at 121°C followed by 1 hour at 177°C. The modules were then heated in 50 vol.% H₂ / 50 vol.% CO₂ to temperatures of 100°C, 150°C and 200°C in successive thermal cycles. The only H₂ and CO₂ permeance that should be seen is the permeance through the polyimide tubing itself, which is selective. High permeance or non-selective flow indicates a leak through the potting material or the interfaces between the potting material and the sample and/or module wall.

GE ID: module 20 was 0.07 in. diameter polyimide tubing potted with Aremco-Bond™ 631. The maximum operating temperature was 200°C, according to the manufacturer. The module was heated to 100°C and cooled back to room temperature while maintaining a pressure gradient of 6 psi between the process gas inlet and sweep side of the membrane. During the heat-up, no flow through the membrane was seen until temperature was above 70°C. At 100°C, H₂/CO₂ selectivity of 7 was recorded. Upon cooling, the flow through the membrane did not increase and the module showed no leaks.

A second heating cycle was done to 150°C. The heating behavior matched the previous thermal cycle, and at 150°C, H₂/CO₂ selectivity was around 8. The hydrogen permeance was 0.3 GPU at temperature. During cooling, the permeance value at each temperature was slightly higher than it had been during heating. In addition, there were a few areas in the cooling ramp where the permeance values increased unexpectedly. This behavior indicated possible seal leaks at the potting material. The permeance as a function of temperature is shown in Figure G-18. Based on the behavior at 150°C and the maximum operating temperature, the module was not heated to 200°C.

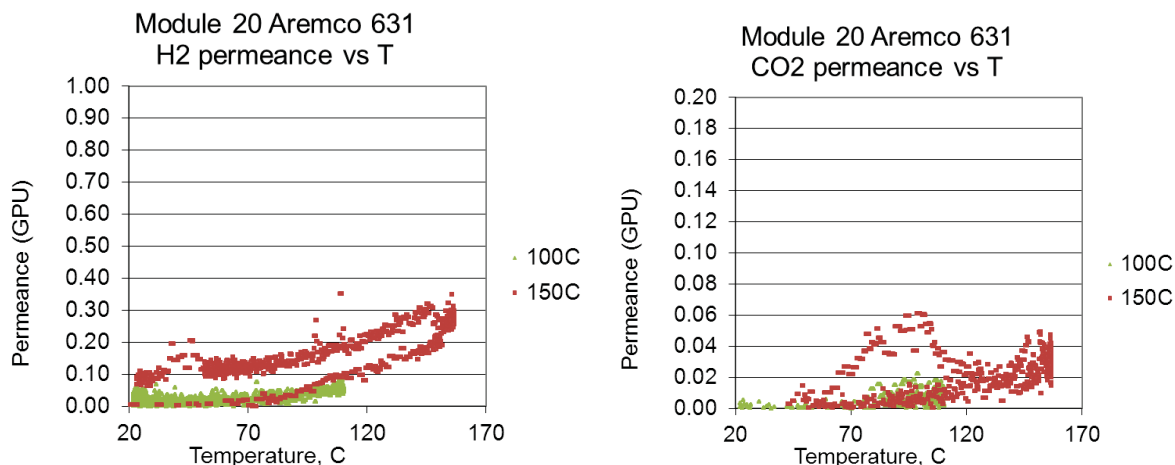
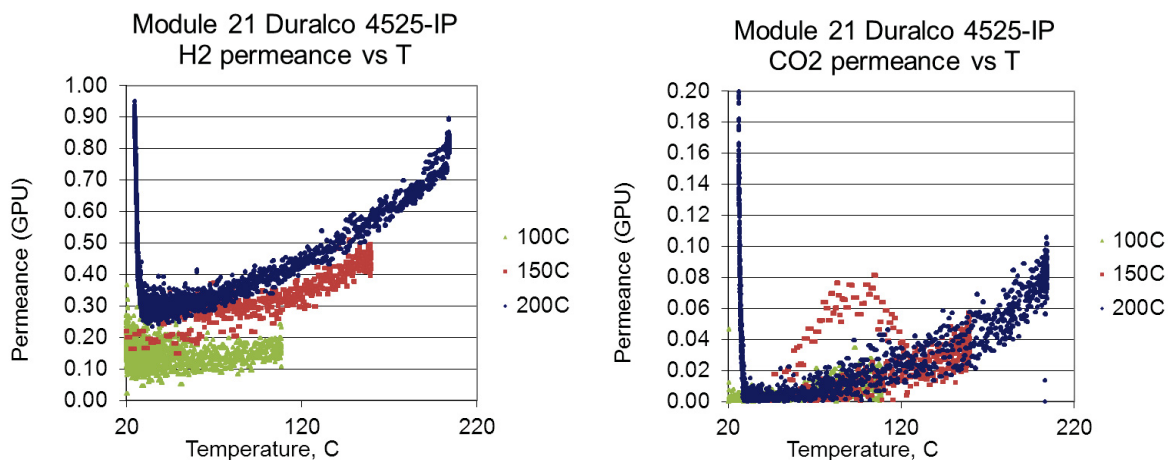


Figure G-18. Permeance increase with temperature for hollow fiber module potted with Aremco Bond 631 epoxy: (a) hydrogen, (b) carbon dioxide.

Module 21 was potted with Duralco™ 4525-IP, which had a maximum operating temperature of 260°C. The material cured at room temperature, with an additional elevated temperature post-cure. Previous testing has shown that the post cure may be important for this process. The module was heated and cooled successively to 100°C, 150°C and 200°C. At the end of cooling, after the 200°C heat, there was a large increase in H₂ and CO₂ permeance, accompanied by a selectivity drop to 1, indicating a viscous leak. No further heating was done on the module. The module performance is shown in Figure G-



19.

Figure G-19. Permeance increase with temperature for hollow fiber module potted with Cotronics 4525-IP epoxy: (a) hydrogen, (b) carbon dioxide.

At 150°C, the H₂ permeance was 0.5 GPU with a selectivity of about 10. There was a slight increase in CO₂ permeance during cooling from 150°C, but at the end of cooling, the CO₂ permeance was zero. Additionally, the 200°C heating and cooling cycle looks good, with no unexpected behavior until the leak at the end of cooling. This module was run at the same pressure gradient as module 20.

From this data, it is apparent that the module could be heated to 150°C and cooled with no negative effects. The module could also be heated to temperatures as high as 200°C while still showing good performance. The only limitation is that the module cannot survive multiple heating cycles to temperatures as high as 200°C. It is possible that some modules will be more robust than others and may survive cooling from 200°C. Conservatively, 150°C was chosen as a maximum testing limit for hollow

fiber modules, so that the modules could survive multiple heating ramps. This was necessary so that modules can be tested at GE and then shipped to WRI for further testing.

Based on the data from these modules plus previous tests, the H₂ permeance of polyimide tubing with a 50 µm wall at 150°C was approximately 0.4 GPU with H₂/CO₂ selectivity close to 10. Duralco™ 4525-IP was chosen as the potting material to be used in future testing. The studies with polyimide tubing helped in deconvoluting the gas leakage from the hollow fiber and potting material. Using dense polyimide tubing, the defects in the hollow fibers were eliminated and appropriate epoxy sealing materials were selected.

Hollow Fiber Membrane Module Fabrication

Bench Testing

Initial module testing suggested that the fiber quality varied among individual fibers. The first modules were made with fibers that had passed only a visual inspection after imidization. After assembled modules showed leaks during bench screening (N₂ permeance measurement) or mixed gas testing, it was decided to screen the fiber bundles prior to module assembly. After screening several fiber bundles and continuing to find leaks, it was determined that the polyimide fibers would need to be individually screened. While the system sensitivity was limited, it could detect N₂ permeance of 10 GPU or higher. If a fiber did not show a detectable leak (N₂ permeance less than 10 GPU), the fiber was considered a pass.

Polyimide hollow fibers were grouped into bundles of 1-10 fibers and assembled into modules to be tested for H₂ and CO₂ gas separation performance. The bundle of fibers were enclosed in a stainless steel shell and potted on both ends with an epoxy or other suitable material to make a hermetic seal between the module and the fibers. The module was then tested in the H₂/CO₂ test system. The assembly and potting of a module was a time consuming process. In addition, leaks may develop either at the potting material or within the fibers themselves during module assembly. The screening of the polyimide fibers prior to module assembly was an important step to ensure that only good fibers were being incorporated into modules and to determine if damage to the fibers was occurring during module assembly or potting. This preliminary screening test resulted in time and module parts saved and increased experimental clarity about when leaks were occurring in the system, if they were any leaks.

Individual fibers or bundles of polyimide hollow fibers were potted inside 316 SS Swagelok® port connectors. The fibers were inserted through the port connector and held in place with a rolled length of Teflon® tape. The Teflon® also held the liquid epoxy in place during potting. Alternatively, a glass wool can be used. The fibers were then potted with Devcon® 5 Minute® epoxy. The fibers were potted first on the top side, close to the Teflon® tape. Once the epoxy was cured, the fibers were potted on the other end of the port connector. Potted fiber bundles are shown below in Figure G-20. Each fiber was then sealed on the other end with a small amount of 5 Minute® epoxy, as shown in Figure G-21.



Figure G-20. Potted hollow fibers for screening.



Figure G-21. Potted hollow fibers for screening.

The potted hollow fibers were then connected to the bench top permeance test set-up using 0.25 in. Swagelok[®] fittings. The test-set up consisted of a gas source (house plumbing or cylinder), a 0-100 sccm mass flow controller which could measure pressure, and appropriate fixturing to connect a mounted sample to system. House nitrogen was used as the gas source for the hollow fibers.

The fibers were pressurized with N₂ and the rate of pressure drop was measured. The procedure is summarized in Appendix H.

Appendix H. H₂/CO₂ Gas Permeability Testing of Hollow Fibers

Four modules were assembled with VTECTM polyimide fibers (Spin 4, states 1 and 7 and Spin 5, state 4) that had been tested to verify that they were free of large viscous defects. Based on the N₂ permeance testing results, all of the fibers were expected to be dense. This was supported by microstructural evaluation in the SEM. Each module was filled with 5 fibers and potted with Cotronics epoxy. A cross section of potted fibers is shown in **Error! Reference source not found.H-1**.

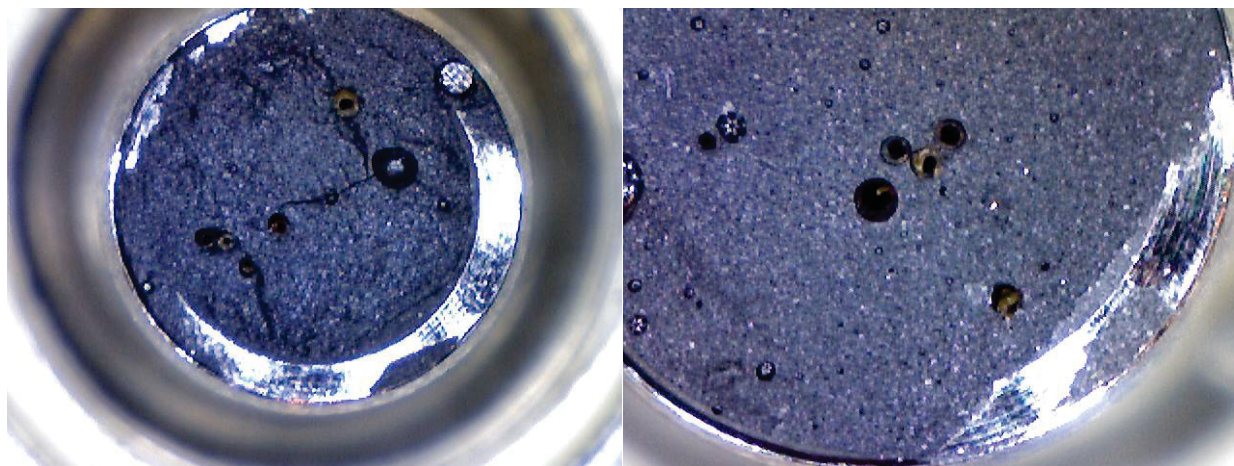


Figure H-1. Cross section of potted VTEC fibers potted in module with DuralcoTM 4525-IP.

The modules were heated to 150°C in ideal syngas (50 vol.% H₂ / 50 vol.% CO₂) to measure permeance of H₂ and CO₂ and H₂/CO₂ selectivity. The modules showed similar performance to each other and similar permeance to polyimide tubing, confirming that the fibers were dense. All of the modules survived heating to 150°C and cooling to back to room temperature. The H₂/CO₂ selectivity values ranged from 4–15. The range of selectivities measured was wide due to noise in the mass spectrometer signal due to low CO₂ concentrations.

The H₂ permeance and selectivity of the 3 modules was similar, with H₂ permeance ~ 0.1 GPU and selectivity ~ 10 at 150°C. The CO₂ permeance was close to the minimum detectable for the system, meaning there is noise in the measurement. The testing results from the modules are shown in Figure H-2.

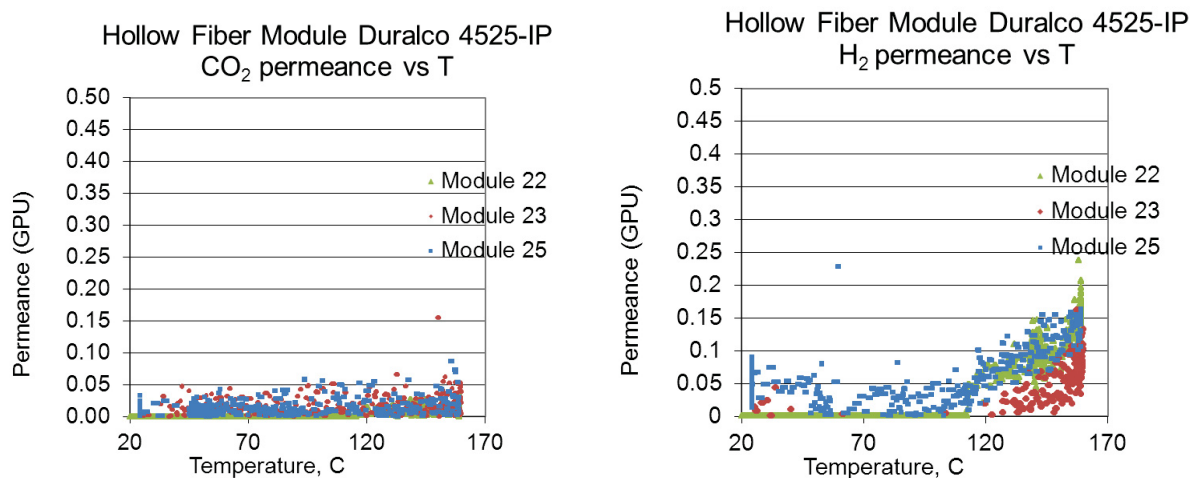


Figure H-2. Permeance increase with temperature for hollow fiber modules potted with Cotronics 4525-IP epoxy: (a) hydrogen, (b) carbon dioxide.

The behavior of permeance with temperature was the same for heating and cooling for both H₂ and CO₂, indicated no leaks or changes in the fibers during the heating cycle. The values were on the same order of magnitude as the values measured for polyimide tubing, emphasizing that the fibers must be dense. The H₂ and CO₂ permeance values of the fibers seem slightly lower than the tubing, which may be within the error of the measurement or due to a slightly greater wall thickness than the tubing. Two modules were sent to WRI for syngas testing.

Appendix I. Summary of Tasks, Major Milestones and, Deliverables

Task 1. Model performance of the membrane reactor and system

Subtask 1.1. Develop detailed WGS-MR model.(Q1)

Milestone (Q1): WGS-MR model and initial membrane performance targets - Completed

Subtask 1.2. Develop integrated system model and perform economic analysis. (Q2-4)

Milestone (Q3): Integrated system model and refined membrane targets for NH₃ application - Completed

Deliverable (Q4): Economic analysis for coal-to-ammonia and broader gasification market impact - Delivered

Task 2. Develop hydrogen selective polymer materials. (Q4) - Completed

Task 3. Develop manufacturing processes for supports with defect-free intermediate layers and membrane modules (porous supports).

Subtask 3.1. Define intermediate layer targets (Q1)

Milestone (Q1): Intermediate layer microstructural targets - Completed

Subtask 3.2. Screen and optimize processes for intermediate layer deposition (Q2-4)

Milestone (Q3): Down-selected intermediate layer deposition process - Completed

Deliverable (Q4): Optimized intermediate layer process on 5 cm tube - Delivered

Subtask 3.3. Integrate polymer onto optimized intermediate layer (Q5-Q11)

Deliverable (Q8): Optimized intermediate layer process on 20 cm tube - Delivered

Deliverable (Q11): Optimized intermediate layer process on 70 cm tube - Delivered

Subtask 3.4. Determination of physical parameters of the module (Q5)

Milestone (Q5): Membrane module design trade-off analysis - Completed

Subtask 3.5. Mechanical design of the membrane module (Q6-Q7)

Milestone (Q7): Design for tube-in-shell membrane module - Completed

Subtask 3.6. Design and fabrication of sub-scale modules for experimental validation (Q8-Q11)

Milestone (Q9): Subscale module with 20 cm tube for testing - Completed

Deliverable (Q11): Subscale module with 70 cm tube for testing - Delivered

Subtask 3.7. Design and fabrication of hollow fibers for experimental validation (Q8-Q11)

Milestone (Q10): Develop hollow fibers for testing - Completed

Deliverable (Q12): Subscale module with hollow fibers for testing - Delivered

Task 4: Validate membrane performance under realistic testing conditions. Demonstrate the economic and environmental benefits of hydrogen produced from WGS-MR process for ammonia/fertilizer plants. (Q6 – Q12) – Validation Completed

Task 5: Deliver Project Final Report of DOE-HQ, EERE-AMO - Completed